PMFSEL REPORT 91-1
JULY 1991

REINFORCED CONCRETE FRAME CONNECTIONS REHABILITATED BY JACKETING

by

Sergio M. Alcocer

and

James O. Jirsa

Sponsored by
National Science Foundation
Grant No. ECE-8610946

ABSTRACT

Little experimental work has been conducted to verify the performance of concrete jacketing of frame elements and its suitability as a rehabilitation technique. Designers of this scheme have faced the dilemma of analyzing and designing rehabilitated structures without guidelines. An experimental program was developed to evaluate the effectiveness of jacketing of frame elements. Four reinforced concrete large-scale frame connections with flexible columns were tested after being repaired or strengthened by jacketing only columns, or both columns and beams. The subassemblages represented an existing structure designed according to Mexican and American practices typical of 1950's construction with non-ductile detailing. The specimen condition prior to rehabilitation and the layout of the column longitudinal reinforcement were also varied. The subassemblages were tested to large deformation levels applying a bidirectional cyclic loading history.

The prime objectives of the study were as follows:

1. The effect of jacketing on the hysteretic response of the subassemblages, especially with regard to stiffness degradation and energy dissipation.

2. The mechanism of joint shear resistance in rehabilitated connections with a special structural steel cage used to provide joint confinement.

3. The effect of damage due to prior loading on the response of a jacketed beam-column joint.

4. The influence of the layout of the column longitudinal steel, in particular with respect to bond along bars bundled or in the corner of the column jacket or distributed along the face of the column.

5. The slab participation in the positive and negative moment capacities of the floor system.

6. The constructability of the jacketing scheme.

The program was part of the coordinated research effort between Mexican and American engineers implemented after the 1985 Mexico earthquake, and sponsored by the National Science Foundation (USA) and Consejo Nacional de Ciencia y Tecnologia (Mexico).

ACKNOWLEDGEMENTS

The research was conducted at the Phil M. Ferguson Structural Engineering Laboratory at the University of Texas at Austin. Financial support for the experimental program was provided by the National Science Foundation under grant ECE-8610946 (Mexico Earthquake Program). Additional funding was provided to Dr. Alcocer by the Consejo Nacional de Ciencia y Tecnologia (CONACYT - Mexico).

This report is based on the Ph.D. dissertation of Dr. Sergio M. Alcocer under the direction of Dr. James O. Jirsa. Dr. Michael E. Kreger provided counsel and support throughout the project.

The authors would like to acknowledge the contributions of the following Mexican and American colleagues: Dr. Roberto Meli (Universidad Nacional Autonoma de Mexico), the late Prof. Francisco Robles, and Prof. Jesus Iglesias (Universidad Autonoma Metropolitana), Dr. Horacio Ramirez de Alba (Universidad Autonoma del Estado de Mexico), and Loring Wyllie (H.J. Degenkolb Associates). These engineers participated in the coordinated research effort between Mexico and U.S. implemented after the 1985 Mexico earthquake and helped immeasurably in the detailed planning of the test specimens and test program.

The invaluable assistance and cooperation of the staff of the Ferguson Structural Engineering Laboratory is gratefully acknowledged. Special thanks are expressed to Sharon Cunningham and Jean Gerhke who helped prepare the report. The assistance of numerous students (J.E. Martinez, J. Sanchez, R. Cook, J. Buckman, H. Bouadi, R. Bravo, T. Estrel, B. Falconer, G. Guimaraes, J. Jimenez, T. Powers, G. Ramirez, A. Santolamazza and S. Shah) during the construction, preparation and testing of the specimens is greatly appreciated.

TABLE OF CONTENTS

LIST OF TABLES

LIST OF FIGURES

CHAPTER I - INTRODUCTION

1.1 GENERAL

Recent earthquakes in many different parts of the world have shown the vulnerability of existing structures to moderate and severe ground motions. The 1985 Mexico earthquake and the 1989 Loma Prieta event demonstrated the disastrous consequences of inadequate structures, as well as the benefits of a systematic review and rehabilitation program. Owners are finding the rehabilitation of structures as a reasonable way to provide safety to building occupants and to protect their investments. However, for existing structures, the problems of identifying weaknesses, assessing the condition of the structure, designing techniques for correcting deficiencies, and developing economic and rapid construction procedures have not had the attention of structural engineers and researchers. Rehabilitation is a complex problem since well-understood methods for new construction may not apply. Just as every building is unique, the solution for buildings requiring repair or strengthening for improved seismic response must also be adapted to each structure. Occupancy, social, economic, and technical issues affect any solution.

The experience in Mexico City following the 1985 earthquake increased the worldwide interest regarding the need for reducing the risk posed by hazardous structures. In the U.S. for example, a considerable effort has been underway to develop evaluation and design guidelines for rehabilitation of structures (Ref. 25). In the aftermath of the earthquake, more than a thousand buildings were rehabilitated, many of which had flexible columns with non-ductile detailing and showed joint distress. In this chapter, background on joint behavior and on rehabilitation of frame connections is presented. The objectives and organization of this study are also described.

1.2 BACKGROUND

1.2.1 Joint Behavior in Moment Resisting Frames. Intensive research carried out in several countries over the last two decades has led to the identification of critical features of joint behavior (Refs. 13, 19, 21, 26, 27, 29, 31). Joints in moment resisting frames are normally subjected to large shear forces when adjoining beams develop their maximum flexural strengths. Generally, it is preferable to ensure that the columns above and below a joint remain elastic while beam hinging develops. The primary attention has focused on force transfer mechanisms across the cracked joint core.

Under seismic effects, bending moments and shears are generated in beams and columns which introduce internal stresses into the joint core (Figures 1.1a and 1.1b, taken from Ref. 13). Two force transfer mechanisms have been recognized. The diagonal compression strut mechanism (Figure 1.1c) is formed along the main diagonal of the joint panel as the resultant of the horizontal and vertical compression stresses acting at the beam

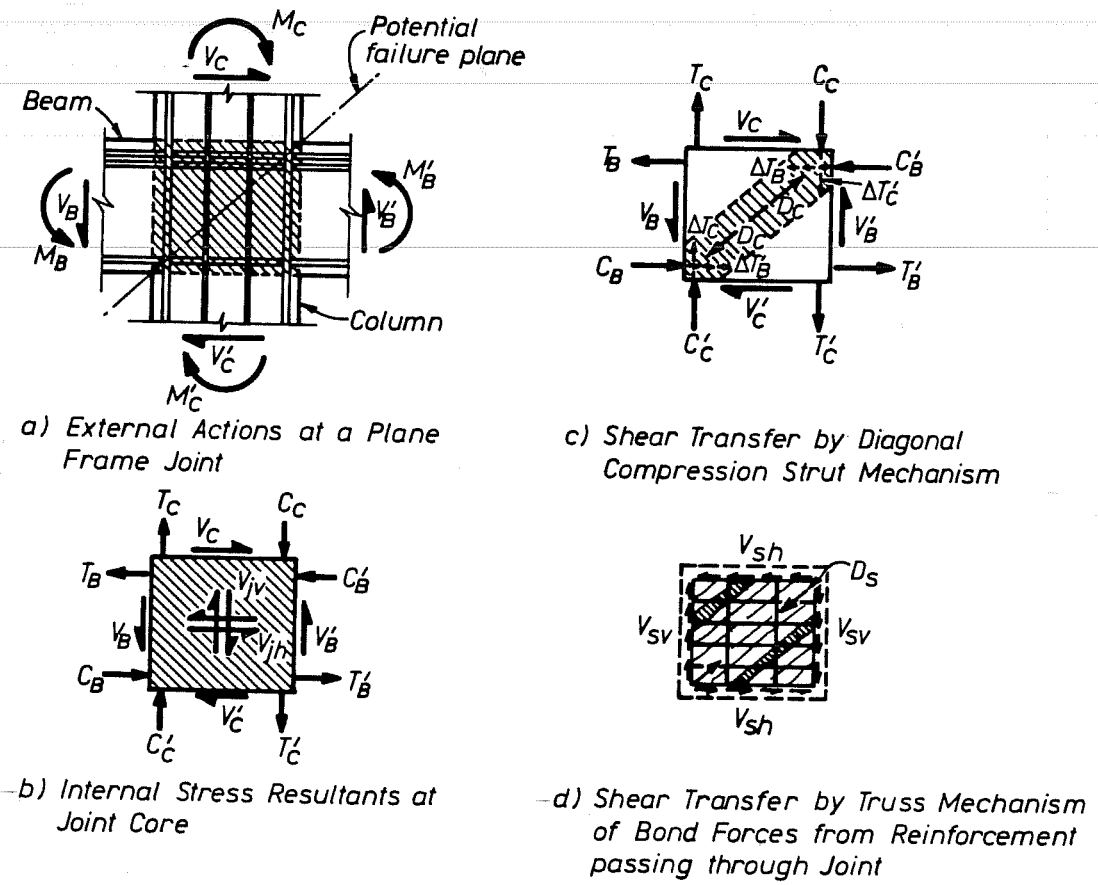

Figure 1.1 Joint Shear Transfer Mechanisms (from Ref. 13).

and column critical sections. It is important to note that the strut exists regardless of the bond situation within the joint. In the second mechanism, referred to as truss mechanism (Figure 1.1d), Figure 1.1 small diagonal struts are distributed in the joint panel, and are balanced by tensile stresses in the horizontal and vertical reinforcement, and by bond stresses along beam bars and exterior column bars. The truss mechanism is possible only when good bond is maintained along beam and column reinforcement. However, perfect bond generally cannot be preserved along the beam reinforcement after beam hinging. Once bond deteriorates, force transfer in the truss mechanism gradually decreases, and the diagonal strut carries most of the shear forces in the joint.

Research results have indicated that joint shear strength increases with concrete strength. Tests have shown that a minimum amount of transverse steel must be provided to preserve the joint concrete and the shear strength. Also, it has been noted that increasing the amount of joint lateral reinforcement does not lead to higher joint shear strengths. Test data indicate that lateral beams, whether unloaded or loaded, enhance the joint performance because they help to maintain the integrity of the core. Beam width also appeared to influence the behavior. In many experimental programs, different levels of constant axial loads have been applied to the columns. Results show that column axial load does not influence the joint strength. In some specimens the floor slab has been included. Slab participation in joint confinement and flexural beam capacities has been reported. Particularly, the participation of the slab steel with the beam reinforcement resisting negative moments has been noted. It has been recognized that the bar size relative to joint dimensions strongly affects the stiffness and energy dissipation capacity. Moreover, bond deterioration modifies the joint shear transfer mechanism. Design guidelines for beam-column joints are given in the American Concrete Institute 352 Committee Recommendations and the American Concrete Institute Building Code Requirements (Refs. 4, 2, 3). The guidelines are intended for new structures. No design recommendations exist for rehabilitated frame connections.

1.2.2 Rehabilitation Techniques for Frame Connections. Typically, frame connections have been rehabilitated by one or a combination of the following basic methods: 1) a local repair scheme, which includes epoxy resin injection or replacement of damaged concrete and steel; 2) steel jacketing; and 3) concrete jacketing (Ref. 46). A brief review of the applicability of the techniques and relevant conclusions from experimental studies of rehabilitation of frame connections is presented.

1.2.2.1 Local Repair Schemes.

Epoxy Resin Injection: The technique is recommended for the restoration of concrete elements with low levels of damage, no crushed or spalled concrete, no fracture or buckling of steel and small crack widths. Pressure injection of the resin is the method most commonly used. Vacuum may also be applied for injection. Procedures for injection techniques can be found elsewhere (Ref. 45).

Replacement: When crack widths are larger than 5.0 mm., and concrete crushing or steel buckling is observed, the damaged section of the element should be replaced with new material to restore the strength and stiffness of the member. To allow placement of new concrete in joints and beams, holes must be drilled in the slab. Before removal of damaged sections, the structure must be temporarily shored.

Most of the research reported on rehabilitation of joints has used local schemes (Refs. 17, 20, 30, 34, 38, 41). In almost all cases, the structures showed damage concentrated in the beams near the joint, and minor distress in the joint. Typically, the location of the most damaged beam region was moved in the repaired structure. This

phenomenon should be assessed to avoid causing severe distress in the joint during future earthquakes. In general, epoxy injection was successful for restoring the shear and flexural strengths of the members. In some cases in which large portions of the members were injected, higher strength than the original was reached (Refs. 20, 30, 41). In all tests, the energy dissipation and stiffness of the repaired structure were lower since it is impossible to inject the microcracks. In some programs, the stiffness was restored to 85% of the original value, while in others only 50%. The behavior of injected members depends on the quality of the repair. Generally, epoxy injection did not restore the bond between concrete and steel reinforcement because concrete pulverized along the bar prevents epoxy from saturating the region. However, French et al. (Ref. 20), concluded that both pressure injection and vacuum injection techniques restored bond between concrete and steel effectively. Replacement of damaged material has been used to restore the bond capacity of bars (Refs. 30, 41). In some buildings, joint concrete has been replaced to restore strength, stiffness and energy dissipation characteristics to the original values. This technique is very labor intensive, particularly for interior joints.

1.2.2.2 Steel Jacketing. Addition of steel elements surrounding a member can be used to restore and to enhance the behavior. If the member is damaged, a local repair technique could be used prior to jacketing. Steel jacketing involves creating a concrete-steel composite section by placing a skeleton made of steel angles and straps; or by attaching plates to the members using adhesives and bolts; or by encasing the member with steel plates or rolled shapes, and filling the space between the casing and the member with non-shrinkage or expansive cement grout. Steel jacketing has been used extensively to rehabilitate structures but little data is available on its effectiveness, particularly to upgrade joint performance. Migliacci et al. (Ref. 34), reported the behavior of exterior frame connections jacketed by a steel skeleton made of steel angles and straps. To improve the confinement of the beam and columns, the straps of two specimens were prestressed by pre-heating. From the results it is concluded that steel jacketing enhanced the strength and energy dissipation capacity observed in the original structure. The specimens with pre-heated straps showed more stable behavior. However, prestressing obtained by pre-heating should not be relied on since it is difficult to control in the field.

1.2.2.3 Concrete Jacketing. The purpose of concrete jacketing is to enhance the axial, flexural and shear strengths, and stiffness of any element, damaged or undamaged, by wrapping it with an additional cage that could be formed either by new longitudinal steel plus ties or by welded wire fabric, and new cast-in-place or shotcreted concrete cover (Refs. 12, 45, 46). For flexural capacity, reinforcement in the jackets should be made continuous using holes drilled in the structure to allow passage of the transverse and longitudinal reinforcement. The connection can be locally jacketed to increase the stiffness and shear strength, or forming part of an overall jacketing scheme which includes beams and columns (Figures 1.2 and 1.3, respectively, taken from Ref. 46). The latter approach is intended Figure 1.2 to rehabilitate the connection and to enhance the strength, stiffness and energy dissipation capacity of the frame. Very few attempts have been made to assess experimentally the behavior of jacketed frame connections. Corazao and Durrani (Ref. 17),

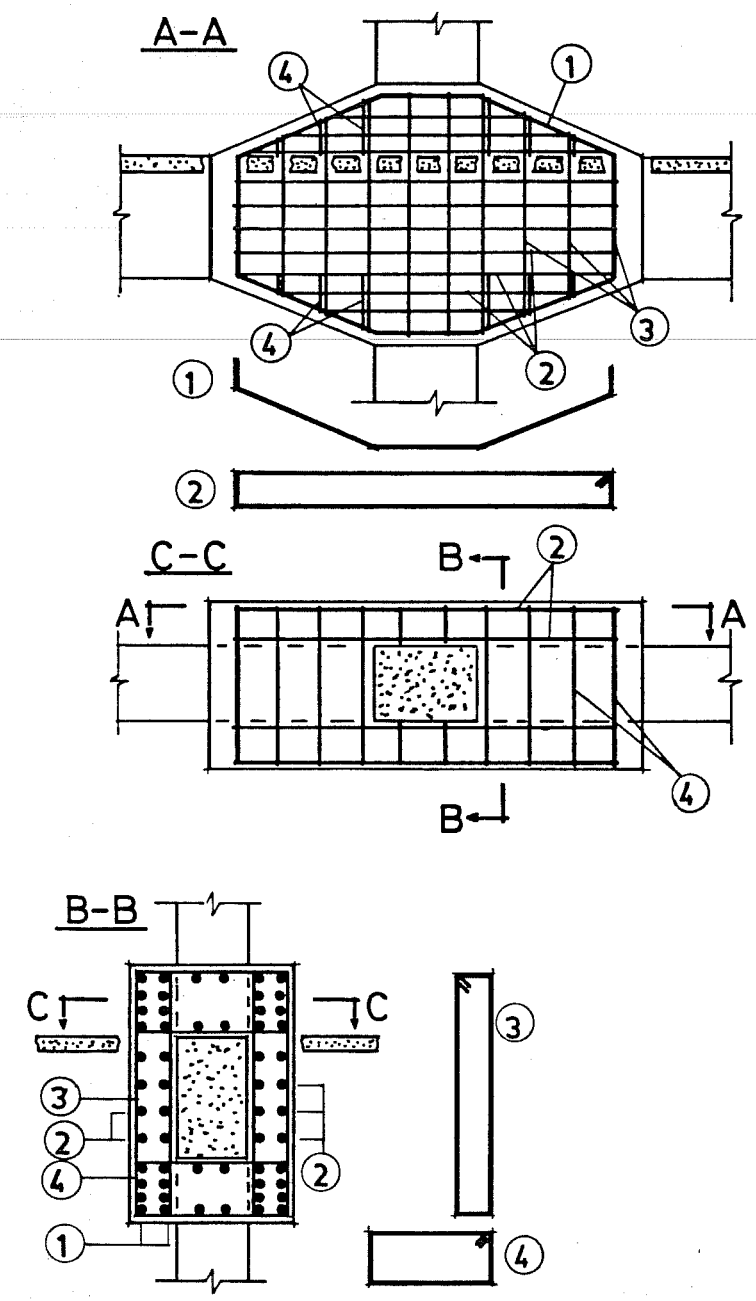

1 - longitudinal bars
2 - horizontal ties
3 - vertical stirrups
4 - vertical stirrups

Figure 1.2 Local Jacketing of Joint (from Ref. 46).

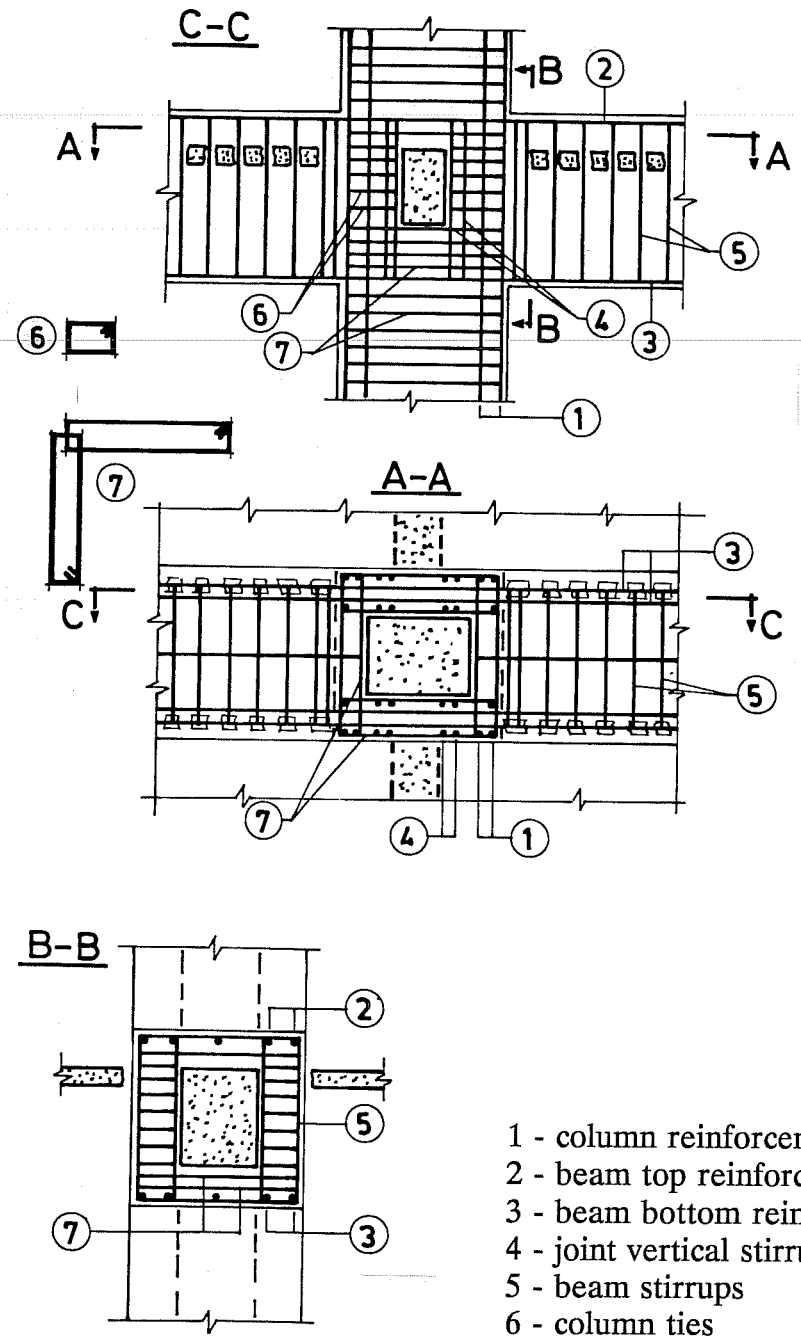

Figure 1.3 Jacketing of Beams, Columns and Joint (from Ref. 46).

reported on some tests of frame connections repaired by jacketing the columns, and by jacketing the columns and a portion of the beams adjacent to the joint. For joint confinement, holes were drilled into the beams and ties were placed around the joint and bent in-situ with 135-deg hooks. Although the size of the specimens is not likely to represent an actual structure and assessment of the experimental data is very limited, the authors concluded that column jacketing restored only the strength of the structure but failed to restore the stiffness and energy dissipation capacity. Jacketing of columns and a portion of the beams next to the joint, restored the strength, stiffness and energy dissipation capacity and moved the beam hinge location.

One of the most common solutions for rehabilitation of concrete frame buildings in Mexico City after the 1985 earthquake, was concrete jacketing of the structural members (Refs. 5, 24). Jacketing of columns only and jacketing of columns and beams both was compatible with the structural system of the building. Jacket reinforcement was continuous to enhance the strength, stiffness and energy dissipation characteristics of the moment resisting frame. One of the advantages of jacketing was the reduced foundation strengthening required as compared with buildings in which shear walls were added. Many buildings had a box type foundation that helped distribute the forces transferred from the superstructure. In some cases, only strengthening of grade beams was necessary which was done generally by jacketing. In general, foundation rehabilitation was expensive and difficult. Different layouts of column longitudinal reinforcement were used. Figure 1.4 shows a jacketed column in which the bars were bundled to reduce slab perforation and to

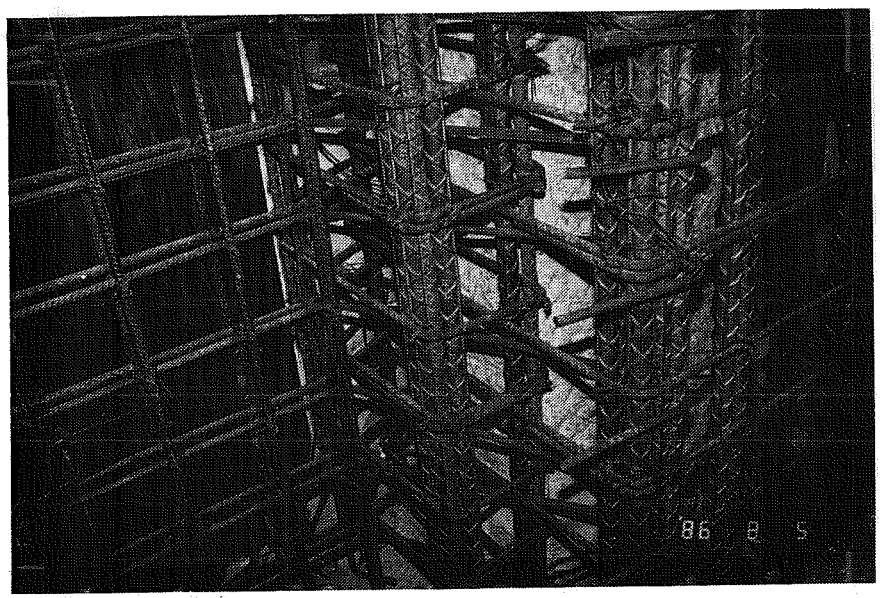

Figure 1.4 Column Jacketing Using Bundled Bars

facilitate construction. However, the use of bundles might affect the structure's performance since bond along the bars could be damaged during large load reversals. Distributed reinforcement around the column was also used in many cases (Figure 1.5). There is no

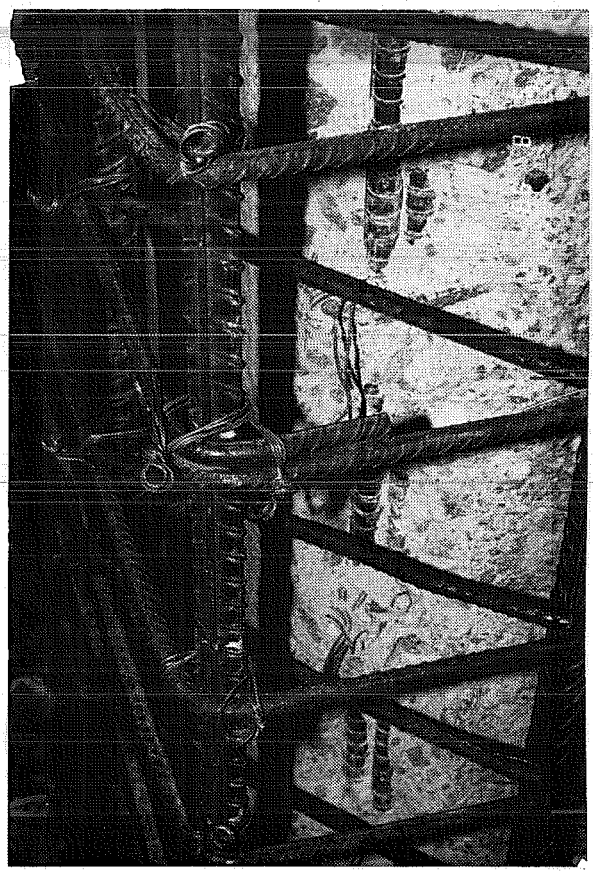

Figure 1.5 Column Jacketing Using Distributed Reinforcement

experimental evidence regarding the comparative performance of bundles versus distributed reinforcement in jacketed frame columns subjected to earthquake loads.

1.3 OBJECTIVES AND SCOPE

Little experimental work has been conducted to verify the performance of concrete jacketing of frame elements and its suitability as a rehabilitation technique. Designers of this scheme have faced the dilemma of analyzing and designing rehabilitated structures without guidelines. An experimental program was developed at the University of Texas at Austin to evaluate the effectiveness of jacketing of frame elements. Four reinforced concrete large-scale frame connections with flexible columns were tested after being repaired or strengthened by jacketing only columns, or both columns and beams. The subassemblages represented an existing structure designed according to Mexican and American practices typical of 1950's construction with non-ductile detailing. The specimen condition prior to rehabilitation and the layout of the column longitudinal reinforcement were also varied. The subassemblages were tested to large deformation levels applying a bidirectional cyclic loading history. The program was part of the coordinated research effort

between Mexican and American engineers implemented after the 1985 Mexico earthquake, and sponsored by the National Science Foundation (USA) and Consejo Nacional de Ciencia y Tecnologia (Mexico).

The objectives of this study are to investigate the following:

1) The effect of jacketing on the hysteretic response of the subassemblages, especially in regard to stiffness degradation and energy dissipation.
2) The mechanism of joint shear resistance in rehabilitated connections and the use of structural steel for joint confinement.
3) The effect of a damaged core on the response.
4) The influence of the layout of the column longitudinal steel, in particular with respect to bond along bundled or distributed bars.
5) The slab participation in the positive and negative moment capacities of the floor system.
6) The composite behavior of the jacketed members.
7) The constructability of a jacketing scheme.

1.4 ORGANIZATION

The study is divided into seven chapters. Chapter II describes the fabrication, loading program and instrumentation of the specimens. In Chapter III, the general behavior of the structures is presented, and the response envelopes and story shear behavior compared. In Chapter IV, the internal behavior of the subassemblages is assessed through the examination of strain gauge data. In Chapter V, an analysis of test results is presented. An evaluation of the joint shear strength and slab participation to beam bending capacity is included. The construction and design considerations are discussed in Chapter VI. Chapter VII contains a summary of the test results, and the conclusions.

CHAPTER II -- EXPERIMENTAL PROGRAM

2.1 INTRODUCTION

Four large-scale identical reinforced concrete frame connections were constructed and rehabilitated by jacketing the columns only, or both the columns and beams. The specimens represented an interior joint of a lower story of a multistory building and were subjected to a severe bidirectional cyclic load history. In each test, the existing structure was the same and was designed according to American and Mexican design practices of the 1950's. The first specimen was tested to failure (test **O**, i.e. **O**riginal connection), repaired by jacketing the column with bundled longitudinal reinforcement, and retested (test **RB**, i.e. **R**epaired with **B**undled bars). The second specimen was undamaged prior to jacketing to permit a comparison of the effect of a damaged core on the response (test **SB**, i.e. **S**trengthened with **B**undles). To compare the influence of bundles, the columns of the third model were jacketed with the longitudinal reinforcement distributed around the perimeter (test **SD**, i.e. **S**trengthened with **D**istributed reinforcement). In the fourth specimen, the column was jacketed using distributed bars, and the beams were jacketed and longitudinal steel added to increase the flexural capacity moderately (test **SD-B**, i.e. **S**trengthened with **D**istributed reinforcement and jacketed **B**eams). The experimental program is summarized in Table 2.1.

Table 2.1 Summary of Experimental Program

Test	Specimen Before Test	Jacketing		Bundled Column Bars
		Columns	Beams	
O	Undamaged	-	-	-
RB	Damaged	*		*
SB	Undamaged	*		*
SD	Undamaged	*		
SD-B	Undamaged	*	*	

2.2 SPECIMEN DETAILS

The dimensions of the specimens are shown in Figure 2.1. All specimens consisted of orthogonal beams 17 ft. long framing into a column 13.9 ft. high at midheight. The existing structure had beams with 8 by 20 in. section and a square column with 12 in. sides.

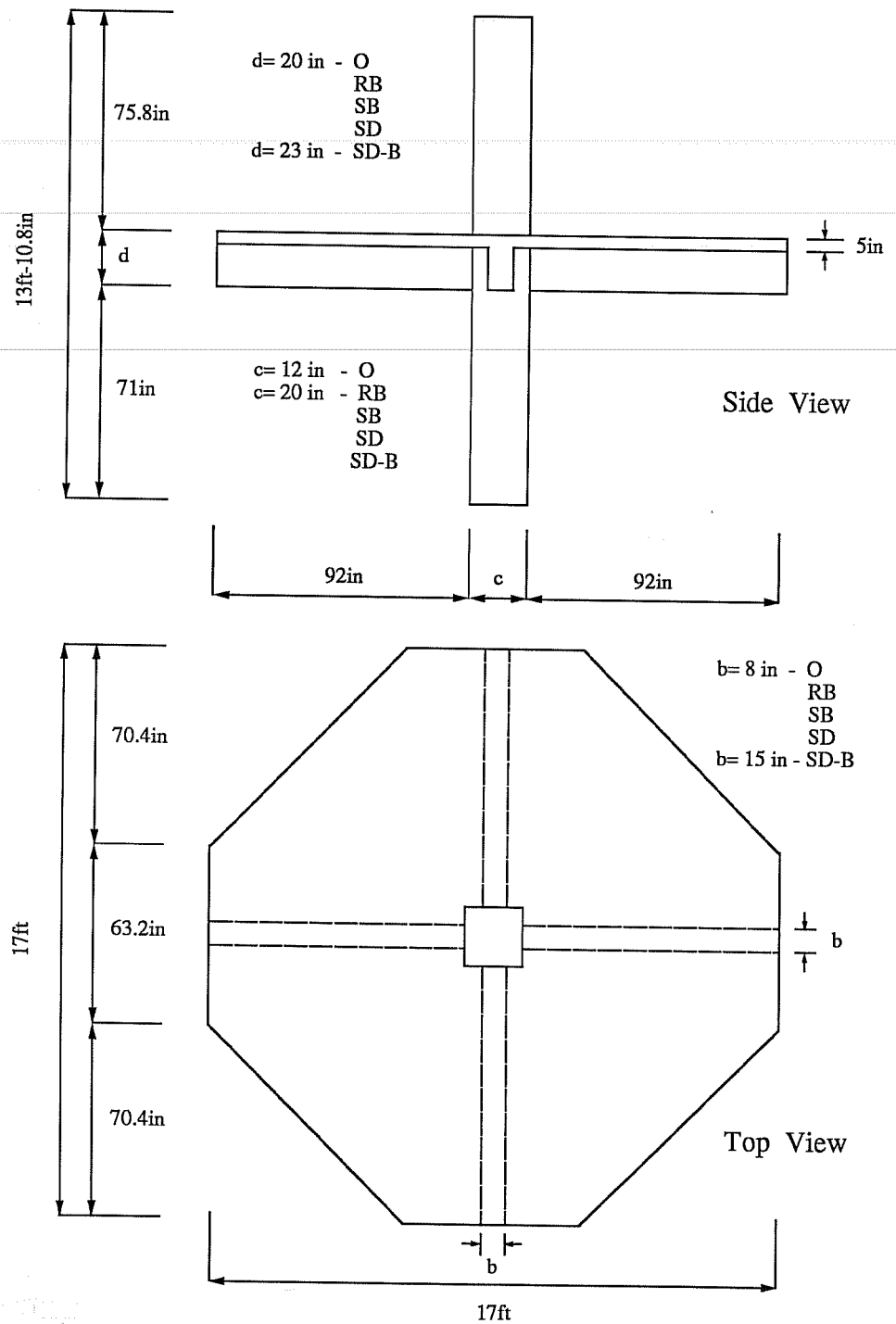

Figure 2.1 Specimen Dimensions

In all rehabilitated specimens, the column jacket was 4 in. thick so that the column section increased to 20 in. sides. For specimen SD-B, the beam jacket increased the section to 15 by 23 in.. Beam span and lower column height shown in Figure 2.1 correspond to specimens RB, SB and SD. A slab of 5 in. thickness was used in all tests. Slab corners were removed to permit transportation through the laboratory. Specimens with similar geometry have been tested in other programs at The University of Texas at Austin (Refs. 21, 29). Beam and column dimensions corresponded to a full-scale structure designed according to Mexican practice (Ref. 18). Although reinforcement detailing was that of American design practice, beam and column dimensions corresponded to a 2/3 scale model since larger clear cover than in Mexican practice is used (Refs. 2, 3).

Concrete in the existing structure was assumed to have a design compressive strength of 3500 psi., whereas the design strength for the concrete jackets was 4000 psi.. The compressive strength of concrete cylinders at 28 days and at the time of the test, as well as the age at testing, are presented in Table 2.2.

Table 2.2 Uniaxial Compressive Strength of Concrete Cylinders

Structural Element	Test				
	O	RB	SB	SD	SD-B
Original Specimen					
Lower column, beams, slab	2270[a] (2340)[b] [55][c]	2270 (2340) [143]	3660 (3960) [86]	2550 (2730) [90]	2540 (2670) [120]
Upper column	2460 (2460) [28]	2460 (2680) [116]	N/A (3300) [65]	2610 (2700) [64]	2440 (2660) [112]
Jacket					
Lower column, and beams in SD-B	-	4850 (5110) [44]	5140 (5750) [49]	5500 (5500) [33]	5350 (5830) [42]
Upper Column	-	4440 (4630) [32]	5780 (5870) [44]	6000 (6000) [27]	5390 (5390) [28]

[a] 28-day compressive strength, psi.
[b] ( ): compressive strength at time of test, psi.
[c] [ ]: age at testing, days.

ASTM A615 Grade 60 steel was used for all reinforcing bars. ASTM A36 structural steel was used in the joint confinement cage described later. Steel tensile properties are presented in Tables 2.3 and 2.4. Specimen details and reinforcement ratios, based on gross concrete areas are given in Table 2.5.

Table 2.3 Reinforcing Steel Properties

Bar Size #	Test	f_y [ksi]	ϵ_y [%]	f_u [ksi]
3	O, RB	67.3	0.23	110.3
3	SB, SD, SD-B	65.5	0.23	106.9
4	SD-B	61.2	0.21	103.4
5	SD-B	61.6	0.21	105.1
6	All	62.2	0.21	107.0
7	All	64.4	0.22	91.4
9	RB, SB, SD	62.3	0.21	108.8
10	SD-B	62.5	0.22	102.5

Table 2.4 Structural Steel Properties

Cage Component	Test	f_y [ksi]	ϵ_y [%]	f_u [ksi]
Angle	RB	44.3	0.15	68.0
	SB, SD	41.9	0.14	66.7
	SD-B	42.8	0.15	68.0
Flat Bar	RB, SB	42.8	0.15	64.8
	SD, SD-B	43.0	0.15	66.0

Table 2.5 Specimen Details

Test	Beam Reinforcement			Column Reinforcement		Slab Reinforcement	
	Longitudinal		Transverse	Longitudinal	Transverse	Top	Bottom
	Top	Bottom					
O	4#7 (1.5%)	4#7 (1.5%)	#3 @ 5 in.	8#6 (2.4%)	2-#3 @ 6 in.	#3 @ 12 in. (0.2%)	#3 @ 24 in. (0.1%)
RB[a]	4#7 (1.5%)	4#7 (1.5%)	#3 @ 5 in.	8#6 12#9 (3.9%)[c]	2-#3 @ 6 in. #4 @ 3 in.	#3 @ 12 in. (0.2%)	#3 @ 24 in. (0.1%)
SB[a]	4#7 (1.5%)	4#7 (1.5%)	#3 @ 5 in.	8#6 12#9 (3.9%)[c]	2-#3 @ 6 in. #4 @ 3 in.	#3 @ 12 in. (0.2%)	#3 @ 24 in. (0.1%)
SD[b]	4#7 (1.5%)	4#7 (1.5%)	#3 @ 5 in.	8#6 12#9 (3.9%)[c]	2-#3 @ 6 in. #4 @ 3 in. #3 @ 3 in.[d]	#3 @ 12 in. (0.2%)	#3 @ 24 in. (0.1%)
SD-B[b]	4#7 2#5 (0.9%)[c]	4#7 2#4 (0.8%)[c]	#3 @ 5 in. #3 @ 4 in.	8#6 12#10 (4.7%)[c]	2-#3 @ 6 in. #4 @ 3 in. #3 @ 3 in.[d]	#3 @ 12 in. (0.2%)	#3 @ 24 in. (0.1%)

[a] Column jacket - bundled bars.
[b] Column jacket - distributed reinforcement.
[c] Steel ratio includes original and jacket reinforcement.
[d] Corner ties.

The existing structure was designed according to Mexican and American practices of the 1950's. The characteristics typical of buildings from that period include flexible columns, non-ductile detailing, and "strong beam - weak column" systems (Ref. 9). Many buildings that collapsed during the 1985 Mexico earthquake had such features (Refs. 24, 43). In the existing structure, beam reinforcement was provided so that the jacketed column would be subjected to large shear forces in the joint. Top and bottom beam reinforcement was continuous through the joint. To preclude a shear failure in the beams during testing, closed stirrups were provided to meet the requirements of Refs. 2 and 3. The flexural capacity of the beams was greater than that of the columns. The spacing of the column transverse steel was half of the spacing required by Ref. 1. It is important to note that transverse steel was not provided in the joint. This did not meet the requirements of ACI 318-83 (nor ACI 318-89) but was more representative of 1950's construction in which there were no ties in the joint. Reinforcement details of the original specimen are shown in Figure 2.2. The column and beams had 1 in. clear cover.

Rehabilitated specimens were designed so that the flexural strength of the column was greater than that of the beams. However, the joint shear forces were still large. When the column dimensions were increased to improve flexural capacity, joint shear strength increased since it was directly proportional to the column area. To produce forces on the joint at levels near the shear strength, large beam moments must be developed, and to maintain a column strength greater than beam strength, a high column steel ratio is necessary. Large joint shear forces and high column steel ratios should be avoided in practice because of performance and construction reasons, but had to be considered in this case for the joint to be stressed severely.

Details of the reinforcement for specimens RB and SB are illustrated in Figure 2.3. The column jacket was reinforced with three continuous bundled bars placed at the corners through perforations in the slab. Transverse steel was provided following the recommendations of Refs. 2 and 3, and consisted of two L-shaped ties that overlapped in diagonally opposite corners. Transverse steel was placed above and below the joint region. It is important to note that the tie hooks required a special bend detail because bundled bars were placed in the corner. After the 90-deg bend, a small straight segment was provided before the 135-deg hook bend, to accommodate two column bars. The hook specified could not be bent by the steel fabricator because the extension was too small. The hooks were bent in the laboratory.

Specimens SD and SD-B had distributed column longitudinal steel around the perimeter as shown in Figures 2.4 and 2.5. One bar was located in the corner and the other two were placed against the existing beams faces. Main transverse steel was similar to that of RB and SB, but additional corner ties were placed between bars away from the corners. Corner ties with 180-deg hooks extended into the joint region. Corner ties with 90-deg and 135-deg hooks were positioned 2 ft. above the slab and below the beams following ACI requirements. Beams of specimen SD-B were also jacketed. Reinforcement was added to increase beam flexural capacity moderately and to produce high shear stresses in the joint.

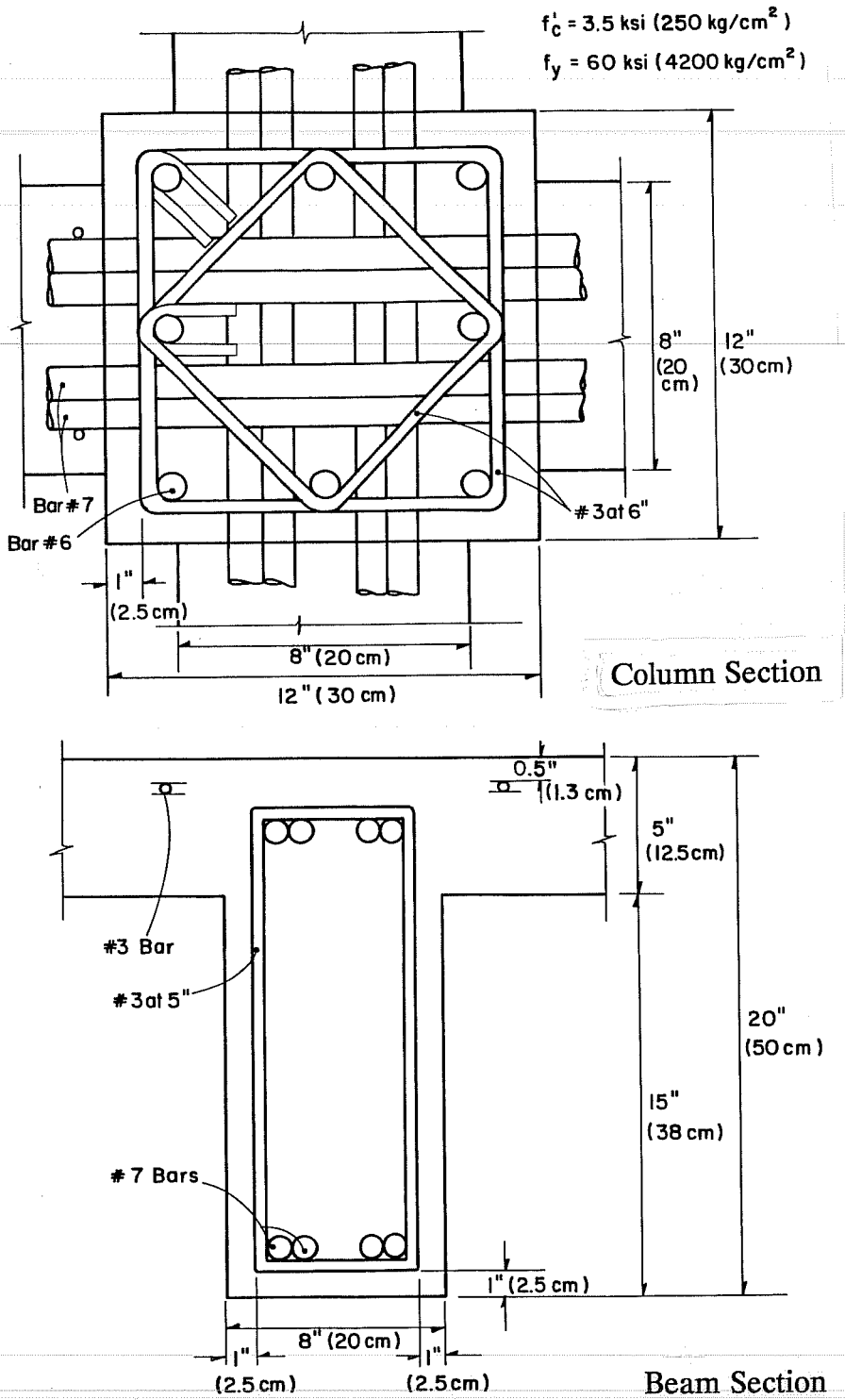

Figure 2.2 Original Specimen - Reinforcement Details

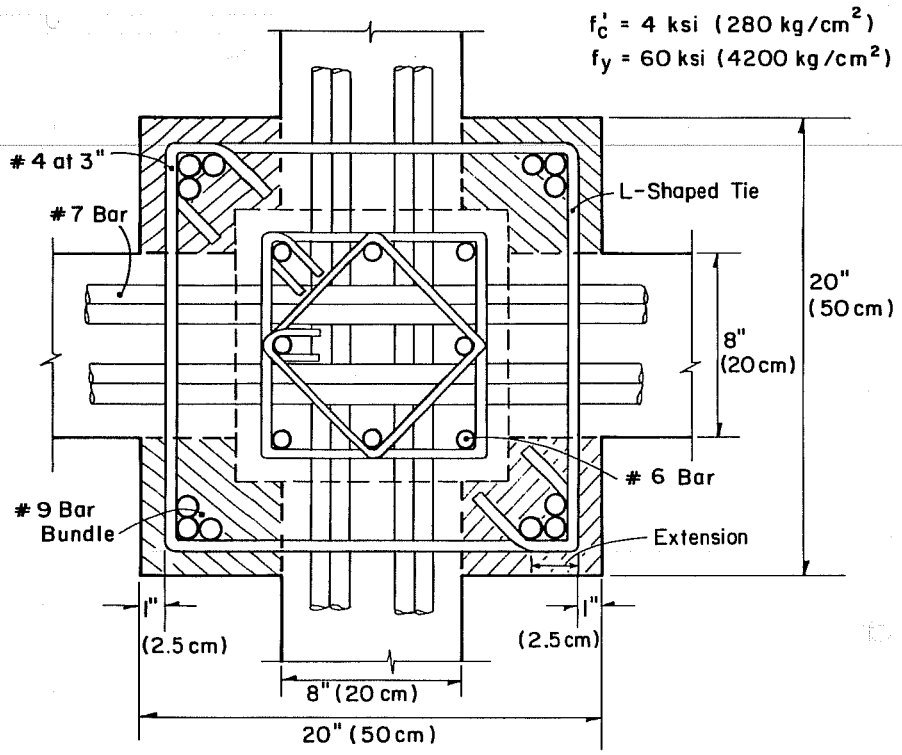

Figure 2.3 Specimens RB and SB - Reinforcement Details

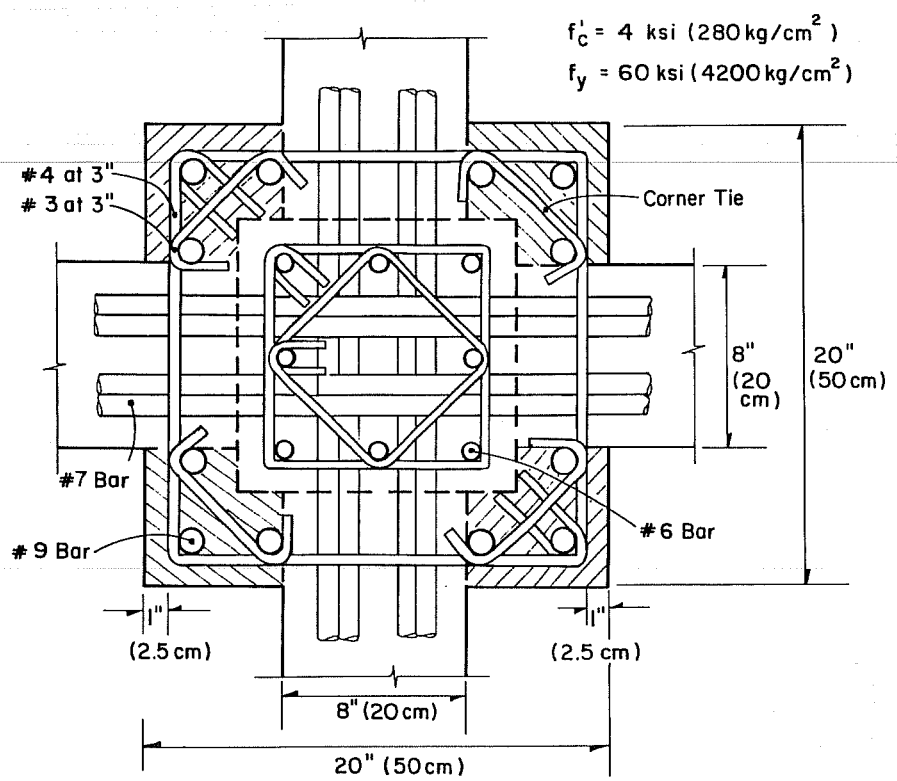

Figure 2.4 Specimen SD - Reinforcement Details

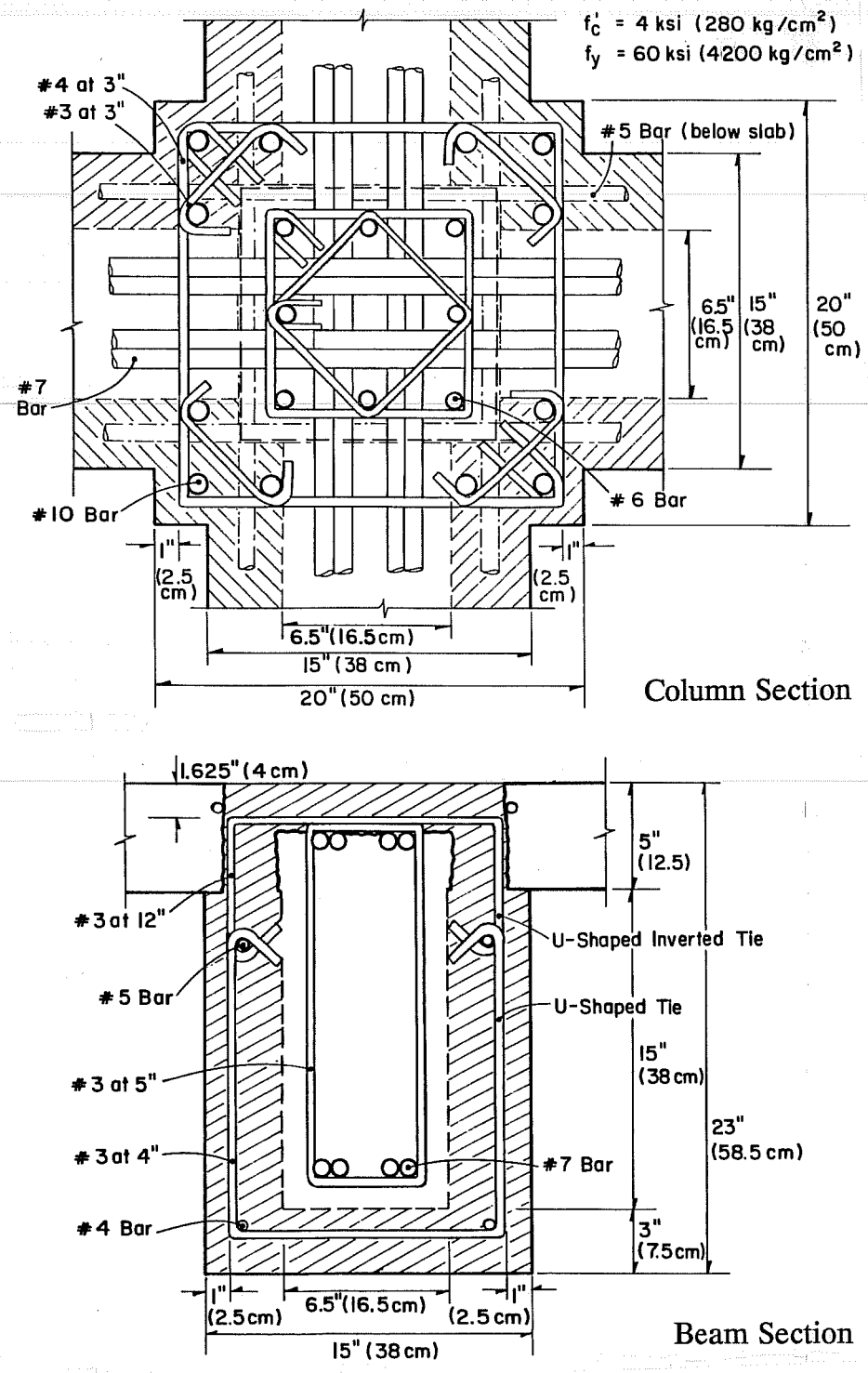

Figure 2.5 Specimen SD-B - Reinforcement Details.

Top bars crossed the orthogonal beams through holes, and bottom bars were placed under the soffit of the existing beams, at each side of the existing column. Beam transverse steel consisted of sets of U-shaped ties fixed to the top jacket bars, and of inverted U-shaped ties placed through perforations in the slab. Closely spaced ties were placed near the joint region, where beam hinging was expected to occur. Away from the joint, the ties were spaced at 12 in., with two U-shaped ties fixed to the top jacket bars between the sets. U-shaped ties had 135-deg hooks. The jacketed beams and jacketed columns for all specimens had 1 in. clear cover.

To confine the joint concrete not confined by transverse beams, and to confine the column bars, a structural steel cage was welded around the joint for all rehabilitated specimens, as illustrated in Figure 2.6. The cage consisted of structural steel angles and flat steel bars welded in situ. A36 steel was used. The cage eliminated the need for ties and the need to drill holes through the beams for placing the ties. Steel angles were dimensioned to provide confinement to the core equivalent to spiral reinforcement. An efficiency factor of 1/3 relative to the confinement of spirals was assumed in design.

Slab reinforcement (Figure 2.7) consisted of a top and a bottom layer of continuous #3 bars. Top reinforcement was spaced at 12 in., and the bottom steel at 24 in.. The closest slab bars to the column for both layers were placed at a section that would later correspond to the face of the jacketed column. Top and bottom reinforcement ratios were 0.2% and 0.1%, respectively. Slab reinforcement had a half-inch cover.

2.3 SPECIMEN FABRICATION

2.3.1 Existing Structures. The existing structures were built on a shored wooden platform. Wooden forms were protected with lacquer and the gaps were closed with tape to prevent bleeding of the concrete that would occur during casting. Prior to assembling the reinforcing cages, steel bars were instrumented with strain gauges. A column cage was constructed and moved to the formwork platform into a position that allowed beam cages to be assembled. Beam cages were fabricated over the column cage (Figure 2.8), and the entire assembly was lowered into the platform. Slab reinforcement was assembled and held in place by slab bolsters (Figure 2.9).

Casting of the specimen was done in two stages. The lower column, beams, joint and slab were cast first. The upper column was cast a few days later after the specimen was located in the test setup on the reaction floor. A construction joint was made across the column section several inches above the slab. Ready-mix concrete, with 3/8 in. maximum size coarse aggregate, was used throughout. Concrete was placed with an overhead crane and a bucket. Consolidation of concrete was achieved with portable electric vibrators. Specimens and concrete cylinders were cured in the laboratory and no special curing provisions were taken.

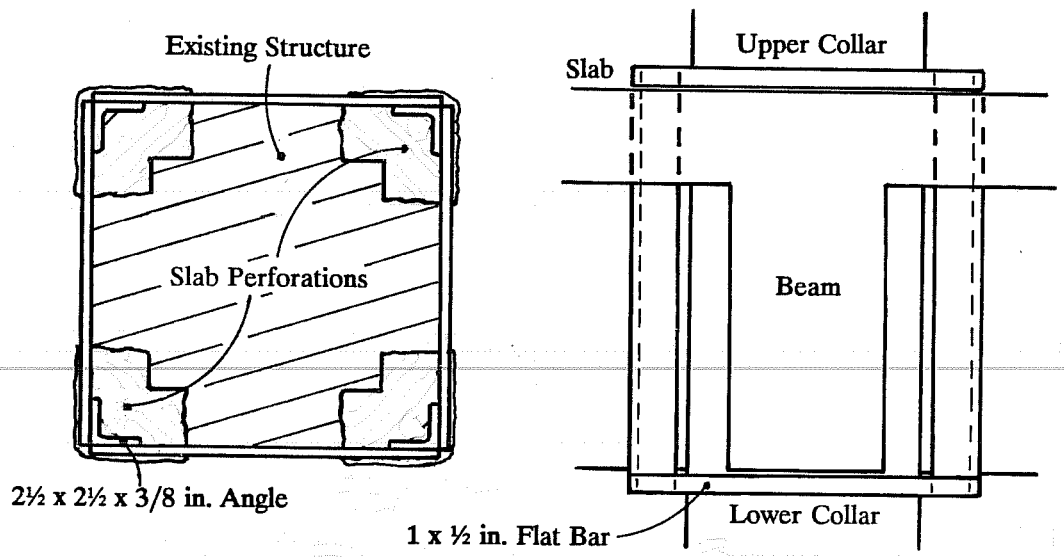

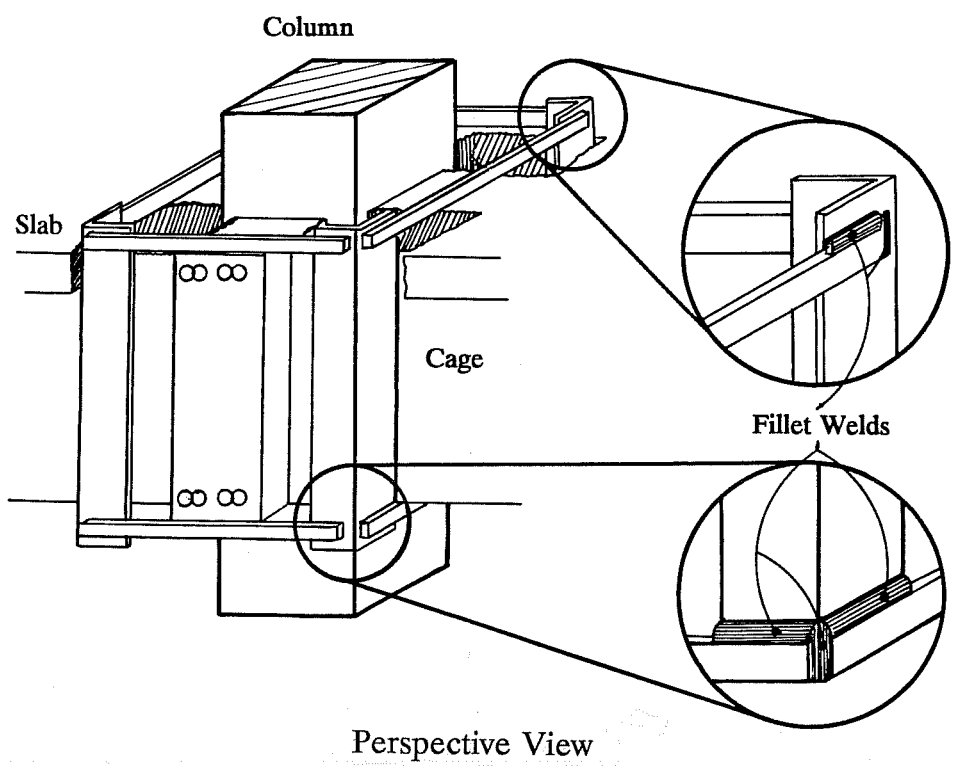

Figure 2.6 Joint Confinement Cage

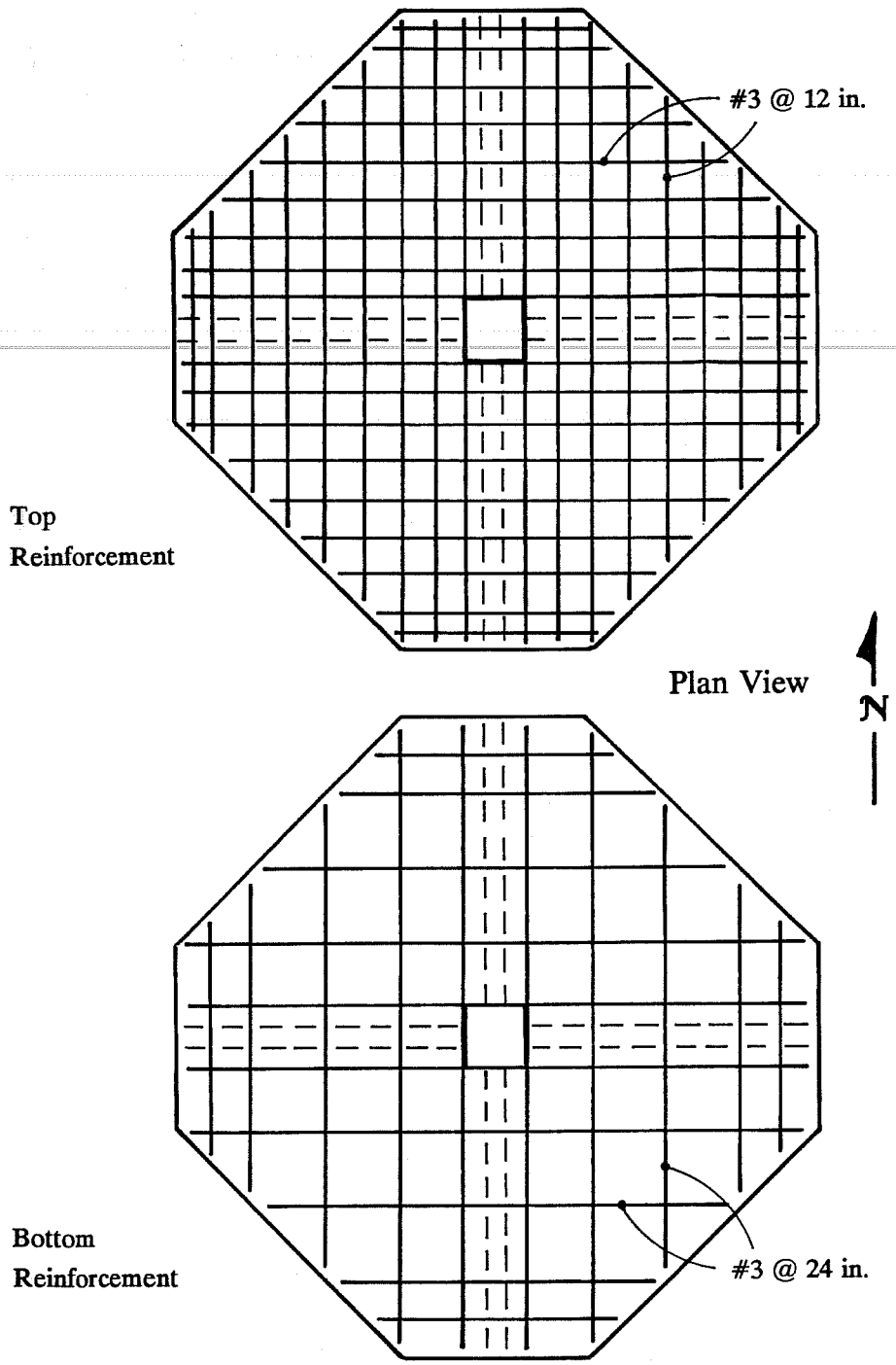

Figure 2.7 Slab Reinforcement

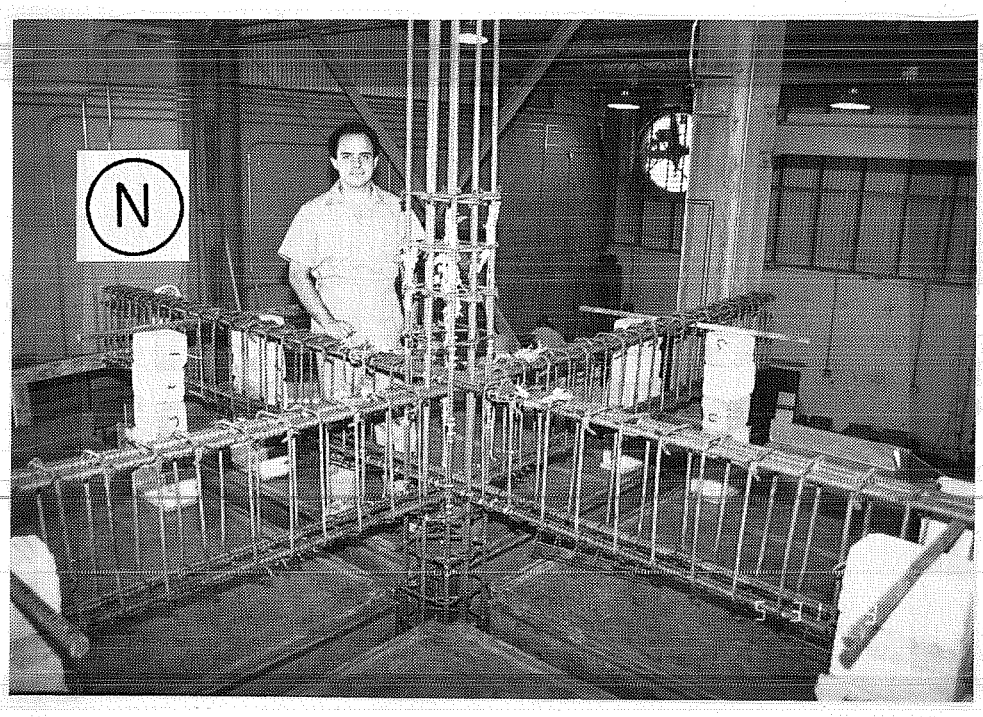

Figure 2.8 Original Specimen - Steel Cage

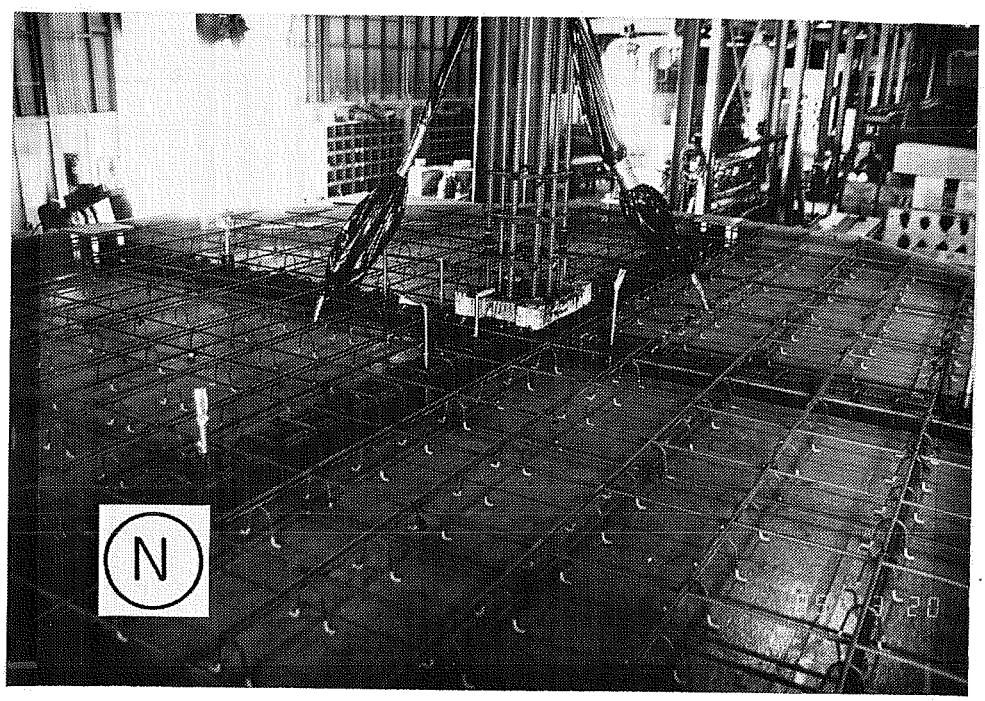

Figure 2.9 Original Specimen - Before Casting

2.3.2 Rehabilitated Specimens

2.3.2.1 Column Jacket Reinforcement. The column jacket was constructed in a similar fashion for all specimens. The only difference was specimen RB which required the removal of loose concrete (from test O) and the replacement of some malfunctioning strain gauges. The specimen was loaded to zero deflection at beam ends before the rehabilitation process started. The beams and slab were not modified or repaired. Spalled concrete in the bottom of the beams next to the jacketed column was replaced using mortar (Ref. 33).

Perforations through the slab along the beam sides were made with an electric jackhammer. The hole size was limited by the first slab bar that was placed intentionally at the face of the jacketed column; however, the hole was made as large as possible to facilitate placement of the concrete.

To improve bond conditions between the existing concrete and the concrete of the jacket, column surfaces were roughened. Exposure of the outermost aggregate was done with hand chipping hammers. To remove small particles and dust, column surfaces were brushed with a thick brush and vacuum cleaned.

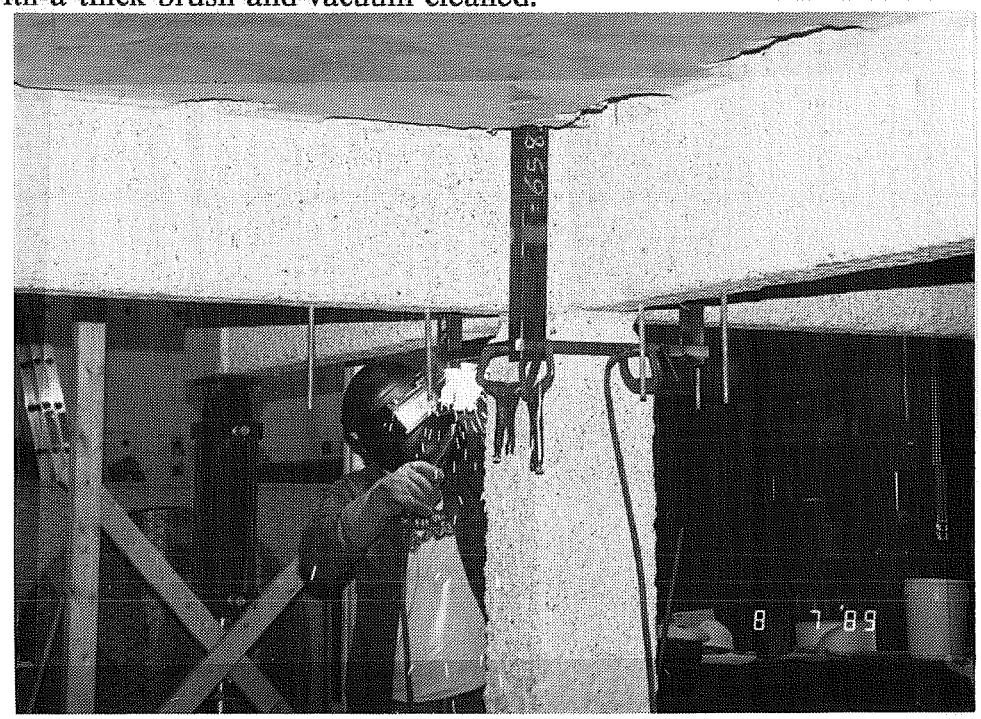

Figure 2.10 Jacketed Specimens - Assemblage of Joint Confinement Cage

Afterward, the joint confinement cage was assembled as shown in Figure 2.10. The upper collar and the steel angles were fillet-welded in the shop. The cage was then inserted into the slab perforations and leveled. Finally, the flat bars from the lower collar were welded in situ to the steel angles.

The L-shaped ties, for the jacket transverse steel, were stacked at the base of the lower column, alternating the diagonal of overlapping corners at each layer. The ties for an entire column were aligned vertically with the joint cage as shown in Figure 2.11. Next, jacket longitudinal reinforcement was lowered through the slab perforations, and the ties were lifted to position and securely tied. For specimens SD and SD-B, the additional corner ties were placed in the joint region and below the beams before lowering the jacket bars. The column jacket cage of specimen SD is shown in Figure 2.12. For specimens RB and SB, securing the transverse steel required some laborious work because the bar ties were not long enough to be wrapped around the bundle. The bar tie had to be passed between the corner bar and one of the adjacent bars, and was wrapped around two column bars and the transverse steel. In specimens SD and SD-B, this problem was not encountered. However, the placement and fastening of the joint corner ties involved laborious detailing.

2.3.2.2 Beam Jacket Reinforcement. Beams in specimen SD-B were also jacketed. The beams were 1.5 in. narrower in this case to reduce the amount of concrete removed during the rehabilitation process. Nevertheless, it was necessary to roughen all beam surfaces along the length, i.e. sides and bottom, in the same manner as column surfaces. The reduction in beam width also decreased the steel congestion of the jacket reinforcement of beams and column around the joint.

The slab was perforated in an alternate pattern along the edge of the beams as shown in Figures 2.13 and 2.14. Perforations were initiated with a series of holes along the boundaries of each perforation. To reduce concrete spalling from the slab lower surface, a piece of lumber was shored against the slab while the holes were drilled. The perforations were completed with an electric jackhammer. A transverse groove was cut into the beam top cover to place the inverted U-shaped ties in the beam. Concrete was placed and consolidated through the slab perforations. The time required for surface preparation and slab perforations for specimen SD-B was nine times that required for surface preparation for the specimens with jacketed columns only.

The final reinforcement cage of specimen SD-B is shown in Figure 2.15. Top reinforcement (2-#5 bars) in the beam jacket, passed through orthogonal beams in 1.25-inch diameter holes which were drilled several inches below the slab. Bottom reinforcement was placed in horizontal grooves in the existing column. The reinforcement for the column jacket was assembled first. Next, the inverted U-shaped ties were placed through the transverse slab grooves (Figure 2.16). The U-shaped ties were placed in groups of three along the beams as high as possible. Because the beam width was somewhat larger than the distance between hook extensions of the U-shaped ties, the hooks bore against the beam faces so that the ties hung due to friction. Afterward, the top bars were inserted, and the U-shaped ties were lowered to the final position and secured. Finally, the bottom bars (2-#4) were placed and secured.

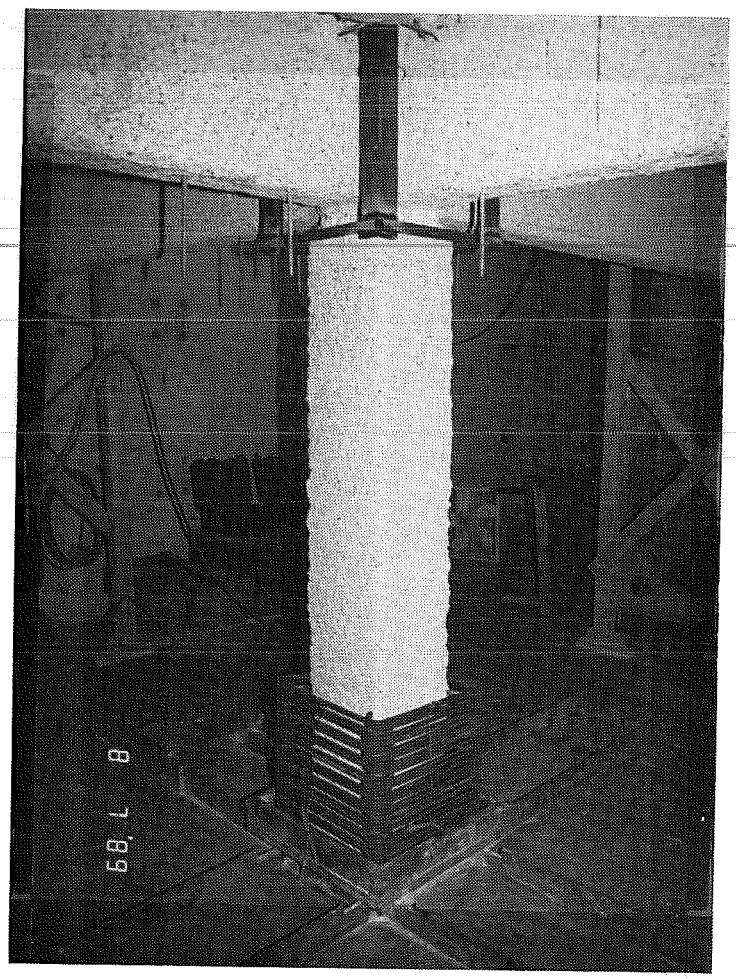

Figure 2.11 Jacketed Specimens - Column Transverse Steel

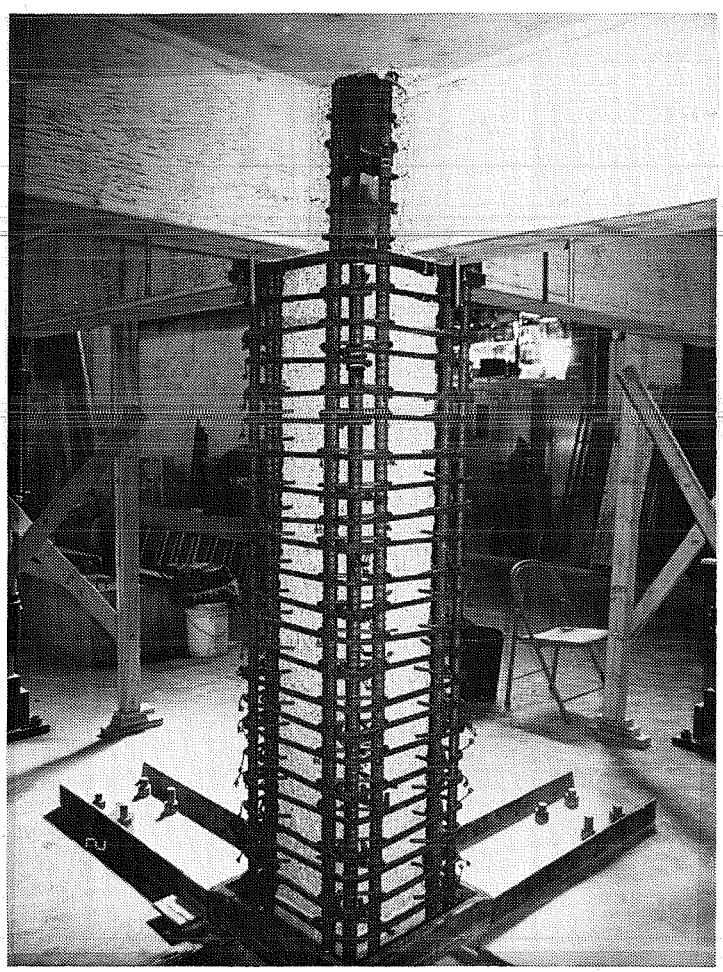

Figure 2.12 Jacketed Specimens - Column Cage

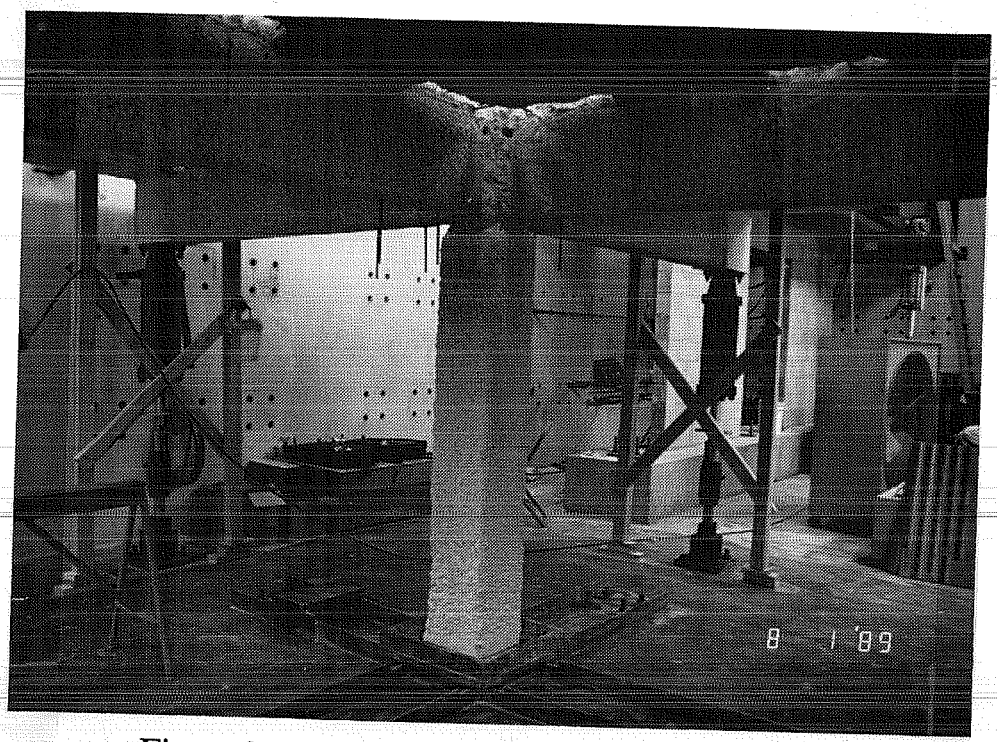

Figure 2.13 Specimen SD-B - Surface Preparation

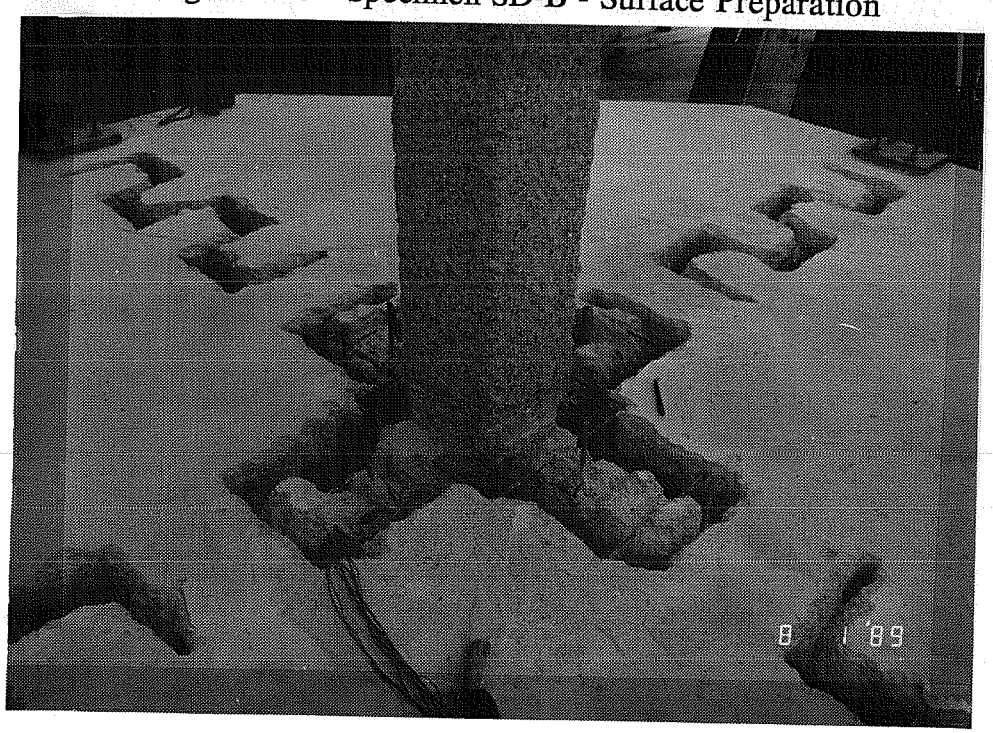

Figure 2.14 Specimen SD-B - Slab Perforations

Figure 2.15 Specimen SD-B - Reinforcement Cage

Figure 2.16 Specimen SD-B - Assemblage of Beam Jacket

2.3.2.3 Formwork and Concrete Placement. Formwork for the new concrete jackets was designed and constructed with large tolerances to match easily the contour of the existing frame elements and to eliminate laborious detailing. Gaps between the forms and the original structure were partially sealed to allow air release during casting. Open gaps were closed during casting with wooden shims. This was particularly the case of specimen SD-B in which long gaps were intentionally left between beam forms and the slab. In specimen RB, poor consolidation of the column jacket under the east and south beams, and under the slab in the northeast and northwest joint corners was noted. Cavities were dry-packed with mortar and did not appear to affect the overall response. Column forms were segmented to facilitate placement of instrumentation inserts. For specimen SD-B, as shown in Figure 2.17, the construction of large forms were needed for the beam jackets. Supporting frames were erected to shore up the forms. A gap, as mentioned above, was left to allow air to escape.

Casting of the column jackets was done in two stages. First, the lower column and the joint were cast (and the beams, for specimen SD-B); several days later, the upper column was cast. Prior to casting, the column surface for specimen RB was saturated. Other specimens were not saturated to avoid excessive free water at the time of casting which might have reduced the concrete strength. The sides of the slab perforations for specimen SD-B were saturated to reduce shrinkage cracking. Congestion in the joint region and high ambient temperatures at the time of casting, required the use of high-range water-reducing admixtures (superplasticizers) to provide the necessary workability without loss of strength. The mix was rich in sand. A 3/8 in. maximum size coarse aggregate was used.

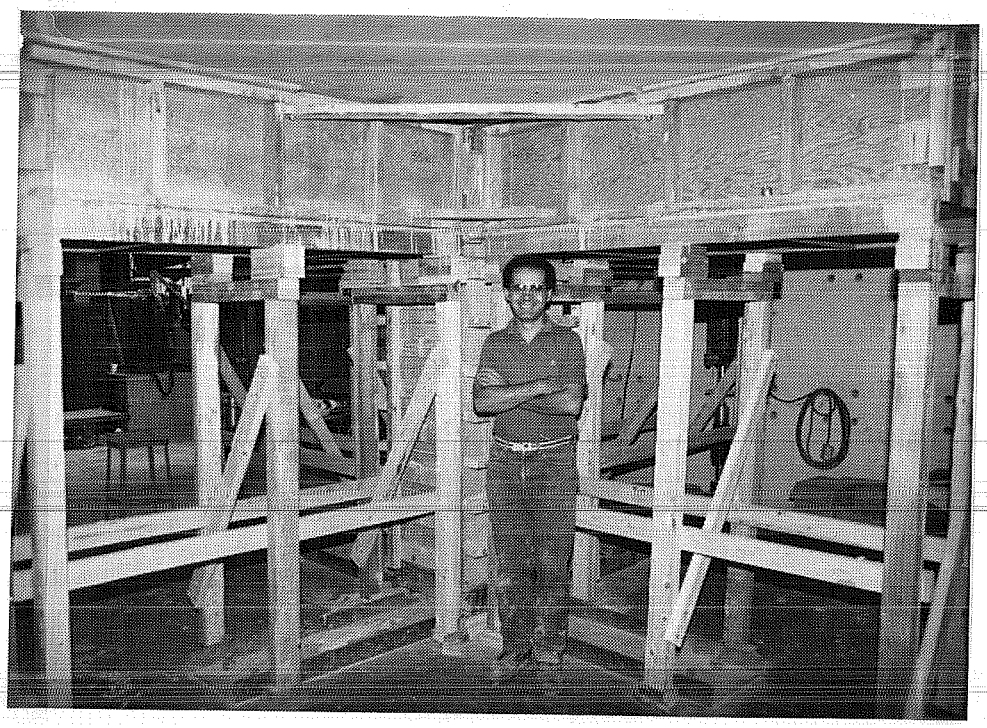

Figure 2.17 Specimen SD-B - Formwork Beam Jacket

Initial slump ranged from 1.25 to 3.5 in., but with the addition of superplasticizer, slump increased to 7.5 to 8.5 in.. The average dose of additive was 20 oz. per hundred pounds of cement. Concrete was placed through the slab perforations using an overhead crane and a bucket. Due to the congestion around the joint, portable electric vibrators were used for concrete consolidation. Concrete jackets and control cylinders were cured in the laboratory and no special curing provisions were taken, except for the beam jacket of specimen SD-B which was moisture-cured for seven days.

2.4 TEST SETUP

The test setup is shown in Figure 2.18. The specimens were mounted on a steel box that rested on an angular spherical bearing contact. The connection allowed rotation with respect to any horizontal axis but restrained lateral movements. Forces were transmitted to the reaction floor through a fixture of structural steel channels. Another steel box was fixed to the upper column and was connected to the reaction wall through structural steel tubes, orthogonally to the wall, and by high strength steel Dywidag bars. The top connection restricted the specimen from displacement in the east-west direction; however, it allowed a small movement in the north-south direction. The top connection was rotationally flexible, and is considered a pinned connection.

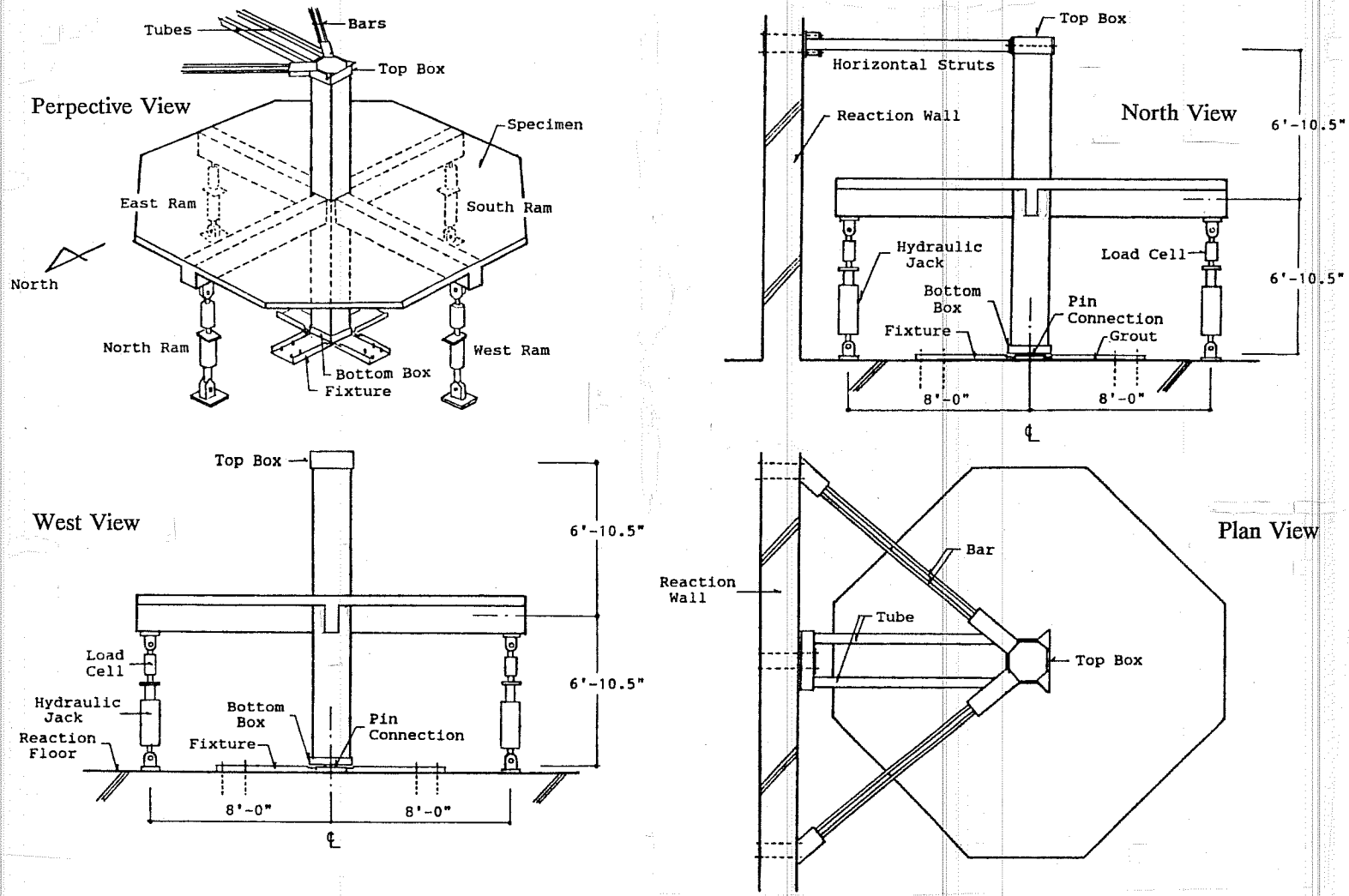

Figure 2.18 Test Setup

Beams were connected to the reaction floor through double-action hydraulic actuators capable of resisting tensile (downward loading) and compressional forces (upward loading). The test was controlled manually with hydraulic hand pumps connected to the rams.

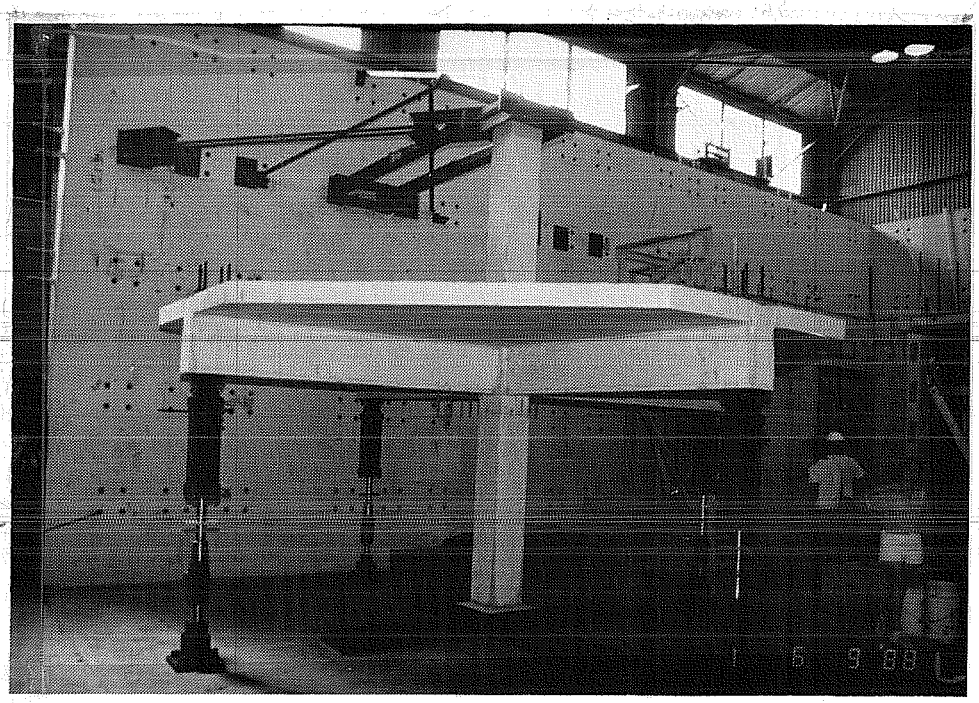

Figure 2.19 Specimen O in Test Setup

Specimens O and SD-B in the test setup are shown in Figures 2.19 and 2.20, respectively.

2.5 LOADING PROGRAM

Specimens were tested using the bidirectional cyclic load history shown in Figure 2.21. The same loading program was applied in the US-New Zealand-Japan-China Cooperative Project on Design of Reinforced Concrete Beam-Column Joints (Ref. 29), and in an experimental project to evaluate the influence of high strength materials in the behavior of joints conducted at The University of Texas at Austin (Ref. 21).

The load history was displacement controlled based on the interstory drift angle and represented a severe load condition for a beam-column joint. The interstory drift angle of a frame structure subjected to lateral loads, sometimes referred to as drift index, is defined by the ratio of the column relative displacement over the column height (Figure 2.22a). For practical and economical reasons, column ends often are pinned and lateral movement is restricted. Beams are pinned at the ends and displaced vertically. In this case the drift

Figure 2.20 Specimens SD-B in Test Setup

angle is defined as the ratio of beam tip displacements to the beam length (Figure 2.22b). The specimens represented an interior joint of a lower story of a building in which the columns would have been subjected to axial load. In this series of tests, no axial load was applied to the column because experimental evidence suggests that axial load has no effect in the joint shear strength (Ref. 29).

Four levels of deformation were applied. Cycles to 0.5% drift angle were applied to simulate loading in the serviceability range. Cycles to 2% drift angle represented what is normally considered the maximum deformation that a structure subjected to earthquake loads should withstand without endangering life safety. Cycles to a 4% drift angle may be considered excessive, but provided interesting and essential information on the behavior of joints under large deformations.

Cycles 1, 2, 3, 5, 6, 9 and 10 were applied in the primary (E-W) direction only. Unidirectional loading in the north-south direction occurred in cycle 4. During cycles 7, 8, 11 and 12 the subassemblage was loaded bidirectionally.

Due to the loading sequence, bidirectional loading occurred in diagonally opposite quadrants. Also, it described an asymmetric loading orbit for drift angles to 2% and 4%. During bidirectional cycles, the loading direction was alternated every quarter cycle. A cycle started with loading in the east-west direction to the specified deformation level. Maintaining the east-west drift angle, the specimen was displaced in the north-south direction. Unloading began in the east-west direction, returning the specimen to zero drift

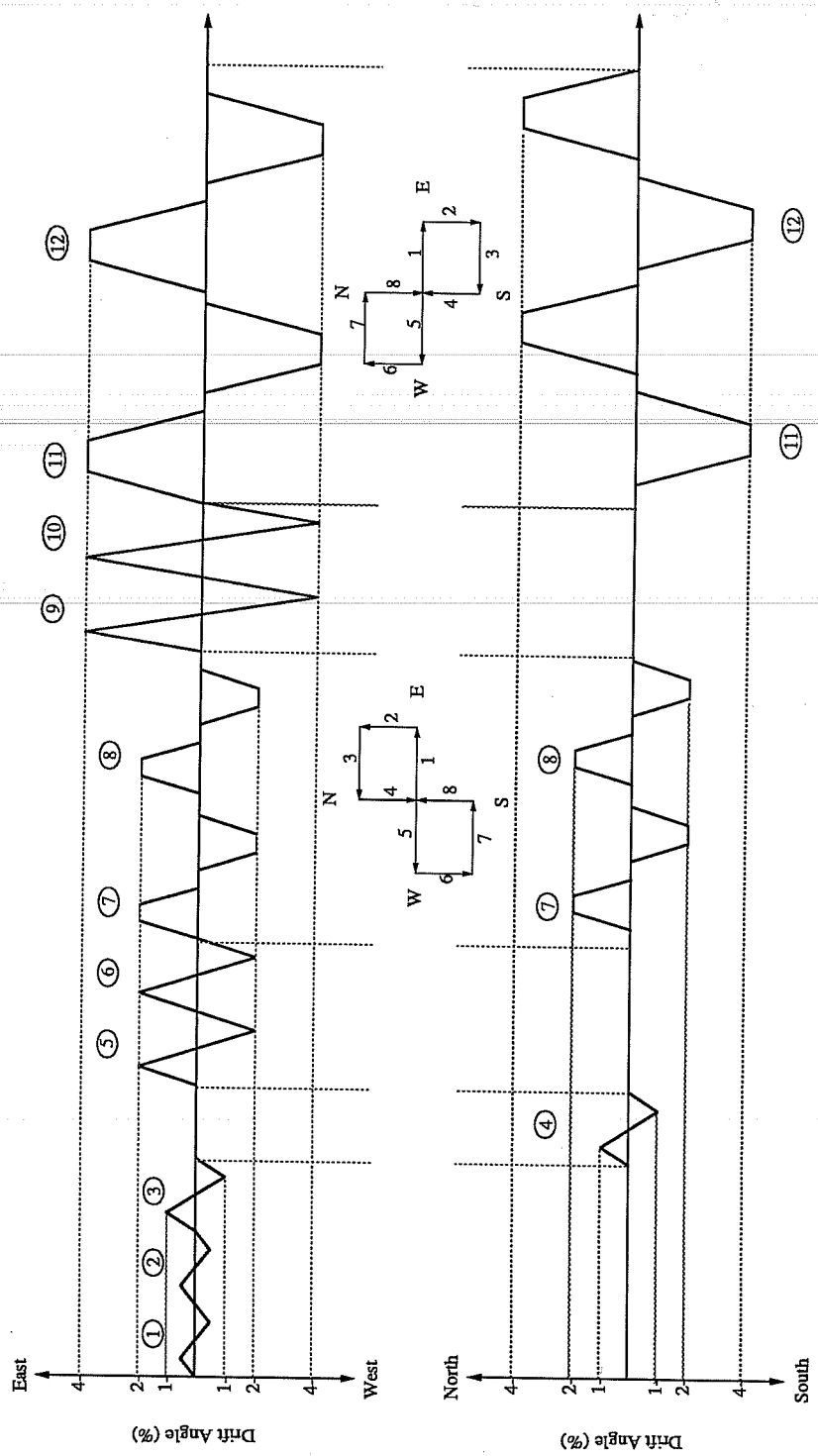

Figure 2.21 Loading History.

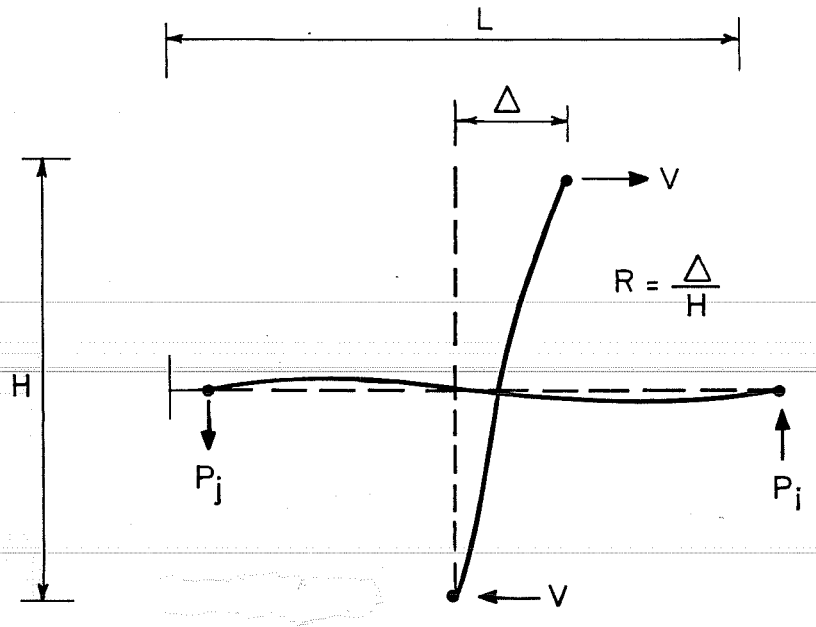

a) Joint in an Idealized Structure

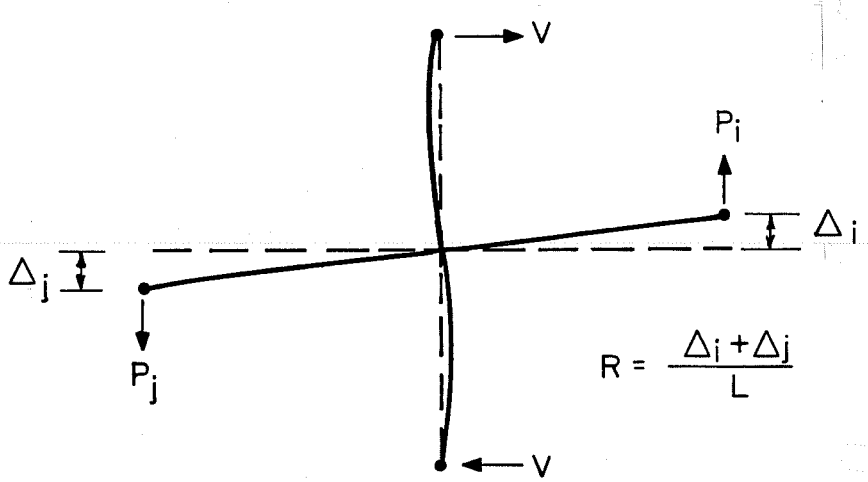

b) Joint in the Laboratory

Figure 2.22 Deflected Shape of Subassemblage

angle. Finally, deformation in the orthogonal direction was reduced to zero. The negative half- cycle was applied similarly. This loading sequence permitted observations of the behavior in two separate directions to be made, while also achieving biaxial effect.

During this study, a positive unidirectional half-cycle, will be defined as upward displacement of the east or the north beams. Consequently, the west beam and the south beam are displaced downwards. During bidirectional cycles, the half-cycle will have the sign of the east-west direction as defined before. Cycles will be denoted, for example, as "cycle 3/pos" or "cycle 11/neg".

2.6 INSTRUMENTATION

2.6.1 Measuring Devices. Specimens were instrumented to obtain as much information as possible regarding the overall response and the load transfer mechanism across the joint. Three types of measuring devices were used: load cells, linear potentiometers and strain gauges.

Loads applied at beam tips were measured with load cells mounted in series with the hydraulic actuators. Beam tip displacements were monitored by 12-in. linear potentiometers. These measurements allowed the calculation of story shear and drift angle. Story shear V and drift angle R are given by (see Figure 2.22)

$$V = (P_i + P_j)\frac{L}{2H} \tag{2.1}$$

$$R = \frac{(\Delta_i + \Delta_j)}{L} \tag{2.2}$$

where $P_{i,j}$ = beam tip loads
L = beam length
H = column height
$\Delta_{i,j}$ = beam tip displacements.

Rigid body motion was measured with two-inch potentiometers located atop the upper column and in the lower steel box. Although the rigid body motion contribution was negligible for the east-west direction, it accounted for up to 12.5% in the north-south direction due to the flexibility of the diagonal Dywidag bars. The measured N-S drift angle was corrected by eliminating the small column lateral movement.

To better understand the behavior of the specimens and help determine the mode of failure, it is useful to obtain the contribution of the different frame elements, namely, beams, columns and joint, to the total deformation and energy dissipation capacity. The instrumentation used to determine the joint shear distortion is shown in Figure 2.23. From these measurements, and assuming the deformation pattern for the specimens shown in Figure 3.1 (Chapter III), it is possible to obtain mathematical expressions for the contributions. Interstory drift and energy dissipation contributions will be discussed in greater detail in Chapters III and V. It is believed that at large drift levels, the inserts of the joint distortion instrumentation impeded the joint cracks from closing thus affecting the readings. This phenomenon occurred in all tests and was observed in other programs with similar instrumentation (Refs. 21, 29). Results are plotted up to the cycle in which instrumentation became unreliable.

Instrumentation used for beam rotations and column rotations is shown in Figure 2.24 and 2.25. Beam rotations were measured with linear potentiometers positioned 2 in. above the slab and below the beam soffit. Similarly, column rotations were measured with linear transducers mounted 2 in. from the column faces. The column and beam deformations included in the rotation measurements, as a result of the position of the potentiometers, were taken into account. In specimen O, since beam deformations were considerably smaller than column deformations, beam rotations were the most affected and therefore were corrected. Conversely, in the rehabilitated specimens, column rotations were corrected for the measured beam deformations. The linear potentiometers were positioned against small steel plates attached to the concrete surface. After several large loading cycles, typically at drifts to 4%, the concrete in the vicinity of the transducer mounting devices sometimes spalled and further measurements were unreliable. Average curvatures are presented up to cycles to 2% drift. Average beam and column curvatures were determined by dividing the measured relative rotation at one section by the length along the member over which they occurred.

Reinforcing steel in the beams, columns, slab and joint confinement cage was instrumented with strain gauges. The locations of the strain gauges in the original specimen, as well as in the beam and column jacketing, are shown in Figures 2.26 to 2.31. In specimen O, and consequently in RB, top beam bars were not instrumented at the W face of the original column, and at the E face of the existing column in bottom bars. Also, existing and jacketed column bars instrumented with five strain gauges were placed in the NW and SE corners and the bars with three gauges in the other corners. In specimen SB, two strain gauges of the beam reinforcement were mislabeled during instrumentation. The labels were exchanged during the analysis of the data and the gauges showed the expected behavior.

To assess the behavior of the joint confinement cage, strain gauges were positioned as illustrated in Figure 2.32. Similarly to column gauges, the NW and SE steel angles were instrumented only for specimen RB.

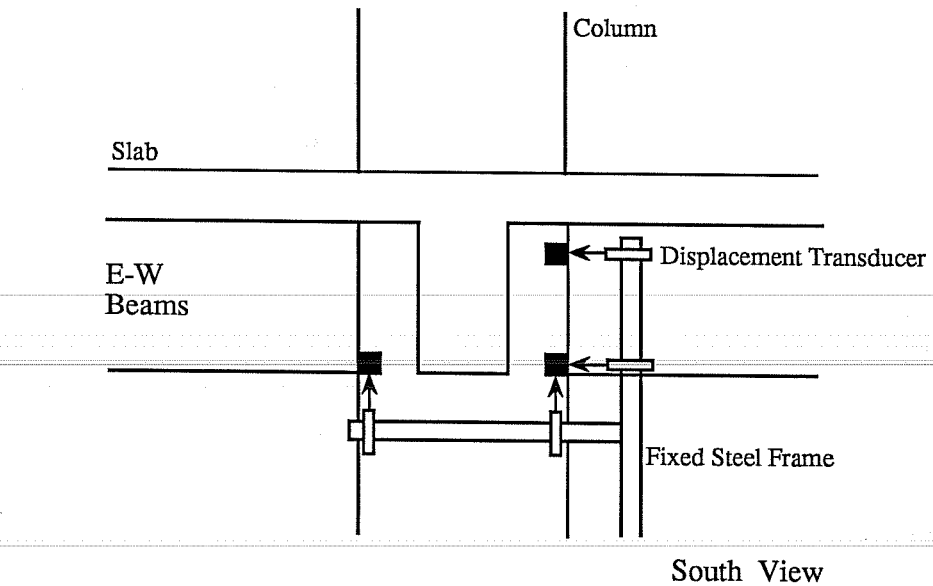

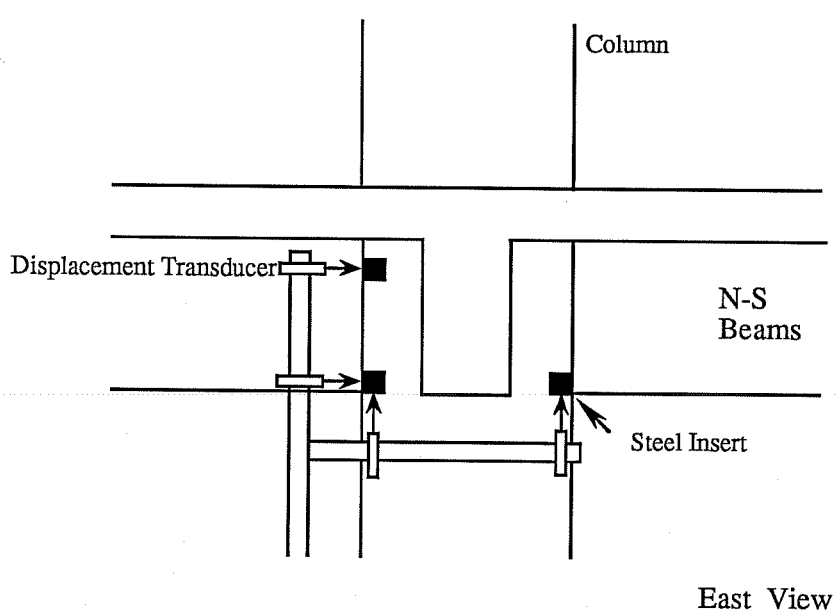

Figure 2.23 Instrumentation for Joint Shear Distortion Measurements

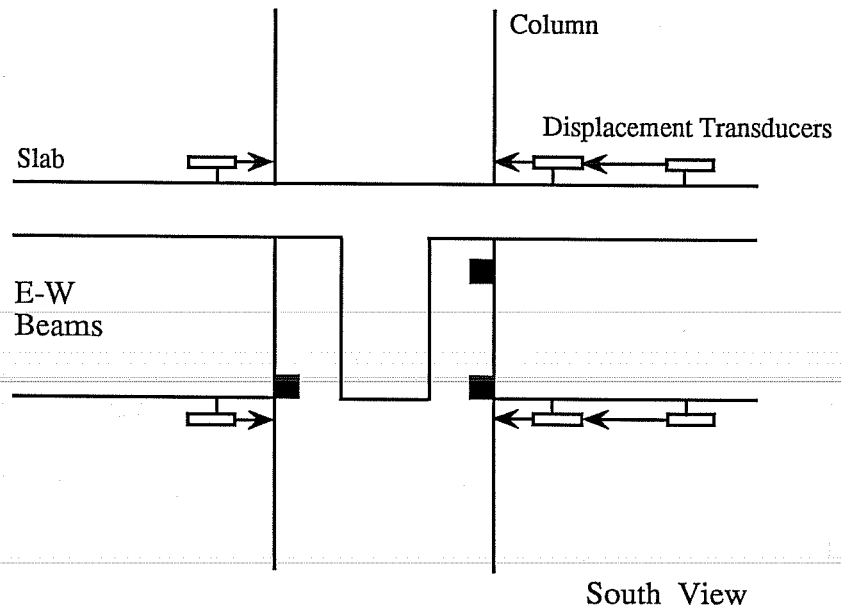

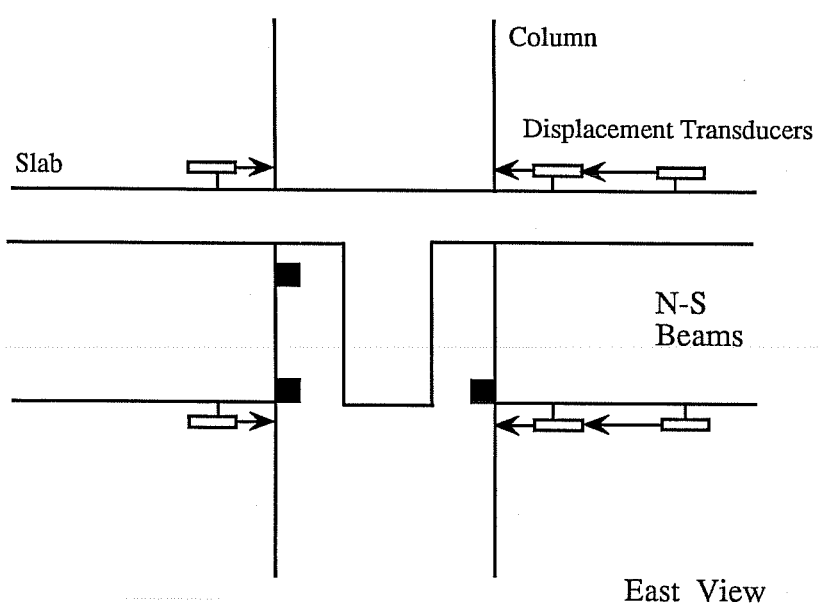

Figure 2.24 Instrumentation for Beam Rotation Measurements

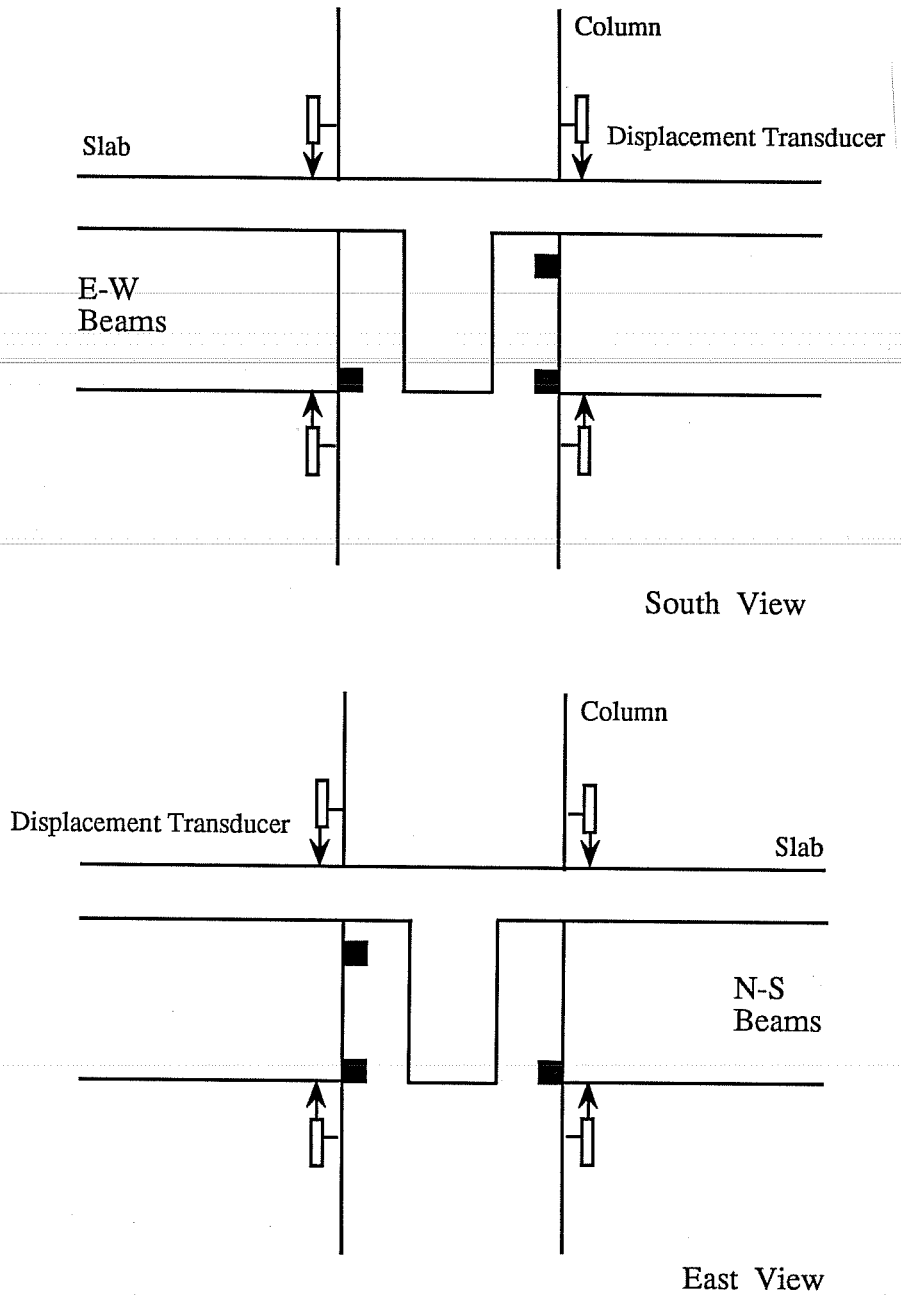

Figure 2.25 Instrumentation for Column Rotation Measurements.

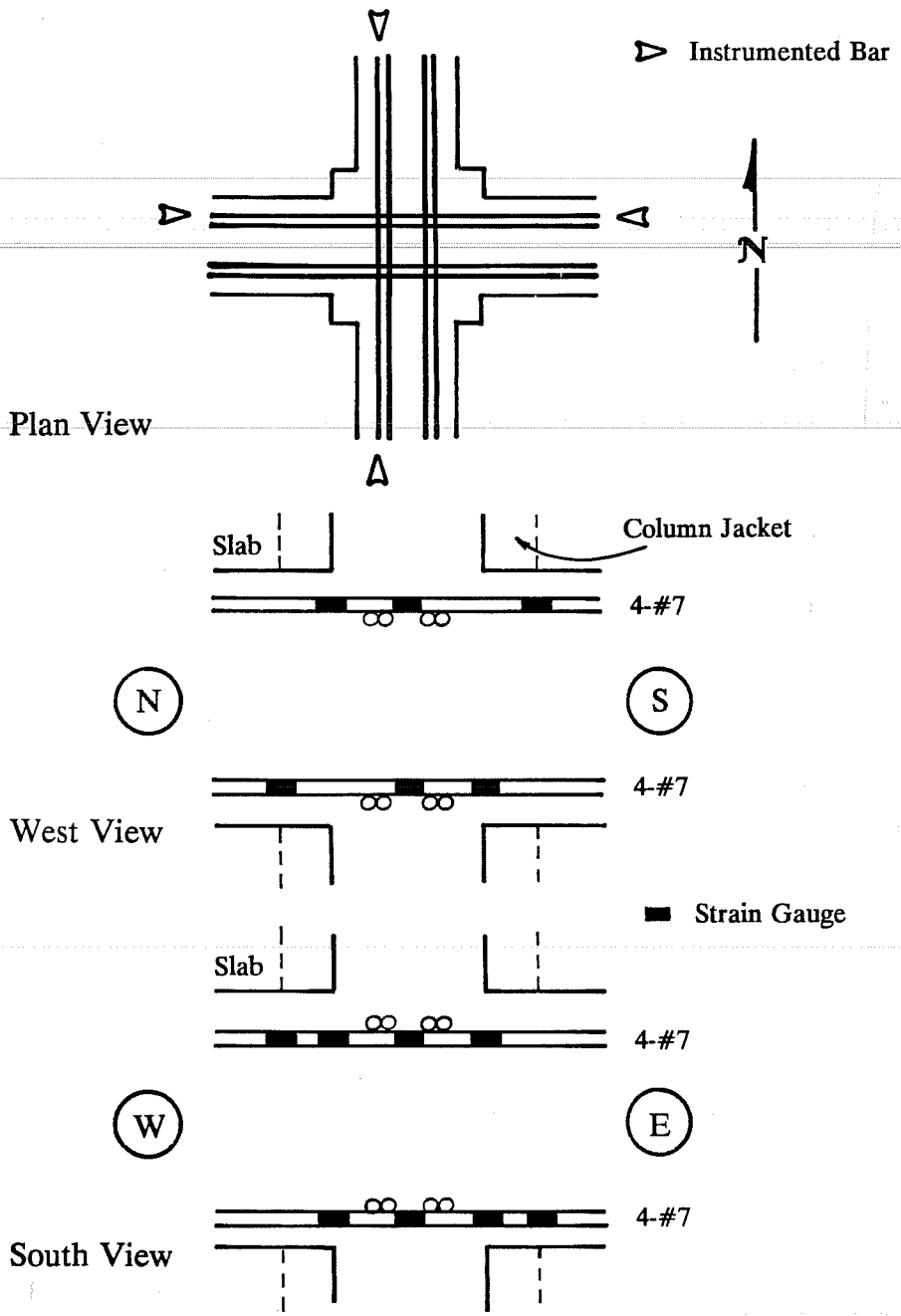

Figure 2.26 Original Beam - Strain Gauge Location

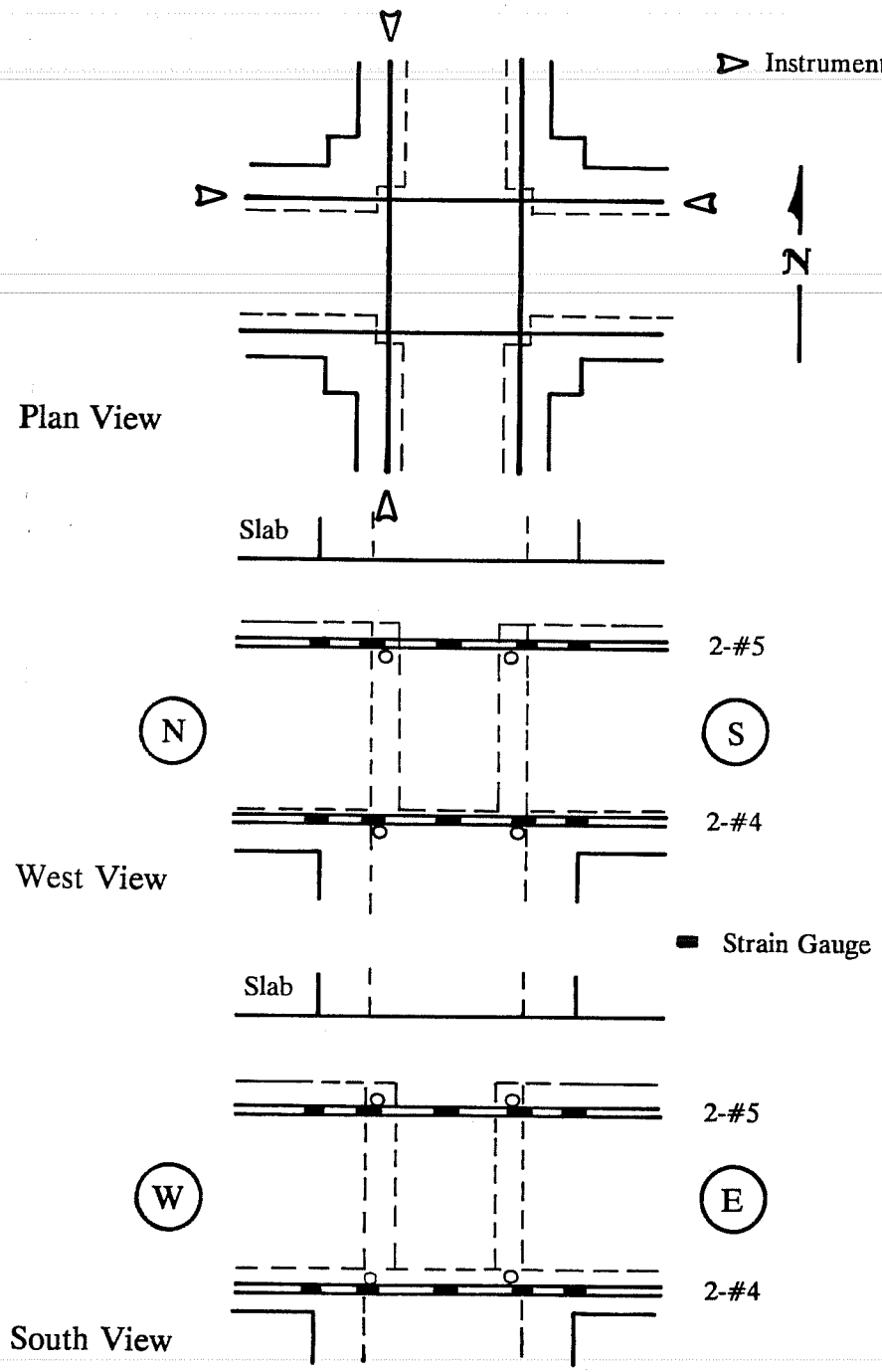

Figure 2.27 Beam Specimen SD-B - Strain Gauge Location

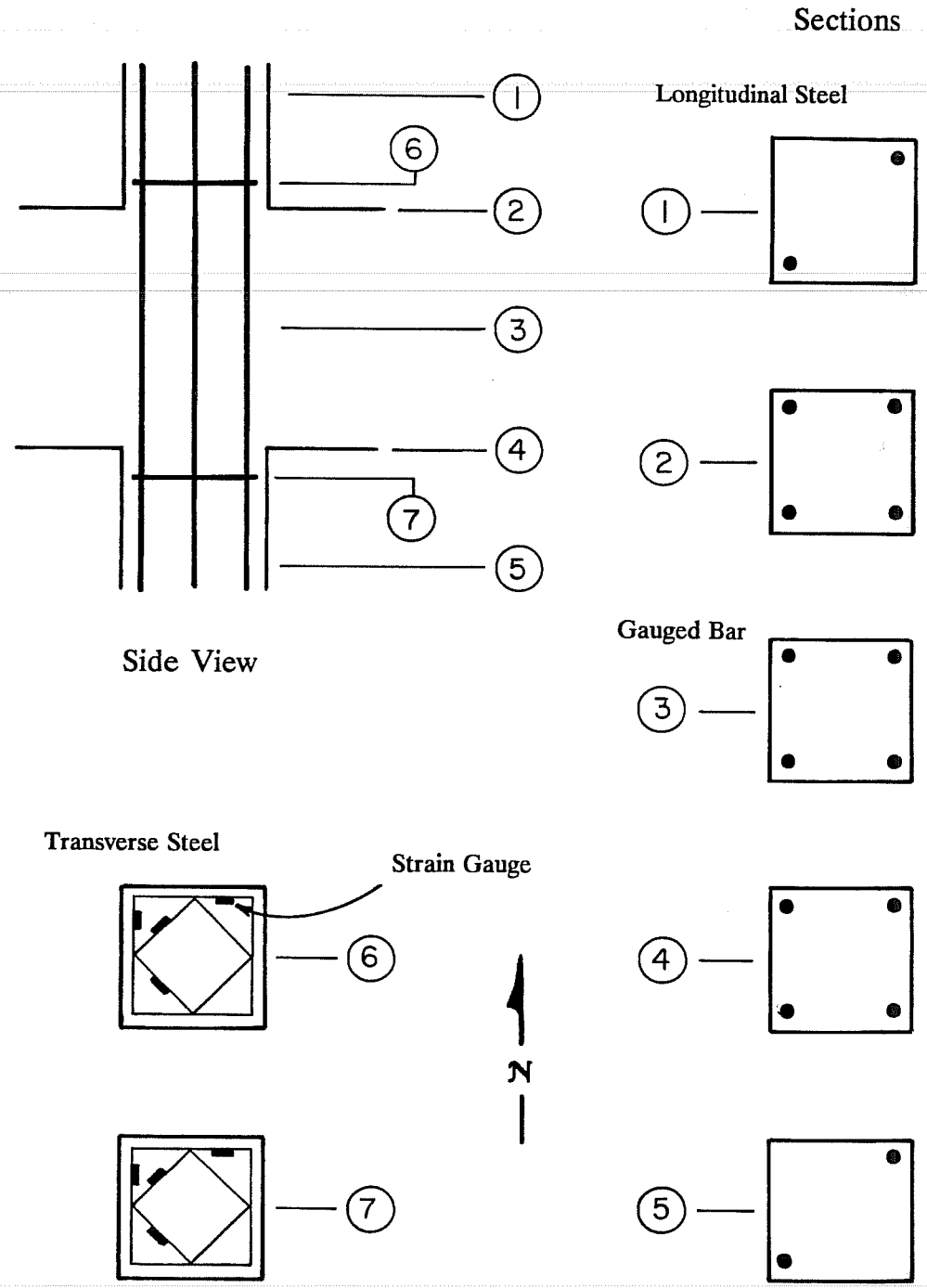

Figure 2.28 Original Column - Strain Gauge Location

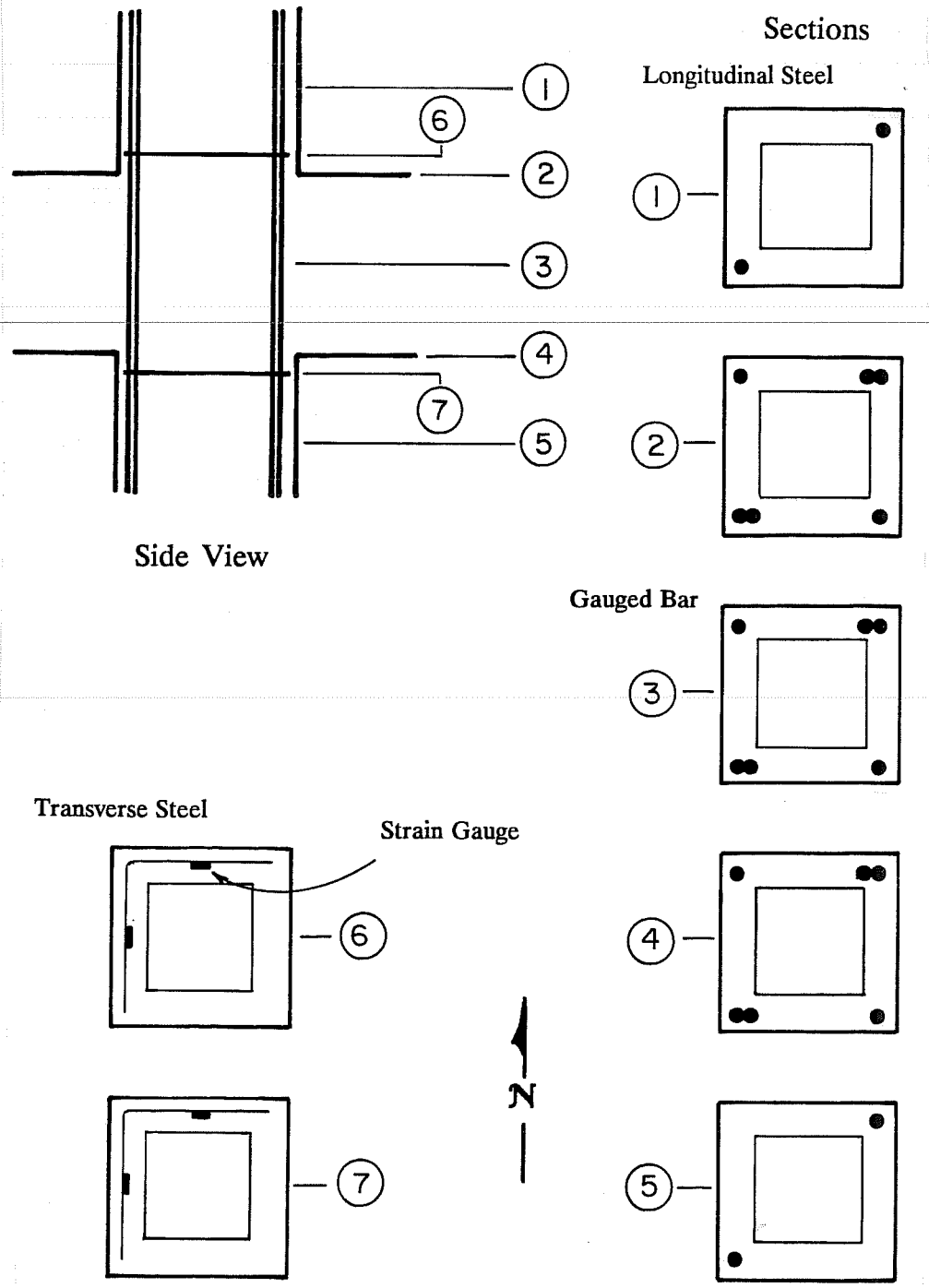

Figure 2.29 Jacketed Column Specimens RB and SB - Strain Gauge Location

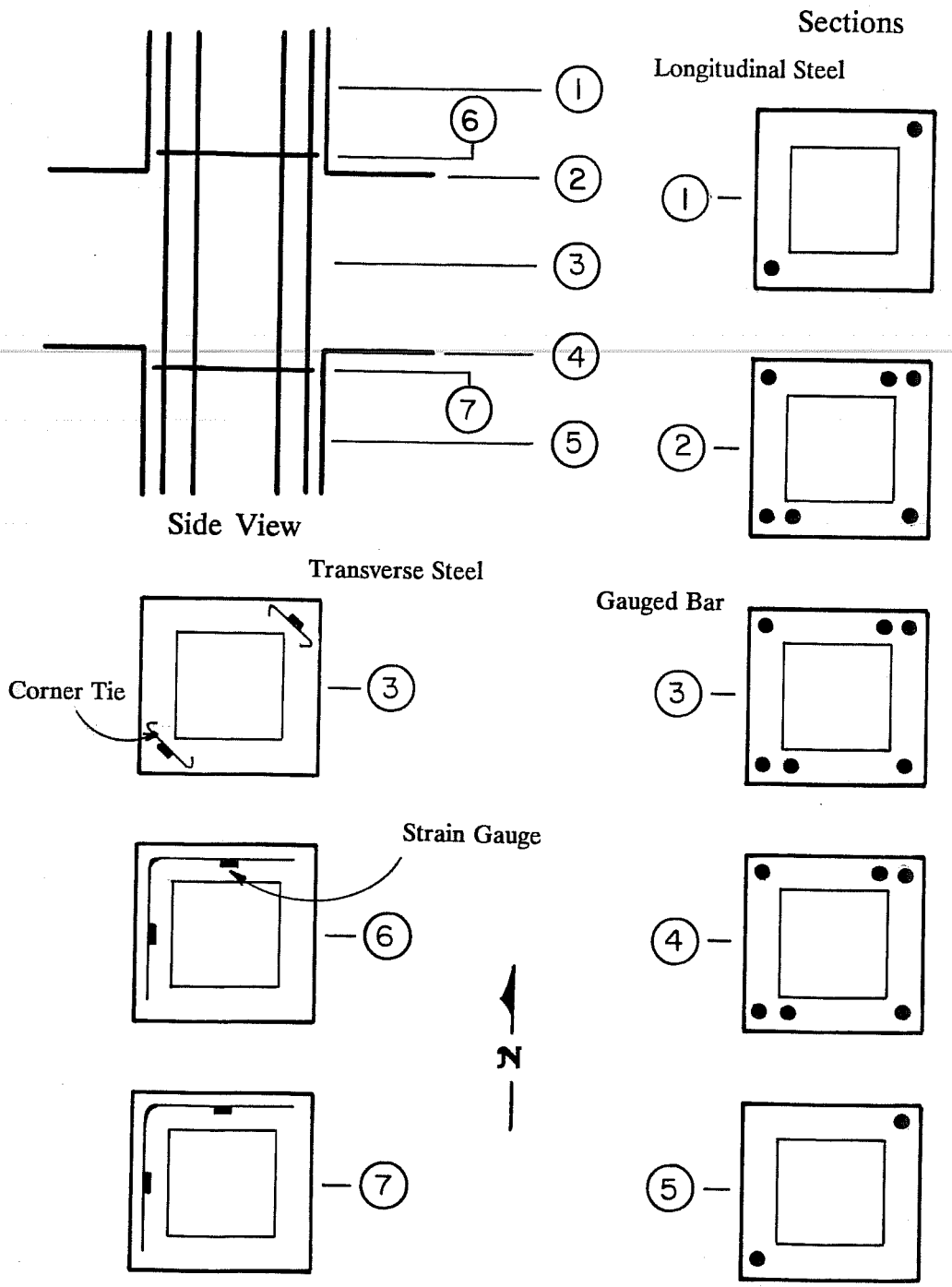

Figure 2.30 Jacketed Column Specimens SD and SD-B - Strain Gauge Location

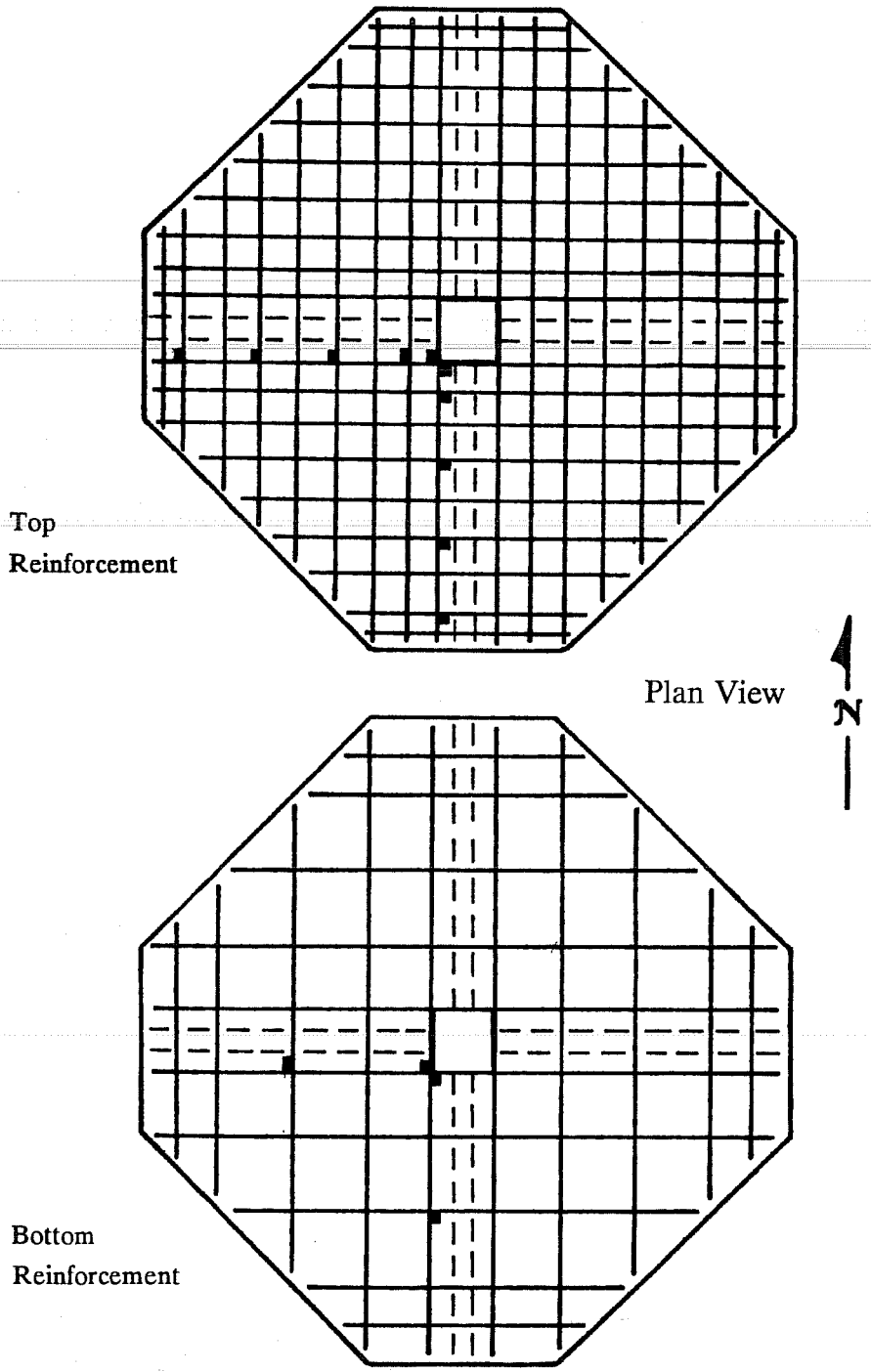

Figure 2.31 Slab - Strain Gauge Location

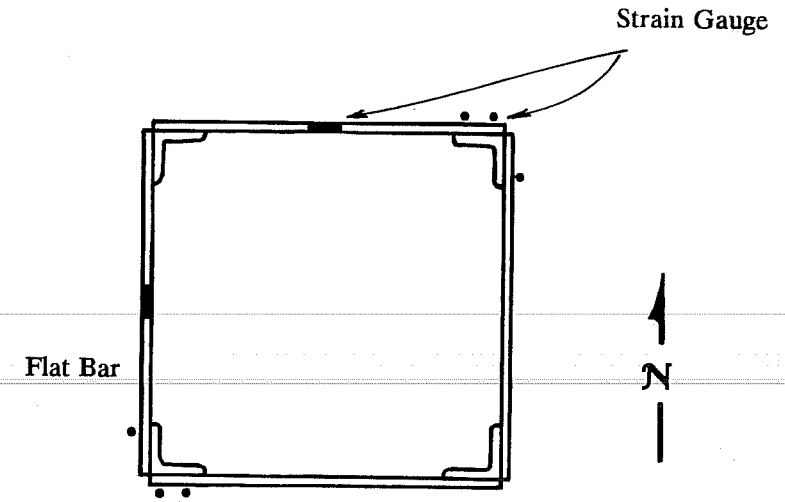

Plan View

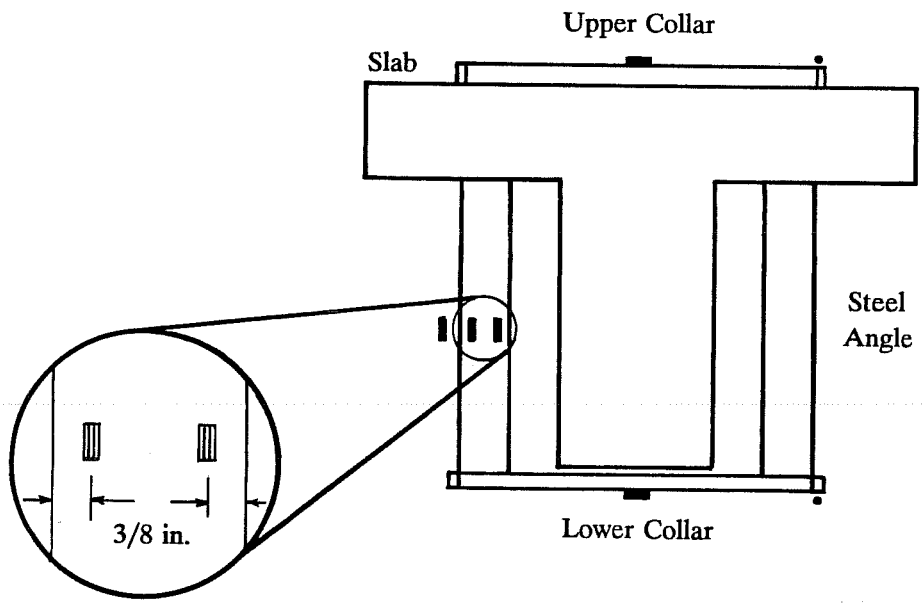

Side View

Figure 2.32 Joint Confinement Cage - Strain Gauge Location

2.6.2 Ultrasonic Pulse Velocity Measurements. Ultrasonic pulse velocity equipment was used on jacketed specimens to monitor degradation of the frame elements and to detect possible delamination between the original concrete and the jackets.

The equipment consisted of a pulse repetition frequency generator, two transducers (a transmitter and a receiver) with a frequency of 50 KHz., and a digital display. Longitudinal wave pulses are generated at a repetition frequency of 10 per second. The instrument displays the time taken for the earliest part of the pulse to reach the receiving transducer measured from the time it leaves the transmitting transducer. The pulse velocity, or travel time if distance is constant, will generally depend only on the properties of the material, and its measurement enables an assessment of the conditions of the material. Transducers may be arranged on the surface of the specimen tested to produce a direct, a

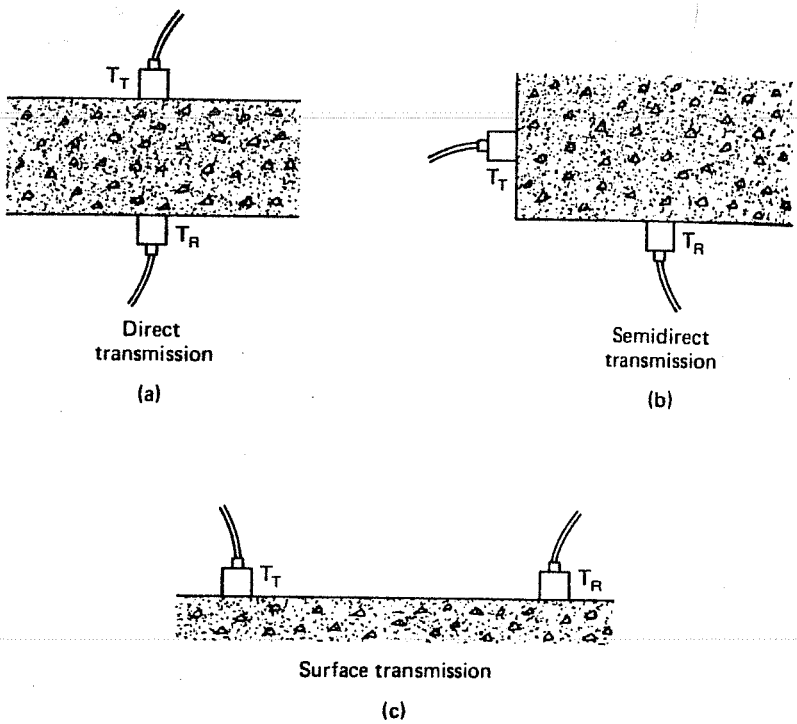

Figure 2.33 Methods of Measuring Pulse Velocity Through Concrete (from Ref. 35).

semi-direct or an indirect (surface) transmission (see Figure 2.33, taken from Ref. 35). Only the first two were used. Readings with pulse velocity are affected, among several others, by the presence of aggregate and steel along the wave path. Hence, position of measuring points was not varied throughout each test. Relative change of travel time was used to correlate degradation in the specimen. Location of measuring points is illustrated in Figure 2.34.

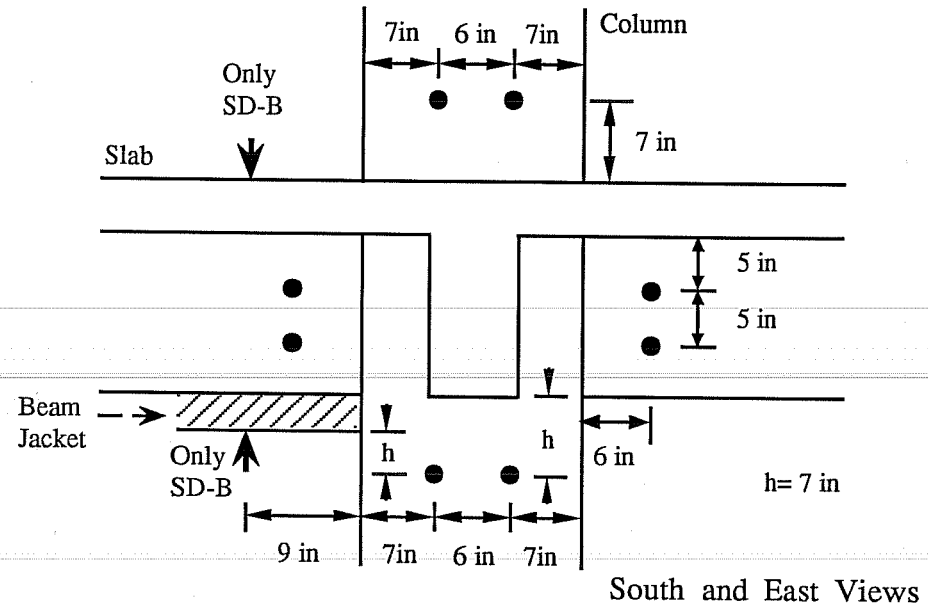

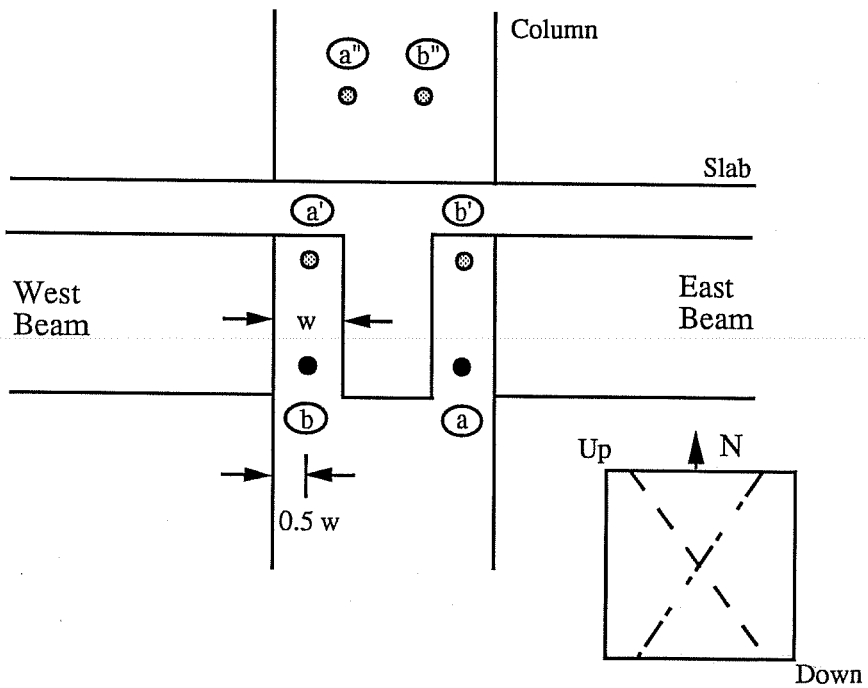

Figure 2.34 Ultrasonic Pulse Velocity Measuring Points.

Direct readings were taken on beam and column faces, in the two loading directions, and from the beam soffit to the slab surface for specimen SD-B. Semi-direct measurements were done across the joint. The first set of joint readings was taken between points in opposite faces of the joint (readings a-a' and b-b'). One point was located in the lower portion of the joint on one side of the beam, and the other in the upper part of the joint, below the slab, on the opposite beam side. The second set was taken between a point in the lower portion of the joint and a diagonally opposite point in the upper column (readings a-a'' and b-b''). At large drifts, joint cracking and spalling, and delamination between the joint cover and the steel angle affected the readings. Near the end of some tests the pulse velocity did not stabilize.

All readings were taken before the test, and after the set of cycles, either unidirectional or bidirectional, at each deformation level. Only joint readings were taken after the first cycle of the set, either unidirectional or bidirectional, at each deformation level. Petroleum jelly was used as the coupling medium between faces of the transducers and the concrete surface.

2.7 DATA ACQUISITION

The test was monitored with X-Y plotters and the displacement was controlled with dial gauges. The instrumentation devices were connected to a scanner, which was controlled by a microcomputer. At each load stage the instrumentation channels were read and a hard copy of the readings was obtained simultaneously. The software used allowed conversion of test data to engineering units in real time to monitor the test. Measurements were saved on floppy disks for further data reduction and analysis of results.

CHAPTER III - GENERAL BEHAVIOR OF THE SPECIMENS

3.1 INTRODUCTION

The overall response of the specimens is presented in this chapter. Crack patterns are described. The story shear versus drift angle relations are shown for both loading directions. Components of drift angle and selected member curvatures are presented. Finally, response envelopes and story shear behavior are discussed. Concepts used throughout the chapter are defined. Most of the results are presented for the E-W direction. Results in the N-S direction are similar and only the differences are noted.

In general, the specimens showed similar hysteretic response, characterized by considerable pinching and stiffness degradation. Strength decay was observed when cycling at large deformation levels. Rehabilitated specimens showed a more favorable energy dissipation mechanism as compared with the failure mode of the existing structure. Jacketing of frame elements improved the response of the existing structure.

3.2 DEFINITION OF RESPONSE CHARACTERISTICS

3.2.1 Components of Drift Angle. Member contributions to specimen deformation give a good indication of the behavior of the specimen and help visualize the possible mode of failure. Under the racking loads imposed on the beams, the specimens were assumed to deform in the pattern shown in Figure 3.1. For illustration purposes, deformations of frame elements in Figure 3.1 are exaggerated. The deformed specimen in an idealized structure and in the laboratory are also shown. Joint deformations were considered to be governed by shear. Beams and columns were assumed to deform in flexure. Both elastic and inelastic deformations were included in the measurements and calculations. Joint distortion was measured with linear potentiometers mounted on a reference frame which was fixed relative to the specimen (see Figure 2.23). Joint distortion γ was calculated as the difference of the vertical joint angle α and the horizontal joint angle β.

Although column ends were pinned and restricted from lateral movement, a fictitious equivalent column deflection associated with the joint distortion could be calculated. From the geometry shown in Figure 3.1, the beam end deflections and equivalent column deflection can be determined as

$$\Delta_b = \Delta_{i\ (or\ j)} - \Delta_1 - \Delta_2 \qquad (3.1)$$

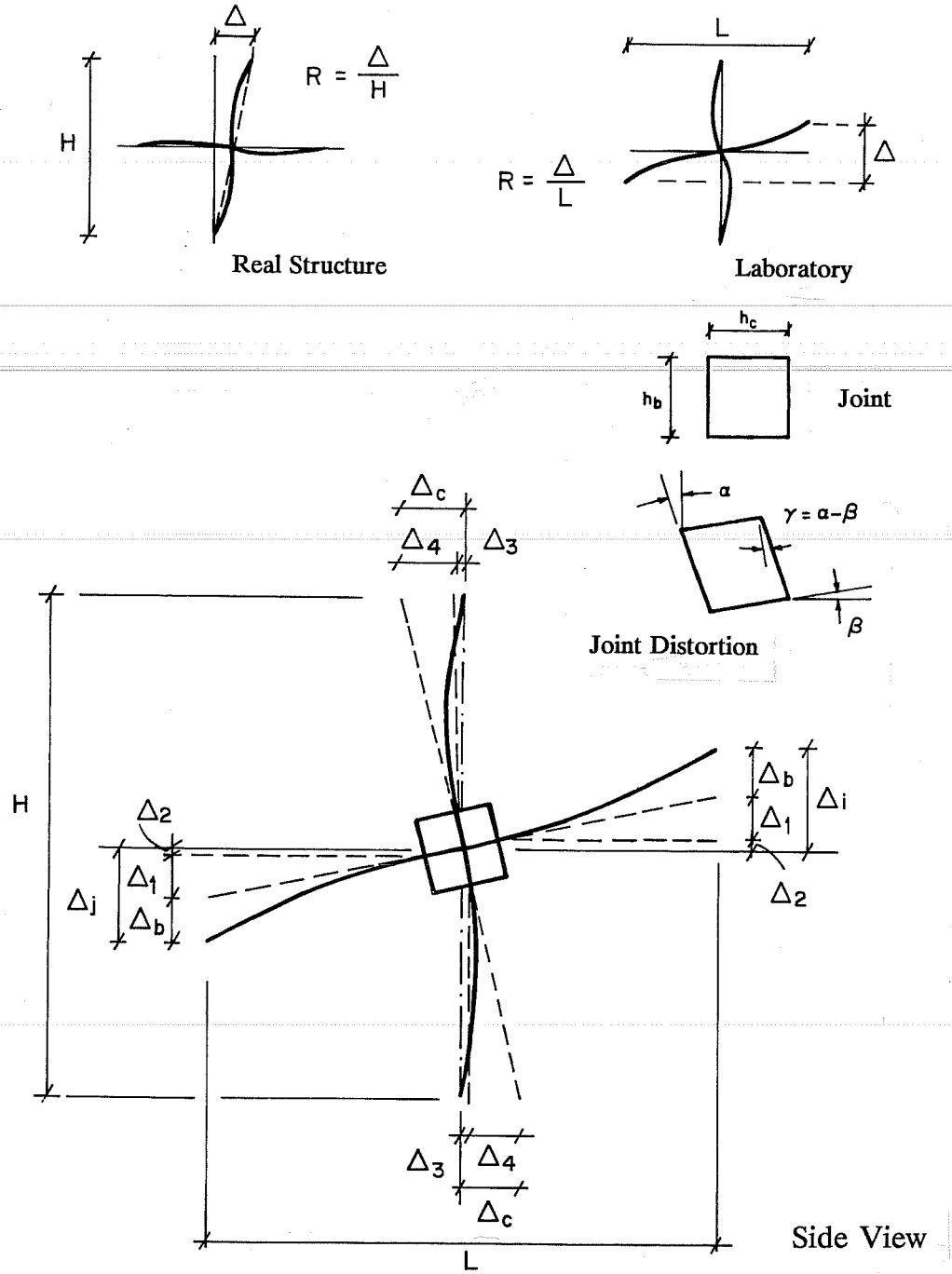

Figure 3.1 Assumed Deformation Pattern

$$\Delta_c = \Delta_3 + \Delta_4 \tag{3.2}$$

where

$$\Delta_1 = \frac{L - h_c}{2}\,\alpha \tag{3.3}$$

$$\Delta_2 = \frac{h_c}{2}\,\beta \tag{3.4}$$

$$\Delta_3 = \frac{h_b}{2}\,\alpha \tag{3.5}$$

and

$$\Delta_4 = \frac{H - h_b}{2}\,\beta \tag{3.6}$$

If the beam angle is defined as

$$\theta_b = \frac{\Delta_b}{L/2} \tag{3.7}$$

and the column angle as

$$\theta_c = \frac{\Delta_c}{H/2} \tag{3.8}$$

substituting Equations 3.1 and 3.2 into Equations 3.7 and 3.8, and using Equations 3.3 through 3.6 and the definition of joint distortion $\gamma = \alpha - \beta$, the beam and column angles can be rewritten as

$$\theta_b = R - \alpha + \frac{h_c}{L}\,\gamma \tag{3.9}$$

and

$$\theta_c = \beta + \frac{h_b}{H}\,\gamma \tag{3.10}$$

where R is the imposed story drift angle.

The drift component attributed to the joint can be written as

$$\gamma' = \gamma \left(1 - \frac{h_b}{H} - \frac{h_c}{L} \right) \tag{3.11}$$

Summation of θ_b, θ_c and γ' equals the imposed drift angle R so that if one drift component increases, other components must decrease. Any of the drift components multiplied by the specimen height H gives the element's contribution to interstory drift. For convenience in the presentation, the components of drift angle were multiplied by one hundred to give values in percent. The column angle depended mainly on the magnitude of the horizontal joint angle β (see Equation 3.9). The beam angle and drift component attributed to joint deformation were governed by the vertical joint angle α (Equations 3.10 and 3.11). In all tests α was larger than β. In cycle 9, for example, α was 2.5 times β in specimen O, 5 times in RB, and 6 times in SD.

3.2.2 Member Curvatures. Beam and column rotations were measured for all tests. Instrumentation used for measuring beam and column rotations is shown in Figure 2.24 and Figure 2.25, respectively. The measurements included elastic and inelastic deformations, as well as slip of beam and column longitudinal reinforcement within the joint. Beam rotations were measured over two regions along the beams (Figure 3.2). Region 1 covered the first 3 to 4 in. next to the column in all four beams. Region 2 included, approximately, the next 12 in. in the east and north beams. Average beam curvatures were calculated from the beam rotations by dividing the measured relative rotations by the length along the member over which the rotation occurred, i.e. the length of Regions 1 and 2. Column rotations were measured over the first 4 to 5 in. of the column above and below the joint in both loading directions. Average column curvatures over the gauge length were calculated. In all specimens, upper column curvatures were calculated over a shorter region than lower column curvatures.

3.3 SPECIMEN O

Specimen O, the first of four identical specimens built to represent the existing structure, was tested to failure applying the bidirectional cyclic loading history with a maximum deformation to 4% drift described in section 2.5. Although the imposed deformation was large for a prototype building subjected to strong ground motions, it provided information on the behavior of beam-column joints with flexible columns to levels expected to cause severe damage. Specimen O was repaired and retested (specimen RB). The ratio of calculated column to beam flexural capacities (in the E-W direction), based on measured material properties and dimensions, was 0.32 (see Chapter V).

Final crack patterns are shown in Figure 3.3. The crack pattern of the northeast quadrant of the specimen during cycle 7/neg to 2% drift, is shown in Figure 3.4. Similar

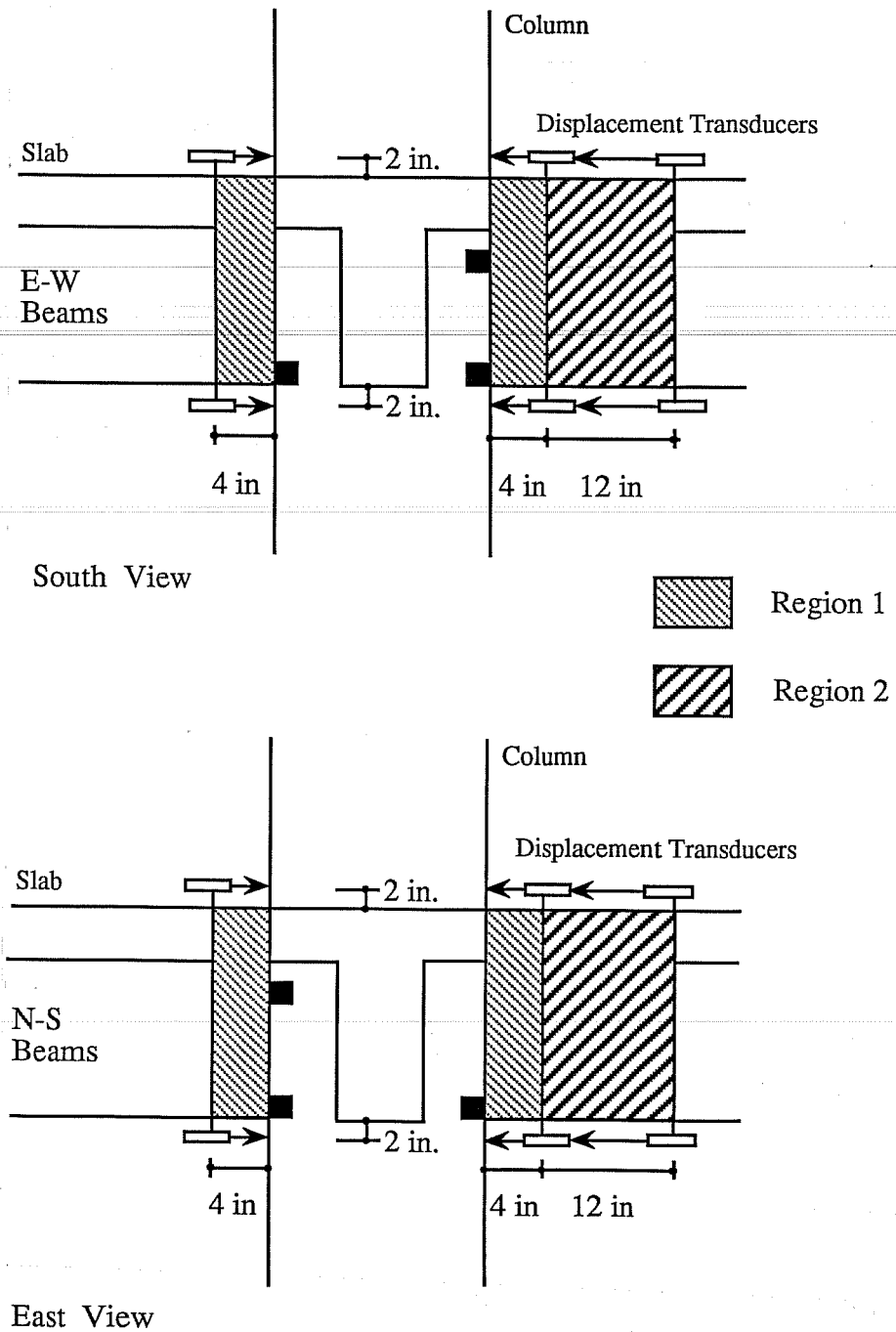

Figure 3.2 Beam Curvature Regions

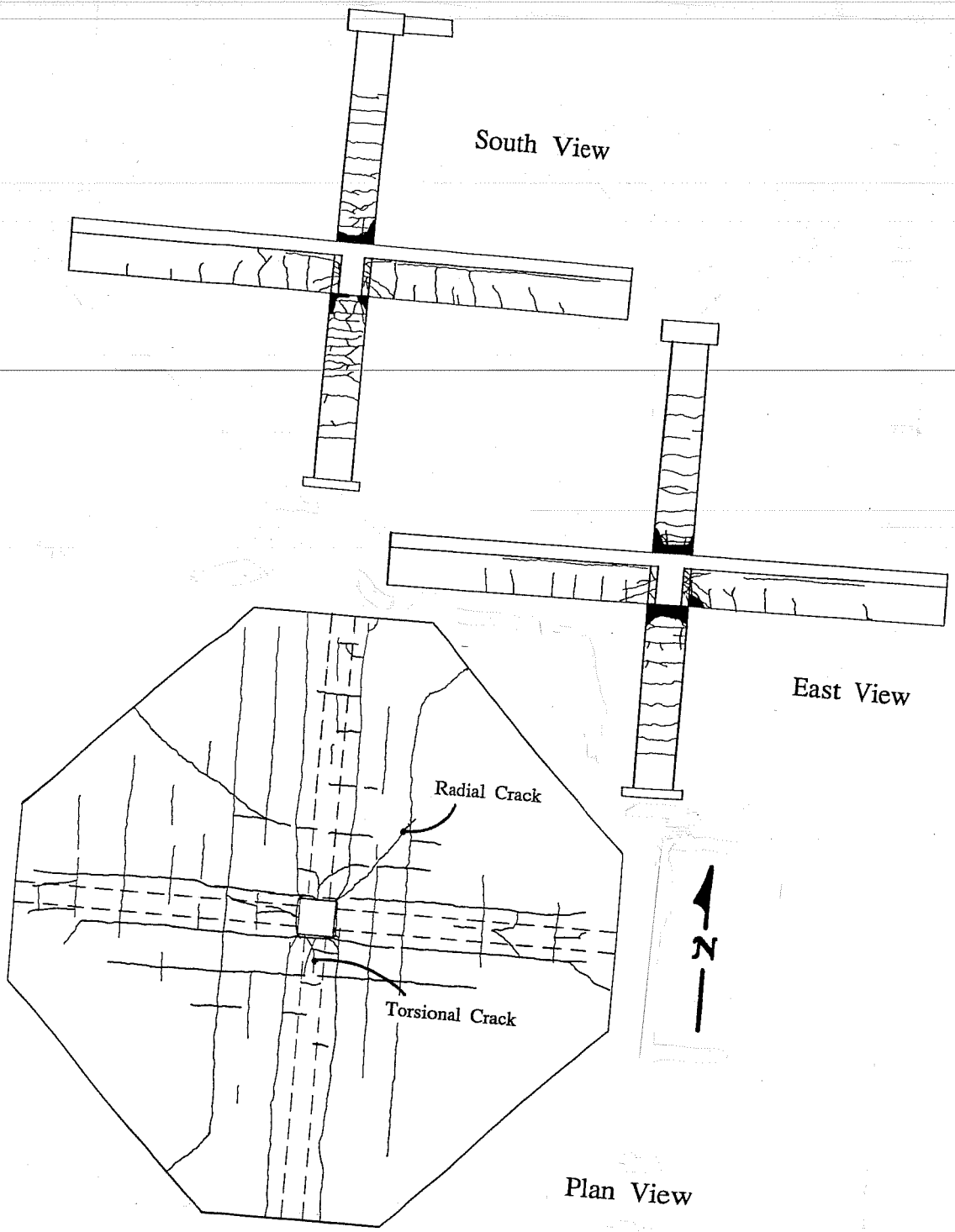

Figure 3.3 Specimen O - Final Crack Patterns

patterns were observed in the other quadrants. The story shear versus drift angle curves are presented in Figures 3.5 and 3.6 for the east-west and north-south components of story shear, respectively. First unidirectional cycles at 1%, 2% and 4% (cycles 3, 5 and 9) are indicated in the E-W direction. In the north-south direction, unidirectional cycle 4 and first bidirectional cycles 7 and 11 are labeled. The ultimate story shears corresponding to joint failure, $V_{u,j}$, and column hinging, $V_{u,col}$, are also shown in the figures. The story shear corresponding to joint failure was based on the joint shear strength recommended in Ref. 4. The story shear to produce column hinging was calculated from measured material properties and dimensions, considering an equivalent rectangular stress block for the concrete and assuming that plane sections remain plane. In Chapter V, a more detailed analysis of the member strengths is given. Figures 3.5 and 3.6 are plotted in the same scale as that used for tests RB, SB and SD so that comparisons among tests can be made. In general, the hysteresis loops for the two loading directions are nearly symmetrical and show considerable pinching, especially at drifts to 4%, and severe stiffness degradation. The hysteresis curves are dominated by the response of the most damaged elements, namely the columns and joint. Severe concrete crushing and spalling were observed in the columns. Columns developed plastic hinges above the slab and below the beam soffit. Yield penetration into the joint and large joint deformations were noted during the test. Consistent with a "strong beam - weak column" system, the beams and slab experienced minor flexural cracking and remained elastic. Specimen failure was precipitated by joint failure. Hysteresis curves in both directions show bidirectional interaction in the form of vertical lines at loading peaks and at zero drift during cycles 7, 8, 11 and 12. A drop in story shear during loading or unloading in the orthogonal direction was observed in all specimens.

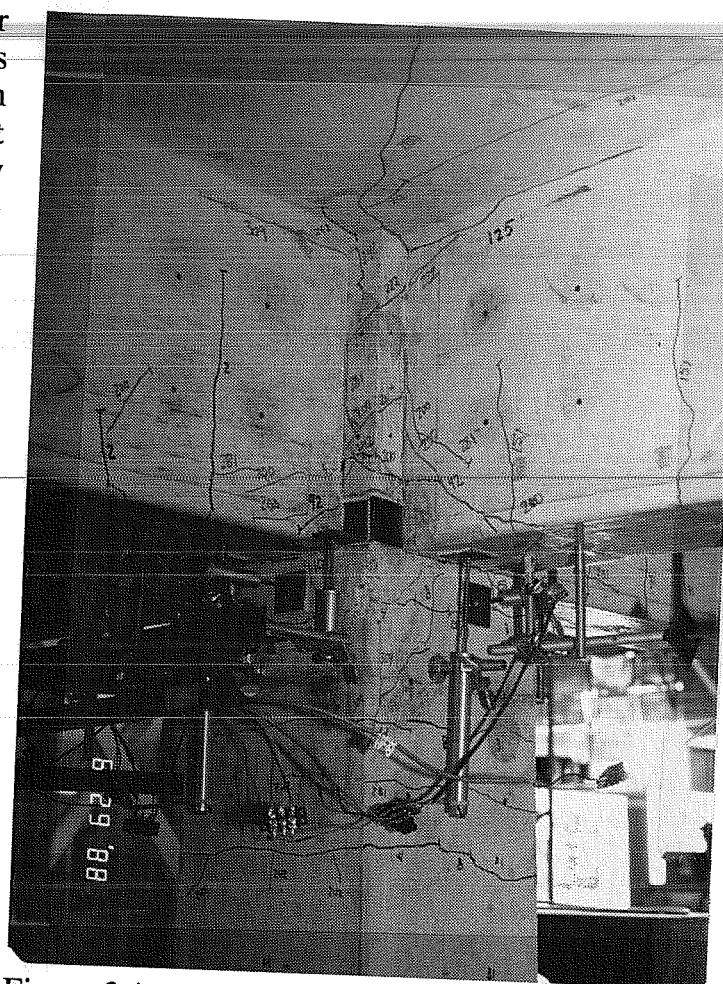

Figure 3.4 Specimen O - Crack Pattern NE Quadrant Cycle 7/neg

The joint strength in the E-W direction was exceeded in cycles 5, 6 and 9. However, considerable stiffness degradation and pinching, partially due to concrete damage, were

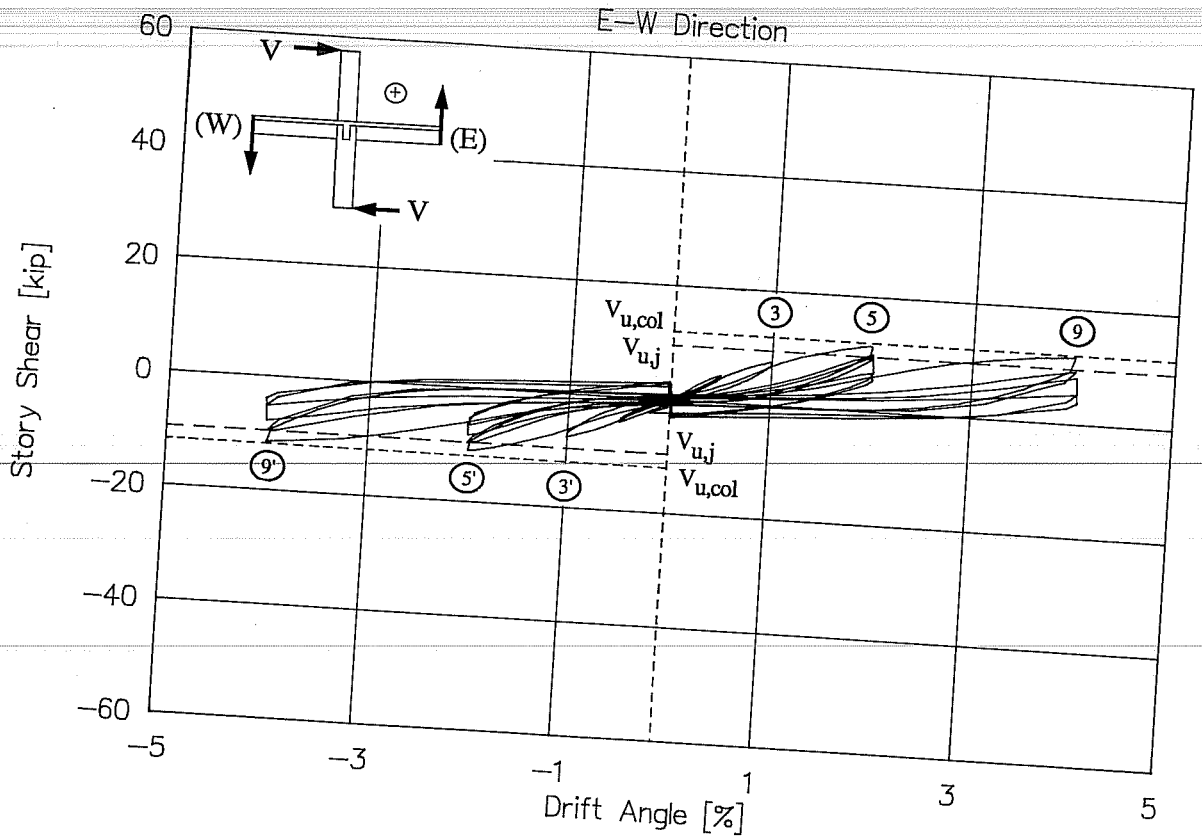

Figure 3.5 Specimen O - Story Shear vs. Drift Angle (E-W Direction).

observed in the hysteresis diagram (Figure 3.5). It is interesting to note that the maximum story shear in the N-S direction was reached in cycle 7 and was smaller than any of the calculated capacities (Figure 3.6). This suggests that the strength of the joint in the N-S direction was affected by the distress and cracking during loading in the E-W direction. The lack of joint confining steel probably exacerbated this problem. This phenomenon is similar to that in which a cracked concrete compression field must resist compression forces at a different inclination than that of the existing cracks. All specimens reached higher measured story shears in the E-W direction than in the N-S direction.

Coinciding with the observation that beams remained elastic, with maximum measured moments of about 1/3 the flexural capacity, the E-W story shear versus beam angle relation was linearly elastic (Figure 3.7). It is clear that beam contribution to drift angle was negligible. Beam curvatures were quite small. East beam curvatures for Regions 1 and 2 (see Figure 3.2) are presented in Figures 3.8 and 3.9, respectively. Similar figures were plotted for other beams (not shown here). East beam shear is considered positive when the beam is deflected upwards. Curvatures in Region 2 were very small (less than 0.0001 in^{-1}). Similar values of curvatures in Region 2 were found in all tests. Cracks which formed early in the test remained almost unaltered throughout the rest of the test with

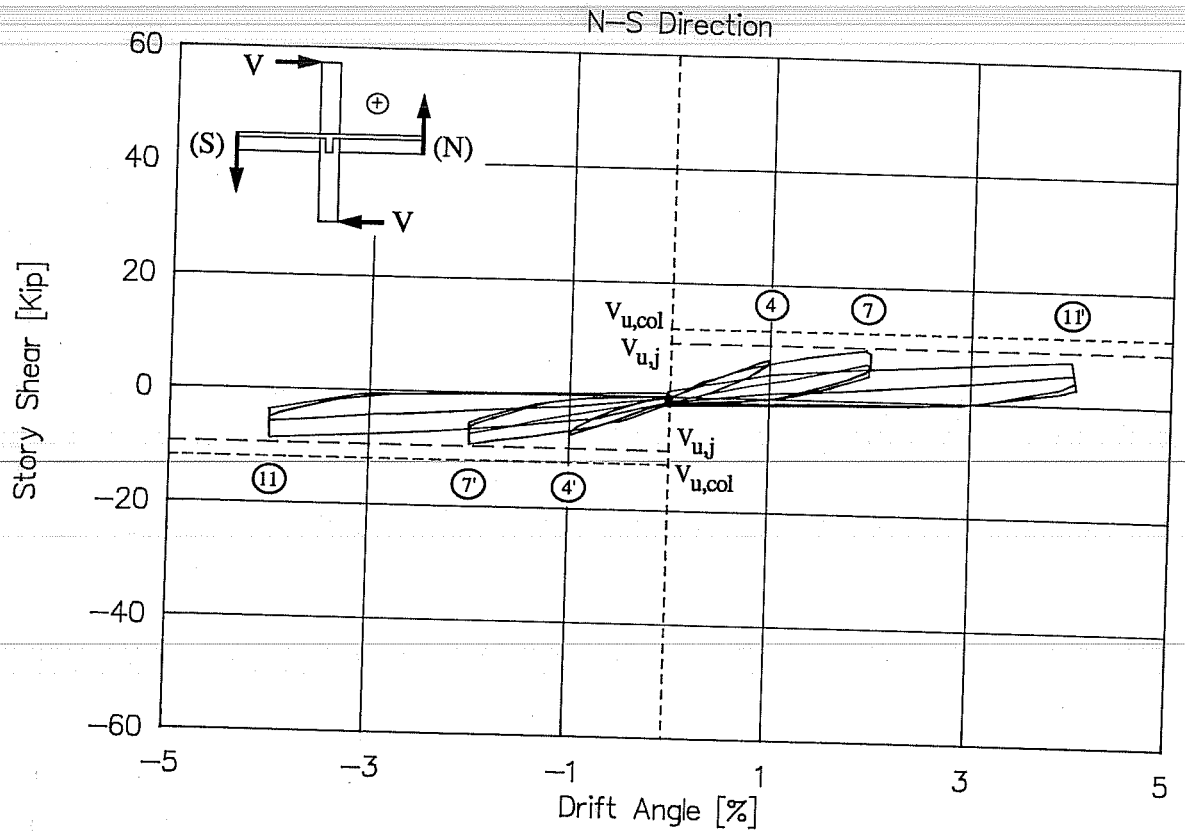

Figure 3.6 Specimen O - Story Shear vs. Drift Angle (N-S Direction).

maximum opening of 0.002 in.. Beams transverse to the loaded direction exhibited torsional cracking in the beam sides and in the top surface of the slab next to the column. Concrete crushed in the bottom faces of the N-S beam in cycles 11 and 12.

The behavior of the columns can be assessed through the E-W story shear versus column angle shown in Figure 3.10. Loops exhibited pinching and stiffness decay, especially at 4% drift, characteristic of column hinges without ductile detailing. The column angle increased at the same rate as the drift angle. The column damage also increased with cycling, particularly at drifts to 2% and 4%. Columns cracked in flexure in all sides. Maximum crack width of flexural column cracks increased by a factor of three from drifts at 0.5% to drifts at 2% (0.013 in.). Cracks were located at the column ties. First concrete crushing and spalling occurred during cycle 7 in the southwest and northeast corners above the slab and below the beam soffits. These corners were subjected to the highest compression due to the bidirectional loading. Cycles 9 and 10 (E-W direction), were characterized by large column and joint crack openings, and concrete crushing. The column crack at the beam soffit opened an average of 1 mm.. Yielding of column bars occurred in cycle 9. During bidirectional cycles 11 and 12, further loss of strength and stiffness deterioration were observed in the hysteretic response. Severe crushing and spalling of

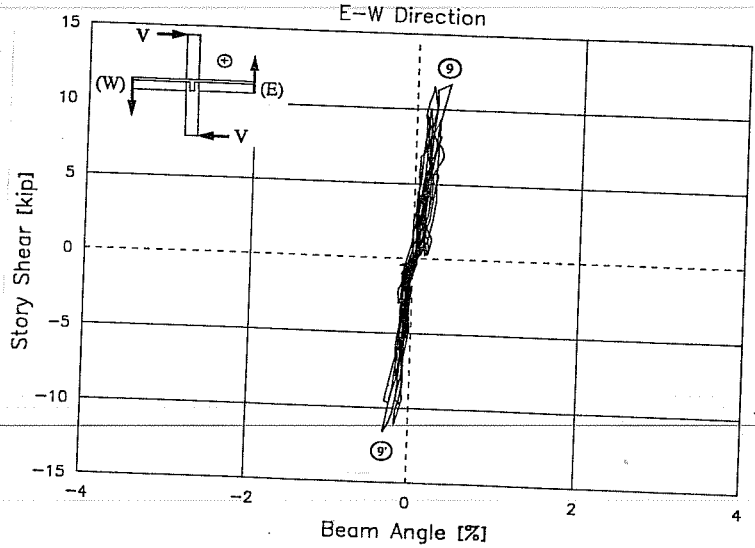

Figure 3.7 Specimen O - Story Shear vs. Beam Angle (E-W Direction).

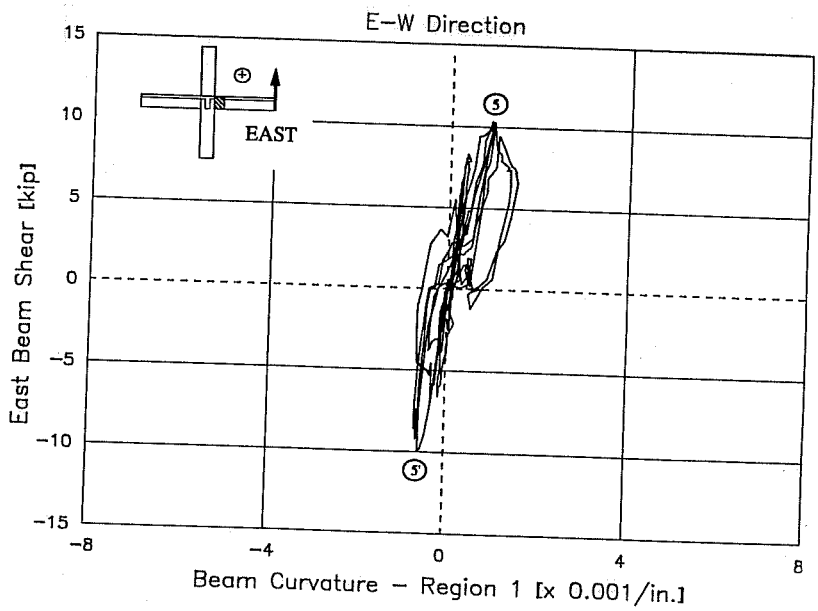

Figure 3.8 Specimen O - East Beam Curvature - Region 1

column concrete occurred in the northwest and southeast quadrants in the joint and above the slab. The northwest corner column bar was exposed below the slab. At the end of the test, it was noted that the northwest corner column bar was separated from the column core. Story shear in the E-W direction versus the upper and lower column curvatures are presented in Figures 3.11 and 3.12, respectively. Typical of "strong beam - weak column"

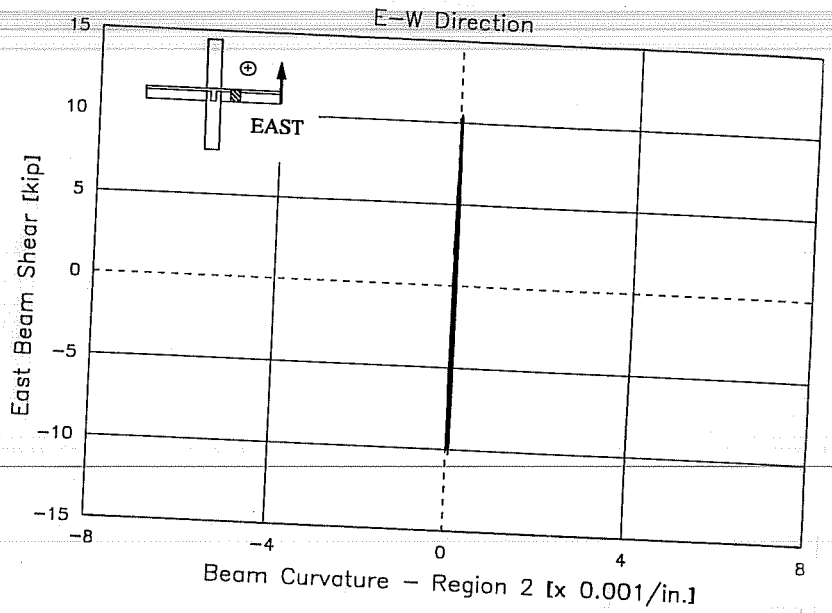

Figure 3.9 Specimen O - East Beam Curvature - Region 2

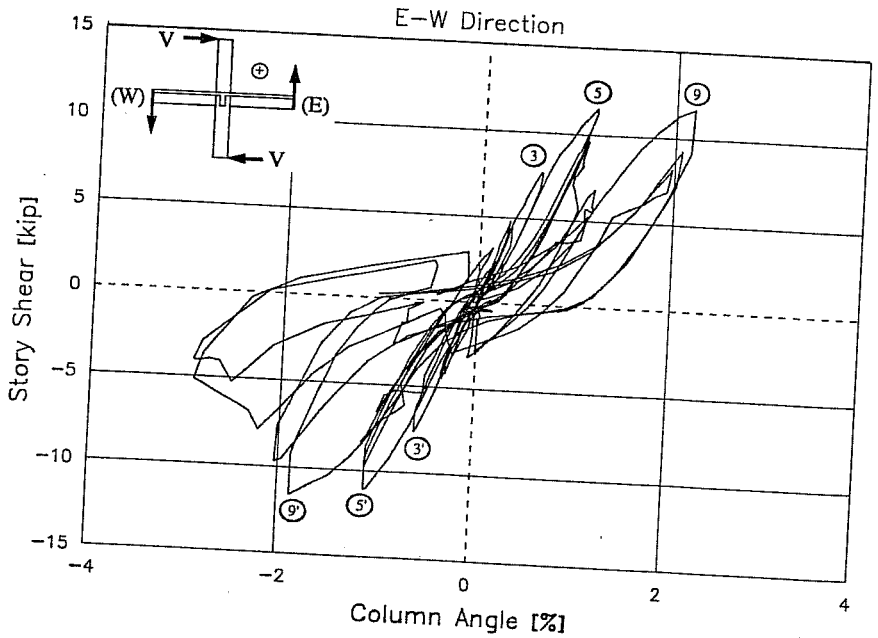

Figure 3.10 Specimen O - Story Shear vs. Column Angle (E-W Direction)

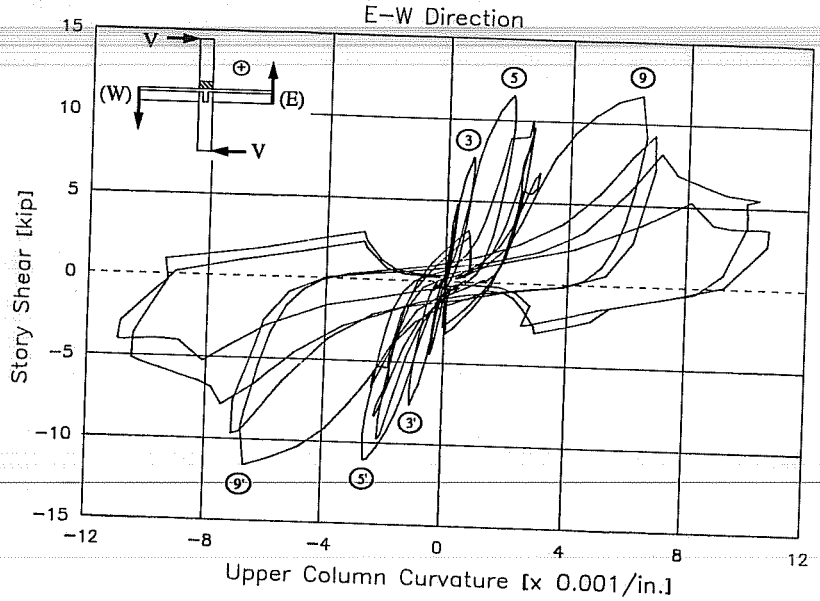

Figure 3.11 Specimen O - Upper Column Curvature (E-W Direction)

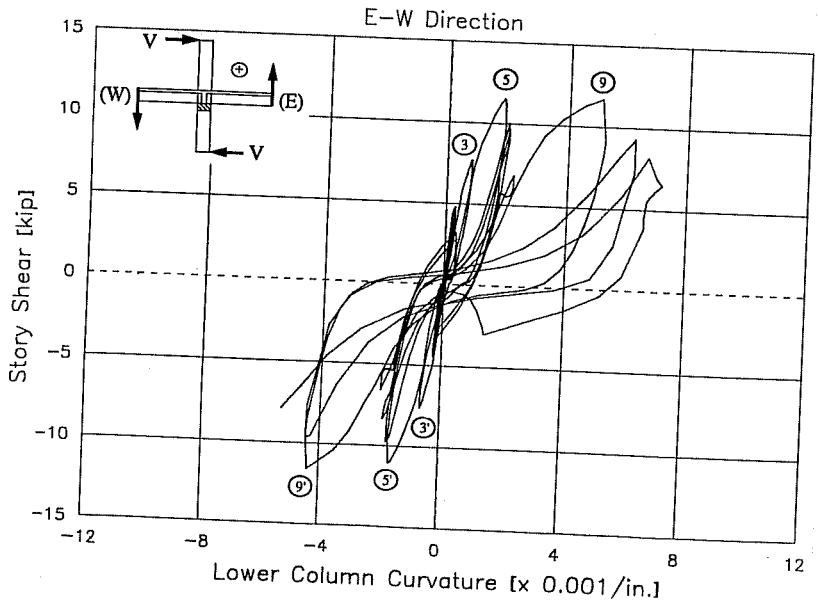

Figure 3.12 Specimen O - Lower Column Curvature (E-W Direction)

systems, column curvatures were much larger than beam curvatures. Curvatures up to 0.011 $in.^{-1}$ were measured in the upper column in cycle 11/neg. Upper column curvatures were 50% larger than lower column curvatures. Because the column was confined by the slab, damage was concentrated in the column. Below the slab, damage was distributed along the column and into the joint, so that the deformation was not concentrated in the column.

The slab developed minor flexural cracking in the top surface which coincided with the slab bars adjacent to the column in each direction. A crack formed at the column face in cycle 3. In cycles 5 and 6, flexural cracks extended across the entire slab width, in the top and bottom surfaces near the column. A crack on the bottom surface of the slab, which started at the column corner, extended towards the free edge (where slab corners were removed). This radial cracking formed during cycle 5/pos (beam deflected upwards). The first beam torsional crack on the top surface of the slab appeared in cycle 5/neg, starting at the south column face and extending obliquely with respect to the south beam axis towards the west (see Figure 3.3). In cycles 7 through 10 new torsional cracks formed in the slab around all four sides of the column. New radial cracks formed and existing cracks extended.

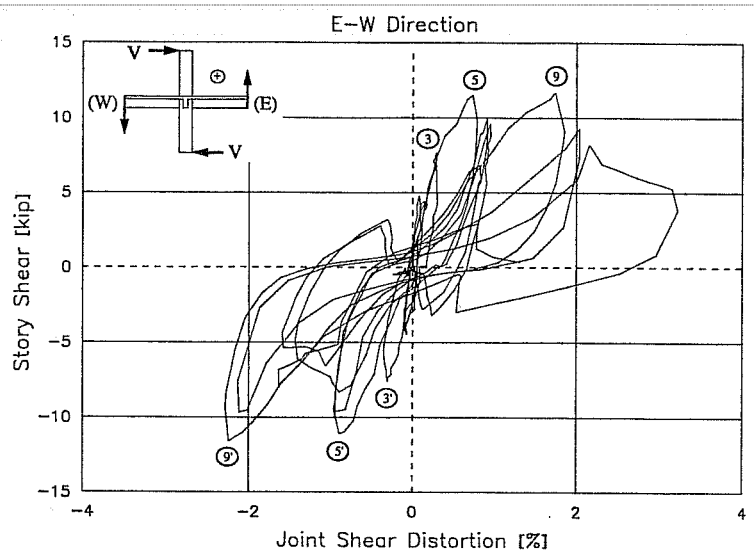

Figure 3.13 Specimen O - Story Shear vs. Joint Shear Distortion (E-W Direction)

Joint behavior can be studied through the E-W story shear versus joint shear distortion relation (Figure 3.13). Loops are symmetrical up to cycle 9 and show considerable pinching, loss of stiffness and strength deterioration typical of joint distress. From cycle 5, the joint shear distortion 15γ increased faster than the imposed drift angle. The joint distress was evident with the formation of inclined and horizontal cracks that extended into the beams. The first inclined joint crack formed in the northwest corner of the column during cycle 1/neg and extended into the north beam. In cycles to 1% drift, new inclined

and horizontal cracks formed which extended as torsional cracks into the transverse beams. In cycles to 2% drift, the joint region showed considerable inclined and horizontal cracking concentrated in the lower half of the joint. Further analysis of strain gauge data confirmed that anchorage of the corner column bar in that section was affected by the cracking (see Chapter IV). Average joint crack widths of 0.016 in. were recorded. Bond deterioration along corner column bars in following cycles might have contributed to narrowing of loops. After column hinging in cycle 9 to 4% drift, maximum forces were applied to the joint. The maximum E-W story shear was reached and surpassed the calculated joint capacity (Figure 3.5). It is likely that failure occurred in cycle 9, after which severe strength decay was noted. The strength degradation is mainly attributed to deterioration of joint concrete.

3.4 SPECIMEN RB

Following the completion of test O, the specimen was loaded to zero deflection at the beam ends (initial position at start of testing). Loose concrete was removed. The subassemblage was repaired by jacketing the columns. Longitudinal reinforcement in the column jacket was bundled in the corners. The beams and slab were not modified or repaired. Specimen RB was tested applying the same load history used for specimen O. The test was terminated before cycle 12 was completed because the specimen was considered to have failed. The ratio of calculated column to beam flexural capacities, based on measured material properties for the E-W direction, was 2.53.

Final crack patterns are illustrated in Figure 3.14. The crack pattern of the NE quadrant during cycle 8/neg to 2% drift is presented in Figure 3.15. The story shear versus drift angle relations for the E-W and N-S directions are presented in Figures 3.16 and 3.17, respectively. In general, cracking in specimen RB was more uniformly distributed than in specimen O. Beams cracked much more because the column was stronger and the beams carried higher forces. Beams yielded at 4% drift. Columns showed only minor flexural cracking compatible with the "strong column - weak beam" design philosophy. Slab cracking was more extensive than in test O. The joint was the most damaged element and failed in shear after beam hinging. Joint distress led to the strength decay observed, particularly at drifts to 4%. Most of the inclined joint cracks occurred in the N-S faces, whereas vertical and horizontal cracks formed in the E-W sides. The joint confinement cage was sufficient to prevent spalling into the joint core. No indication of concrete delamination in the column was found. Although the loops showed higher stiffness and strength than those for specimen O, stiffness and strength degradation, as well as pinching, were noted (see Figures 3.16 and 3.17). Pinching of the curves is partially attributed to joint concrete damage, cracking and spalling, and sliding of the beam relative to the column jacket. In all rehabilitated specimens, bond deterioration along beam bars also contributed to the S-shaped response. Bond distress is discussed in greater detail in Chapter IV in which an analysis of strain gauge data is presented. The measured E-W story shear exceeded the calculated strength in cycles 5, 9 and 10. The hysteresis curves show significant stiffness degradation after cycle 5 due to severe joint cracking which extended into the column.

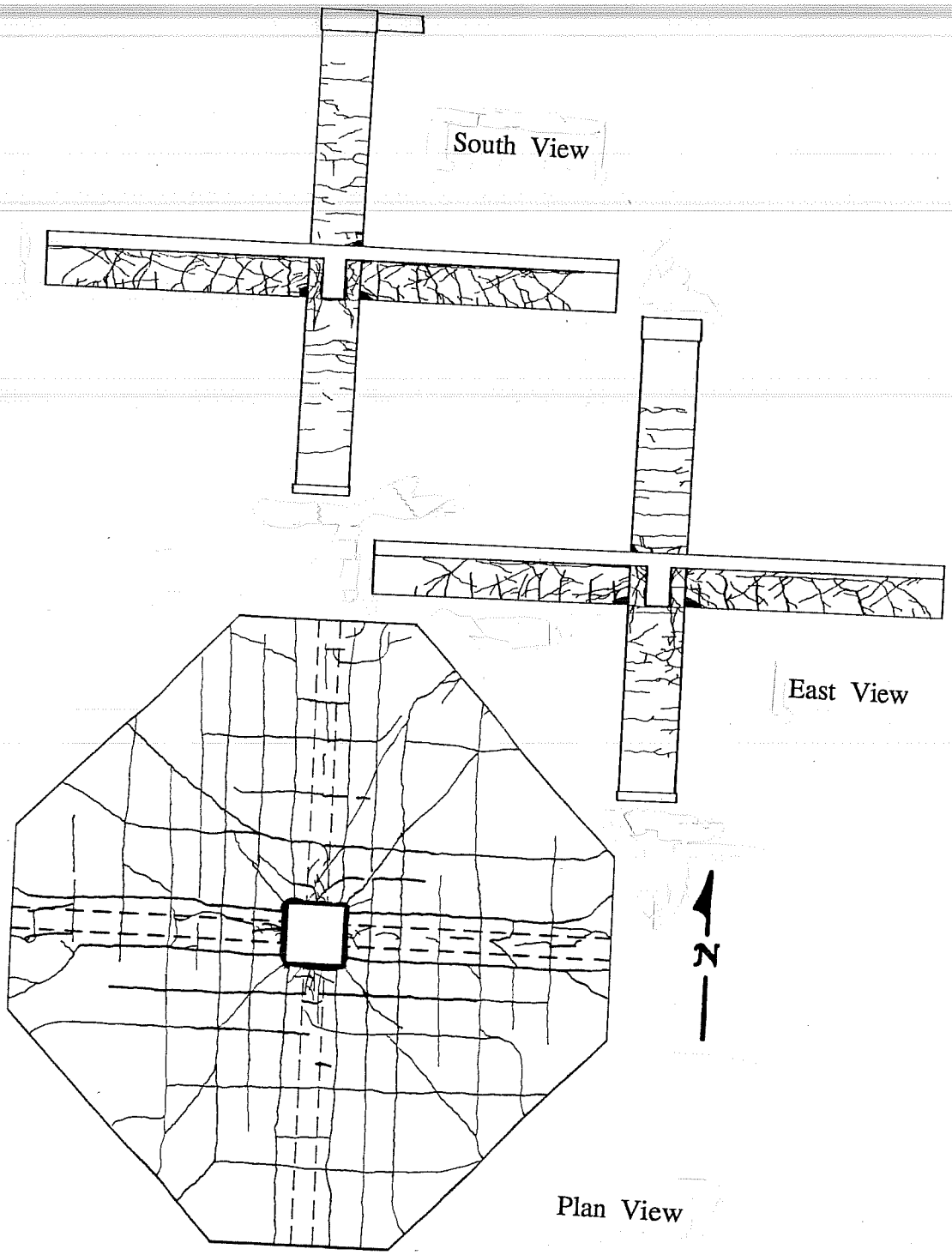

Figure 3.14 Specimen RB - Final Crack Patterns

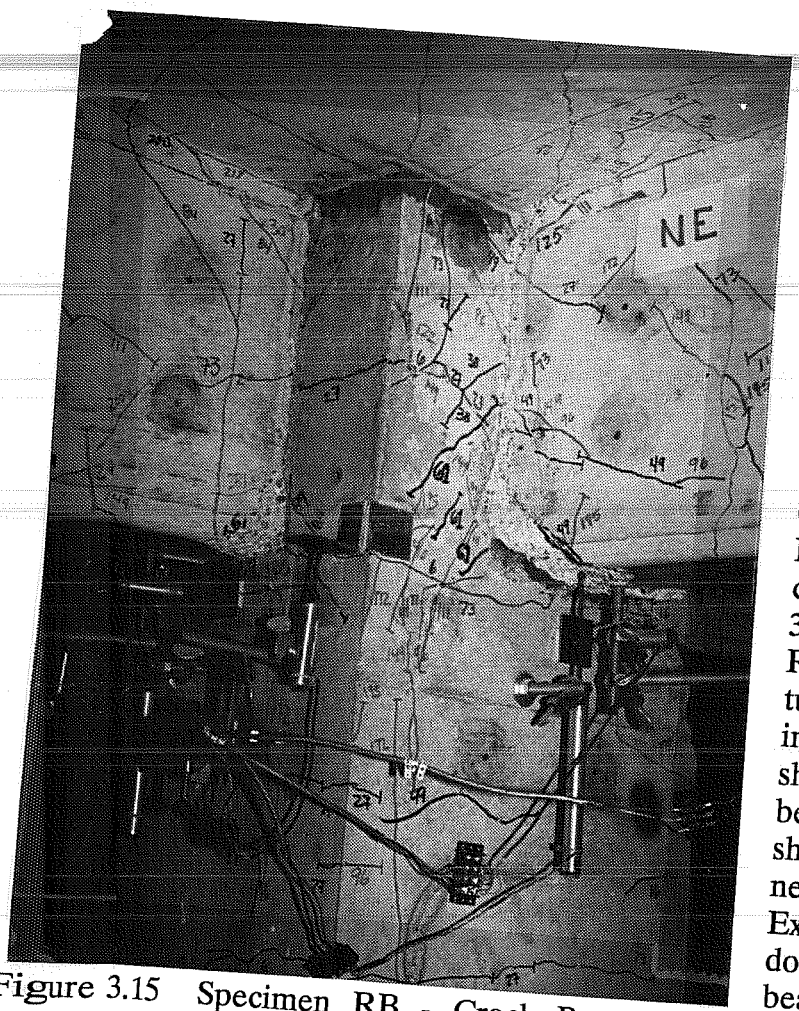

Figure 3.15 Specimen RB - Crack Pattern NE Quadrant Cycle 8/neg

Inclined cracks in the column below the joint probably reduced bond along the column bars and allowed them to slip. The maximum measured story shear occurred in cycle 9 and exceeded $V_{u,j}$ by 28%. Cycles 9 and 10 were characterized by large crack opening and concrete crushing which further reduced the stiffness.

The change in the energy dissipation mechanism of specimen O can be observed by comparing the E-W beam angles and the beam curvatures for specimen O (Figures 3.7 and 3.8) with those for specimen RB (Figures 3.18 and 3.19). Curvature graphs for other beams of specimen RB (not presented here) showed similar behavior. For RB, beam angle and beam curvatures show narrow loops and some stiffness degradation when cycling. Existing beam cracks from test O dominated the crack pattern. No beam cracks formed at the column face. In cycles to 0.5% and 1%, existing beam cracks extended and new cracks formed. Some of the inclined cracks were extensions of cracks in the slab bottom surface. Vertical cracks appeared along the beam - column jacket interface. This type of cracking was observed in all rehabilitated specimens. Transverse beams exhibited torsional cracks some of which extended from joint cracks. Beam torsional cracks were steeper than those noted in test O. Considerable flexural-shear cracking in the east-west beams occurred during cycles 5 and 6. Some small splitting-like cracks appeared on the beam sides along the bottom reinforcement. The crack at the beam - column jacket interface measured 0.040 in. wide. First beam crushing and spalling occurred in the N-S beams during cycle 7/neg (see Figure 3.15). Minor concrete crushing was noticed in the beam - column jacket interface due to the relative movement. Top and bottom beam bars yielded in cycle 9/pos thus producing large forces at the joint which led to joint failure. The beam bottom concrete cover crushed. Inelastic action in beams during cycles to 4% drift, increased the beam curvatures to a maximum value of about 0.006 in.$^{-1}$. At the end of the test, beam bottom reinforcement was exposed and the mortar patch under the east beam was pulverized.

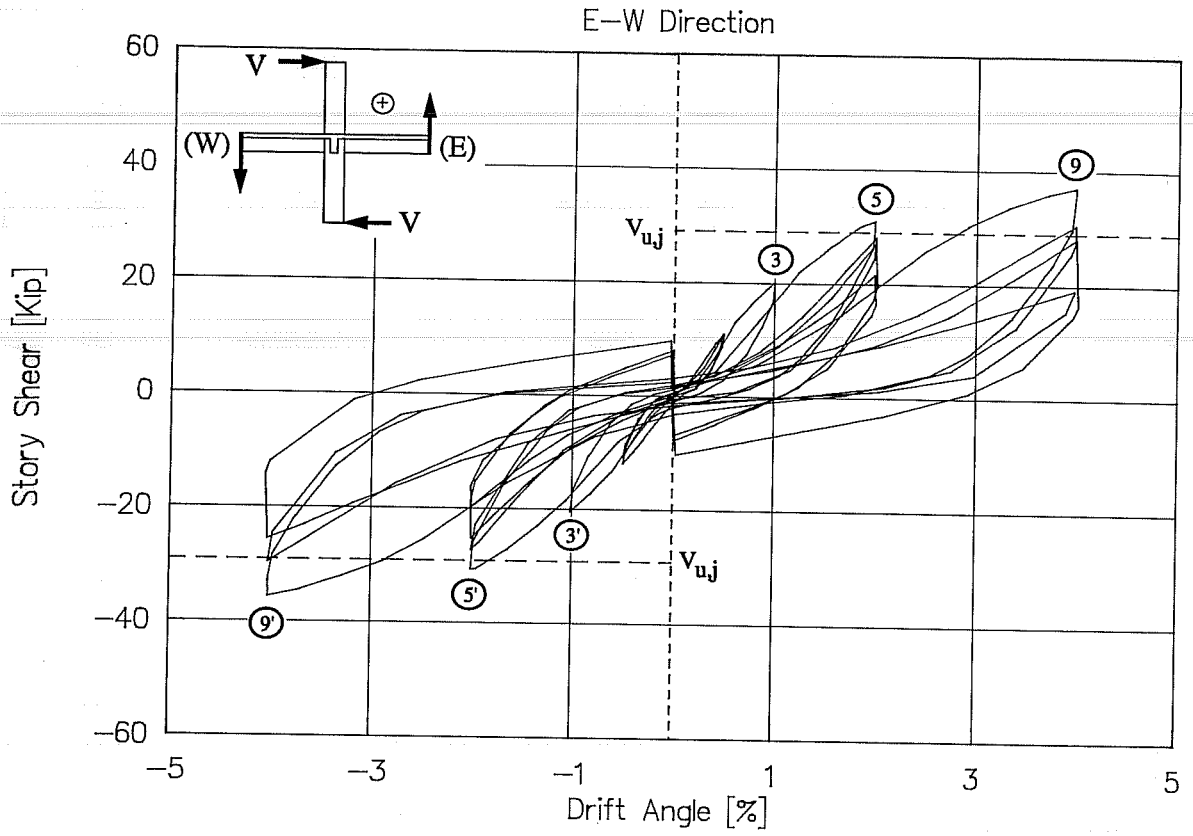

Figure 3.16 Specimen RB - Story Shear vs. Drift Angle (E-W Direction)

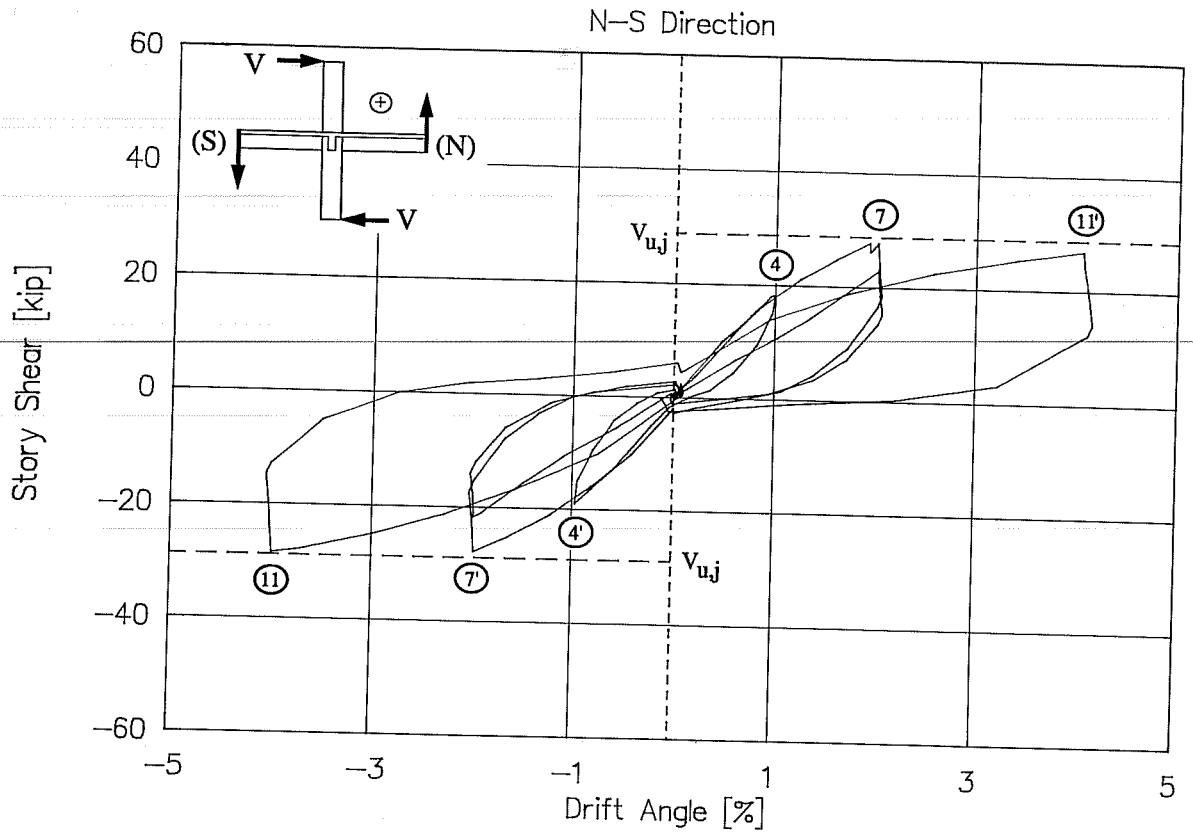

Figure 3.17 Specimen RB - Story Shear vs. Drift Angle (N-S Direction)

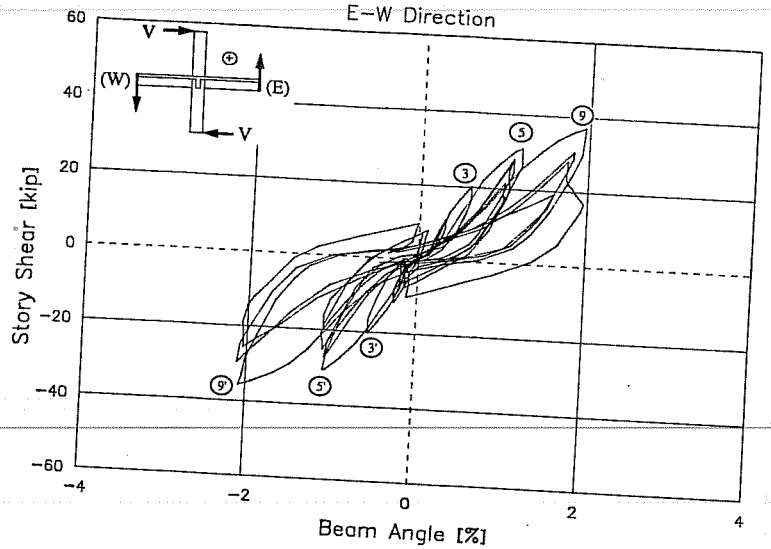

Figure 3.18 Specimen RB - Story Shear vs. Beam Angle (E-W Direction)

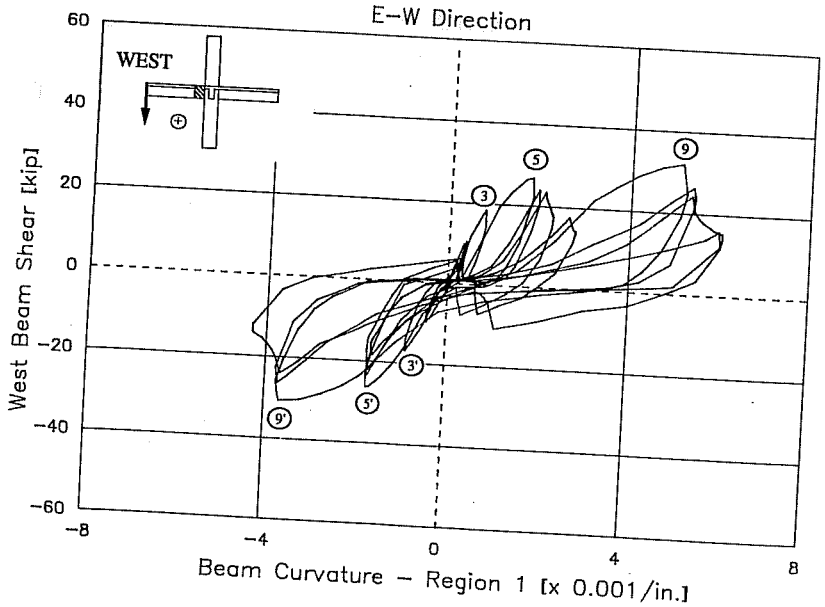

Figure 3.19 Specimen RB - West Beam Curvature - Region 1

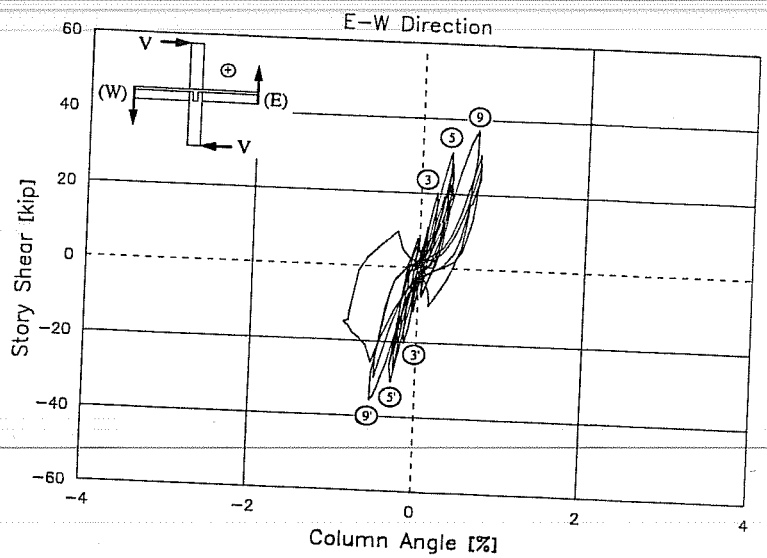

Figure 3.20 Specimen RB - Story Shear vs. Column Angle (E-W Direction)

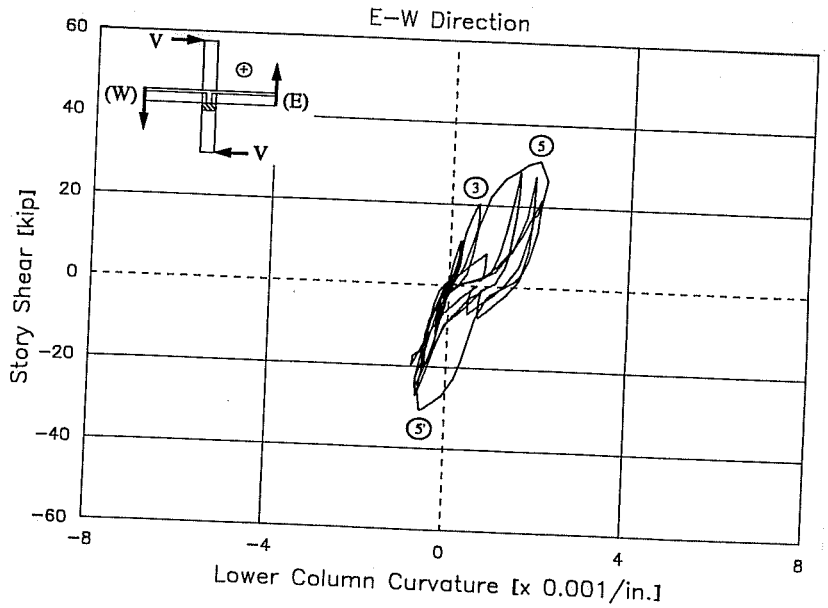

Figure 3.21 Specimen RB - Lower Column Curvature (E-W Direction)

The behavior of columns can be assessed through the column angle curves shown in Figure 3.20. It is evident from the values of θ_c that column contribution to drift angle was very small. Lower column curvatures (Figure 3.21) were concentrated around the joint collar and were smaller than beam curvatures. The upper column showed similar behavior but smaller curvatures were recorded (not presented here). The column faces cracked in flexure early in the test. A column crack formed at the location of the lower steel collar of the joint confinement cage at drifts to 0.5%. Similar cracks formed at this deformation level in all rehabilitated specimens. During cycles 7 and 8, the lower column developed inclined cracks in the northeast and southwest corners which were subjected to the highest compression due to bidirectional loading. During cycle 8, column concrete from the northwest and southwest corners below the beam soffit spalled. In cycles to 4% drift, column cracking was minor (0.002 in.). Column concrete continued to crush at the four corners of the lower column, below the beam soffits, and at the corners of the upper column just above the slab. Joint cracks extended about 8 in. into the column corners, with maximum average widths of 0.06 to 0.08 in.. Concrete damage in the lower column corners next to the joint and bond distress of column bundles in the same zone probably produced the pinching of the column angle and column curvature loops noted in Figures 3.20 and 3.21, respectively.

During cycles to 0.5% and 1% drift (cycles 1 through 4), the slab cracked in flexure in both directions. In cycles 5 and 6, flexural and radial cracks continued extending in top and bottom slab surfaces and beam torsional cracks appeared in the slab. Average slab crack width was 0.08 in. at the column face. First slab concrete crushing occurred in cycle 9 at the E-W column faces. A large crack between the slab and the joint collar was noted. Flexural cracks extended across the entire width in the two slab surfaces. Torsional cracks stopped in the second slab bar. In cycle 11, slab concrete crushed around all the column faces. By the end of the test, considerable crushing and spalling were observed near the joint in the top and bottom slab surfaces. Crushing in the top surface occurred in the concrete between torsional cracks. This type of damage was observed in all the rehabilitated specimens. Concrete in the slab bottom surface next to the column corners was loose. The top slab bars in both directions next to the column separated from the concrete.

Joint performance can be studied through the E-W story shear versus joint shear distortion relation presented in Figure 3.22. The joint distortion loops are symmetrical and nearly linear in the first cycles. The joint showed inclined cracking in the northeast corner as early as cycle 1/pos. Horizontal joint cracks formed at midheight in east and west faces and inclined cracks appeared in north and south faces. In cycle 3, most of the cracking occurred in the joint region. Inclined cracks, up to 0.010 in. wide, formed in the E-W joint sides and were concentrated in the lower half of the joint. Nearly horizontal cracks were noted in the N-S joint sides. During cycle 4 in the N-S direction, inclined joint cracks formed in the east and west sides of the joint and extended to the orthogonal beams as torsional cracks in the two faces of the E-W beams. Vertical joint cracks in north and south faces appeared and were located at midwidth of joint sides. In cycles to 2% drift, considerable strength degradation with increase in joint distortion is noted. Loops also

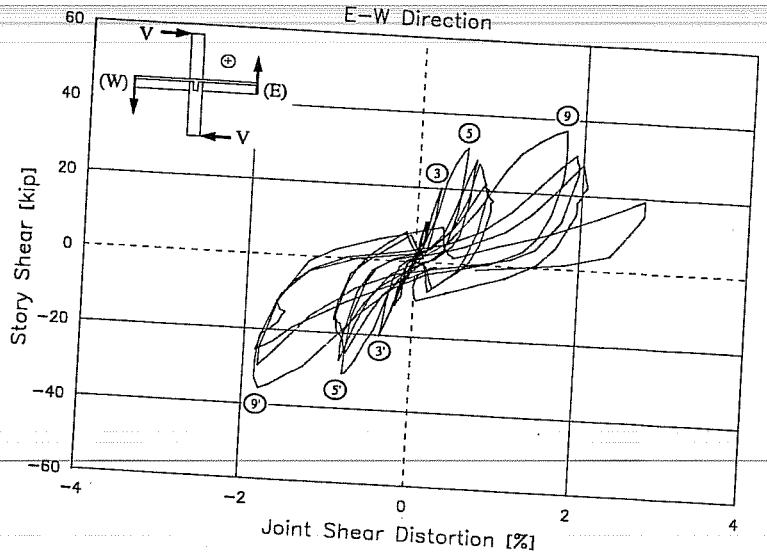

Figure 3.22 Specimen RB - Story Shear vs. Joint Shear Distortion (E-W Direction)

exhibit considerable pinching typical of shear dominated elements. Further deterioration was noted during cycles to 4% drift. Joint distress was severe and joint distortion was quite evident. The steel angle at the northwest joint corner was exposed. The joint distortion increased by a factor of three from cycle 5/pos to cycle 9/pos when the joint failed during cycle 9. After completion of the test, joint cover was easily removed with a chipping hammer but the concrete core seemed sound. It is important to note that no joint transverse steel was provided in the original column core or in the jacketed column. The concrete was assumed to carry the joint shear, and the concrete and column bars were confined by the steel angle in the corners of the jacket (see Figure 2.6).

3.5 SPECIMEN SB

Specimen SB was strengthened by jacketing the column as in specimen RB but there was no damage prior to jacketing. The ratio of calculated column to beam flexural capacities for the E-W direction was 2.68. By comparing tests RB and SB, the influence of damage on the response of the rehabilitated specimen can be assessed.

The final crack patterns are presented in Figure 3.23. The crack pattern in the NE quadrant during cycle 8/pos is shown in Figure 3.24. The hysteretic response for the east-west and north-south components of story shear are presented in Figures 3.25 and 3.26, respectively. Cracks were better distributed than in specimen RB. Most of the damage was concentrated around the joint region. Beam cracking was indicative of beam hinging. Failure of the specimen was due to joint failure after beam hinging. Relative movement between the beam sides and the column jacket was observed, but was less than that noted

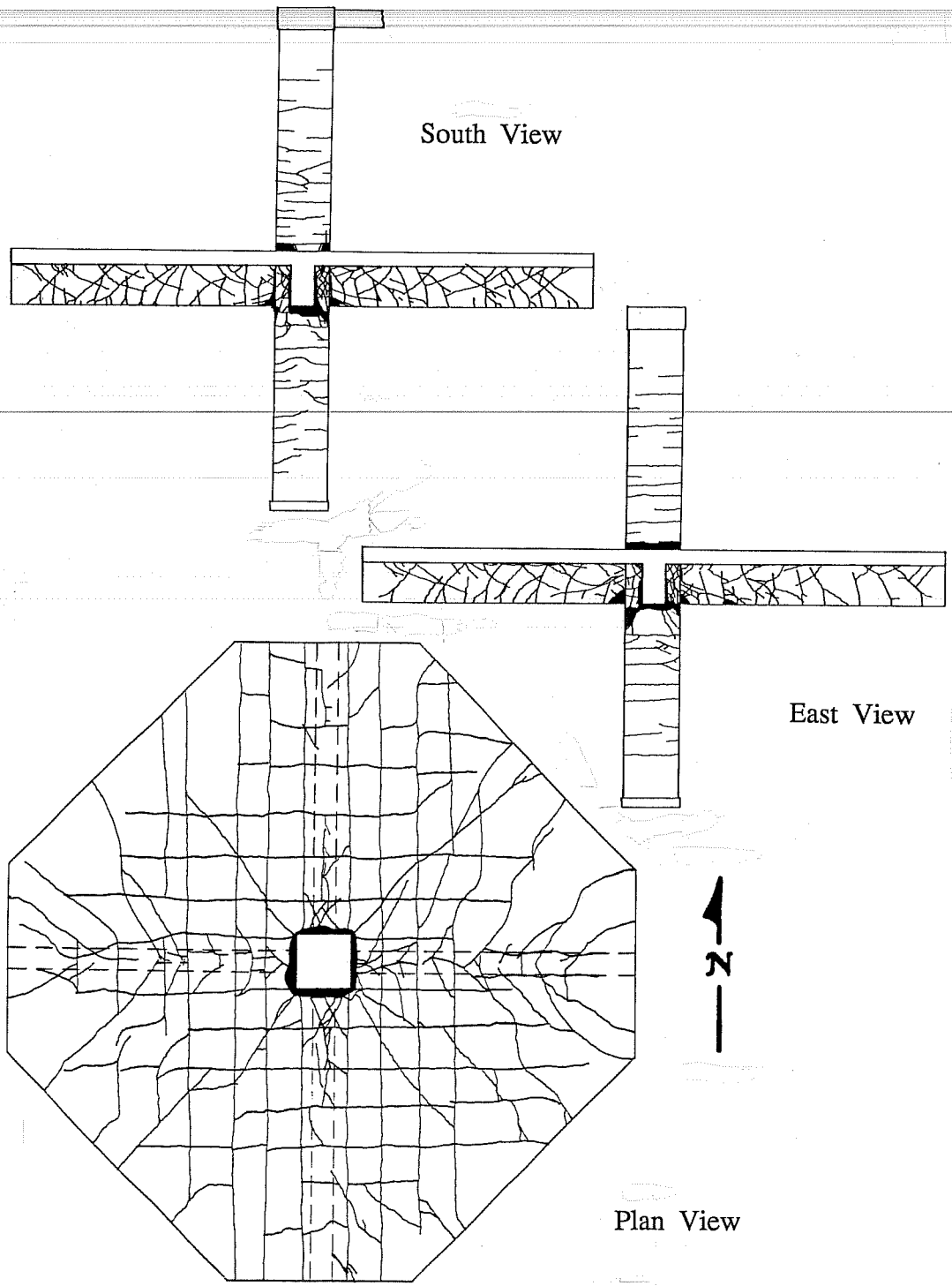

Figure 3.23 Specimen SB - Final Crack Patterns

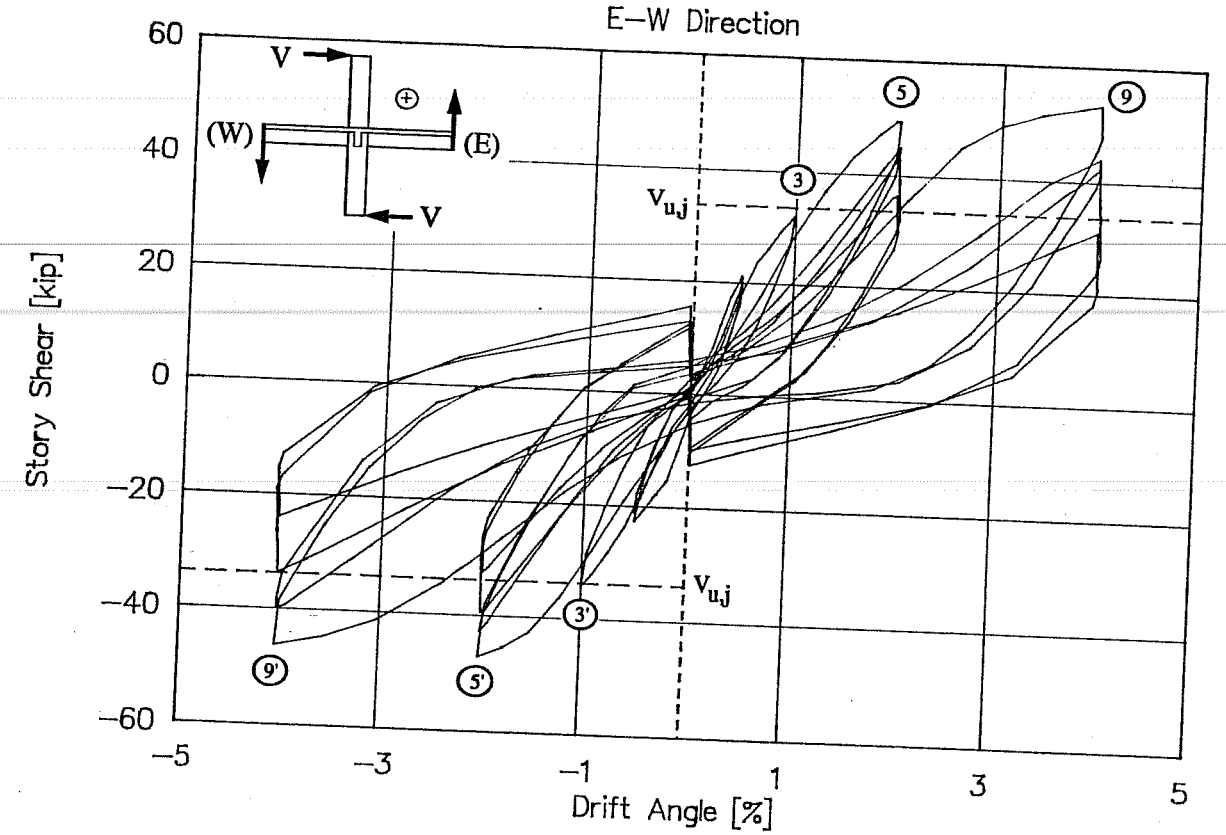

Figure 3.25 Specimen SB - Story Shear vs. Drift Angle (E-W Direction)

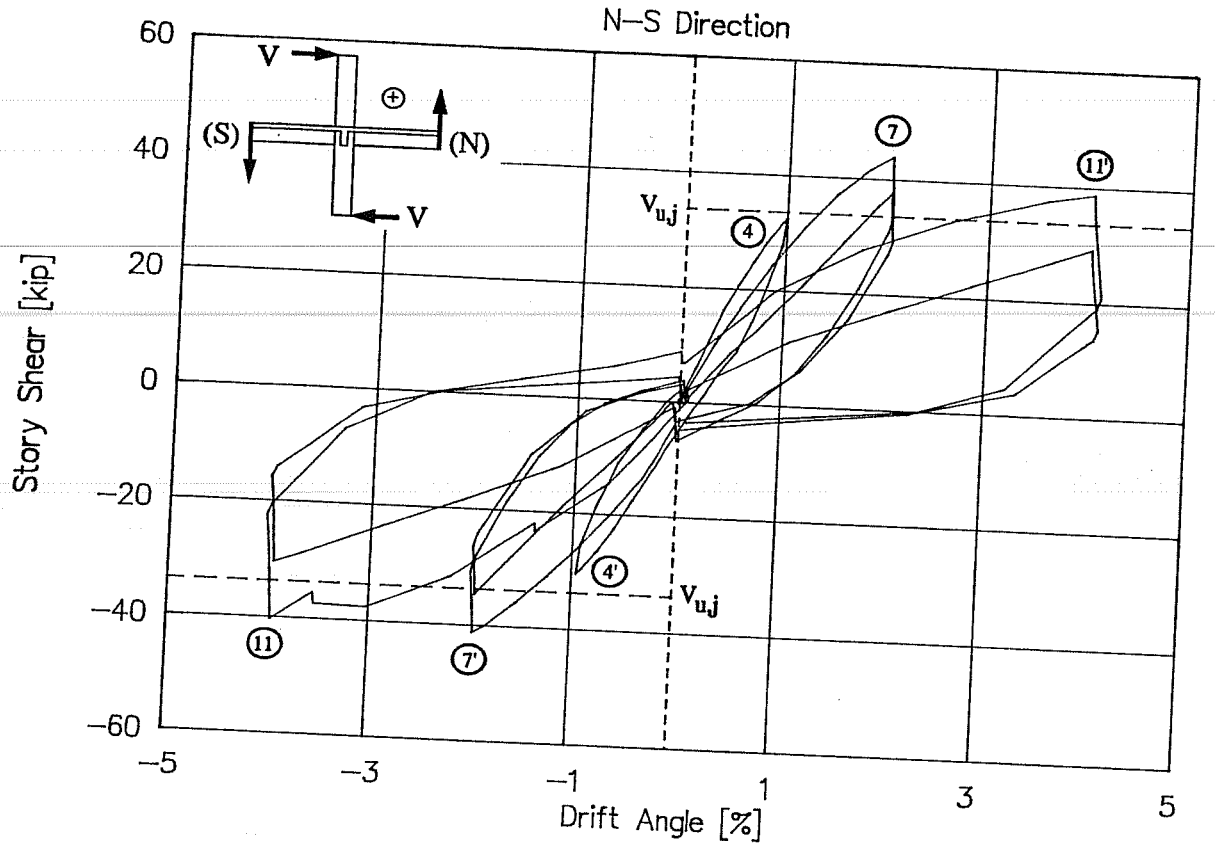

Figure 3.26 Specimen SB - Story Shear vs. Drift Angle (N-S Direction)

cycle 9, when the top and bottom beam reinforcement yielded (see Figure 3.25). Large crack widths in beams and crushing of the slab were noted. Rounding when loading near the peak is also noticed in the beam angle and west beam curvature for Region 1 (Figures 3.27 and 3.28, respectively). Similar curvature relationships were for E, N and S beams (not shown). In general, beam curvatures were stiffer during downward loading. Maximum curvatures of about 0.004 $in.^{-1}$ were recorded after yielding. In subsequent cycles, beam angle and beam curvature show further stiffness degradation and pinching. North-south beams showed larger curvatures than E-W beams and ranged from 0.006 to 0.008 $in.^{-1}$ in cycles to 4%. North-south beam curvatures increased by a factor of two to three from cycles at 2% to cycles at 4% drift. During bidirectional cycles 11 and 12, severe crushing occurred which accelerated the decay in stiffness and energy dissipation characteristics. Beam concrete spalled between the torsional cracks. After the test, N-S beam bottom bars were exposed.

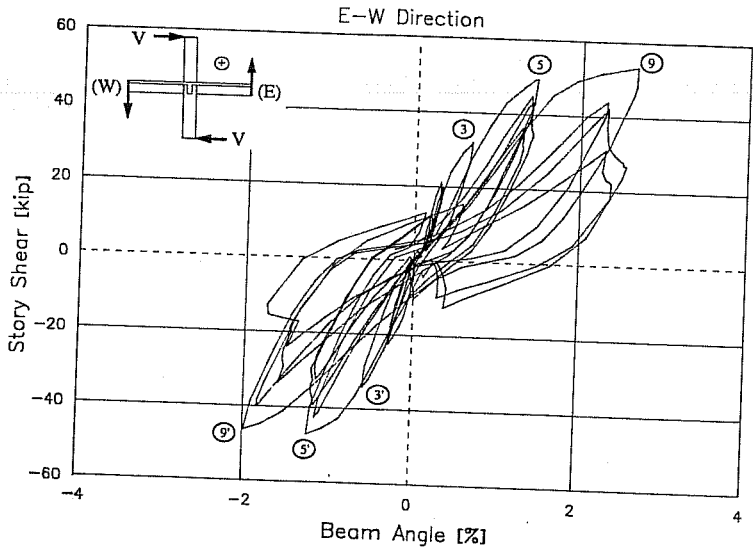

Figure 3.27 Specimen SB - Story Shear vs. Beam Angle (E-W Direction)

Column flexural cracking was minor. Column elastic behavior is evident in the column angle relationship in Figure 3.29 and in the lower column curvature of Figure 3.30. Upper column curvatures showed similar behavior (not presented). The column angles were stable and exhibited strength degradation due to joint distress. No stiffness degradation was noticed. Narrowing of the loops was credited to cracking and crushing of concrete in the corners. Cracking and crushing around the joint collars might have also led to pinching of the curves. In cycles 7 and 8, significant column crack widths (0.040 to 0.050 in.) were recorded around the joint collar. First crushing of column concrete started below the beam soffits in cycle 7/pos. First crushing at upper column corners was noted during cycle 7/neg (see Figure 3.24). In cycles to 4% drift, the column concrete crushed around the joint

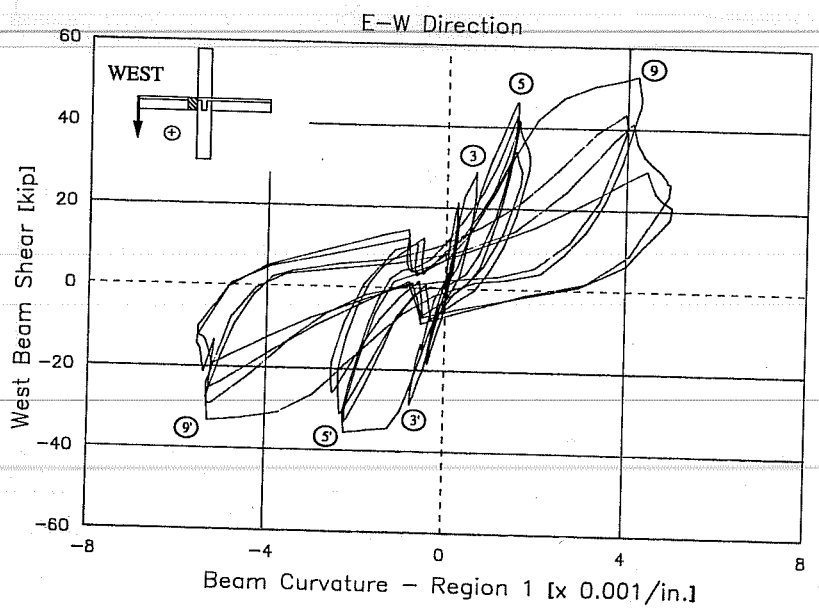

Figure 3.28 Specimen SB - West Beam Curvature - Region 1

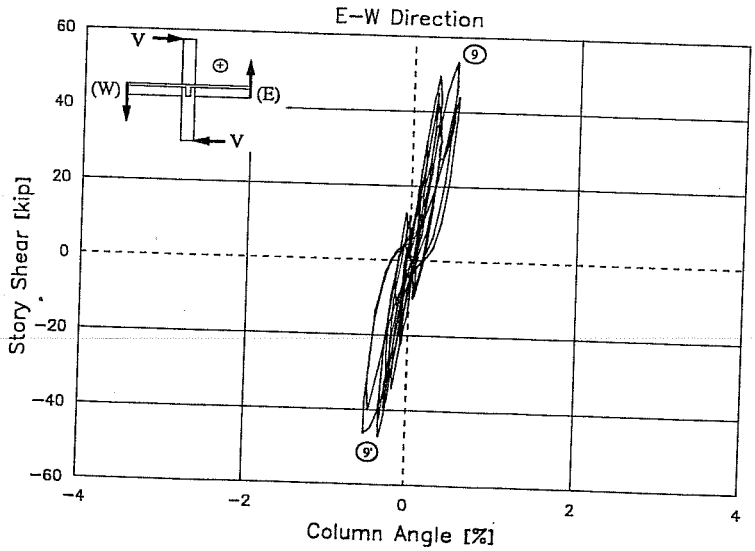

Figure 3.29 Specimen SB - Story Shear vs. Column Angle (E-W Direction)

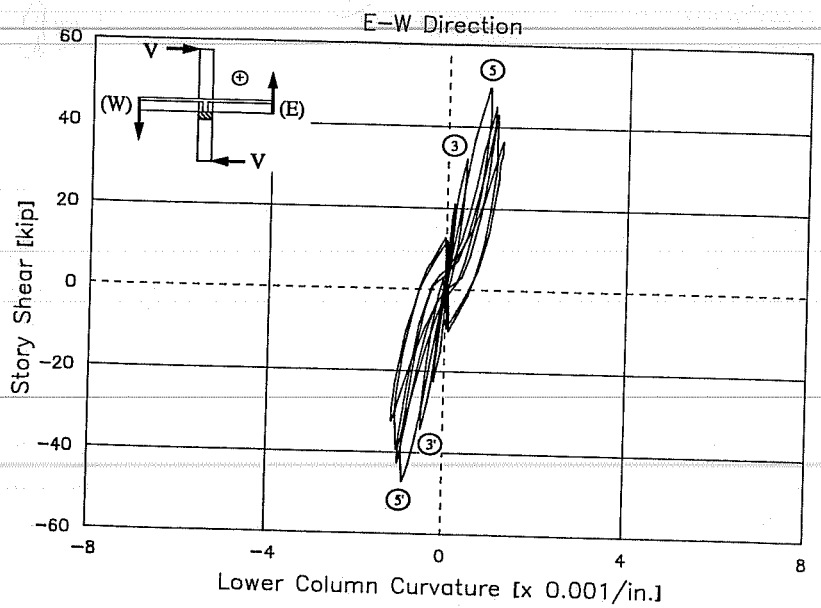

Figure 3.30 Specimen SB - Lower Column Curvature (E-W Direction)

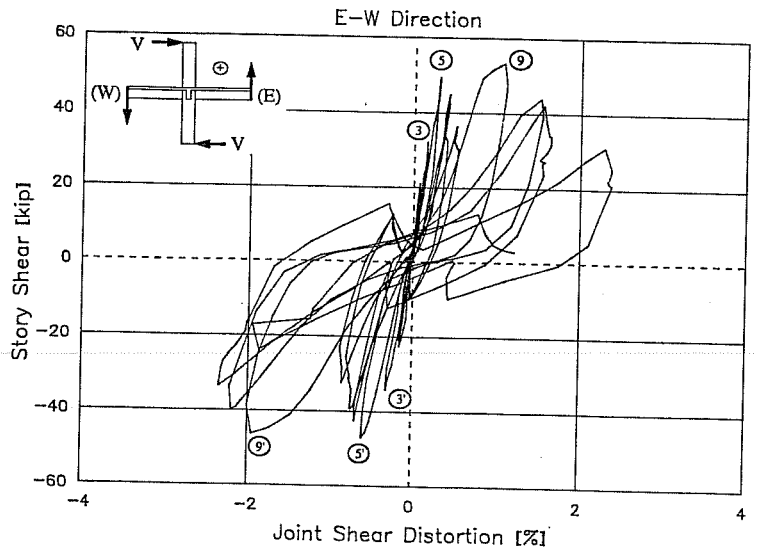

Figure 3.31 Specimen SB - Story Shear vs. Joint Shear Distortion (E-W Direction)

collars and progressed towards the lower column corners. A gap between the slab and the collar was noted in the tension side of the upper column, particularly near the corners.

In cycles 1 and 2, slab flexural cracks formed in both surfaces and coincided with the slab reinforcement. The first slab crack formed at the column face. At 1% drift, slab cracks in both surfaces extended, some of them across the entire slab width and depth. When loading in the N-S direction during cycle 4, flexural cracks coincided with the E-W reinforcement. The first slab radial crack appeared in the SE quadrant when the top slab surface was in tension. The first torsional cracks (cycle 5/pos) formed on top of the N-S beams and ran towards the beam deflected upwards. In cycle 6, slab bars adjacent to the column yielded. Some slab cracks extended the full width of the slab. During bidirectional cycles 7 and 8 new slab radial and beam torsional cracks formed. Radial cracks bisected the NE and SW quadrants when beams in those quadrants were displaced downwards. In the slab bottom surface, radial cracks opened as much as 0.060 in.. In cycles 9 and 10, the crack at the column face had a width of 0.060 in.. First crushing was noted. New cracks on top of the N-S beam formed almost parallel to the beam axis between the second and fourth E-W slab bars. During bidirectional cycles 11 and 12, concrete crushed around the column. Large slab cracks parallel to beam sides were noted in the bottom surface near the column. Radial cracks were formed in the NW and SE quadrants in the two slab surfaces. Similarly to RB, top reinforcement in both directions next to the column was separated from the slab concrete.

Joint behavior can be assessed through the story shear versus joint shear distortion curves presented in Figure 3.31. Joint response was almost linear up to cycle 5. The joint first cracked during cycle 1/neg. After cycle 4, the joint showed extensive inclined cracking, well distributed along the joint height, and one horizontal crack in the E side at midheight. Some joint cracks extended into the E-W beams in the form of torsional cracks and few into the lower column towards the column corner edge. During unidirectional cycles 5 and 6, inclined joint cracks extended into the lower column 7 to 15 in. below the beam soffit. The extension was more noticeable in the north and south joint sides. In cycles to 2% drift, the joint distortion loops widened and the strength decayed due to shear degradation of joint concrete. The N-S component of joint distortion showed similar behavior but distortion was smaller (not presented here). Failure of the joint was evident in cycle 9 in which large joint bulging and severe crushing and spalling were observed. In subsequent cycles, joint cover was severely cracked and at the NW corner spalling was observed. When loading, bending of the joint steel angles could be seen. The effect of bidirectional cycles on the response diagrams was more noticeable during cycles 11 and 12 because the drop of the story shear was larger than during cycles 7 and 8. After the test, the joint cover was loose but no spalling penetrated into the core. Joint steel angles and some column bundled bars were observed to be separated from the column core. The joint steel angles and the lower collar in the north face were removed (Figure 3.32). Concrete between the steel angle and the bundle was cracked. The lower joint collar had a deflection caused by bearing of the beam on the collar under downward displacements.

3.6 SPECIMEN SD

Column longitudinal reinforcement in the jacket consisted of continuous bars distributed around the perimeter. The existing structure was undamaged prior to jacketing. The ratio of calculated column to beam flexural capacities for the E-W direction was 2.65. Results from test SD are useful to compare the effect of bundled and distributed reinforcement on the behavior of the subassemblages. The test was terminated after cycle 11. The specimen was severely damaged and had lost considerable strength.

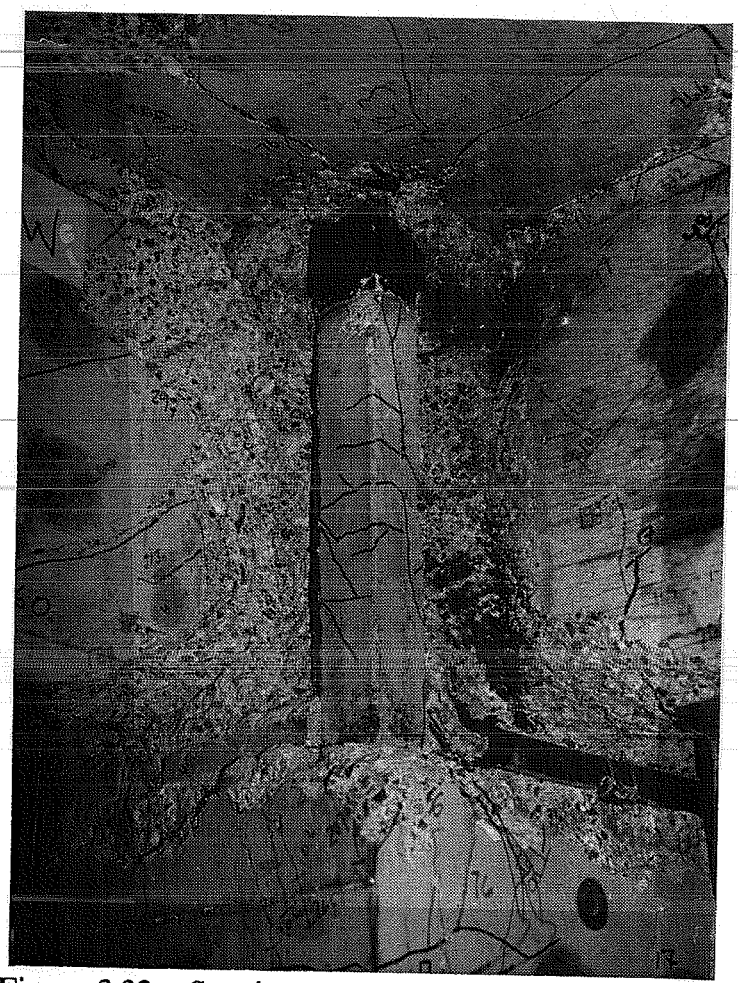

Figure 3.32 Specimen SB - NW Quadrant After Removal of Joint Steel Angle

Final crack patterns for specimen SD are shown in Figure 3.33. The crack pattern of the SW quadrant in cycle 7/neg is presented in Figure 3.34. The story shear versus drift angle relations for the E-W and N-S directions are presented in Figures 3.35 and 3.36, respectively. Specimen SD had fewer beam cracks but they were wider than in the beams of SB. Concrete crushing in the beams was more extensive than in SB and the slab was less damaged. Specimen SD had more and wider joint cracks. Beam hinging was obvious. East-west beam crushing into the joint was more extensive than N-S beam crushing. The upper and lower columns showed almost no concrete distress. No sign of delamination between the column concretes was found. E-W and N-S top slab bars adjacent to the column separated from the concrete. The hysteresis diagram was characterized by stiffness degradation, loss of strength, and pinching of the loops, at 2% drift and especially during cycles to 4%. The response was governed by the most stressed elements, namely the beams and joint. Slab bars, and top and bottom beam reinforcement yielded in cycle 5. In subsequent cycles to 2% drift, the hysteresis diagram showed degradation of stiffness and strength associated with large crack openings, beam crushing and joint distress (Figure 3.35). At 4% drift, the joint was the most damaged element and failed in shear compression during cycle 9. The strength decay was due mainly to joint shear degradation. The response in both directions showed ductile behavior associated with the formation of beam hinges. The predicted capacity was almost equalled in cycles to 1% drift in the two loading directions (cycles 3 and 4). Nearly all

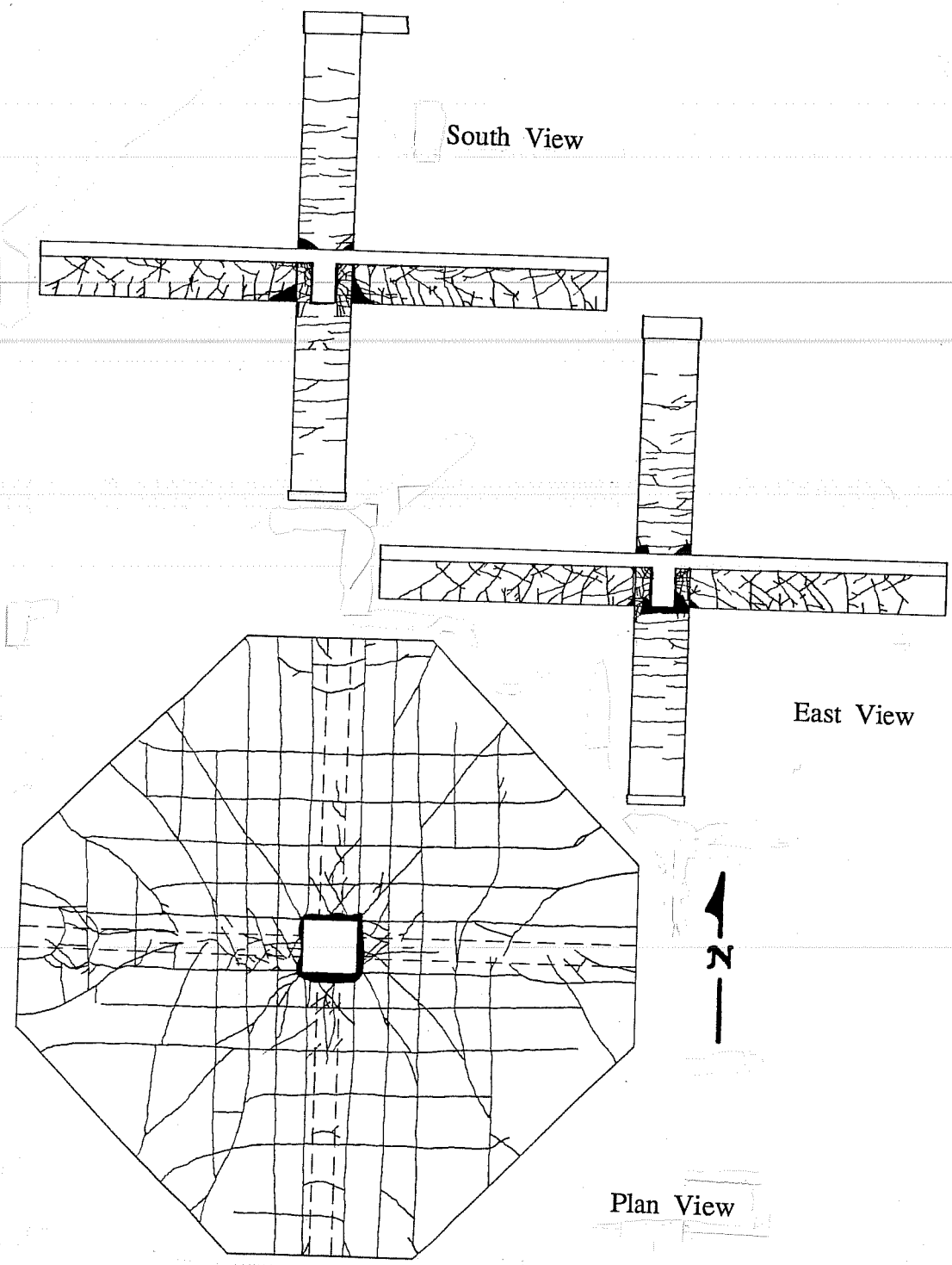

Figure 3.33 Specimen SD - Final Crack Patterns

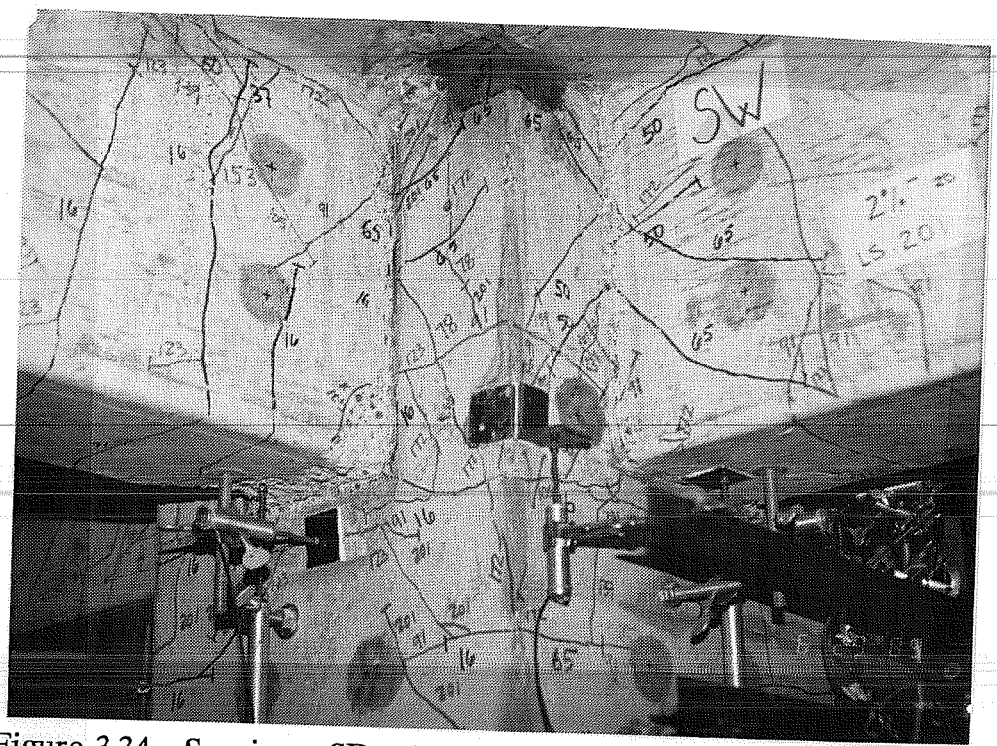

Figure 3.34 Specimen SD - Crack Pattern SW Quadrant Cycle 7/neg

subsequent story shears were above the calculated capacity (Figures 3.35 and 3.36). In cycle 9, the maximum measured E-W story shear surpassed $V_{u,j}$ by 45%.

The behavior of the beams can be evaluated through the beam angle and west beam curvature for Region 1 (Figures 3.37 and 3.38, respectively). Similar graphs were plotted for other beams (not shown). Beam angle curves and beam curvatures were almost linear up to cycle 3. During cycles 1 and 2, E-W beams cracked in flexure. Beam cracks adjacent to the column (3 to 4 in. away from the face) extended the depth of beam web. In cycle 3, flexural and inclined cracks extended. North-south beams cracked in torsion. When loading in cycle 4, flexural cracks formed in the N-S beams and torsional cracks in the E-W beams. In cycle 5, beam angle and beam curvature loops widened after yielding of the slab and beam bars. Crack openings up to 0.007 in. were recorded. North-south beam torsional cracks extended up to 20 in. from the column face and generally stopped at a section corresponding to the location of the second E-W slab bar. During bidirectional cycles, most of the damage occurred in the N-S direction. Concrete in the north-south beam crushed in the bottom faces between the torsional cracks. Top and bottom beam reinforcement yielding is evident in the beam angle and west beam curvature curves for cycle 9. In the east-west beams bottom cover crushed and spalled, exposing the bottom reinforcement near the column. Beam crack widths of 0.060 in. were recorded. Torsional cracks in the N-S beams opened 0.030 in.. Further cycling to 4% drift steadily narrowed the loops. Relative movement between beam and column jacket caused crushing of the concrete and a crack opening of 0.040 in.. In cycle 11, E-W beam crushing penetrated into the column core.

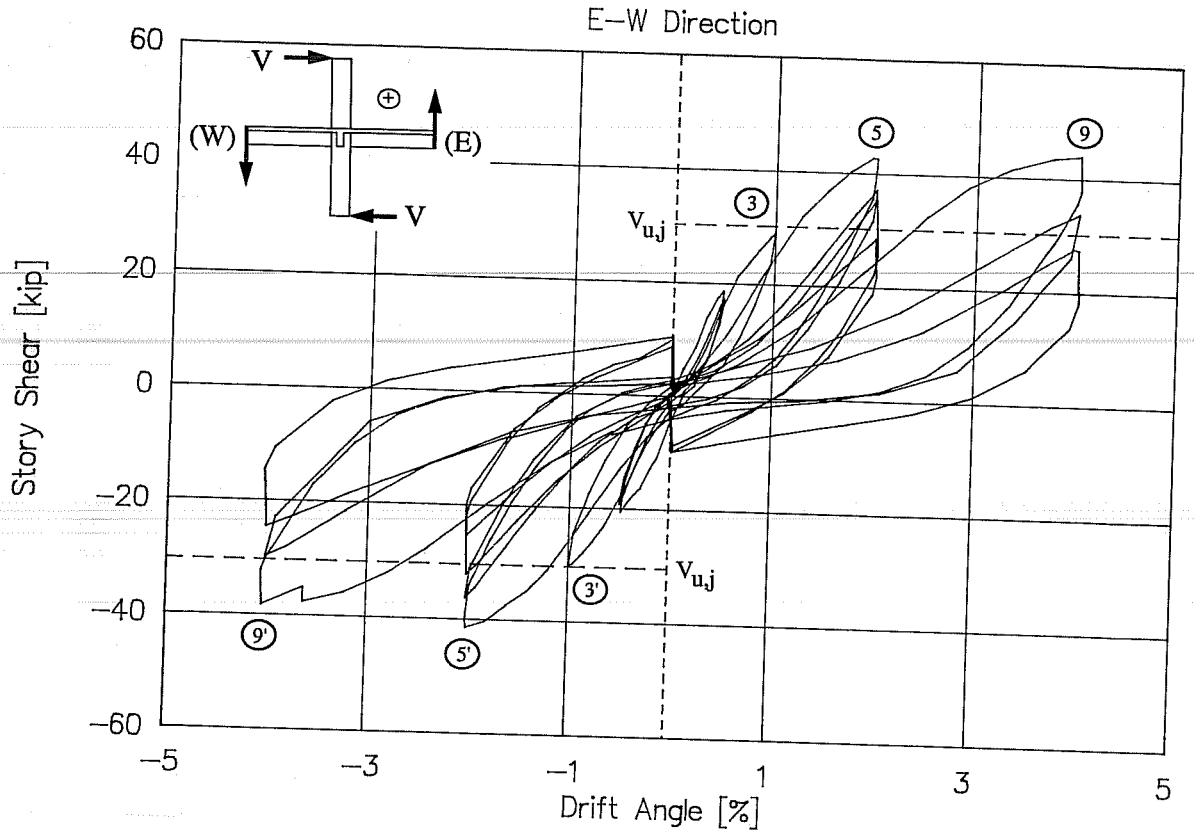

Figure 3.35 Specimen SD - Story Shear vs. Drift Angle (E-W Direction)

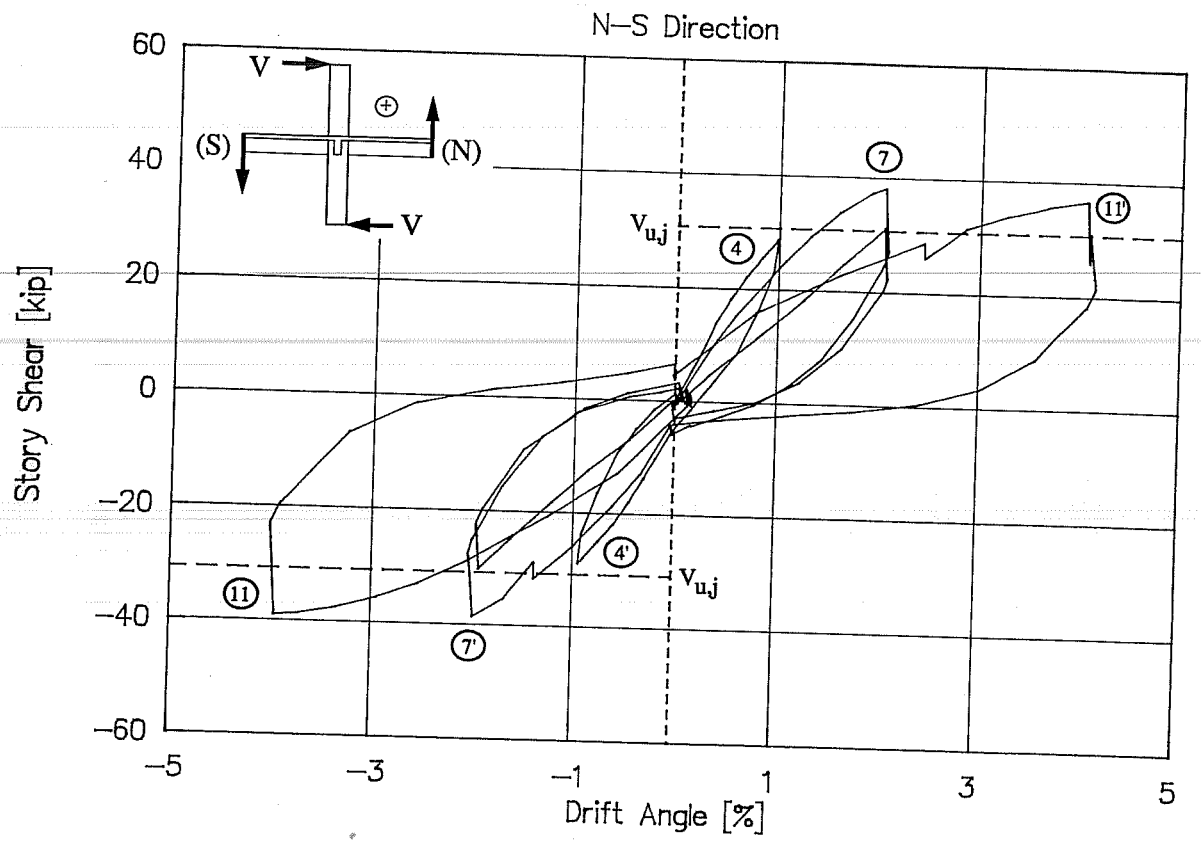

Figure 3.36 Specimen SD - Story Shear vs. Drift Angle (N-S Direction)

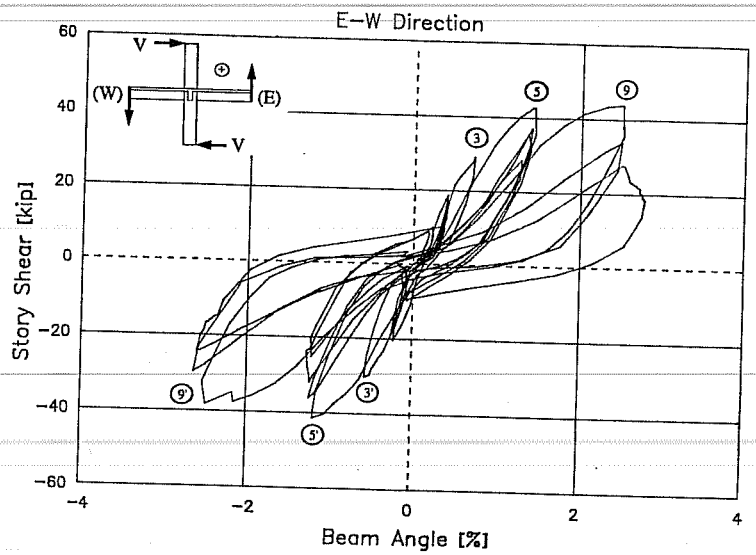

Figure 3.37 Specimen SD - Story Shear vs. Beam Angle (E-W Direction)

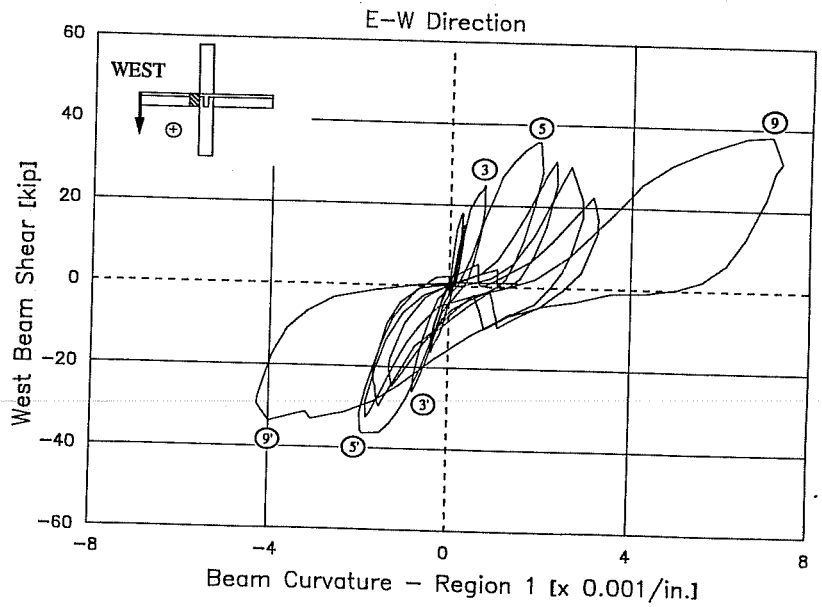

Figure 3.38 Specimen SD - West Beam Curvature - Region 1

After the loose concrete was removed, bottom bars were partially exposed in the four beams next to the column. Maximum curvature in the north beam was about 0.007 $in.^{-1}$ and 0.006 $in.^{-1}$ in the south beam. Beams of specimen SD had larger curvatures than SB at the same load level (see Figure 3.28).

The column angle was much smaller than the beam angle consistent with minor column distress (Figure 3.39). The column angle was nearly linear throughout the test and increased less than the imposed drift angle. During cycles 7 and 8, column concrete crushed and spalled around the lower joint collar and in the NE and SW corners below the beam soffits. At the end of the test, the column bars placed against the beam sides were exposed in the lower half of the joint. The lower column curvature for the E-W direction is presented in Figure 3.40. Upper column curvature showed comparable response. Column curvatures were slightly higher than those for SB at the same load level (see Figure 3.30). Similarly to RB and SB, column curvatures were smaller than beam curvatures.

In cycles 1 and 2, slab cracks formed in the region of higher bending moment following the N-S reinforcement. Only the cracks at the N-S column faces extended the full slab width. During cycle 2, bending and radial cracks formed in the slab bottom surface. The slab flexural cracking increased and extended across the entire slab width in cycle 3. In cycle 4/neg, the first beam torsional crack appeared in the slab. Torsional cracks started at the E-W column faces and propagated towards the south. In cycles 5 and 6, flexural cracks extended and some reached the free edges. Torsional cracks formed on top of the N-S beam. Slab concrete crushed at the E face of the column. During bidirectional cycles 7 and 8, radial cracking formed in the slab top surface along the NE - SW diagonal. After yielding of the slab and beam bars in cycle 9, there was additional concrete crushing in the slab at the east and west column faces. Large crack openings at the column faces were measured (0.030 to 0.040 in.). The first three flexural cracks at each side of the E-W column faces extended the entire slab width. New radial cracks in the bottom surface appeared. Splitting cracks developed in the top surface of the E-W beam during cycles 9/neg and 10/pos.

Up to cycle 3, the joint behavior was linear as illustrated in the joint shear distortion graph (Figure 3.41). The first joint crack formed during cycle 3/pos in the southwest corner and by the end of the cycle, inclined cracking was noted in all four corners of the joint and was well distributed along the joint height. The first horizontal joint crack appeared at midheight in the east face of the SE corner during cycle 4/pos. Yielding of the beam reinforcement in cycle 5 increased the shear stresses applied to the joint. The joint distortion showed nonlinear behavior. Joint distortion increased with cycling while the strength decayed. In cycles 7 and 8, a number of steep joint cracks formed in the lower half and extended about 8 in. into the lower column. These cracks reached the edge of the column corner (see Figure 3.34). The cover at the SW joint corner was loose. In unidirectional cycles to 4% drift, new vertical, horizontal and inclined cracks appeared and were well distributed around all joint sides. Cracks widths ranged from 0.002 to 0.040 in., and the joint cover was loosened. During cycle 11, considerable crushing and spalling were

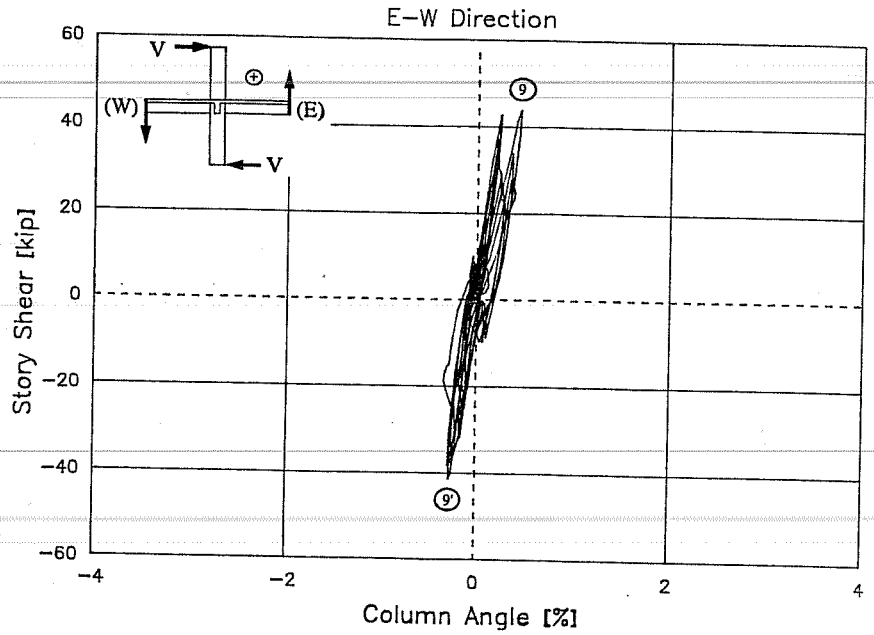

Figure 3.39 Specimen SD - Story Shear vs. Column Angle (E-W Direction)

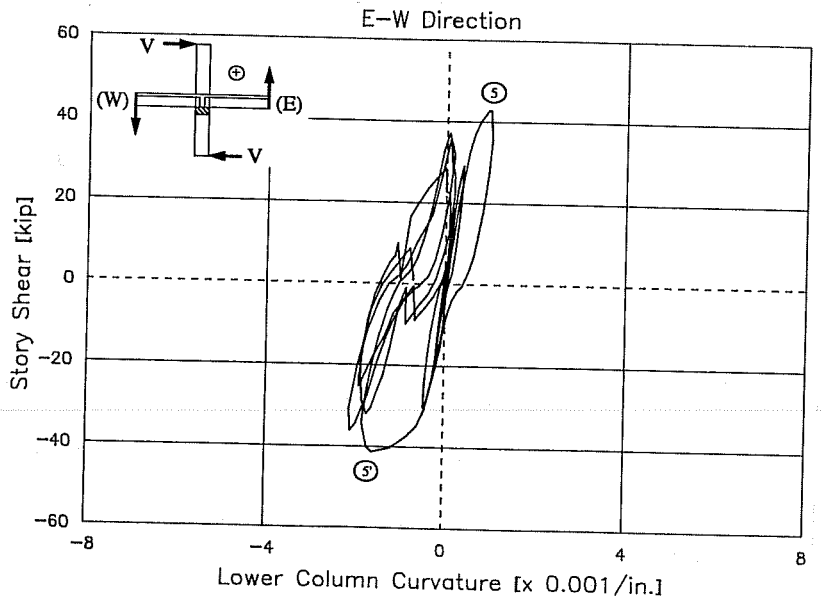

Figure 3.40 Specimen SD - Lower Column Curvature (E-W Direction)

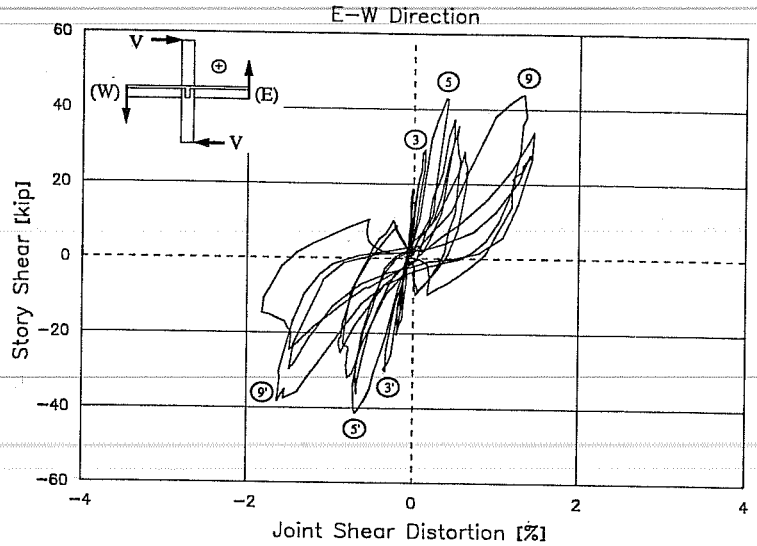

Figure 3.41 Specimen SD - Story Shear vs. Joint Shear Distortion (E-W Direction)

observed. The cover of the NW joint corner spalled. A 3/4 in. gap between the slab and the upper steel collar was noted near the column corners. After the test, loose concrete was removed. Although the steel angle in the NW corner was bent, column bar buckling was not observed. The steel angles at the north side were removed. Concrete between the angle and the corner bar was cracked. In the NE corner, concrete in the lower half was loose (Figure 3.42). East-west joint sides were more damaged than N-S faces. Column bars and cornerties in the E-W sides were exposed. However, no evidence of bond distress was noticed. The strap was bent in the same fashion as in SB. Comparison of joint shear distortions measured in specimens SB and SD (Figures 3.31 and 3.41, respectively), at the same load level and load cycles, shows that the joint of SD was more flexible. The layout of the column reinforcement and the concrete strength might have contributed to the difference. It is interesting to note that joint shear distortion in the N-S direction was almost 50% larger than that in the E-W direction. The N-S beam angle was smaller in turn. This observation coincides with less damage noted in the N-S beams throughout the test.

3.7 SPECIMEN SD-B

The specimen was strengthened by jacketing both the column and beams. Column reinforcement (12-#10 bars) was distributed around the perimeter of the column. The beams were jacketed and longitudinal steel was added to increase the bending strength moderately. The ratio of calculated column to beam flexural capacities for the E-W direction was 2.29.

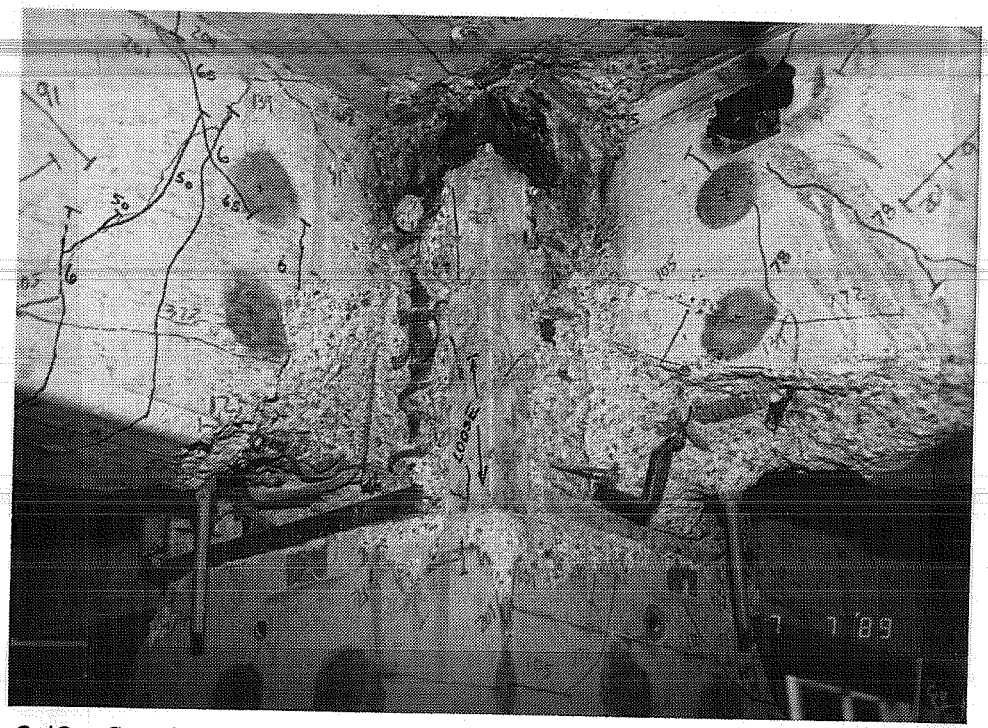

Figure 3.42 Specimen SD - NE Quadrant After Removal of Joint Steel Angle

Final crack patterns are presented in Figure 3.43. The crack pattern of the NE corner in cycle 8/pos to 2% drift is shown in Figure 3.44. The story shear versus drift angle relations for the E-W and N-S directions are shown in Figures 3.45 and 3.46, respectively. The specimen showed severe distress around the joint region. Torsional cracking and crushing of beams were particularly noticeable. Cracking was characteristic of beam hinging. The E-W beam cracked at the column faces, but the column remained essentially undamaged. No indication of concrete delamination between the jackets and original concrete was found. During the rehabilitation process, perforations in the slab along the beam edges were made to place the concrete for the beam jackets. No evidence of distress was found around such perforations. In general, the hysteresis diagrams are symmetrical and show considerable stiffness and strength deterioration during cycles to 4% drift angle. Pinching of the hysteresis loops is mainly attributed to joint shear distress, beam torsional damage, large crack openings, and crushing and spalling in beams. The specimen just reached the calculated capacity in the E-W direction. When subsequent cycles were applied at these deformations, the strength decayed below the calculated capacity. In cycle 3, first yielding of the slab reinforcement and jacketed beam bottom reinforcement occurred. In cycle 5, yielding of beam and slab reinforcement continued and first crushing of beam concrete was noted. Stiffness deterioration and pinching of the loops, evident at subsequent cycles to 2%, are the result of the onset of concrete damage. During cycle 9/pos, top and bottom steel in the beams (original and jacket), and in the slab elongated further. The specimen reached the maximum strength with large forces applied to the joint. Joint failure occurred during cycle 9. The story shear decreased 47% between cycles 9 and 12. The

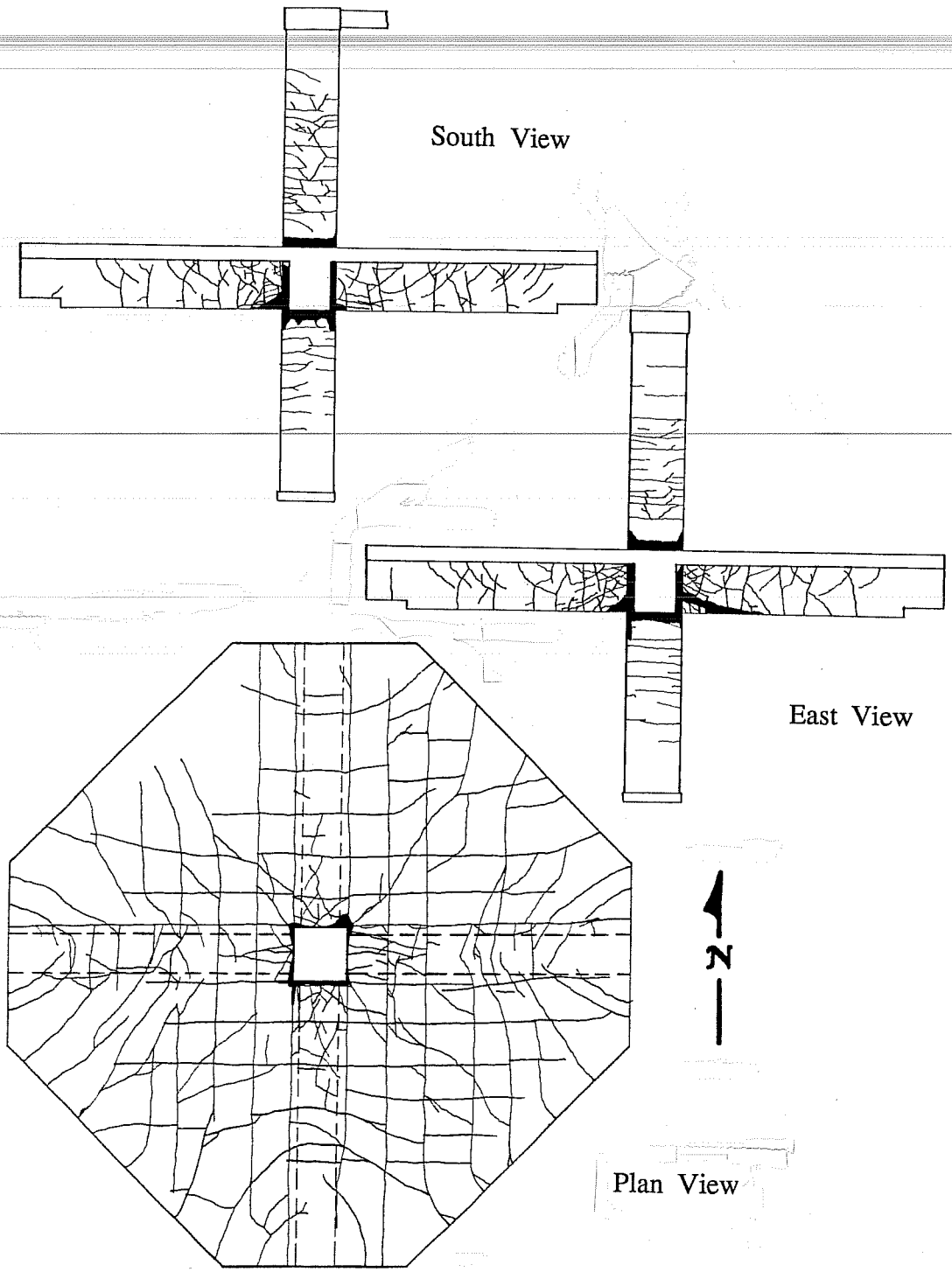

Figure 3.43 Specimen SD-B - Final Crack Patterns

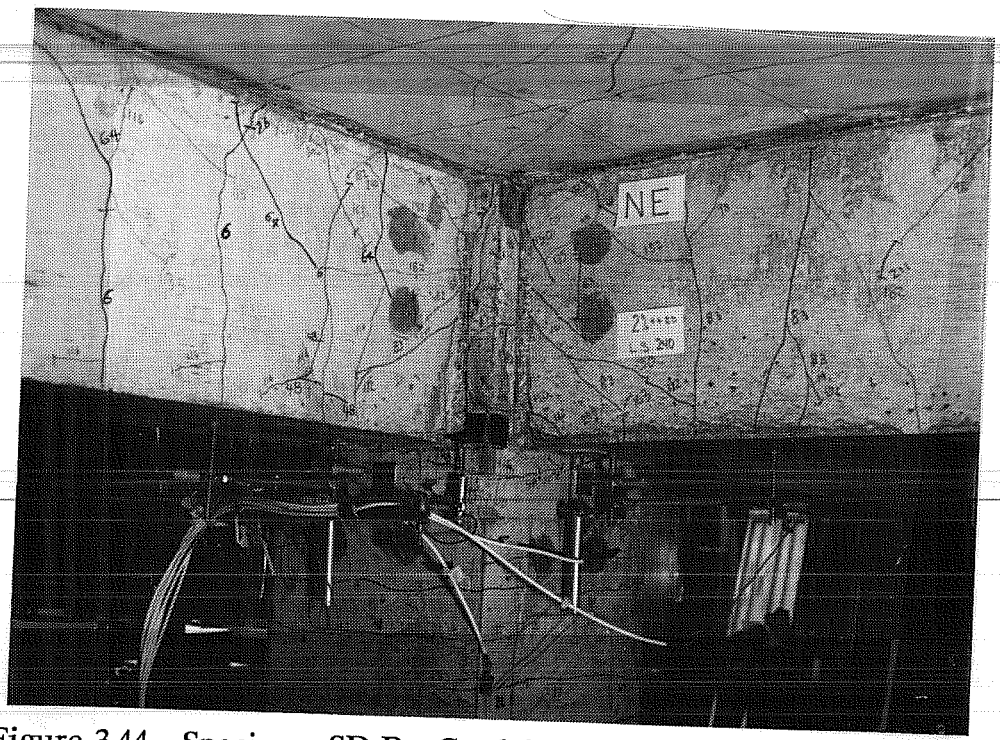

Figure 3.44 Specimen SD-B - Crack Pattern NE Quadrant Cycle 8/pos

response of the subassemblage in the N-S direction (Figure 3.46) showed similar behavior. It is interesting to note that in this direction, the specimen did not reach the calculated capacity $V_{u,j}$. The joint had failed in the E-W direction during cycle 9, so that cracking in the core and alternate loading affected the N-S strength in cycle 11. In this cycle, spalling of joint and the N-S beam cover probably accelerated the strength reduction.

During cycles 1 and 2, beam crack widths of 0.005 in. were recorded. The first torsional crack appeared in the N-S beam in cycle 1/pos. In cycle 3, beam crack openings increased by a factor of three from those recorded in cycles 1 and 2. During cycle 4, the E-W beam showed torsional cracks which stopped at the section corresponding to the location of the second slab bar. Cycle 5 was characterized by yielding of the beam reinforcement and concrete damage. Cycles to 2% drift marked the onset of nonlinear behavior of the beam angle and west beam curvature for Region 1 (Figures 3.47 and 3.48, respectively). For other beams, curves were similar (not shown). Beam cracking was shear dominated. Crack openings of 0.040 in. at the column face and of 0.016 in. at a section 10 in. from the column face were recorded. The west beam bottom cover crushed. The N-S beam cracked considerably in torsion. Torsional cracks started from joint midheight and from the intersection of the beam-column-slab. Some were extensions of joint shear cracks. In cycles 7 and 8, considerable beam cracking and crushing continued (see Figure 3.44). In cycle 9, yielding is evident in the beam angle and W beam curvatures. The curvature loops were stiffer and wider when the beam was displaced downwards (causing tension in the slab). N-S beams were cracked largely in torsion and considerable concrete spalling

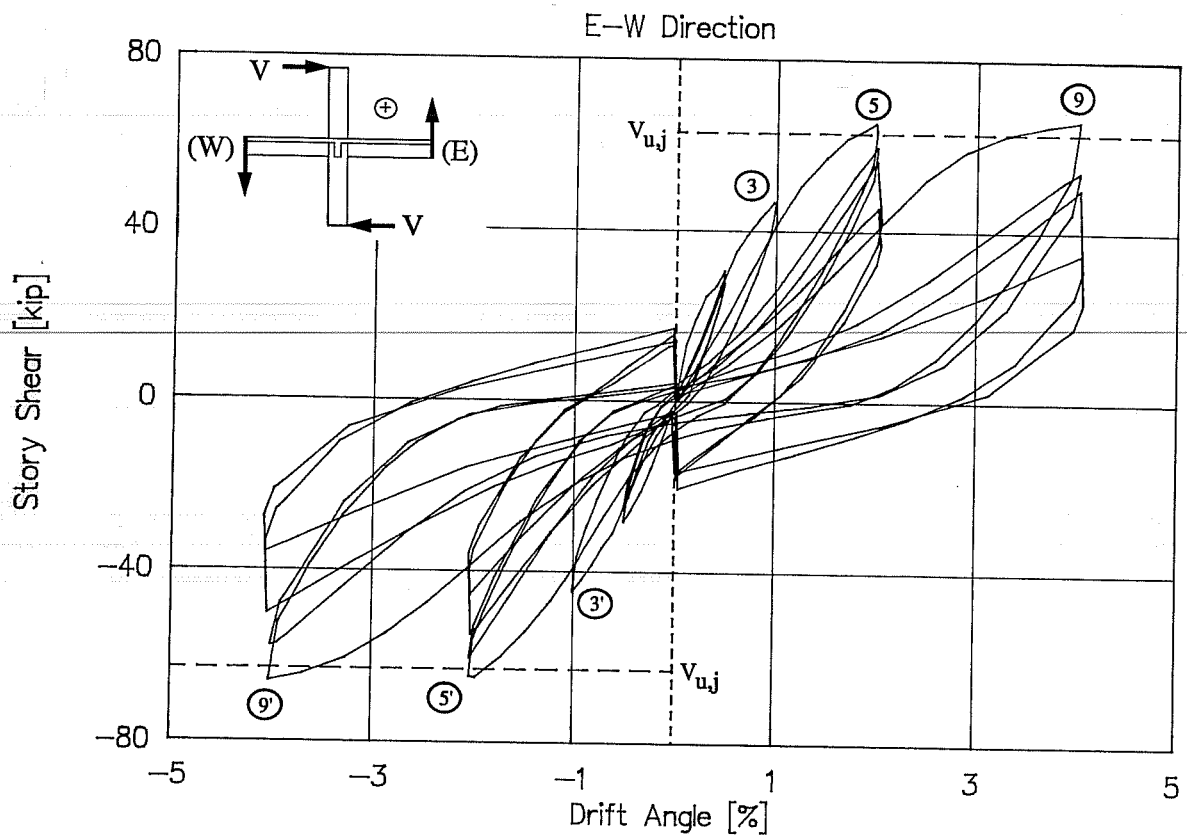

Figure 3.45 Specimen SD-B - Story Shear vs. Drift Angle (E-W Direction)

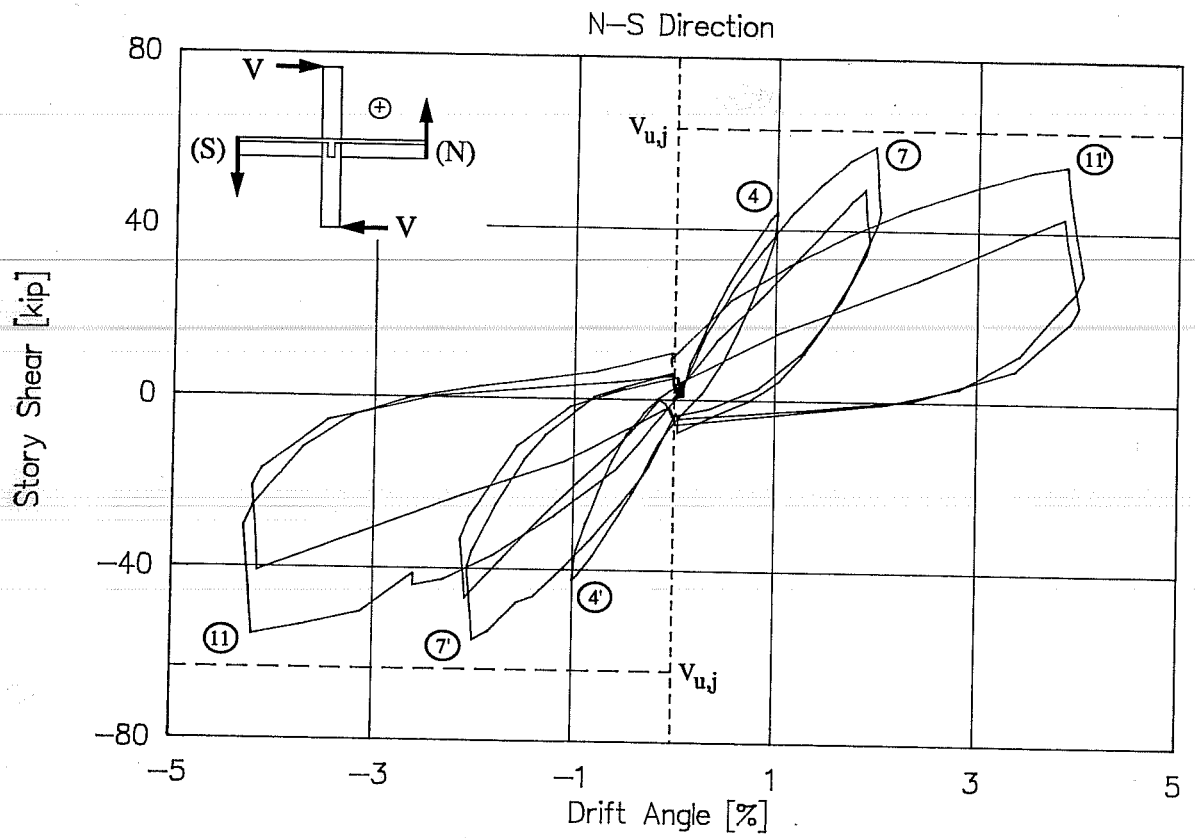

Figure 3.46 Specimen SD-B - Story Shear vs. Drift angle (N-S Direction)

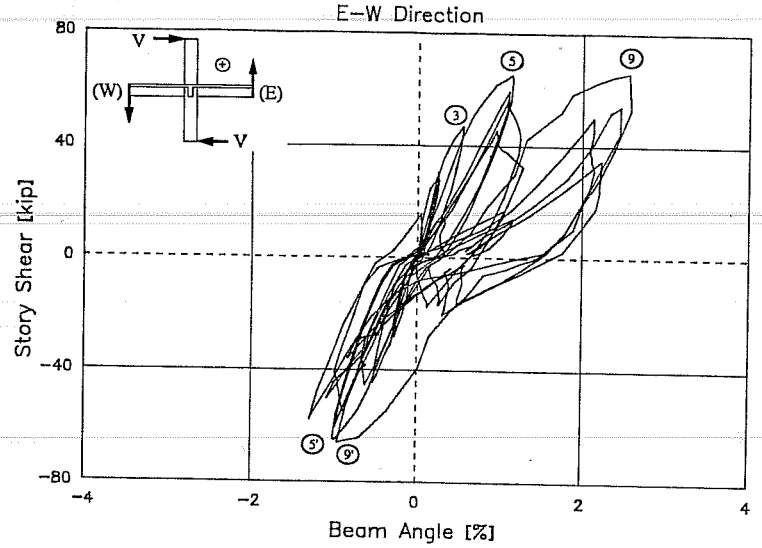

Figure 3.47 Specimen SD-B - Story Shear vs. Beam Angle (E-W Direction)

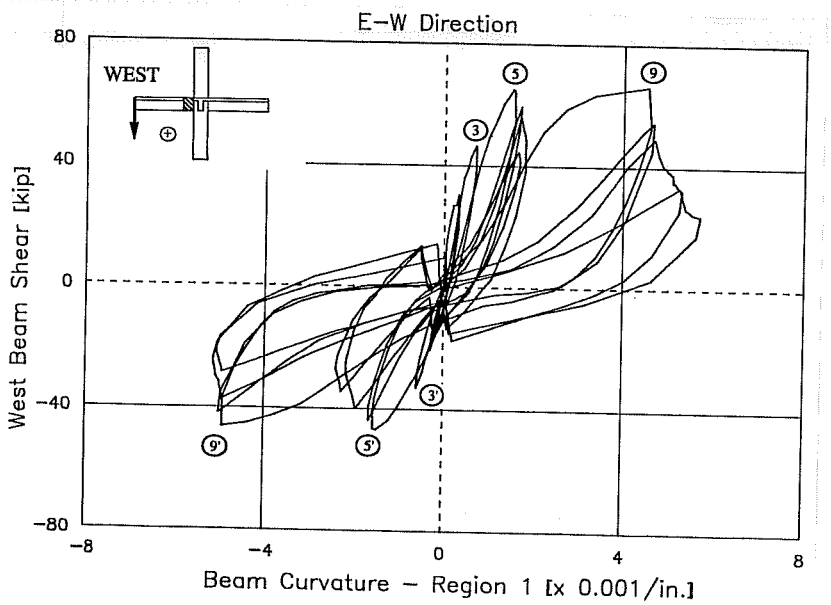

Figure 3.48 Specimen SD-B - West Beam Curvature - Region 1

occurred in a pattern typical of torsional distress. A torsional crack appeared in the N-S beam soffit. In cycles 11 and 12, jacketed bottom beam reinforcement near the column was exposed and significant spalling in the N-S beams continued. Maximum curvatures in the N-S direction were 0.008 $in.^{-1}$ (north beam) and 0.006 $in.^{-1}$ (south beam), which are larger than for E-W beams thus coinciding with the greater amount of beam distress observed. After the test, loose concrete was removed. Bottom reinforcement of the jacketed beam (2-#4

bars) was completely exposed in all beams and bar buckling next to the column face was observed. Damage in the NE corner is shown in Figure 3.49.

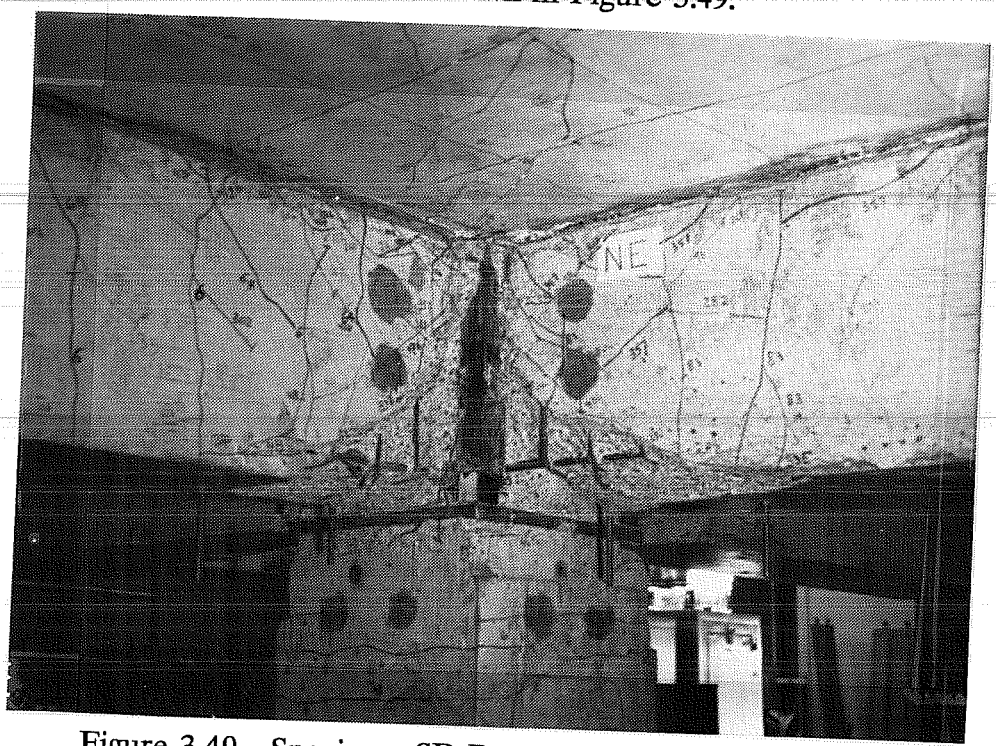

Figure 3.49 Specimen SD-B - NE Quadrant After Test

Similarly to other rehabilitated specimens, the column angle and lower column curvatures showed elastic behavior throughout the test (Figures 3.50 and 3.51, respectively). Column cracks remained very narrow (0.003 in.). In cycles to 2% drift, column crushing occurred first at the upper and lower joint collar in E-W faces. Damage was concentrated around the joint and the upper and lower joint steel flat bars were exposed after cycle 8. The NW column corner crushed below the beam soffit. Some pinching is noted in the column angle curves, especially in the last cycles, due to the damage around the joint region. The column angle increased slower than the imposed drift angle. At the end of the test, upper and lower column corners next to the joint were spalled.

The slab cracked in both the top and bottom surfaces. The first slab crack formed at the column face and extended the entire width. Some cracks extended through the slab depth. Cracks in the bottom surface coincided with the location of the top layer of slab reinforcement. By cycle 4, all cracks had formed along the slab bars. Inclined slab cracks formed near the hydraulic actuators. First beam torsional crack appeared on the top surface of the south beam in cycle 3/neg. and on top of the west beam in cycle 4/neg. In cycles 5 and 6, new flexural cracks formed between the slab reinforcement. A considerable number of inclined slab cracks appeared next to the rams. At the column face, the slab crack was 0.040 in. wide. More torsional cracks formed but did not extend beyond the second E-W

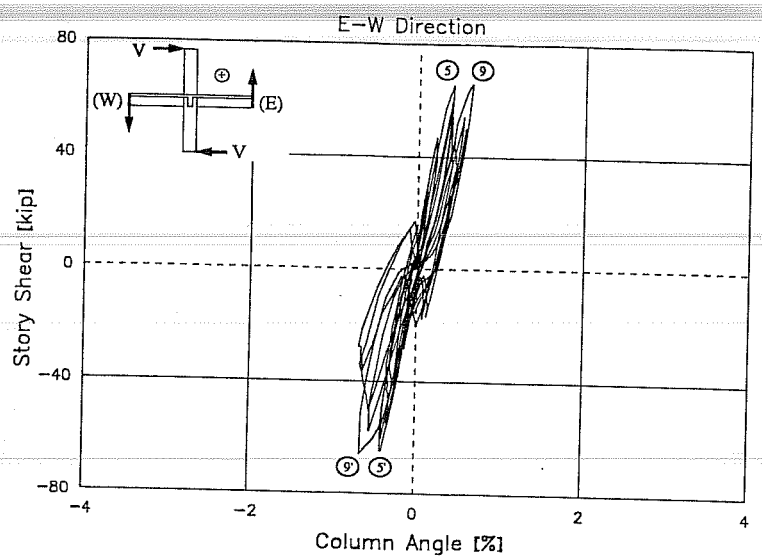

Figure 3.50 Specimen SD-B Story Shear vs. Column Angle (E-W Direction)

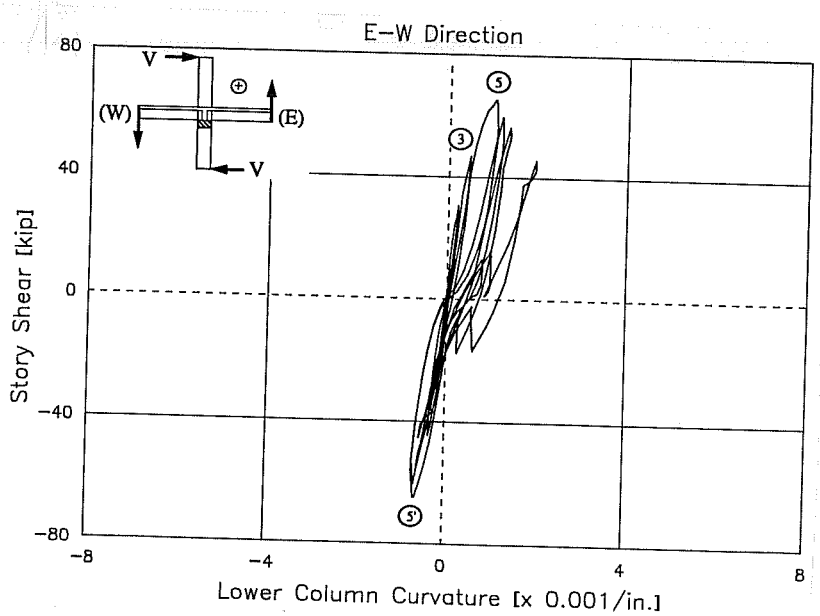

Figure 3.51 Specimen SD-B - Lower Column Curvature (E-W Direction)

slab bar. Radial cracking was developed in the NW and SE quadrants in both slab surfaces by cycle 8. In cycles to 4% drift, the slab exhibited large crack openings in both surfaces. When loading upwards, cracks in the bottom surface opened. Slab concrete crushed at the column faces. On top of the E-W beams, splitting cracks nearly parallel to beam axis were noted. Additional torsional cracks appeared. Some torsional cracks extended beyond the second slab bar. After the test, crushed concrete was removed. Slab damage was

concentrated around the column faces but was less than that in SB. Crushing occurred along the slab bars and between the torsional cracks. Some pieces of concrete were loose.

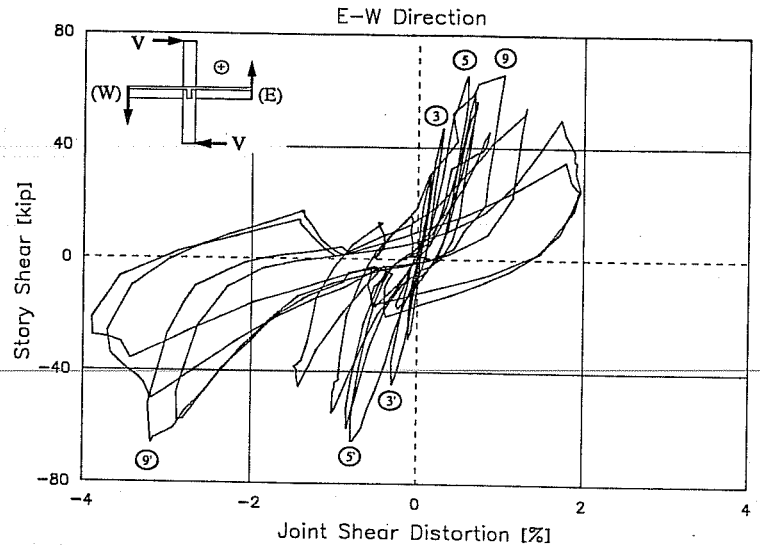

Figure 3.52 Specimen SD-B - Story Shear vs. Joint Shear Distortion (E-W Direction)

Joint first cracked in the SW corner during cycle 2/neg. In cycle 3, well distributed inclined joint cracks were noted. In cycle 4, inclined joint cracks formed in the north and south joint sides and were 0.009 in. wide. Vertical joint cracks near the corner edge in E and W faces were noticed. Cycle 5, in which beam and slab reinforcement yielded, marked the onset of inelastic behavior within the joint (Figure 3.52). It is clear that the loops widened and the strength decayed with cycling. The joint was cracked extensively. Inclined cracks extended into the lower column corners. During bidirectional cycles 7 and 8, joint distress increased and spalling of the cover was observed along almost the entire height of the NW joint corner. Large damage was produced in cycle 9 to 4% drift after beam yielding. Deterioration of the specimen response at this deformation is mainly credited to the joint. Strength decay associated with increasing values of joint distortion is noted in Figure 3.52. Joint concrete crushed and spalled considerably. Crushing along the beam-column interface was noted. Deformation of the joint steel angle was evident and was noted to be compatible with the imposed column curvature. Cycles 11 and 12 were characterized by more joint distress and larger distortions. Joint crushing continued and the steel angles at the four corners were exposed at the end of the test.

3.8 DRIFT ANGLE AND STORY SHEAR ORBITS

The orbits for E-W and N-S drift angle for specimen SB are presented in Figure 3.53. Similar curves are available for the other tests (not shown here). The load history was

displacement controlled. Due to the loading sequence, bidirectional cycles occurred in diagonally opposite quadrants. While the specimen was loaded in one direction, the deformations in the orthogonal direction were kept constant.

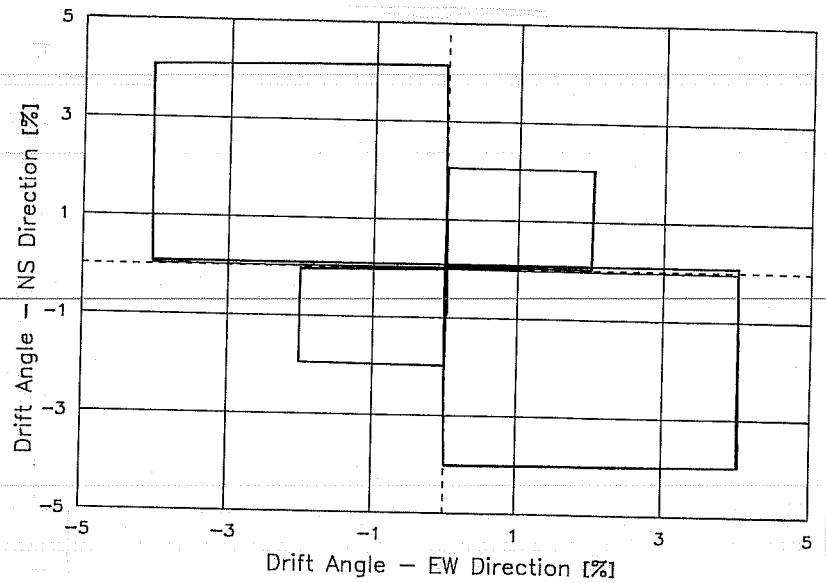

Figure 3.53 Drift Angle Orbits (Specimen SB)

The story shear orbits for specimen SB are shown in Figure 3.54. Story shear orbits of other specimens are similar (not shown). When the specimen was deformed in one direction, the story shear in the other direction changed, even though the deformation was constant. During the second bidirectional cycles, story shear decreased. The reduction was larger in cycles to 4% drift angle (quadrants II and IV).

For illustration purposes, the orbits corresponding to bidirectional cycle 7 are redrawn in Figure 3.55. Before this cycle, the specimen had been subjected to two complete cycles of E-W deformation to 2% drift angle. At the end of cycle 6, the specimen had zero drift angle in the two loading directions. E-W story shear was 4.0 kip and N-S story shear was practically zero (point A'). Cycle 7 started eastward until 2% drift was reached (point B). The peak E-W story shear was 43.1 kip (point B'). Next, the specimen was deformed in the N-S direction to 2% drift angle (point C) and a load of 44.1 kip was reached. As N-S loading was progressing, the E-W story shear gradually decreased to 33.8 kip (point C'). Unloading took place in the east-west direction first (points D and D'). The N-S story shear dropped to 33.5 kip. At zero E-W story shear, the permanent deformation in this direction was 0.8% drift (points X and X'). During unloading in the N-S direction, points D to E, E-W story shear changed by 11 kip. The permanent drift at zero N-S story shear was 0.7% (points Y and Y'). Drift angle orbit for the negative half-cycle followed path EFGHI and the story shear orbit followed path E'F'G'H'I'. Similar features can be observed in the

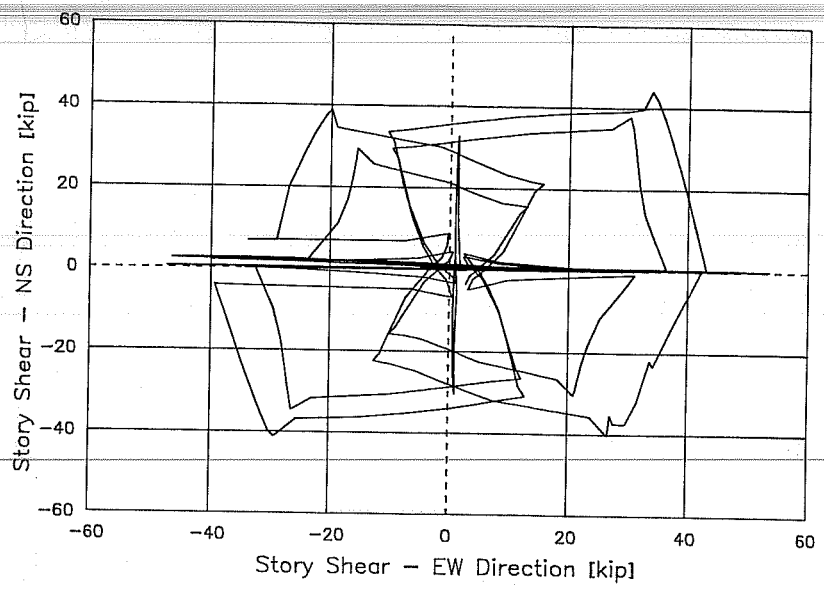

Figure 3.54 Story Shear Orbits (Specimen SB)

response in negative cycles. Bidirectional interaction was evident through vertical segments in the hysteresis response diagrams at peak deformations and at zero drift.

The reduction in story shear in one direction during bidirectional cycles is mainly attributed to the distress and damage produced in that direction during loading and unloading in the orthogonal direction. To illustrate this idea, the initial stiffness of all specimens in the N-S direction was smaller than that in the orthogonal direction. The first three E-W loading cycles caused some damage (flexural column cracks, for example) which affected the stiffness in the N-S direction.

3.9 RESPONSE ENVELOPES AND STORY SHEAR BEHAVIOR

The overall response of the specimens can be compared using envelope curves. The envelopes for positive cycles in the E-W direction are presented in Figure 3.56. Curves for negative cycles are similar due to the symmetric nature of the hysteresis diagram. Specimens maintained their strength even at deformations to 4% drift angle.

The strength of specimen RB was 2.8 times greater at 2% drift and 3.2 times at 4% drift than the strength of specimen O. At 0.5% drift, specimen RB was 2.3 times stiffer than specimen O.

Comparison of RB and SB shows that by jacketing the most damaged elements, the columns and joint, the strength at 2% drift and stiffness at 0.5% drift were 63% and 52%,

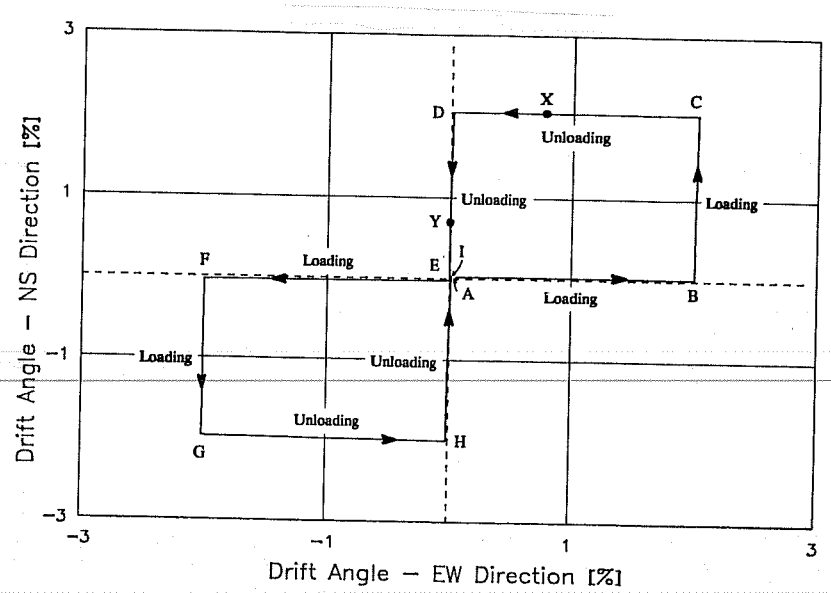

a) Drift Angle

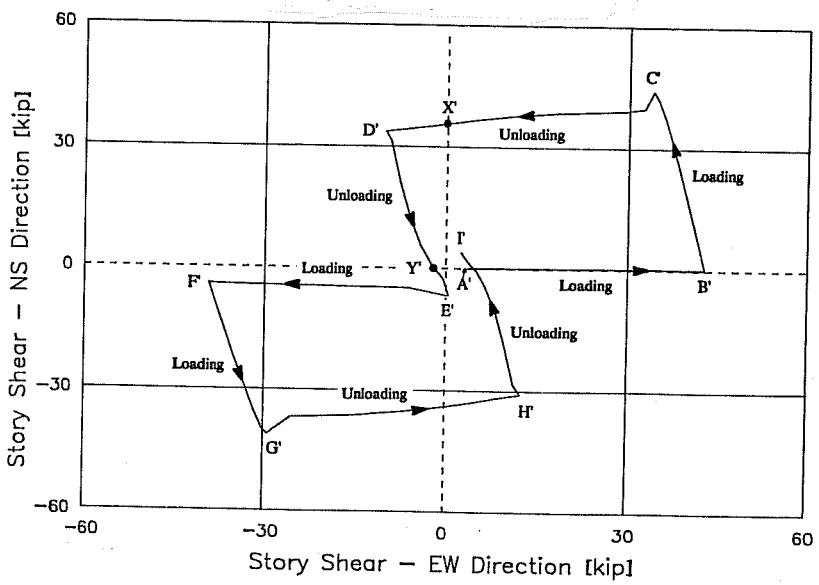

b) Story Shear

Figure 3.55 Orbits Cycle 7 (Specimen SB)

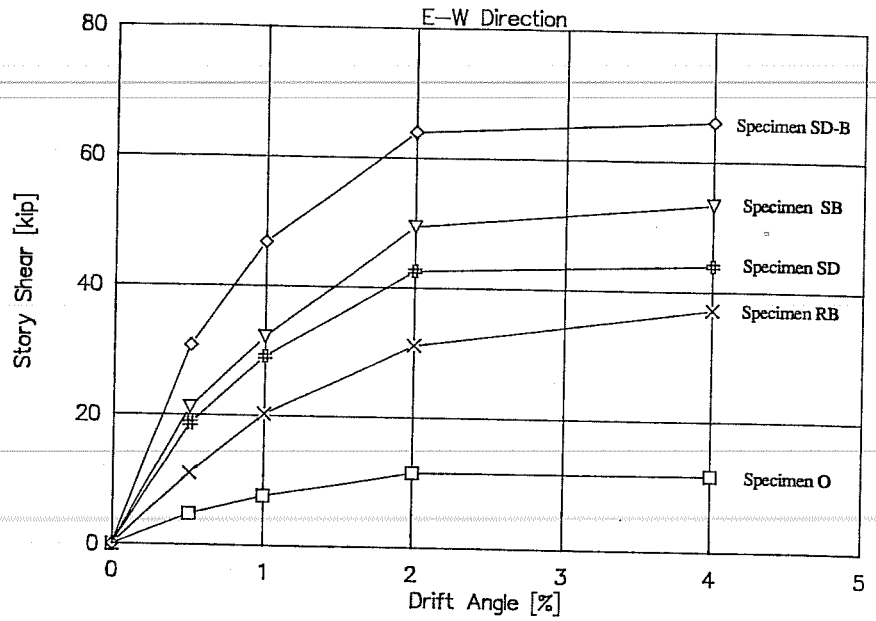

Figure 3.56 Response Envelopes (E-W Direction)

respectively, of the values obtained in the undamaged specimen. The strength of RB at 4% drift angle was 70% of that of SB.

Among the rehabilitated specimens with only columns jacketed, specimen SB was the stiffest and strongest because of the location of the jacket bars and the strength of the concrete. The performance of specimen SD was nearly equal to that of SB. At 0.5% drift, stiffness for SD was 88% of the stiffness for SB. Strength at 2% drift was 86% and at 4% drift was 82% of the values obtained in test SB. However, specimen SD dissipated, in relative terms, little more energy than any other test. Energy dissipation characteristics will be discussed in Chapter V.

As expected, specimen SD-B was the stiffest and strongest specimen since the beams were also jacketed. Initial stiffness was 6.4 times the stiffness for test O. The strength was 5.7 times that of specimen O, both at 2% and 4% drift.

The story shear reached at loading peaks is shown in Figure 3.57. Highest story shears were reached in the first cycles to 2% or 4% drift (cycles 5 and 9). Moreover, for all tests, except RB and SB, the strength reached at cycle 5 was virtually the same in cycle 9 suggesting that beam (or column in O) capacity was reached followed by failure of the joint. Loss of strength at cycles to the same level of maximum deformation supports the idea of shear failure of the joint. It is significant to note the effect of bidirectional loading on the response when comparing the decrement of strength between subsequent unidirectional cycles (say 5 and 6) and subsequent bidirectional cycles (7 and 8, for example).

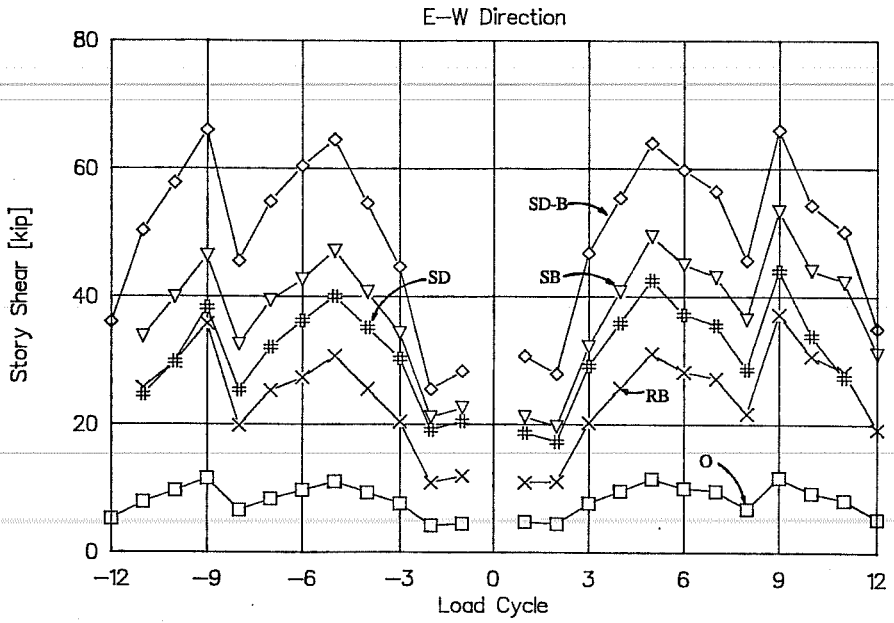

Figure 3.57 Story Shear Response (E-W Direction)

Table 3.1 contains the calculated and measured maximum story shears for unidirectional and bidirectional cycles. The bidirectional resultant was taken as the maximum value given by the square root of the sum of the squares of E-W and N-S story shear components during peak biaxial displacements (same point on the shear orbit).

Table 3.1 Calculated and Measured Maximum Story Shears

Test	Unidirectional Cycles (E-W)			Bidirectional Cycles					
	Calculated V_u [kip]	Measured V_{max} [kip]	Cycle	Calculated V_u[a] [kip]		Measured V_{max} [kip]			
				E-W	N-S	E-W	N-S	Biaxial Resultant[d]	Cycle
O	9.6[a]/12.0[b]	11.7	9/pos	9.6	9.5	6.1	9.2	11.0	7/neg
RB	29.1[a]/36.8[c]	37.2	9/pos	29.1	28.8	20.0	27.8	34.3	7/pos
SB	33.7[a]/37.0[c]	53.4	9/pos	33.7	33.7	33.8	44.1	55.5	7/pos
SD	30.3[a]/36.3[c]	44.0	9/pos	30.3	30.8	26.1	38.4	46.4	7/pos
SD-B	62.9[a]/49.3[c]	66.1	9/pos	62.9	63.4	42.8	59.7	73.5	7/pos

[a] Based on ultimate joint capacity.

[b] Based on column hinging.

[c] Based on beam hinging, assuming T-beam section as described in Chapter V.

[d] Square root of the sum of the squares of measured story shear components.

CHAPTER IV - INTERNAL BEHAVIOR OF THE SPECIMENS

4.1 INTRODUCTION

An assessment of the internal behavior of the specimens is presented. Selected strain gauge data, useful for understanding the behavior of the members and the possible failure mode, is shown. Results of the ultrasonic pulse velocity measurements in the beams, columns and joint are discussed. The effectiveness of jacketing as a repair technique is evaluated by comparing tests O and RB. Comparison of specimens RB and SB permits an examination of the influence of a damaged core on the response of the subassemblage. Specimen SD is compared with SB to investigate the effect of distributed reinforcement around the perimeter of the jacketed column. Finally, specimens SD and SD-B are compared to assess the consequences of beam jacketing on performance.

The existing structure (test O) developed column hinging typical of a "strong beam - weak column" structural system. Pinching of the hysteretic response was caused mainly by joint shear distress and bond loss along the column bars. All rehabilitated specimens showed beam hinging. More favorable energy dissipation mechanisms formed in the rehabilitated specimens, in which the columns remained elastic and the slabs were more stressed than in test O. Bond deterioration along the beam reinforcement contributed to pinching of the story shear versus drift angle diagrams. The joint steel cages confined the joint core effectively. Ultrasonic pulse velocity results indicated composite behavior of the jacketed members.

4.2 ANALYSIS OF STRAIN GAUGE DATA

Strain gauges were placed on beam, column, slab and joint reinforcing steel as described in Chapter II (see Figures 2.26 through 2.32). Due to the large number of strain gauges, selected results are presented at locations which are considered to illustrate best the conclusions obtained. Strains and stresses under E-W loading are presented. In general, the strain behavior reflected during N-S loading is comparable with that in the E-W direction. Large strains in the reinforcing steel occurred at cycles to 4% drift. Several gauges malfunctioned at this stage and made the interpretation difficult. For convenience in the presentation of data, strains were multiplied by ten thousand to give values in percent.

Strain data was converted to stress using a stress-strain model for steel which accounts for cyclic loading and the Bauschinger effect (Ref. 47). It has been recognized that the representation of the stress-strain relation might not be very successful unless detailed test data is available for a particular bar subjected to alternating loads (Refs. 6, 42). The steel properties, reported in Chapter II and used in the stress-strain model, were measured in bar coupons during monotonic tensile tests. Therefore, the calculated stress must be considered as an index to explain qualitatively the tendencies in the response. Stress

analysis in cycles to large drifts became difficult due to large strains above yield and the effect of the previous loading history.

Average bond stresses u_m were computed between gauge locations along column and beam bars. It is important to note that beam gauges were not located at all faces of the jacketed column (see section 2.6.1, Chapter II). In bundled bars, bond stresses were obtained along individual bars. Two calculated bond indexes are defined and compared with measured bond stresses. The design bond index ***DBI***, is an average bond stress over the basic development length of a bar specified by Section 12.2.2 of ACI Building Code Requirements (Refs. 2, 3). The maximum bond index ***MBI*** is an average bond stress based on the assumption that bar has developed tensile yielding at one end and compressive yielding at the other end simultaneously. The three bond indexes were computed using the following expressions

Measured bond stress

$$u_m = \frac{(f_1 - f_2)\, d_b}{4l} \tag{4.1}$$

Design bond index ***DBI***

$$DBI = \frac{\sqrt{f_c'}}{0.04\,\pi\, d_b} \tag{4.2}$$

Maximum bond index ***MBI***

$$MBI = \frac{f_y\, d_b}{2l} \tag{4.3}$$

where

$f_{1,2}$	=	bar stress
d_b	=	bar diameter
l	=	distance between strain gauges
f_y	=	bar yield strength
f_c'	=	concrete compressive strength.

In general, values of u_m and ***MBI*** were calculated over a length of 16 in. for beam bars and over 20 in. for column bars. A zero bond stress does not necessarily means bond loss but indicates that forces with the same magnitude and opposite direction are applied at the ends of the length l . If $u_m = 0$ and is calculated between two contiguous gauges (say between the faces of the existing column and the jacketed column), it might indicate bond deterioration along the bar.

4.3 COMPARISON OF SPECIMENS O AND RB

To study the effectiveness of jacketing as a repair technique tests O and RB are compared.

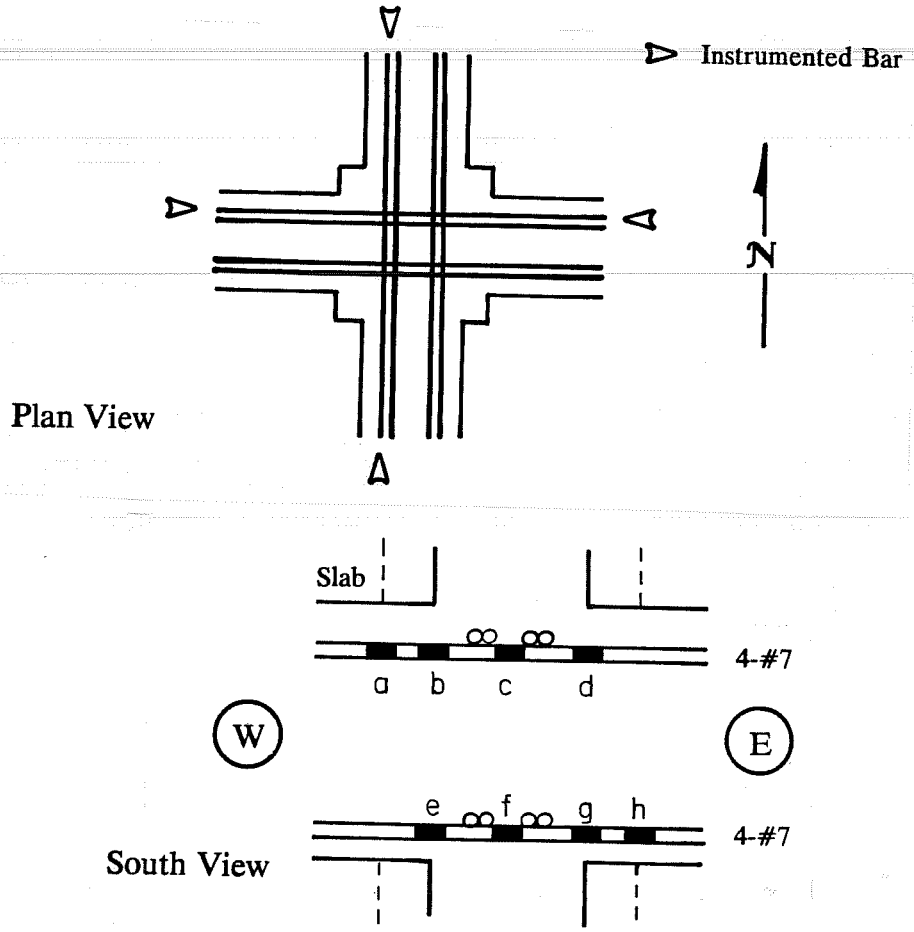

Figure 4.1 Beam Strain Gauge Location

4.3.1 Specimen O

4.3.1.1 Beams. In Figure 4.1, the beam gauge location is shown. In all specimens, top and bottom bars of the existing beams were instrumented with strain gauges. Specimen O, and consequently RB, was not instrumented at locations "b" and "g". Beam bars showed elastic behavior throughout the test. Maximum tensile strain was 3/4 of yield and was recorded at position "e" in cycle 9/neg. In Figure 4.2, the story shear versus strain at location "a" is shown. Positive loading (downward displacement) induced tension in the slab and compression in the bottom portion of the beam. Under negative loading, tensile strains

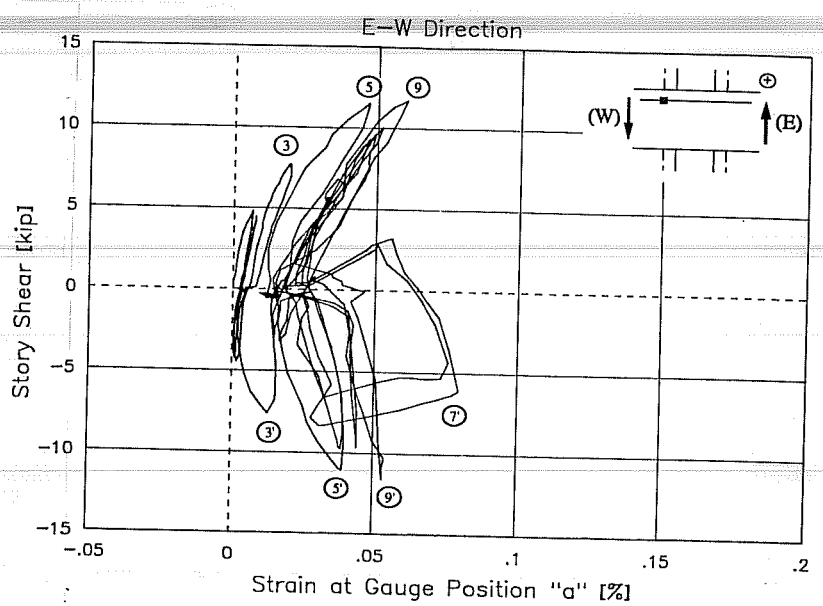

Figure 4.2 Specimen O - Story Shear vs. Strain at Gauge Position "a"

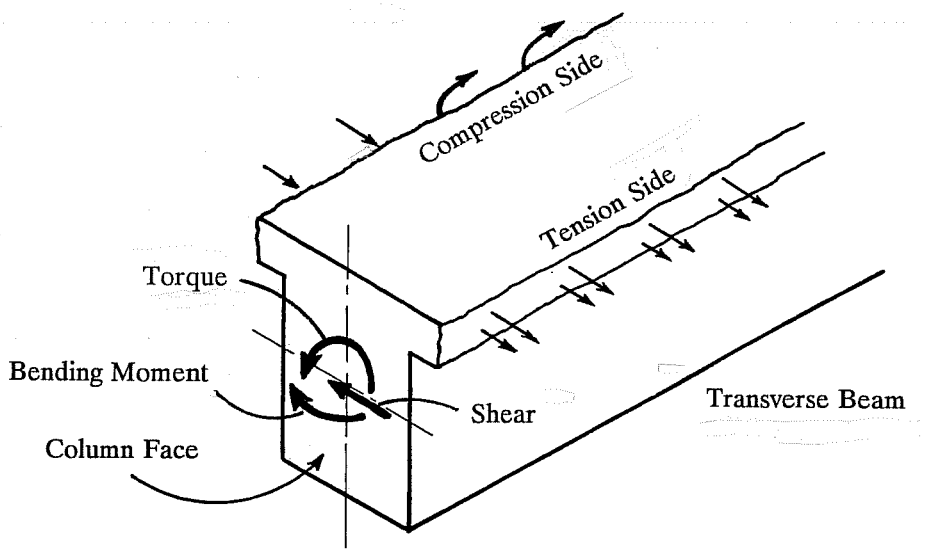

Figure 4.3 Transverse Beam Subjected to Slab Forces

were recorded which were the result of the neutral axis lying above the top bars. The top reinforcement was placed 3.5 in. below the top slab surface. The compressive force of the flexural moment was resisted by the concrete above the top bars. Bottom slab bars, located at nearly the same level as the top beam reinforcement, displayed the same response. Bidirectional interaction was especially noted in cycles 7/neg and 8/neg (see Figure 4.2). No sign of bond loss was observed along beam bars. Bond stresses were very low. Maximum bond stresses calculated between gauge locations "a" and "d", and between "e" and

"h" (16 in. spacing) were 530 and 570 psi., respectively, at cycles to 4% drift. The design bond index was ***DBI*** =440 psi. and the maximum bond index was ***MBI*** =1760 psi..

When the specimens were deformed in one direction, E-W for illustrative purposes, the transfer of slab forces produced shear, bending with respect to the column axis, and torsional moments in the transverse beams (N-S beam) as shown in Figure 4.3. Under negative moment, a portion of the slab participates in the flexural response of the T-beam section and imposes a shear force, and bending and torsional moments on the transverse beam. The remainder of the slab, on both sides of the T-section, acts as a shallow flexural member which also imposes torsion on the N-S beam. Similar response is expected when the slab is deformed in positive curvature. Crack patterns in all the specimens showed beam torsional cracks in the transverse beam, some of which extended from joint shear cracks. Most of the torsional distress occurred close to the column. Torsion of reinforced concrete beams can be studied using the truss analogy (Ref. 14). This assumes that after cracking, the concrete can carry no tension and that the beam acts as a truss with longitudinal chords and with walls composed of diagonal concrete struts and transverse steel ties (Figure 4.4, taken from Ref. 14). The longitudinal component of the diagonal compression must be balanced by tension in the longitudinal steel. Thus, the primary function of the longitudinal steel is to hold the beam together along its axis. In this series of tests no attempt was made to measure torsional moments or rotations. In the explanations given with regard to torsion of the transverse beam, the observed damage and interpretation of the strain behavior will be assessed. Apart from slab rotations, the magnitude of the torque depends on the torsional stiffness of the transverse beam. With progressive inelastic cyclic loading, the torsional stiffness of the beam was likely to have decayed dramatically.

The effect of compatibility torsion in the N-S beam reinforcement when specimen O was deformed in the E-W direction is observed in Figure 4.5. The E-W story shear versus strain in the top reinforcement at the N face of the original column is shown in Figure 4.5a. The strain in the bottom reinforcement at the S face of the column is presented in Figure 4.5b. In both graphs, strains showed almost no interaction (strains were zero) up to cycle 3, which coincided with the onset of torsional cracking. The bottom gauge measured larger strains than the top gauge. The beam web was more flexible in torsion (warped more) than the upper part which included some slab. When the torsional moment was applied, the beam tended to elongate. The elongation in the web had to be reacted only by the bottom beam bars resulting in higher measured strains in the bottom steel. Most of the torsional cracks occurred in the lower half of the beam web. Torsion of transverse beams and the related beam steel strains were found to interact in all tests. This relationship was partially responsible for the story shear decay in the hysteretic response during biaxial deformation and to the larger energy dissipated (area within the hysteresis loops) during those cycles (see Figures 3.5 and 3.6). At large deformation levels, bulging of the joint core in the direction perpendicular to loading, caused the orthogonal beam flexural cracks to close thus confining the core. Restraint was provided by the beam longitudinal steel resulting in tensile strain.

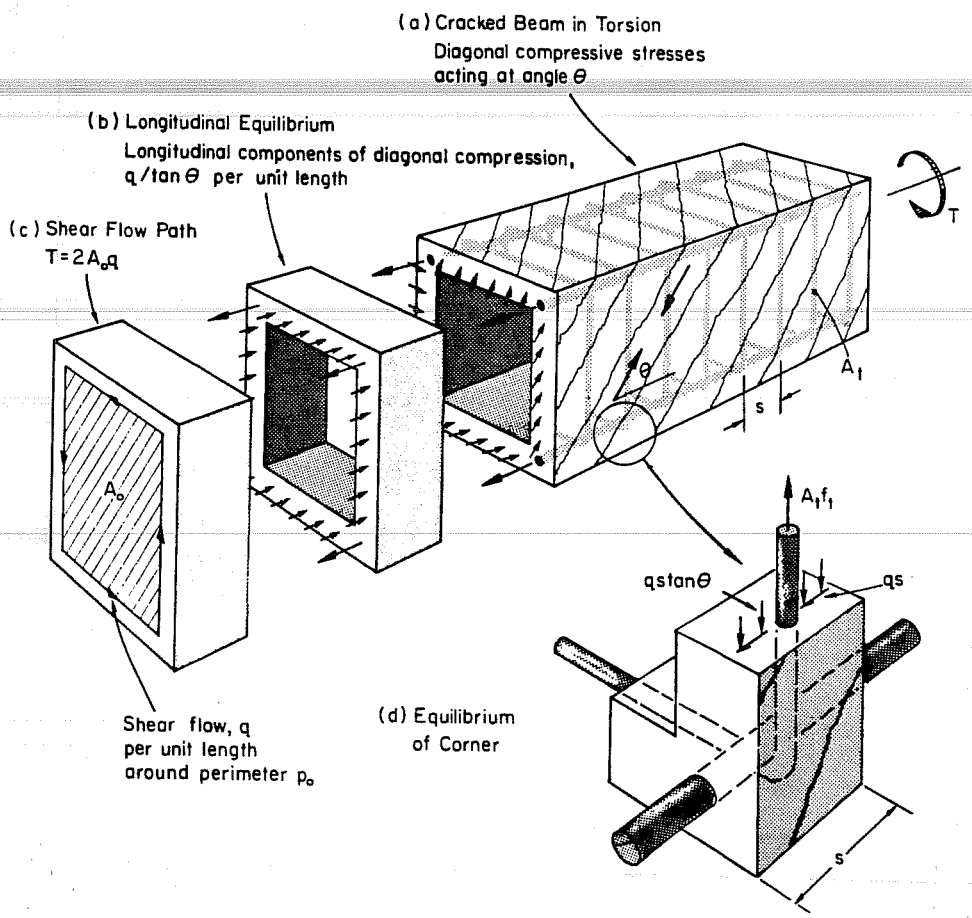

Figure 4.4 Truss Analogy for Beams in Torsion (from Ref. 14)

4.3.1.2 Column. In specimen O, five column gauges were located on the NW and SE corner bars and three on the NE and SW corner bars (see section 2.6.1): 10 in. above the slab in the upper column (gauge "u"), at the top slab surface (gauge "s"), at joint mid-depth (gauge "m"), at the beam web soffit (gauge "w") and 10 in. below the beam soffit in the lower column (gauge "l"). Gauge positions "u", "s", "m", "w" and "l" corresponded to sections 1, 2, 3, 4, and 5, respectively, which are shown in Figure 2.28. Column behavior in test O is studied from strains measured in the SE column bar which was subjected to high stresses in cycles to 4% drift. Similar results were found for other column bars (not shown here).

In Figure 4.6, the E-W story shear versus strain measured at gauge "s" is shown. Positive story shear produced compression in the E face of the upper column, which was contiguous to the bar, and in the W face of the lower column. The wide line in the column cross section in the graph represents the column face in compression during E-W positive cycles. Column bar strains were much larger than beam strains, which is typical of "strong beam - weak column" behavior (see Figure 4.2). In cycle 3/pos, tensile strains were developed because of the position of the neutral axis. It is unlikely that bond distress occurred at this stage because the average bond stress calculated between gauges "s" and "w"

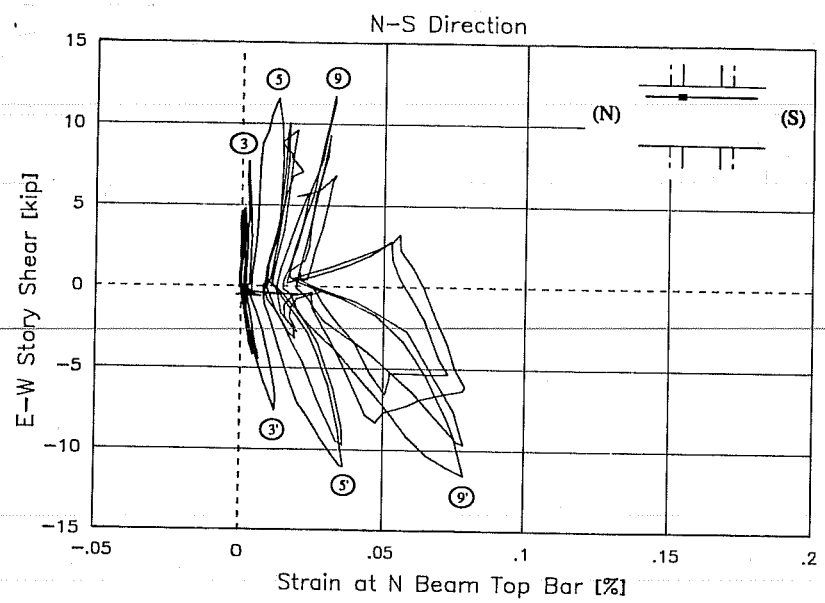

a) Strain at N Beam Top Bar

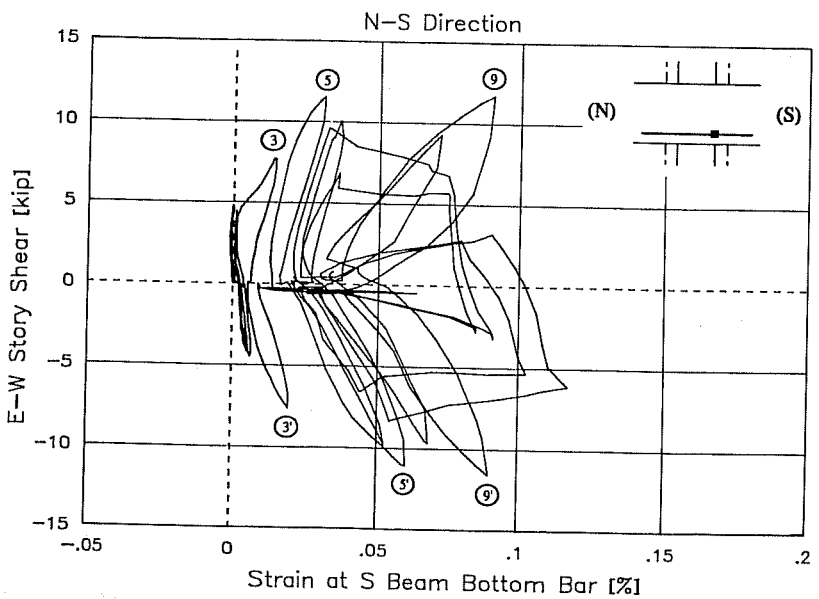

Figure 4.5 Specimen O - E-W Story Shear vs. Strain at N-S Beam Bars

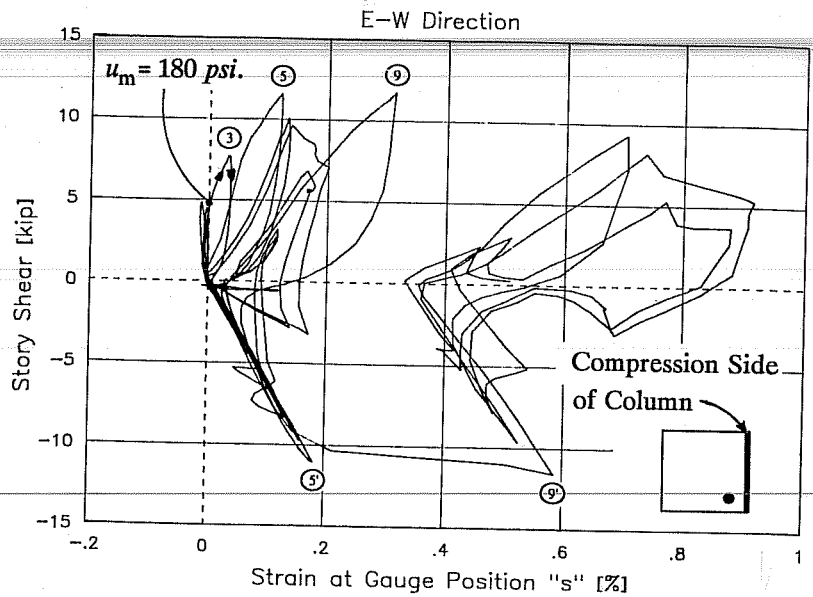

Figure 4.6 Specimen O - Story Shear vs. Strain at Gauge Position "s"

was 180 psi. at zero strain. Both bond indexes were higher than 180 psi.: ***DBI*** =510 psi. and ***MBI*** =1170 psi. The ratio of beam depth to bar diameter was h/d_b =27. During positive half-cycles, strain showed wide loops with some stiffening as loads increased and flexural cracks on the column face closed, redistributing compressive flexural forces to the concrete. Crack closing and the subsequent concrete crushing and spalling contributed to pinching of the hysteresis diagrams discussed in Chapter III (see Figures 3.5 and 3.10). In cycles 10 through 12 at 4% drift, the bar developed larger tensile strains in positive than in negative loading. At this stage, the portion of the bar in the joint below the slab was exposed. The bar was anchored only in the slab. Due to the lack of transverse steel in the joint, forces had to be resisted by a diagonal concrete strut through the joint (see Figure 1.1c), which was controlled by the forces imposed by the column. The joint strut, and the beam and column concrete stress blocks confined the bar assuring its anchorage. The increase in tension at "s", produced an increment in concrete compressive strain at that section leading to concrete crushing and spalling and subsequent progressive bond deterioration. Bar yielded in cycle 9/neg. Strain at location "w" (not shown) exhibited the same behavior as "s". Comparison of "s" and "w" shows that strain at "s" was larger than that at "w" when the bar was required to resist the tensile flexural force. This coincides with the observation that upper column curvatures were larger than lower column curvatures (see Figures 3.11 and 3.12).

To illustrate bond deterioration in column bars over the joint depth, the story shear versus bond stress is shown in Figure 4.7. After cycle 5, a change of phase in the bond stress history occurred and the story shear versus bond stress curves rotated counterclockwise around the origin. In cycle 5, joint cracking, which was concentrated around gauge location "w", affected the column bond capacity. The story shear versus drift

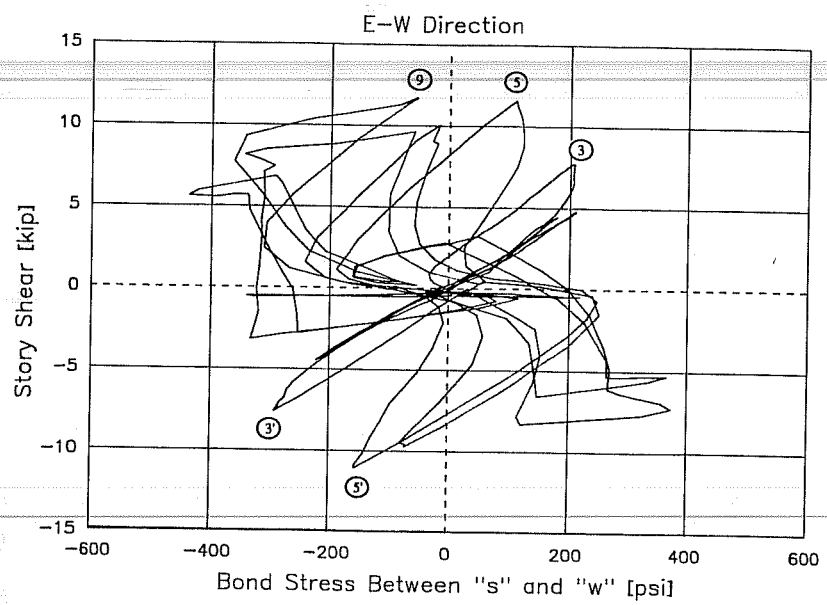

Figure 4.7 Specimen O - Story Shear vs. Bond Stress Between "s" and "w"

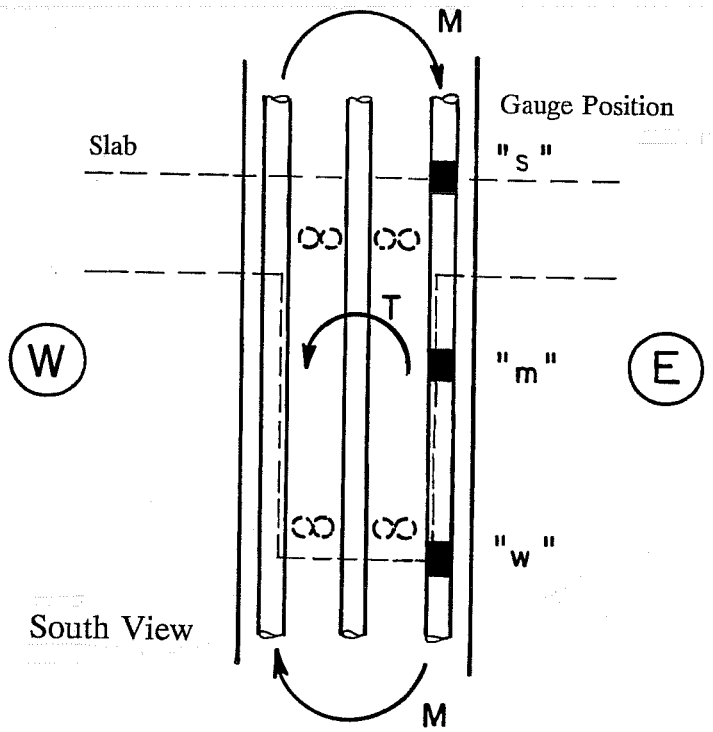

Figure 4.8 Specimen O - Compatibility Torsion at Column Face

angle diagram, as well as the column angle and column curvatures, showed severe stiffness deterioration and pinching (see Figures 3.10 through 3.12). Large concrete damage and joint shear degradation in cycles to 4% further contributed to pinching the loops and reducing energy dissipation. However, bond degradation did not preclude the specimen from attaining maximum strength in cycle 9. In subsequent cycles to 4% drift, bond distress and slip of the column bars contributed to an increase in the column curvatures. Strains at "u" and "l" (not shown) exhibited normal tension-compression loops, which were indicative of good bond at those locations.

As mentioned before, torsion in the transverse beam was transferred to the column faces (Figure 4.8). For illustration purposes, only the total torsional moment at the south face of the column is depicted. During positive loading in the E-W direction, the upper and lower columns were subjected to clockwise flexural moments M which caused compression in the E face of the upper column and in the W face of the lower column. However, the total torque T acted in the opposite direction. The torque caused tensile strains in column bars which were adjacent to the column face in compression. This was the case in positive half- cycles at gauge position "s" (Figure 4.6) and in negative half-cycles at gauge location "w" (not presented here). Column longitudinal steel not only transferred the forces induced by flexural moments but helped to resist torsional moments, which resulted from compatibility of deformation of the transverse beam framing in the joint.

Peak stress distribution along the SE column bar for positive and negative cycles 1, 3, 5 and 9 is presented in Figure 4.9. Upper and lower column gauges "u" and "l" behaved satisfactorily. At locations "s", "m" and "w" only tensile stresses were measured.

4.3.1.3 Slab. In all specimens, strain was measured in both directions in the top and bottom slab reinforcement of the SW quadrant as shown in Figure 4.10. Top gauges were located in two bars next to the column (positions "1" and "2") and thereafter, at one bar every other one (positions "3" through "5"). Bottom gauges were attached to a bar adjacent to the column (position "6") and to a bar close to beam mid-span (position "7"). Top reinforcement was spaced at every 12 in. and the bottom was spaced at every 24 in..

During test O, the slab remained elastic. The E-W story shear versus strain at gauge location "1" is presented in Figure 4.11. Positive loading induced tension in the slab and compression in the beam bottom. From cycle 3/neg, only tensile strains were measured. Tensile strains under upward loading confirmed the position of the neutral axis mentioned in the analysis of beam strains. All instrumented top slab bars showed similar behavior (not presented here). In Figure 4.12, the peak slab strain distribution in the E-W direction for top bars during positive cycles 1, 3, 5, 9 is presented. Bidirectional cycles followed the unidirectional cycles at the same deformation level. In general, strains increased with the imposed drift angle. Maximum strains of half yield strength were reached at 4% drift. Although larger strains were measured next to the column, distribution was fairly uniform. Low slab strains suggested that the slab participation in the flexural response of the T-beam

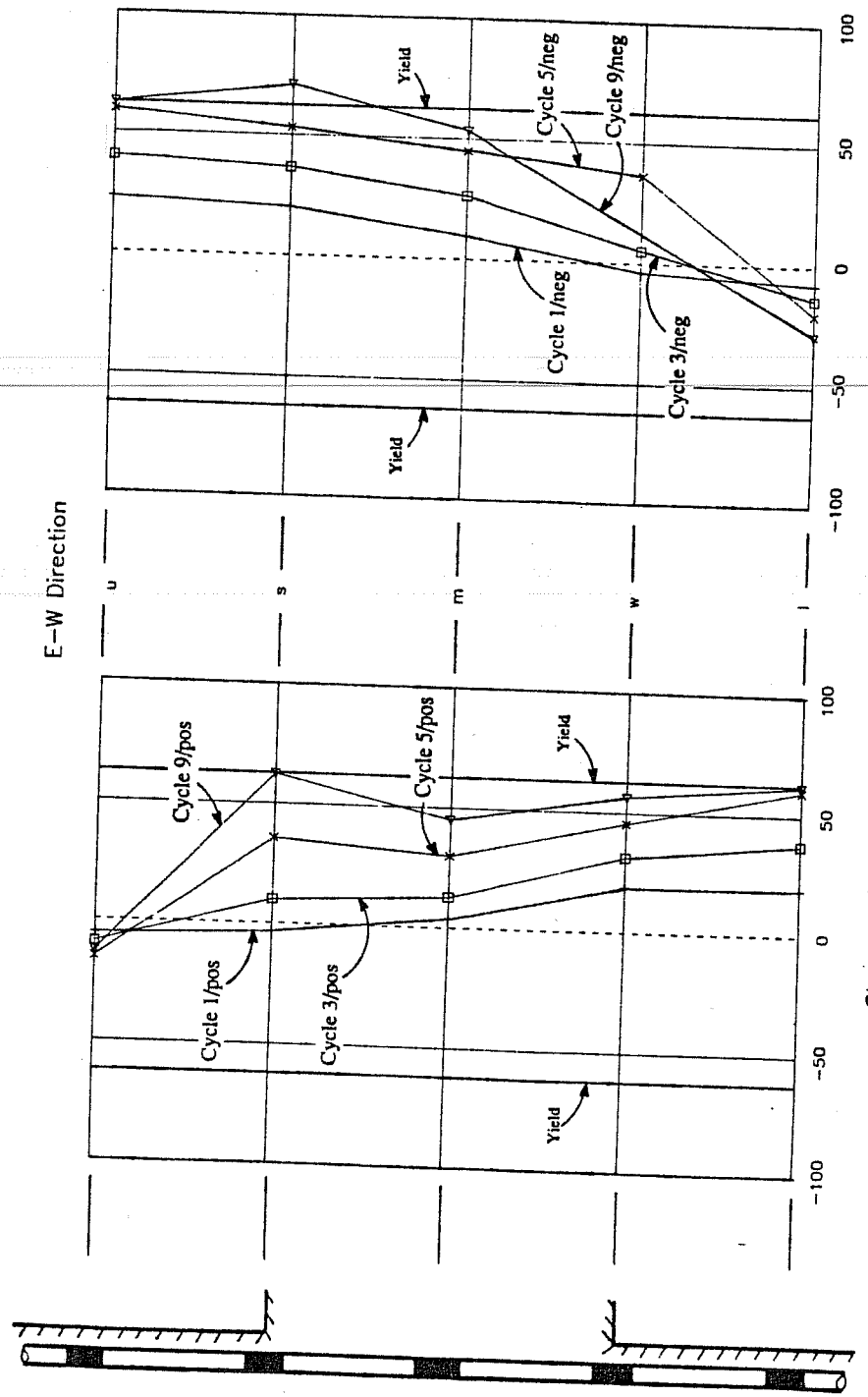

Figure 4.9 Specimen O - Stress Distribution Column Bar

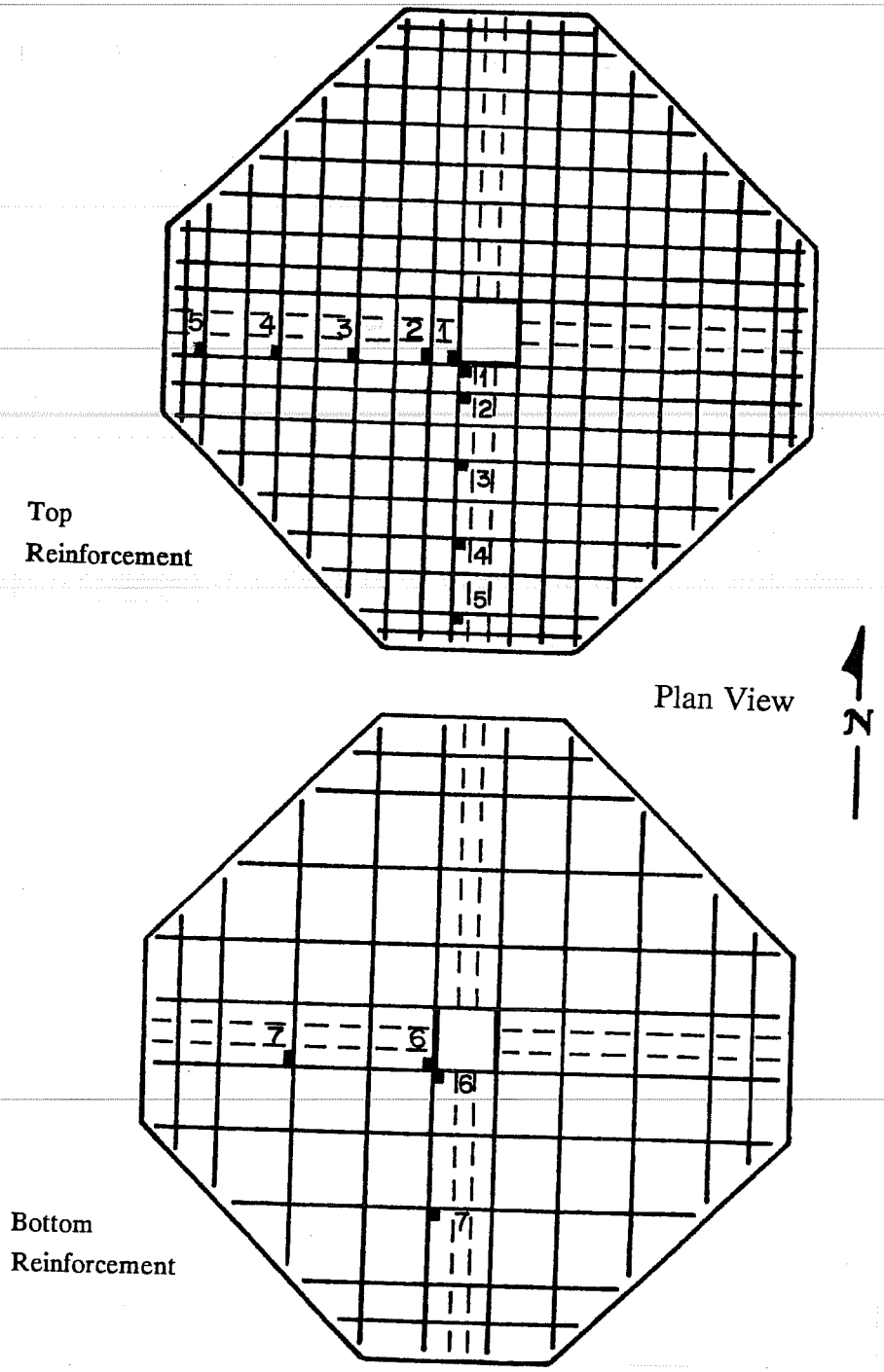

Figure 4.10 Slab Gauge Positions

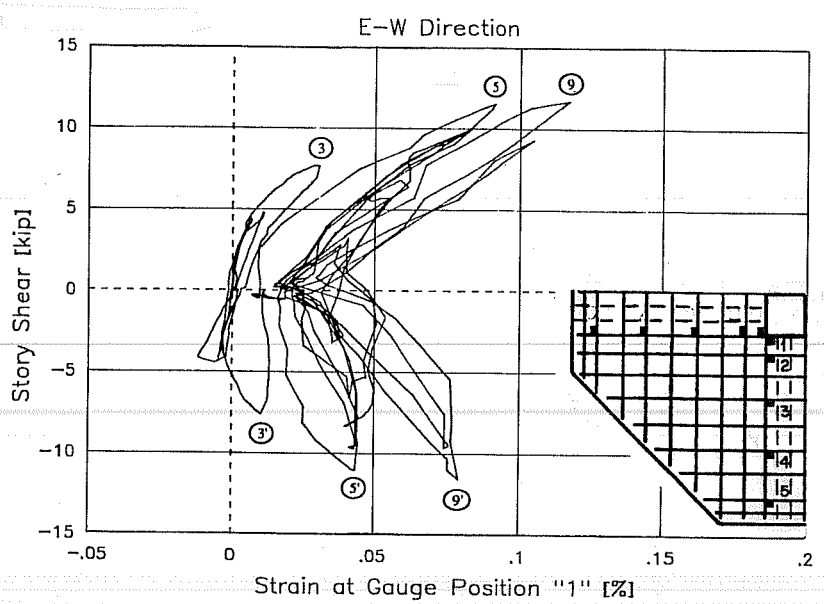

Figure 4.11 Specimen O - Story Shear vs. Strain at Gauge Position "1"

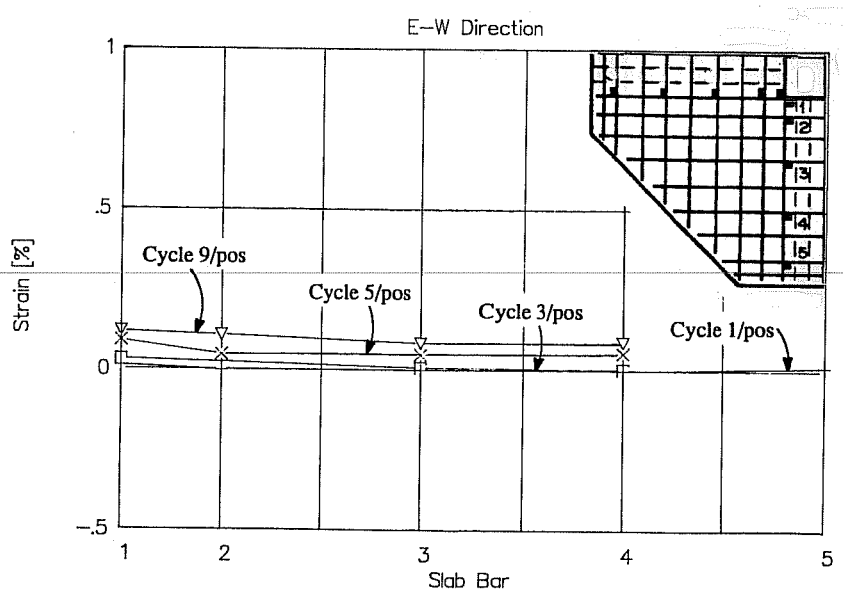

Figure 4.12 Specimen O - Strains Across E-W Top Slab Bars

section (see section 4.3.1.1) was low. Slab participation will be discussed in more detail in Chapter V.

4.3.1.4 Joint. Strains in the column transverse steel above the slab and below the beams were very small. The steel above the slab exhibited lower strains because of the confinement effect of the slab framing into the column.

4.3.2 Specimen RB. After completion of test O, the specimen was loaded to place the beam ends at zero deflection. Estimation of the strain in the reinforcement caused by loading the beams to zero deflection and by material relaxation during the rehabilitation process was not attempted. Due to the failure in test O, the joint core was cracked considerably. Corner column bars were exposed after removal of loose concrete so that the bars were partially surrounded by the concrete of the jacket.

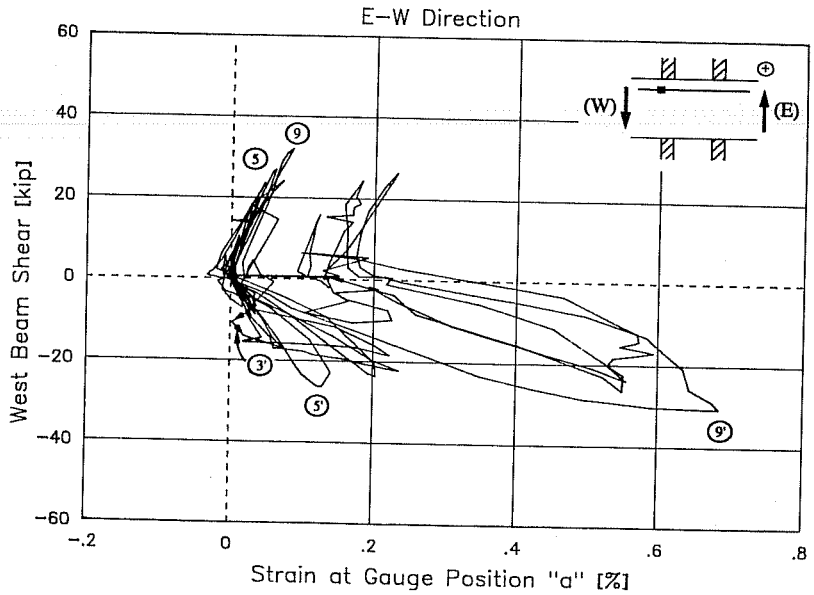

Figure 4.13 Specimen RB - West Beam Shear vs. Strain at Gauge Position "a"

4.3.2.1 Beams. Beam strains were larger in specimen RB than in O. In Figure 4.13, the west beam shear versus strain at gauge location "a" is shown. Figure 4.13 can be compared with Figure 4.2. Positive loading (downward displacement) caused tension in the slab and compression in the bottom portion of the beam. During positive and negative loading, tensile strains were measured. In cycle 3/neg, the strain decreased consistently with the compression imposed by the bending moment on the slab, but before reaching the loading peak, strain increased. From cycle 3, tensile strains during negative loading became increasingly larger than those during positive loading. In subsequent cycles, bond deterioration in the top steel occurred so that the tensile force during negative bending (E

slab in tension) was resisted by the bars unbonded across the joint. The bar was anchored in the compressive side of the joint (W side). Similar behavior was observed at gauge location "d" (not shown here). Bond distress of top bars contributed to pinching of the hysteretic response and loss of energy dissipation capacity (see Figure 3.18). Bond loss was exacerbated by placing 4-#7 in two two-bar bundles which were subjected to load in the previous test (test O). The "top bar effects" (Ref. 23) might have reduced the bar anchorage since the reinforcement was cast above 17 in. of low-strength concrete ($f_c' = 2340$ psi.), which had a 7 in. slump at the time of casting. The column depth to bar diameter ratio, based on the width of the jacketed column and the diameter of a single #7 bar was $h/d_b = 23$. However, the effective h/d_b ratio was smaller because bars were bundled and the beam critical section formed within the column jacket. Yielding of the bar in cycle 9/neg increased the strain gradient in the beam section thus leading to concrete crushing. Concrete damage and bond deterioration contributed to the stiffness degradation observed in the response (see Figure 3.16).

In Figure 4.14, the stress distribution in the E-W direction for positive and negative loading between gauge locations "a" and "d" is shown. Larger tensile stresses were measured in the compressive side of the joint, where the bar anchorage was assured. Stresses in the other side were a little smaller. At 4% drift, maximum average bond stress was 1300 psi. (2.3 times that measured in test O) and three times the design bond index, $DBI = 440$ psi., but smaller than the maximum bond index, $MBI = 1760$ psi..

In Figure 4.15, the west beam shear versus strain at gauge location "e" in the bottom reinforcement is shown. Nearly vertical loops during positive loading in cycles to 4% drift (cycles 9 through 12) indicated bond distress. In test RB, no beam cracks formed near or at the face of the jacketed column and sliding of the beam sides relative to the concrete jacket was observed thus suggesting that the critical section formed inside the column jacket. During upward loading (negative shear), large tensile strains were measured because the critical section was near the original column face. The location of the critical section can be confirmed by the strain at location "h" (Figure 4.16), which showed good bond behavior because the bar was well anchored in the E beam. The bar yielded in cycle 9. Bond distress and slip of bottom bars within the joint were partially responsible for the increase in beam curvatures and pinching of the response.

The stress distribution along E-W bottom beam bars is shown in Figure 4.17. Bottom beam bars were subjected to large compressive forces in one side of the joint and tensile forces in the other side which combined, produced bond deterioration. During upward loading, the bottom steel resisted the tension caused by bending. In the other side of the joint, the beam was loaded downwards causing tension in the top beam reinforcement and in some slab bars. The larger steel area produced a large tensile force which was balanced by compression in the lower portion of the beam. In cycles to large deformation levels, high tensile residual strains in the bottom steel were measured when positive half-cycles were completed. When the next negative half-cycle was applied, compressive stresses were imposed on the bar. After crushing and spalling of beam bottom concrete, bond

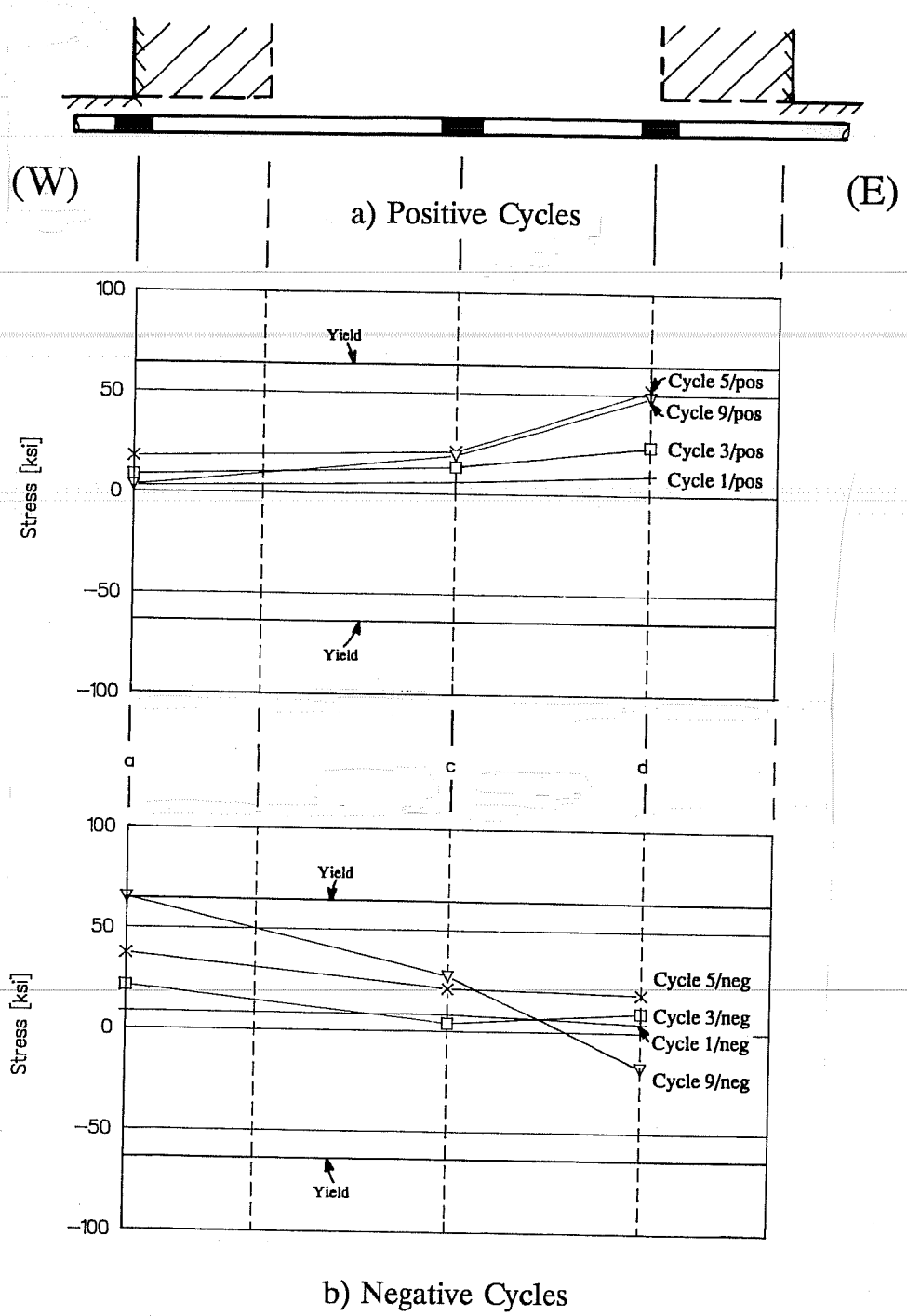

Figure 4.14 Specimen RB - Stress Distribution Top Beam Bar

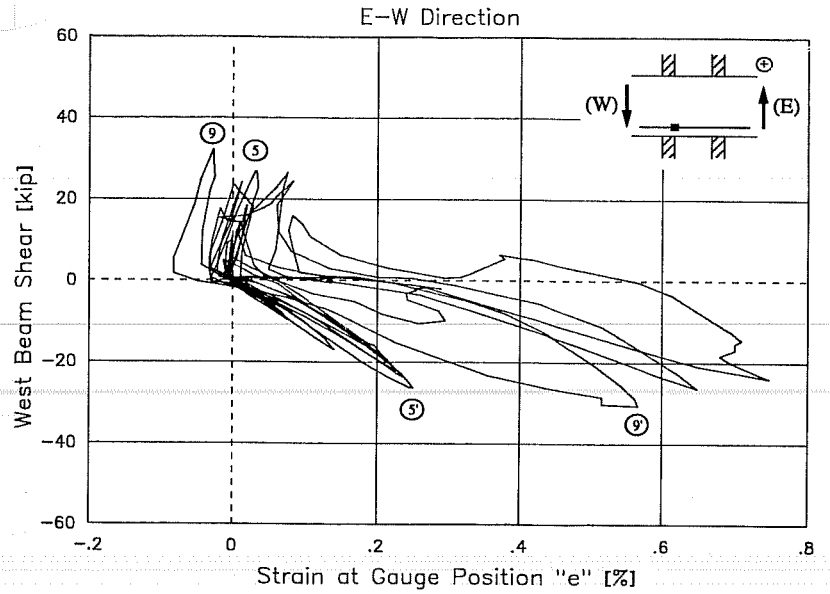

Figure 4.15 Specimen RB - West Beam Shear vs. Strain at Gauge Position "e"

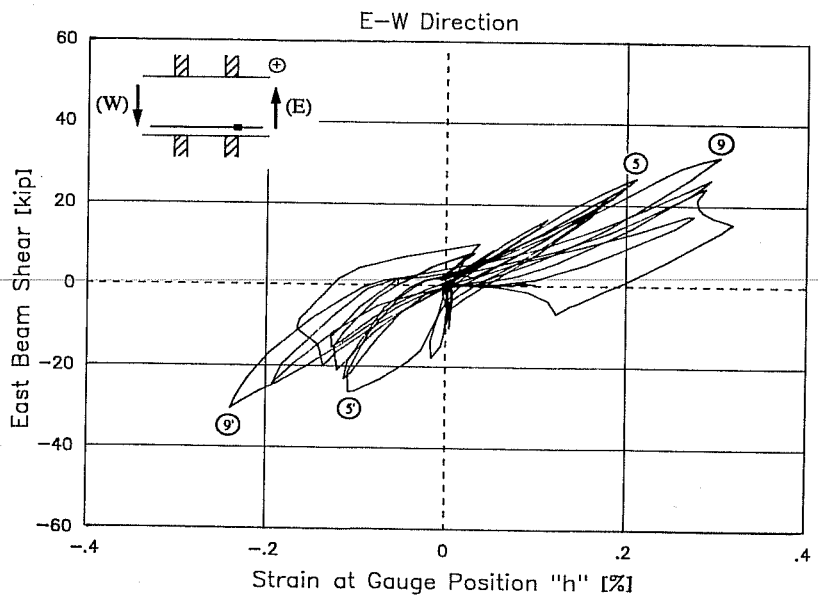

Figure 4.16 Specimen RB - East Beam Shear vs. Strain at Gauge Position "h"

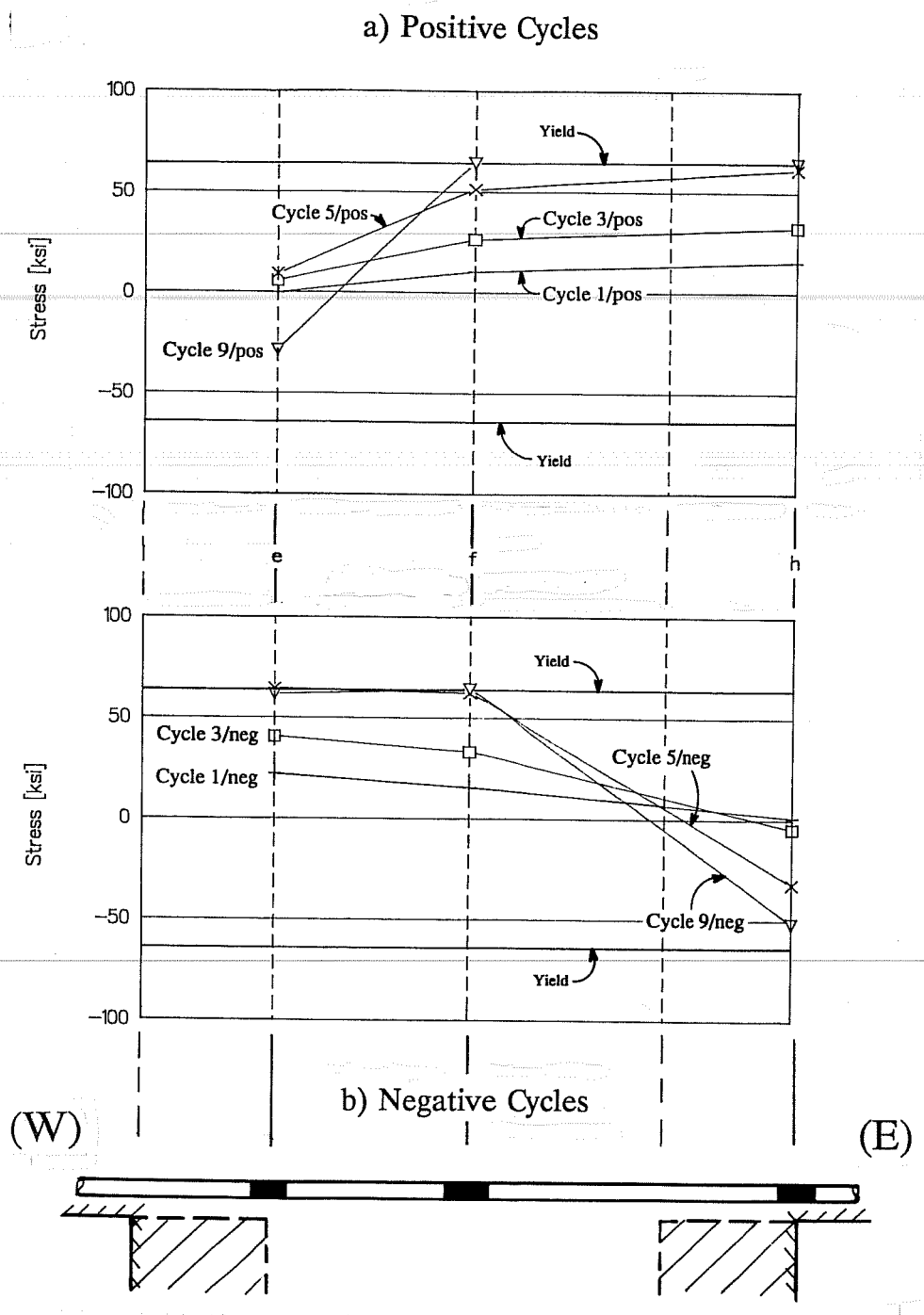

Figure 4.17 Specimen RB - Stress Distribution Bottom Beam Bar

deterioration was intensified. At large drift levels, tensile stresses were constant suggesting that yield penetration and bond loss occurred. Maximum bond stress between "e" and "h" was 1550 psi. during cycle 9/neg.

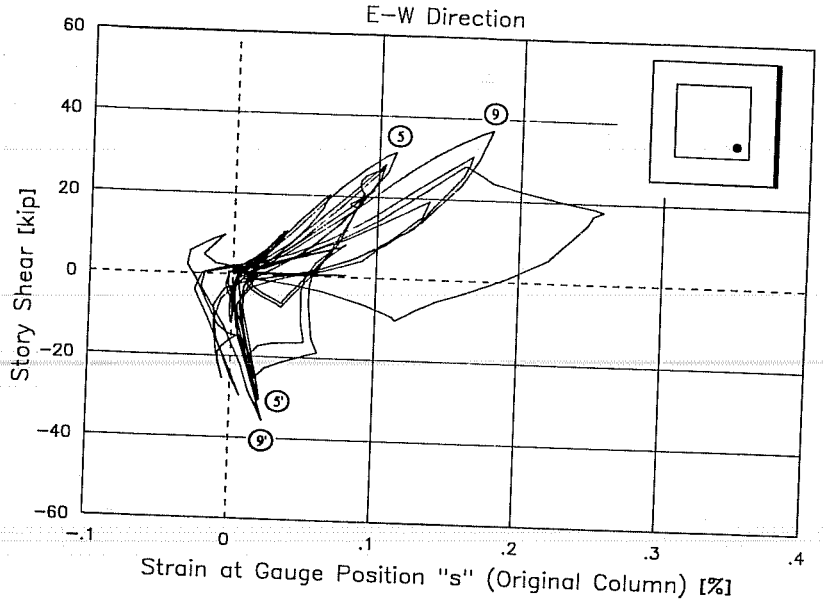

Figure 4.18 Specimen RB - Story Shear vs. Strain at Gauge Position "s" (Original Column)

4.3.2.2 Column. Column strains were smaller than beam strains. Original column bars showed good bond behavior. There was no indication of loss of bond between the original concrete and the jacket. Figure 4.18 shows the story shear versus strain at gauge "s" in the SE original column bar which measured much smaller strains than those in specimen O (Figure 4.6). The bar yielded in cycle 11/pos. Under positive loading, compression was applied to the E face of the upper column. Larger strains were recorded during positive cycles because the original column reinforcement resisted the torsional moment transferred from the transverse beam (Figure 4.8) and resisted the opening of the existing cracks in the original joint core. The same behavior was observed at location "w" (not shown here). At "u" and "l" (not presented) almost zero strain was measured.

The bundled reinforcement of the jacket was instrumented at the same locations as the original column bars (see Figure 2.29). Strains of the SE bundle are presented to compare with the original column reinforcement. Same conclusions were obtained from other bundles. Bundled reinforcement yielded at some locations during cycle 9/pos after beam hinging. In Figure 4.19, the story shear versus strain at gauge location "u" in the corner bar is shown. Good bond behavior can be observed. Consistent with the applied loading, compressive strains were measured in positive cycles and tensile strains in negative cycles. The same behavior was observed at location "l" (not shown).

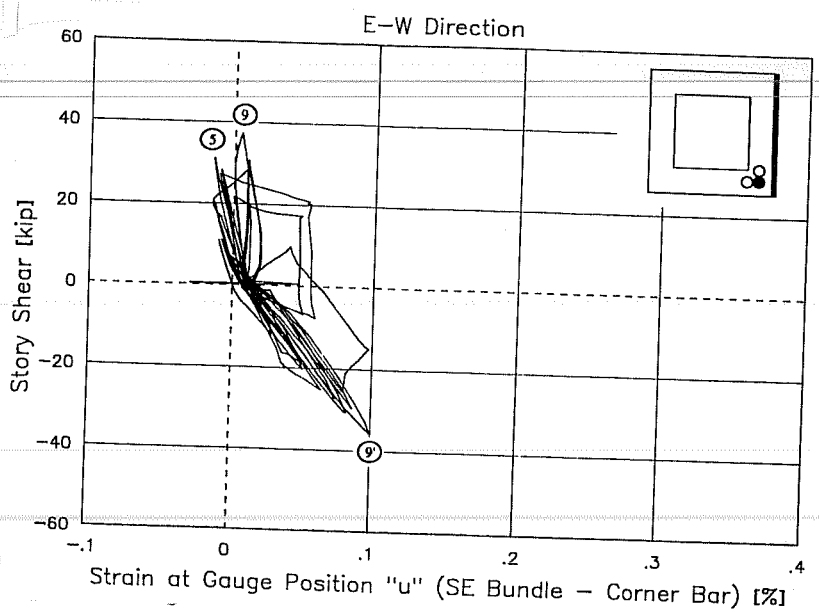

Figure 4.19 Specimen RB - Story Shear vs. Strain at Gauge Position "u" (Jacketed Column - Corner Bar)

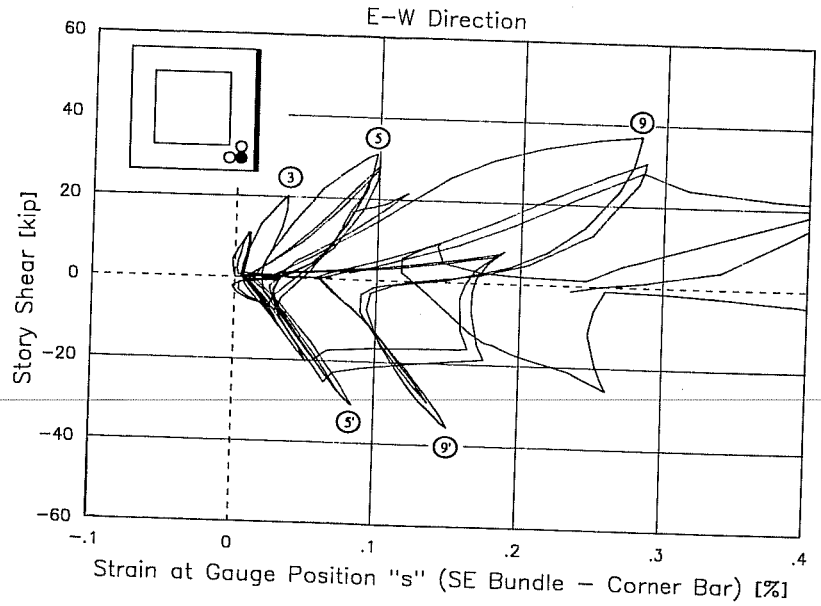

Figure 4.20 Specimen RB - Story Shear vs. Strain at Gauge Position "s" (Jacketed Column - Corner Bar)

In Figure 4.20, the E-W story shear versus strain at gauge location "s" is presented. Bar yielded in cycle 9/pos. From cycle 5, strains for positive cycles increased faster than those in negative loading because the bars were required to balance the vertical component of the joint concrete strut (Figure 4.21a). Similar behavior was observed at "w" (not shown here). Shear forces applied to the joint by the beams and column had to be resisted by a diagonal concrete strut in the joint (see Figure 1.1c). The formation of the strut was evident from the crack pattern observed during the test (Figure 4.22). Most of the inclined cracking (during E-W loading) formed in the N-S joint faces. Since the joint original core was cracked and severely deteriorated after test O, the strut was not formed through the core and the load had to be transferred to the concrete jacket. The joint behaved like a hollow section and the forces were resisted by a pair of parallel struts. In the upper end, the struts were reacted by the jacket of the column, and the beam width and part of the slab. Inside the joint, the vertical component of the strut was balanced by the bundled bars (Figure 4.21a). For illustration purposes, only the idealized pair of diagonal struts and the vertical reaction provided by the bundled bars are drawn in the graph. In the lower end, the axes of the struts did not coincide with the beam axis and the horizontal component was resisted by the lower portion of the steel angles and the lower joint flat bars. An idealization of the horizontal reaction is shown in Figure 4.21b. Early in the test, the strut was inclined about 45° (as first cracks show in Figure 4.22). From cycle 5, the strut became increasingly steeper, matching the steep extension of inclined joint cracks, and the horizontal component of the strut decreased. The horizontal reaction was provided by the column ties and the lower joint flat bars.

The inclined cracking in the lower column affected bond along the bundled bars below the soffit of the beams. The bond distress progressed as cracking extended, especially during bidirectional cycles. Localized slip and bond damage contributed to pinching of the story shear versus drift angle diagram, and of the column angle and lower column curvatures diagrams at 4% drift (see Figures 3.16, 3.20 and 3.21). After cycle 5, a change in phase was observed in the story shear versus bond stress diagram (not shown) similar to that in the column bars of test O (see Figure 4.7). The beam depth to column bar diameter ratio was $h/d_b = 18$.

The stress distribution along the SE corner bar is shown in Figure 4.23. Up to cycle 3/pos, stresses decreased linearly from tension to compression. In subsequent cycles, the bar exhibited larger tensile stresses at the compression side due to the vertical component of the joint strut.

In Figure 4.24, the E-W story shear versus strain at location "w" in the west bar of the SE bundle is presented. The response was similar to that at "s" in the corner bar (Figure 4.20). Load versus strain curves in negative cycles to 4% drift were nearly vertical suggesting bond damage and slip of the bar. C-shaped curves were also observed at locations "m" and "s" (not shown).

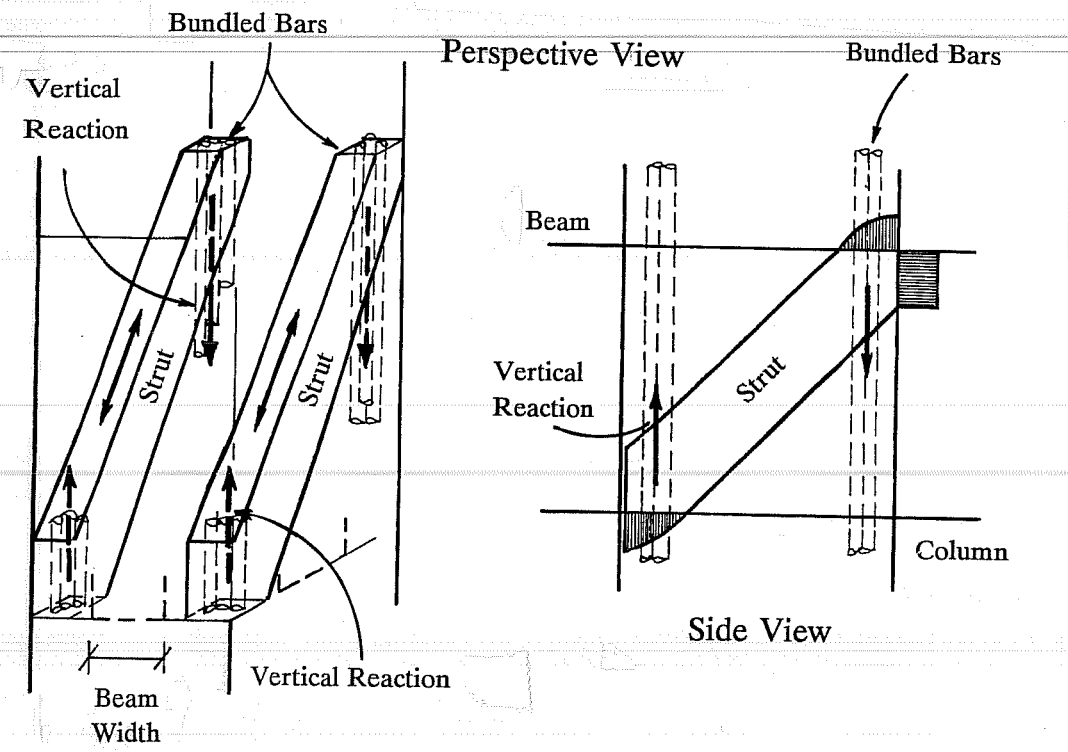

a) Vertical Component of Joint Strut

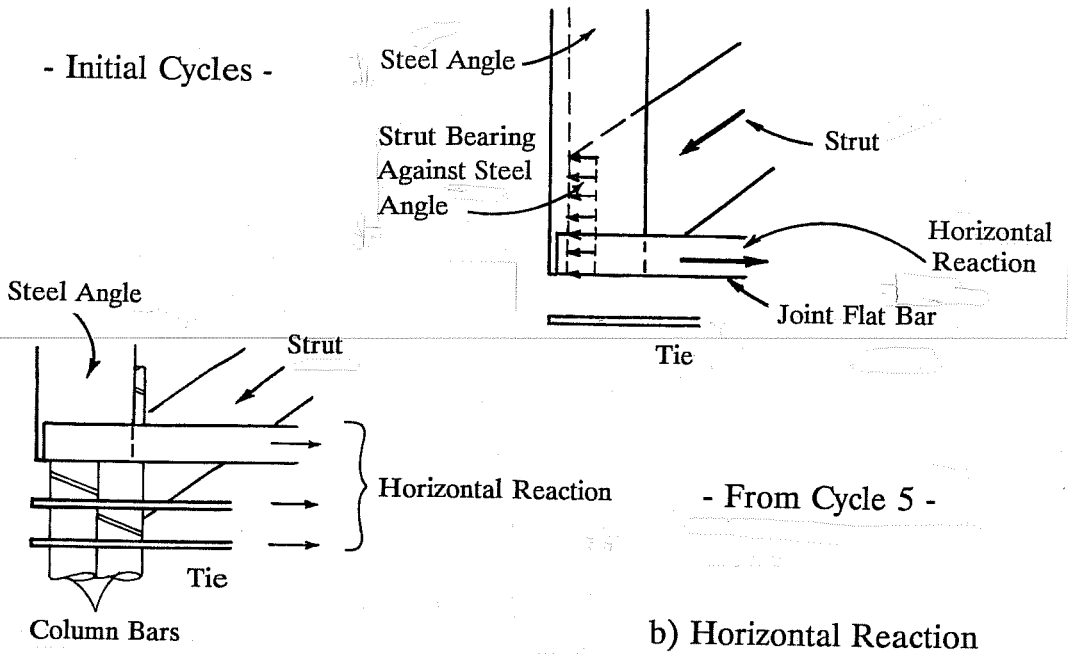

b) Horizontal Reaction

Figure 4.21 Specimen RB - Joint Concrete Struts

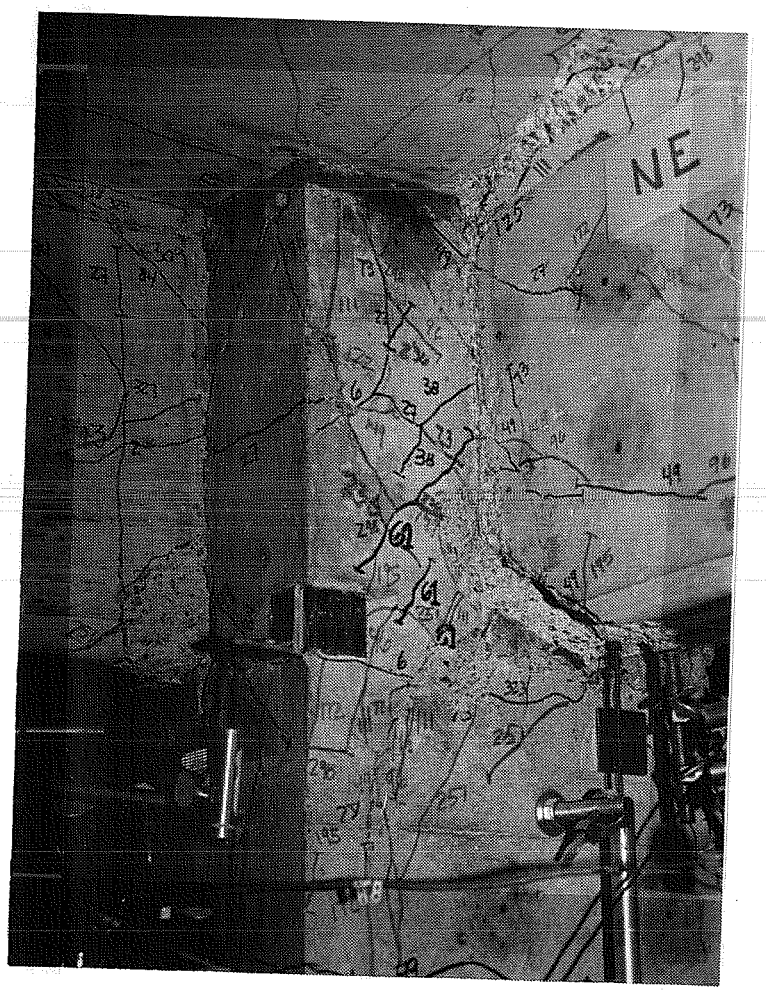

Figure 4.22 Specimen RB - Crack Pattern North Face

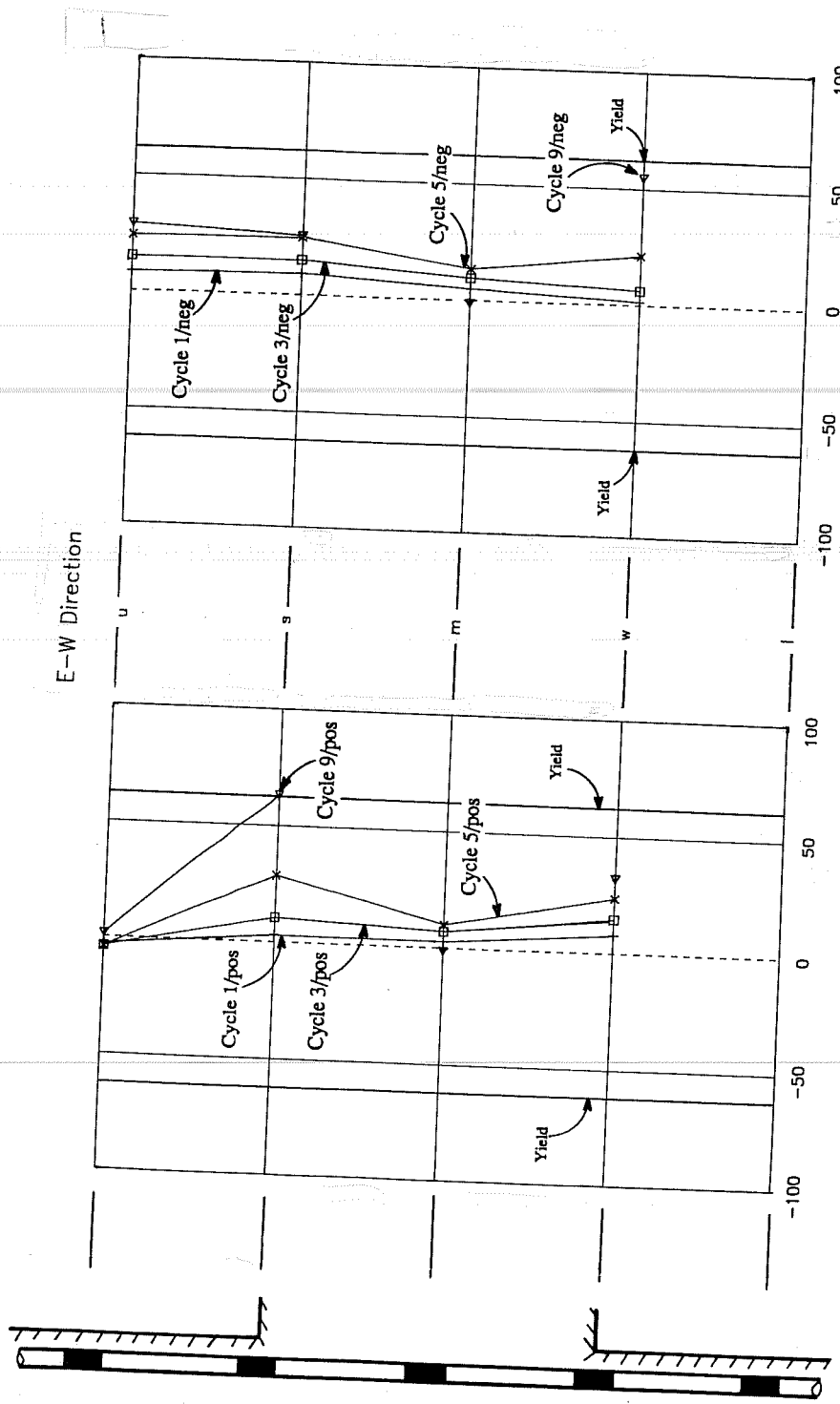

Figure 4.23 Specimen RB - Stress Distribution Column Bar (Jacketed Column - Corner Bar)

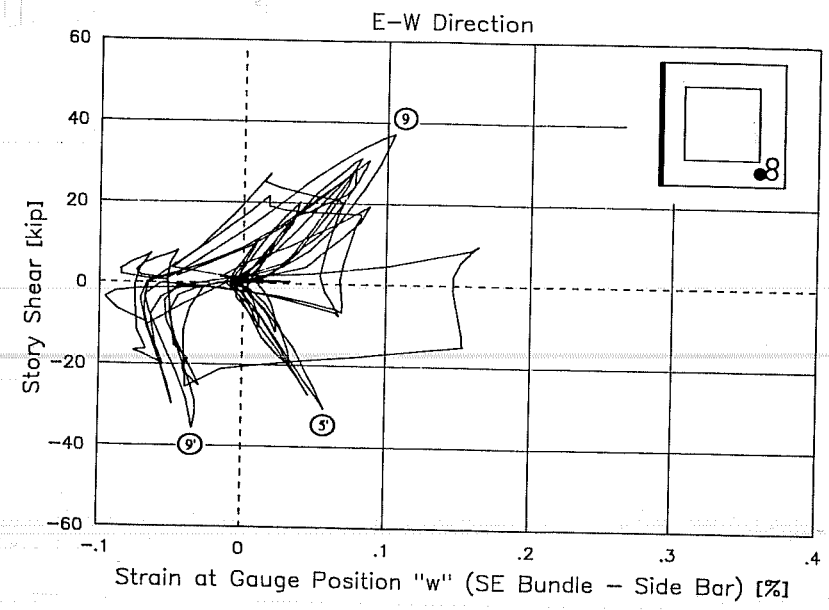

Figure 4.24 Specimen RB - Story Shear vs. Strain at Gauge Position "w" (Jacketed Column - Side Bar)

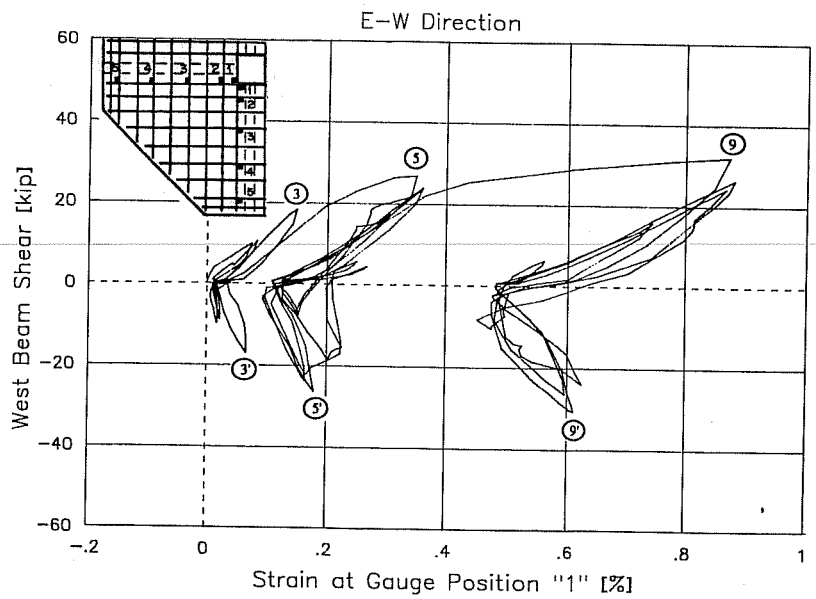

Figure 4.25 Specimen RB - West Beam Shear vs. Strain at Gauge Position "1"

4.3.2.3 Slab. Slab strains increased with increasing drift angle, both during unidirectional and bidirectional cycles. Generally, tensile strains were measured when loading in both positive and negative directions. In Figure 4.25, the west beam shear versus strain at gauge position "1" in the E-W top reinforcement is shown. Larger strains were measured than in test O (see Figure 4.11). Yielding occurred in cycle 5/pos. Large tensile residual strains were measured after positive loading was completed. When negative loading was applied, large compressive stresses were imposed on the bar. Compressive stresses in positions "1" and "2" (with maximum values of 51 and 61 ksi., respectively), caused the bars to buckle as was reported in Chapter III. The stresses were calculated considering the previous strain history and using a stress-strain model for steel which accounted for cyclic loading and the Bauschinger effect (see section 4.2).

The slab strains at positive loading peaks in the top layer for E-W and N-S bars are shown in Figures 4.26 and 4.27, respectively. Strains in bottom bar "6" were smaller than those in top bar "1". Bottom bar "7" showed same magnitude strains as those in top position "3" and "4". Same behavior was observed in all specimens. The strains at peaks of E-W unidirectional cycles 1, 3, 5, and 9 are presented in Figures 4.26a and 4.27a. The peak strains measured in N-S cycle 4 and bidirectional cycles 7 and 11 are illustrated in Figures 4.26b and 4.27b. In general, all specimens showed similar strain distribution across the slab.

During unidirectional cycles (Figure 4.26a), E-W slab strains increased with drift angle. Largest strains were recorded at 4% drift. Top bar strains were larger than bottom bar values. The strain distribution was uniform during first loading cycles. At large drift levels, the largest strains were measured near the column. Slab strains were much larger than those measured for specimen O (see Figure 4.12). It is observed in Figure 4.27a, that the E-W unidirectional cycles caused strains in the N-S reinforcement to balance the in-plane forces generated by the slab (Figure 4.28). In plane forces generated by the slab at the side of the transverse beam tended to rotate the slab quadrant with respect to the column axis. To balance the moment, strains were imposed on the reinforcement in the N-S direction. The largest strain was measured in the bar placed farthest from the column near the beam tip. The restraint provided by the hydraulic actuator against rotation around the beam axis caused the strain at gauge position "5" to be higher than those next to the column.

During cycles 4, 7 and 11, the E-W strain distribution was changed due to loading in the orthogonal direction (Figure 4.26b). In N-S bars the change was more noticeable (Figure 4.27b). During cycle 4, the highest strain was measured next to the column. In bidirectional cycles 7 and 11, the strain distribution was more uniform, particularly between gauges "2" and "5". Largest strains were also recorded at "1" adjacent to the column, which showed yielding in cycle 11/pos. The difference in the strain distribution across both E-W and N-S slab bars when bidirectional loading was applied, compared to that during unidirectional cycles, partially contributed to the drop in story shear observed in the story shear versus drift angle diagram (see Figures 3.16 and 3.17).

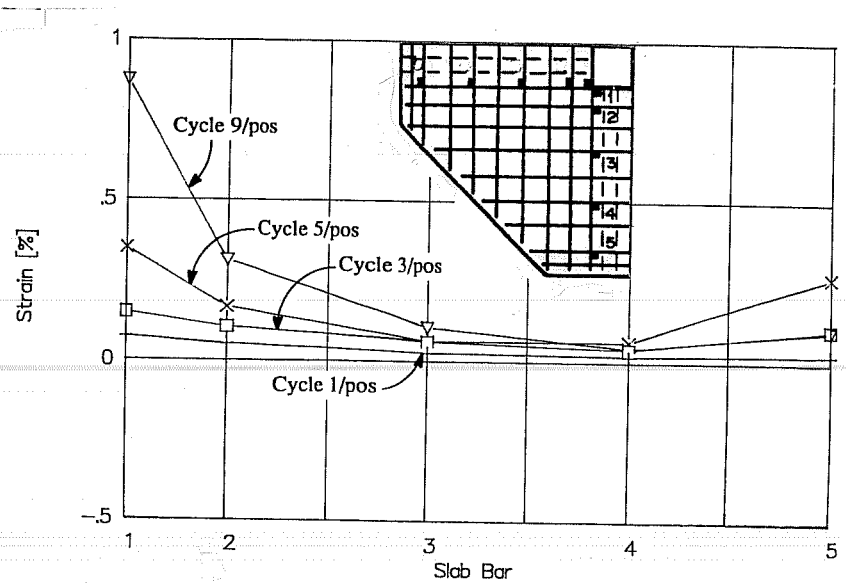

a) Unidirectional Cycles

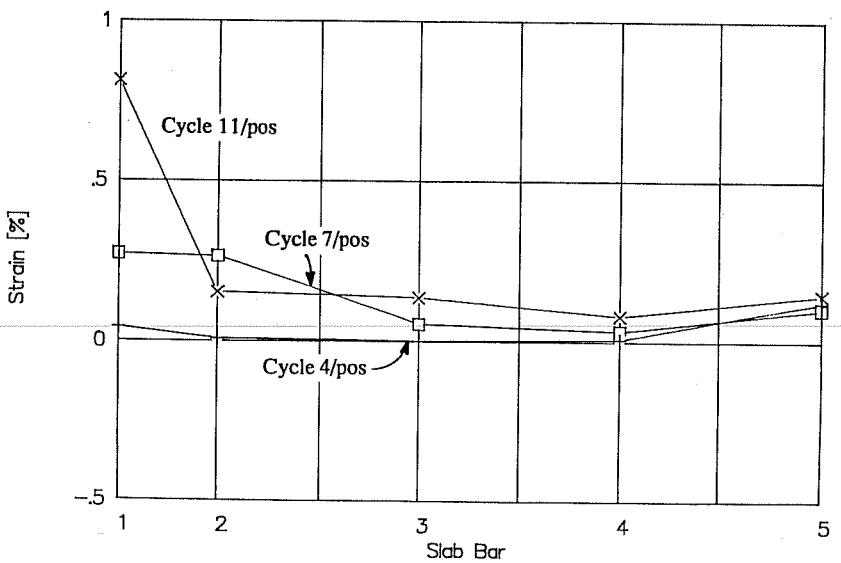

b) Bidirectional Cycles

Figure 4.26 Specimen RB - Strains Across E-W Top Slab Bars

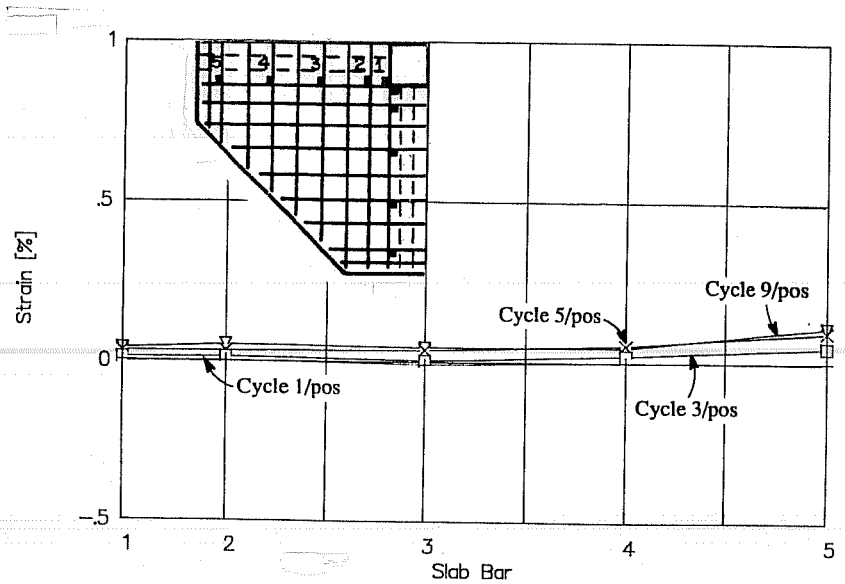

a) Unidirectional Cycles

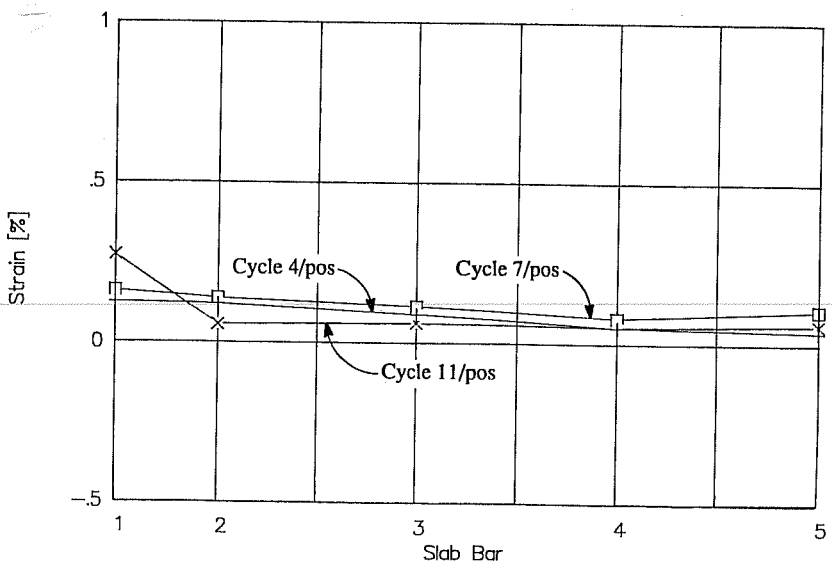

b) Bidirectional Cycles

Figure 4.27 Specimen RB - Strains Across N-S Top Slab Bars

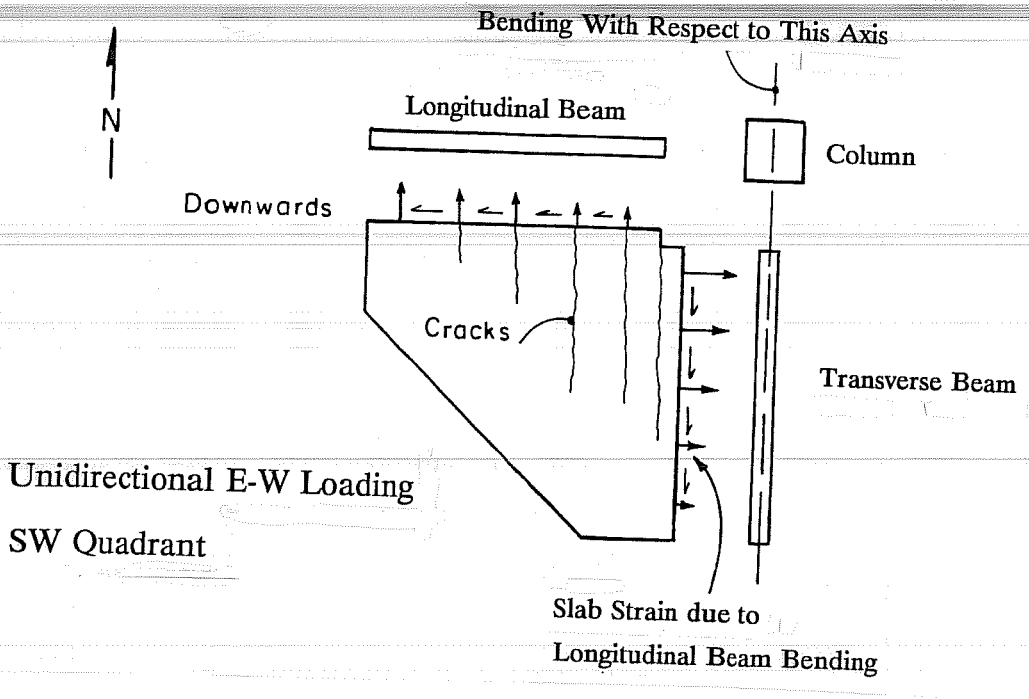

Figure 4.28 In-Plane Slab Forces

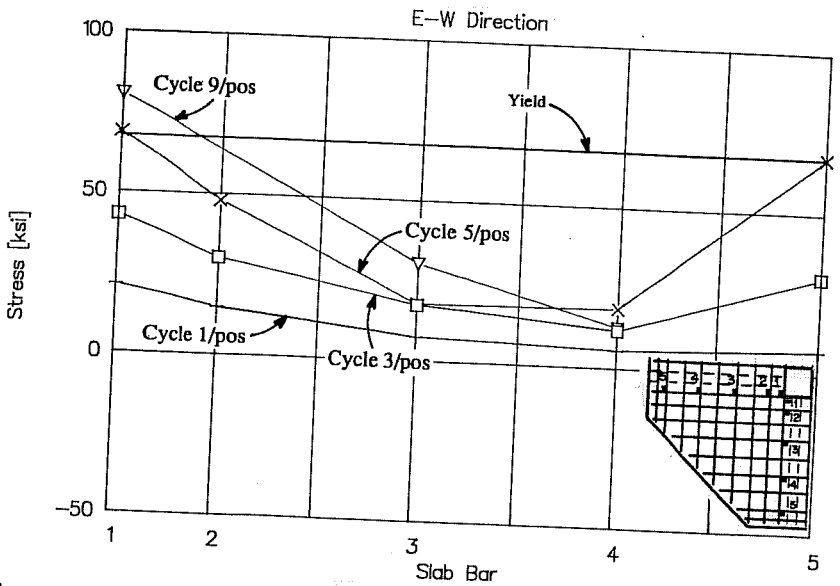

Figure 4.29 Specimen RB - Stresses Across E-W Top Slab Bars

In Figure 4.29, the E-W stress distribution for top bars for positive unidirectional cycles is shown. Stresses were highest in bars closest to the column. Some bars yielded. Bottom bar stresses (not shown) were slightly smaller than top bar stresses at the same location.

4.3.2.4 Joint. Strains in the transverse steel of the existing column and the jacket were measured with gauges located on ties above and below the joint (see Figures 2.28 and 2.29). No ties were placed in the joint region. Gauges placed in the original column ties measured smaller strains than those measured in test O. This was expected since the original column core was surrounded by the concrete shell and confined by transverse steel in the jacket. Gauges located on column transverse steel in the jacket showed elastic behavior with maximum strains of one-half of yield. Larger tensile strains were measured during loading which caused compression on the column face in which the gauge was situated.

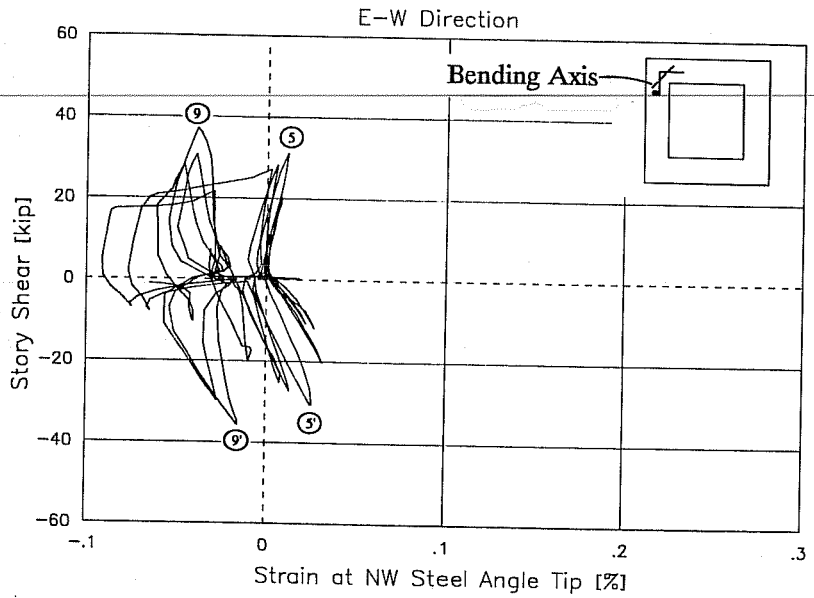

Figure 4.30 Specimen RB - Story Shear vs. Strain at Steel Angle Tip

Only specimen RB had the NW and SE steel angles in the joint gauged, whereas the other specimens were instrumented as shown in Figure 2.32. Gauges were mounted on the outside surface of the steel angles, and at a section corresponding to midheight of the beam web. The joint steel angles proved to be very effective in confining the bars and the concrete, and preventing the concrete other than the cover from spalling. Steel angles yielded in tension at the corner during cycle 9/neg and in compression at the flange tip during cycle 11/neg. Strain data from the steel angle in the NW corner will be presented. The NW corner was in the diagonal subjected to the highest biaxial forces during bidirectional cycles to 4% drift. In Figure 4.30, the story shear versus strain at the south tip of the steel angle is presented. Cycles up to 2% unidirectional drift, showed only tensile strains for both loading directions. Compressive strains were measured at large drift levels in which severe joint concrete spalling and joint deformations were noted (see Figure 3.22). During downward loading, the W beam soffit was bearing on the lower collar, as shown in Figure 4.31, and imposing a tensile force on the steel angles. The magnitude of the tension depended on the bending flexibility of the flat bar and on the deterioration of the beam

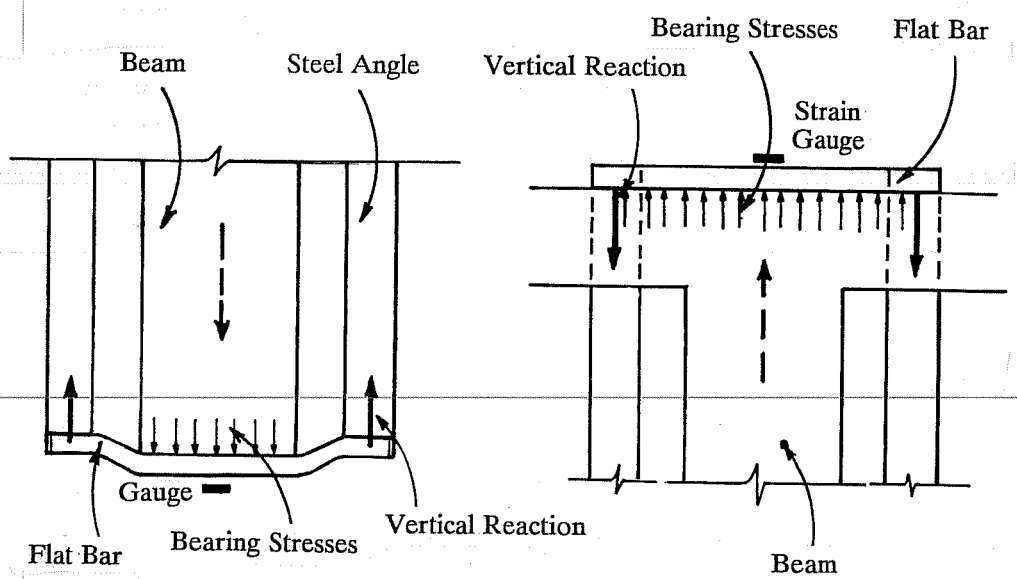

a) Beam Displaced Downwards b) Beam Displaced Upwards

Figure 4.31 Tension on Joint Steel Angles

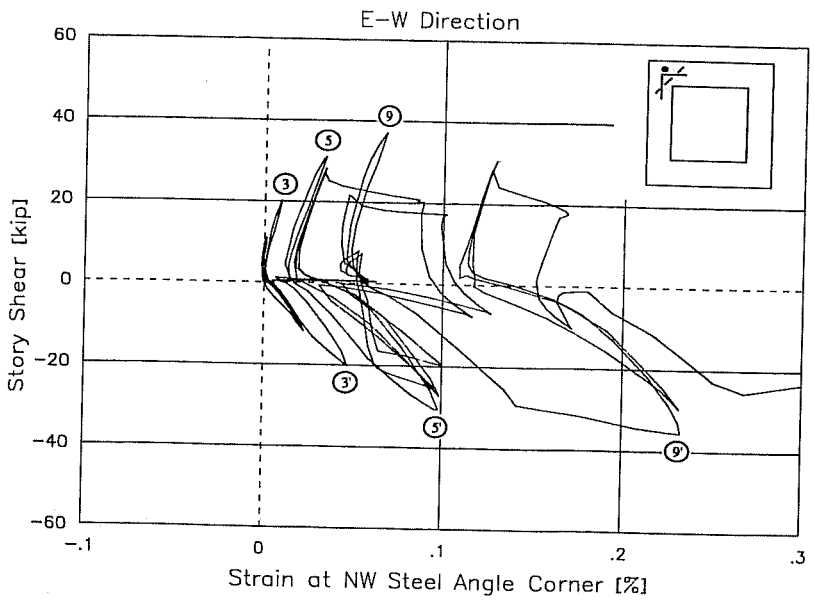

Figure 4.32 Specimen RB - Story Shear vs. Strain at Steel Angle Corner

bottom concrete. Similarly, when loading upwards, the slab reacted against the upper collar and resulted in tension on the steel angles. The tensile force stiffened the steel angle. Bulging of the joint concrete and curvature of column bars were obvious at large drifts during the test. During bidirectional cycles, concrete bulging and bar bowing caused bending of the steel angle with respect to the axis shown in Figure 4.30. Measured compressive strains confirmed bending of the steel angle.

In Figure 4.32, the story shear versus strain at the corner of the steel angle is shown. Only tensile strains were measured due to tension and bending of the steel angle. The strain at loading peaks for the steel angle gauges is shown in Figure 4.33. Tensile strains during first cycles were credited to tension on the steel angle from bearing of the beam and slab on the cage collars. At large deformation levels, bending of the steel angle caused compressive strains in the tip of the flanges and tension in the corner of the steel angle. Nearly symmetric behavior is observed in bidirectional peaks, particularly in cycle 11/pos in which the NW corner was subjected to the highest compression.

Gauges were placed on the top surface of the upper collar and on the bottom surface of the lower collar (see Figures 2.32 and 4.31). In Figure 4.34, the story shear versus strain at the lower flat bar in the N face is presented. Tensile strains were measured throughout. The collar was subjected to flexure caused by bearing of the beam during downward loading (Figure 4.31), and to tension produced by bending of the steel angles and by the horizontal component of the joint concrete struts (see Figure 4.21). Lower strains were measured in the upper collar since bending of the collar, and the reaction against bending of the steel angle were smaller.

4.3.2.5 Ultrasonic Pulse Velocity. Ultrasonic pulse velocity equipment was used to monitor the degradation of frame elements and to detect possible delamination between the original concrete and the jackets. Measurements were taken at the points shown in Figure 2.34. Direct readings were taken in beam and column faces, and semidirect measurements across the joint. The first set of readings ("zero" reading) was taken before the test and served as the basis of comparison for measurements taken during the test. Readings on the beam sides during test RB showed almost no variation throughout the test. Differences from initial readings were due to the presence of inclined flexure-shear cracks along the path of the pulse. Upper column readings in both directions increased 8% on the average during the test. The increase suggests that bond between the original column and the jacket was sound. After cycle 6, readings in the lower column rose 8% on the average, whereas after cycle 8 the measurements increased 40% from the initial readings. No evidence of delamination between the concretes was detected in the column strains. It is likely that flexural and shear column cracks near the joint affected the readings.

Joint measurements tended to increase as test progressed (Figure 4.35). The graph shows readings at the four sets of measurement points normalized with respect to the "zero" reading. Early in the test, large variations were noted because the original joint core was cracked severely from test O. After cycle 4, joint cracking, and delamination between the

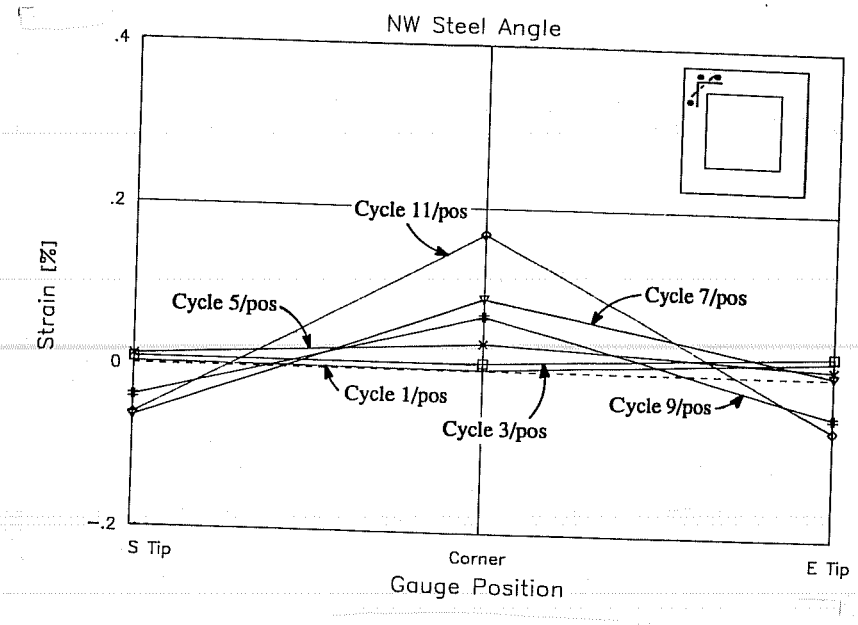

a) Positive Cycles

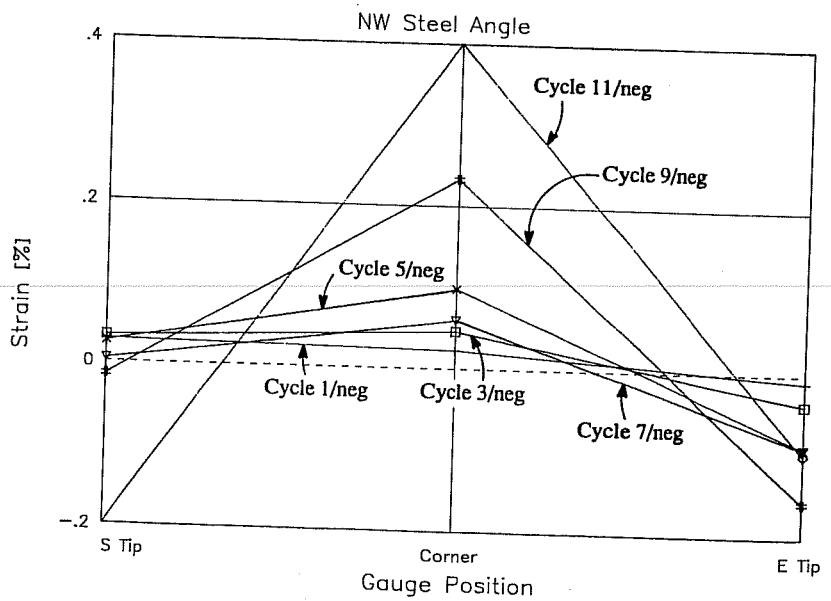

b) Negative Cycles

Figure 4.33 Specimen RB - Strain Distribution Steel Angle

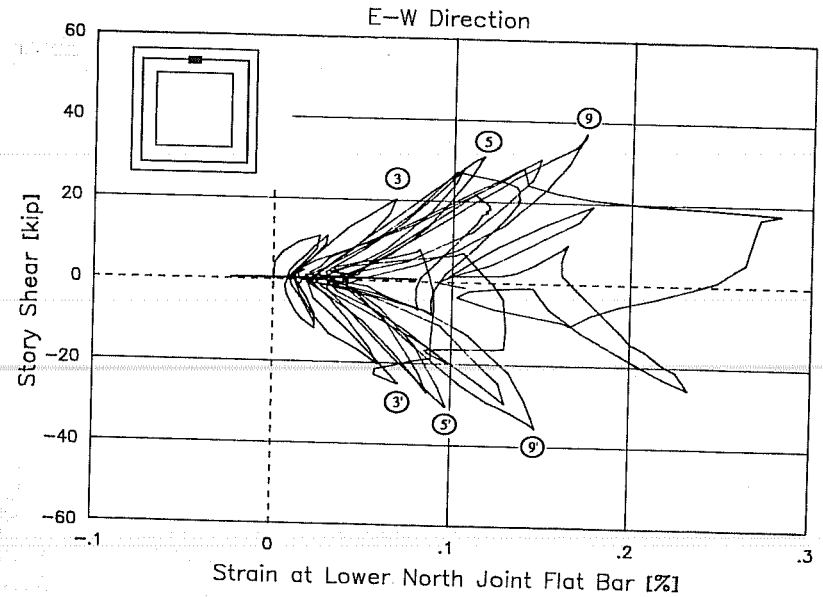

Figure 4.34 Specimen RB - Story Shear vs. Strain at Lower Flat Bar

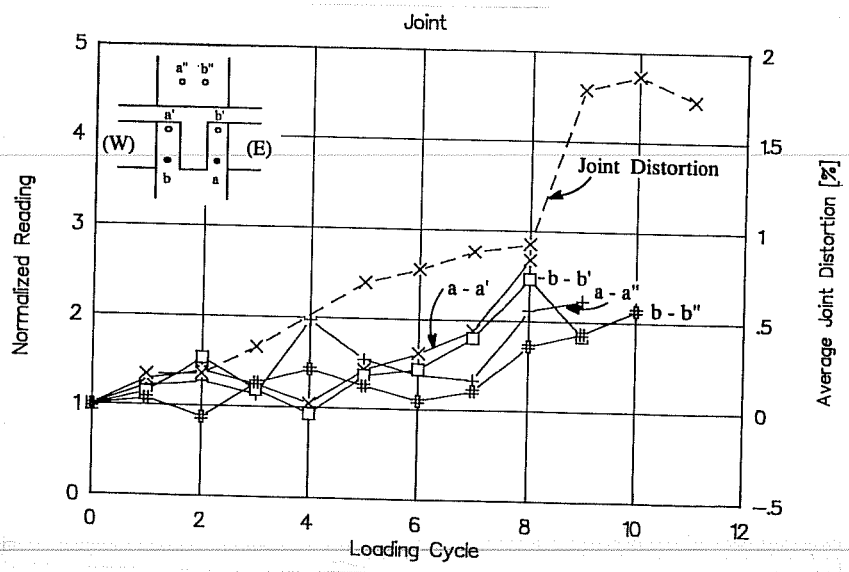

Figure 4.35 Specimen RB - Joint Pulse Velocity Measurement

joint cover and the steel angle were obvious and affected the consistency of the measurements. Joint damage could not be readily correlated with pulse velocity readings.

4.3.3 Summary. Specimen O developed column hinging which precipitated the joint failure. Column bar bond deterioration contributed to pinching of the story shear versus drift angle diagram, especially at 4% drift. Joint shear distortions and concrete damage in the joint also contributed to narrowing of the loops. Considerable damage had occurred before the column bars yielded at 4% drift. It is possible that structures with flexible columns might collapse without developing lateral drift ductilities (relative to first yielding) larger than one. No hinges were developed in the beams.

In the repaired specimen RB, beam hinges formed. Jacketing of the column improved the energy dissipation mechanism. Jacketing was effective as a repair technique. The joint failed after beam hinges formed. Joint distress contributed to pinching, strength decay and "softening" in the load versus deformation response of the specimen. The joint behaved as a hollow section so that forces were resisted by concrete struts in the jacket. The joint steel angles behaved as beam-columns subjected to axial tension. The steel angles prevented spalling of the core concrete. Top and bottom beam bars had virtually no anchorage capacity within the joint at large drift levels. Bond distress caused beam moment capacity reduction, slip of the reinforcement, premature crushing of the concrete and pinching of the force versus deformation response. With the development of beam hinging, slab strains were larger in RB than in test O.

4.4 COMPARISON OF SPECIMENS RB AND SB

To assess the effect on response of damage prior to jacketing, specimens RB and SB are compared.

4.4.1 Beams. Beam bar strains in SB were much larger than in RB. The yielding sequence of the beam reinforcement and slab bars next to the column in the E-W direction, and the load stages in which the bars yielded are shown in Figure 4.36a. Only working gauges are shown. The progression of bond loss is also illustrated for cycles after yielding (Figure 4.36b). Bond along top bars was better than in RB because the tensile strength of the concrete of the existing structure was higher and because the beams were undamaged before the test. In Figure 4.37, the W beam shear versus strain at gauge location "b" is shown. During negative loading (beam upwards), tensile strains were measured because the neutral axis was above the bars. Top beam reinforcement was placed 3 in. below the top slab surface. After yielding, local bond was damaged and the bar slipped after which the strain decreased until reaching the load peak 9/pos. In subsequent cycles, strain remained practically constant because the bar was debonded at this location.

Bottom beam reinforcement first yielded at "g" (see Figure 4.36) thus suggesting that the critical section was located inside the jacket similarly to specimen RB. Bond

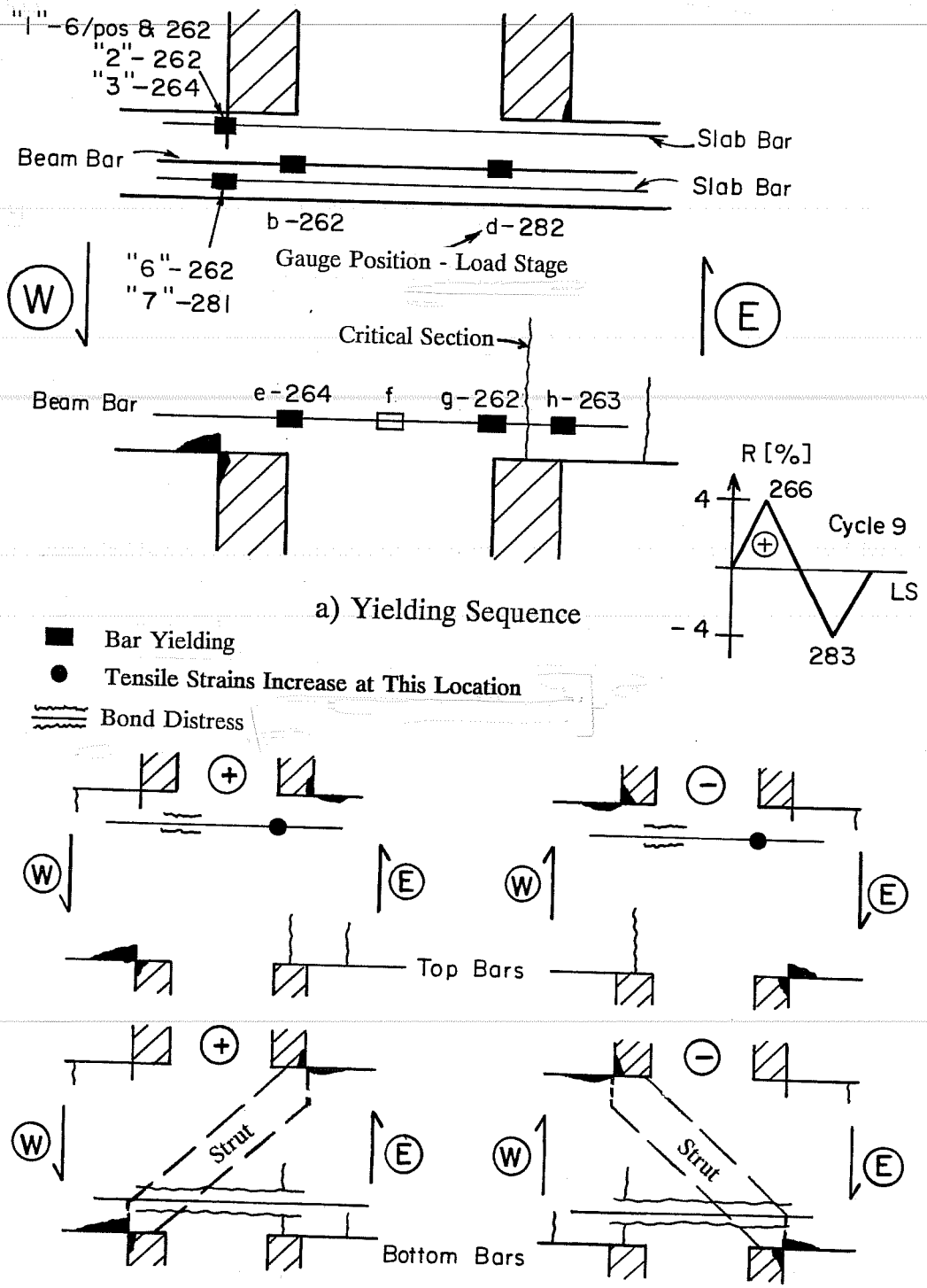

Figure 4.36 Specimen SB - Yielding Sequence (E-W Direction)

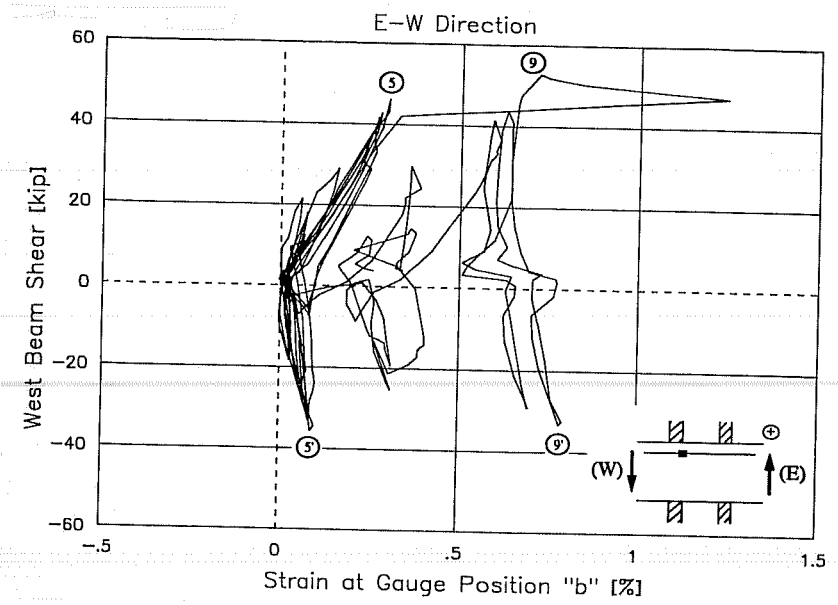

Figure 4.37 Specimen SB - West Beam Shear vs. Strain at Gauge Position "b"

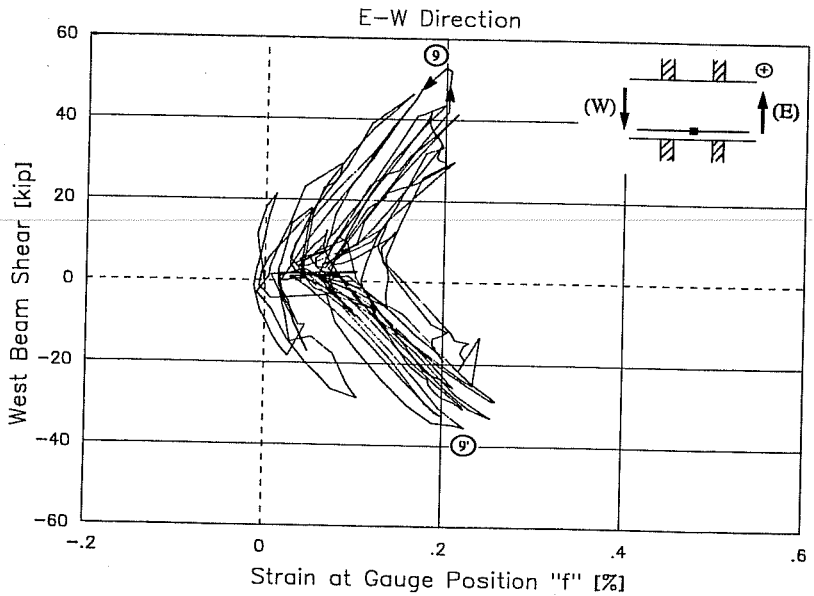

Figure 4.38 Specimen SB - West Beam Shear vs. Strain at Gauge Position "f"

deteriorated due to yield penetration which caused yielding at position "e" two load stages later. The bottom bar was completely debonded through the original column. Bond deterioration progressed in subsequent cycles and constant strain was measured during negative cycles. At gauge location "f" (Figure 4.38), load versus strain curves showed a constant strain segment when loading to cycle 9/pos, and increasing residual tensile strains which were sign of bond distress. Average bond stresses between "e" and "h" changed from 35 psi. in LS 265 to -189 psi. in LS 266. The sign change was indicative of bond damage.

With yielding of the top or bottom reinforcement the neutral axis moved towards the extreme face in compression. The strain gradient increased and crushing was observed in the E side of the slab and in the W beam in cycle 9/pos. Large cracks in the E beam were also observed. Tensile residual strains in the top reinforcement prevented cracks from closing, and reduced the stiffness of the specimen. Before bond damage occurred, joint forces were distributed to the concrete primarily by bond along the column and beam bars (see Figure 1.1d). After debonding of bottom reinforcement, the tension force in the beam reinforcement not transferred to the joint concrete through bond, had to be resisted by concrete at the compression face of the joint where the bar was anchored (see Figure 4.36b, for bottom bars). The magnitude of compressive stresses in the strut increased. The concrete strut was weakened by cyclic loading and the compressive strength was reduced by tensile strains perpendicular to the direction of the strut. The strut eventually failed in shear compression. In subsequent cycles to 4% drift (cycles 10 through 12), top bar bond distress and bond loss in bottom bars contributed to pinching of the story shear versus drift angle response (see Figure 3.25). Beam angle loops (see Figure 3.27) also showed considerable stiffness degradation. Beam curvatures increased after cycle 9 because the reinforcement slipped (see Figure 3.28).

4.4.2 Column. In general, strains in the original column steel were similar to those of RB. Larger strains were measured in SB because larger story shears were applied. At same load level for a given cycle, strains in SB were smaller because the section was stiffer. The original joint core was undamaged before rehabilitation, and the concrete was 70% stronger than in RB.

Bundled reinforcement in the jacket of SB yielded in a few locations. The NE corner bundled bars were subjected to the highest forces during bidirectional cycles to 2% drift. In Figure 4.39, the story shear versus strain at position "s" in the corner bar is shown. Load versus strain curves exhibited normal tension-compression behavior and excellent bond. From cycle 9, positive cycles showed some stiffening as cracks closed, particularly around joint collars. Strains increased after crushing of column concrete around the upper joint collar. Strains at "w" were similar (not shown). In Figure 4.40, the story shear versus strain at position "m" is presented. Nearly symmetrical C-shaped loops and increasing residual strains were evident as the test progressed. Increase in residual strains is sign of locked-in stresses and local bond distress. Anchorage of the bar was assured at sections "s" and "w", in which the surrounding concrete in compression, and the steel angle and collars confined the reinforcement. Bond distress at position "m" was expected because the bar was confined

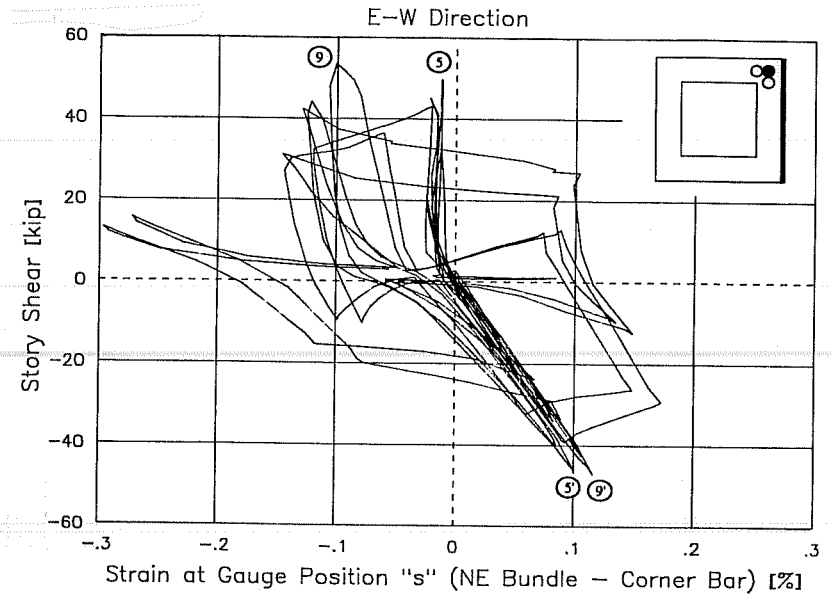

Figure 4.39 Specimen SB - Story Shear vs. Strain at Gauge Position "s" (Jacketed Column - Corner Bar)

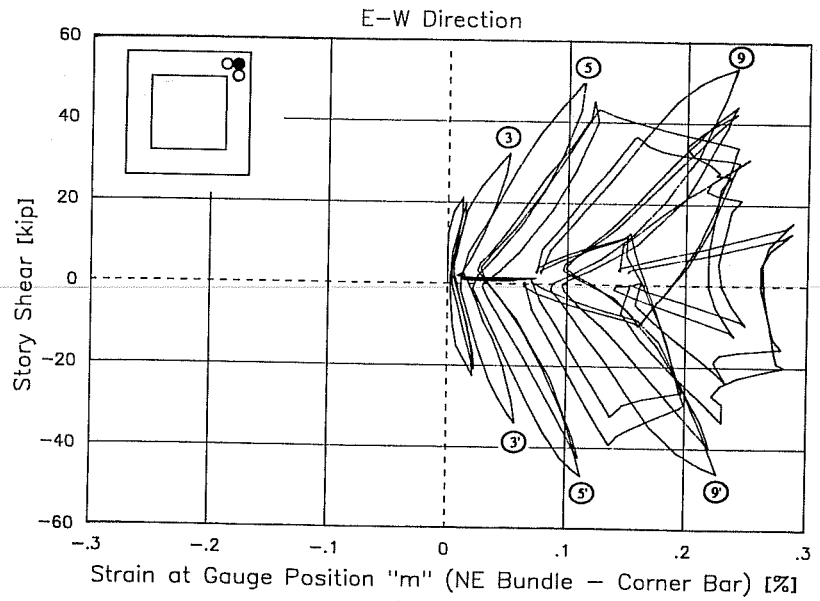

Figure 4.40 Specimen SB - Story Shear vs. Strain at Gauge Position "m" (Jacketed Column - Corner Bar)

only by the steel angle. The maximum average bond stress between "s" and "w" was u_m =1480 psi. (*DBI* =540 psi. and *MBI* =1750 psi.). The beam depth to bar diameter ratio was 18. Larger bond stresses can be calculated between gauges at "m" and "w" during positive cycles and between "s" and "m" during negative loading.

In Figure 4.41, strain at "s" in the W bar of the NE bundle is shown. The tension-compression loops were different from those in test RB (see Figure 4.24). In specimen SB, the joint strut involved both the jacket and the original core, and the strut vertical component was reacted by the concrete in compression across the column width. The bundled bars in the joint were not required to balance the vertical strut component as in RB.

4.4.3 Slab. Yielding of E-W top slab bars was noted in positions "1" through "4" and in positions "6" and "7" for bottom bars. N-S top bars at positions "1", "2" and "3" and bottom bars at "6" yielded during cycle 11/neg when the S beam was displaced downwards. Some bars in both directions strain hardened by the end of the test. Larger strains and more inelastic behavior were observed in the slab in SB than in RB. More crushing and spalling of concrete occurred around the column. Some spalling occurred between beam torsional cracks in the top slab surface. From examination of the deformed shape of the twisted beam (see Figure 4.42, taken from Ref. 14), it can be observed that the walls of the beam do not remain plane surfaces. Because of the curvature of the walls, diagonal compressive strains are maximum, ϵ_{ds}, at the surface and decrease linearly with the distance from the surface. Tensile strain will occur below a certain distance, t_d. The outside concrete spalls off and the inside concrete is in tension. This phenomenon explains the observed concrete spalling between torsional cracks over the beams. Similar distress was found in all rehabilitated specimens but was less severe than in SB.

In Figure 4.43, compressive strains in the first negative half-cycles (upward loading) at position "1" in the E-W direction can be observed (see Figure 4.25 for RB). After yielding in cycles to 2% and 4% drift, a large strain decrease was noted when loading was reversed. Large tensile strains, remaining after positive half-cycles were completed, produced compression stresses in the top reinforcement in the subsequent half-cycle. Peak compressive stresses occurred before the loading peak was reached because compressive forces in slab bars were redistributed to the concrete when the crack closed. Large compressive stresses (up to 84 ksi., computed from the cyclic strain history) caused buckling of the bar.

In Figure 4.44, the strain distribution in the E-W top slab bars for positive unidirectional cycles is presented. In some bars, measured strains at 4% drift were more than four times those measured in test RB, which suggests much larger slab participation. Large slab participation in negative bending is also evident in the stress distribution shown in Figure 4.45 for the E-W direction. At 4% drift, slab bars up to position "4" showed stresses equal to or higher than the yield strength. The large slab participation caused beam

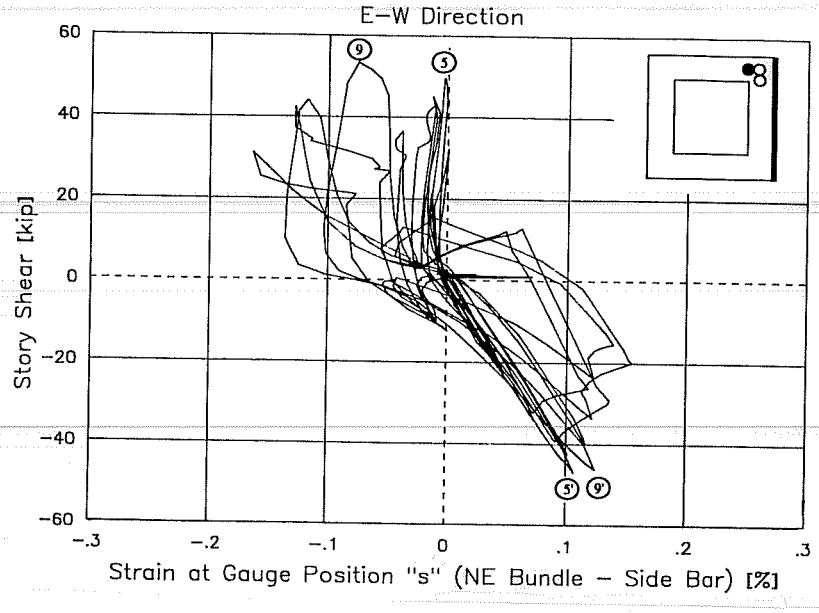

Figure 4.41 Specimen SB - Story Shear vs. Strain at Gauge Position "s" (Jacketed Column - Side Bar)

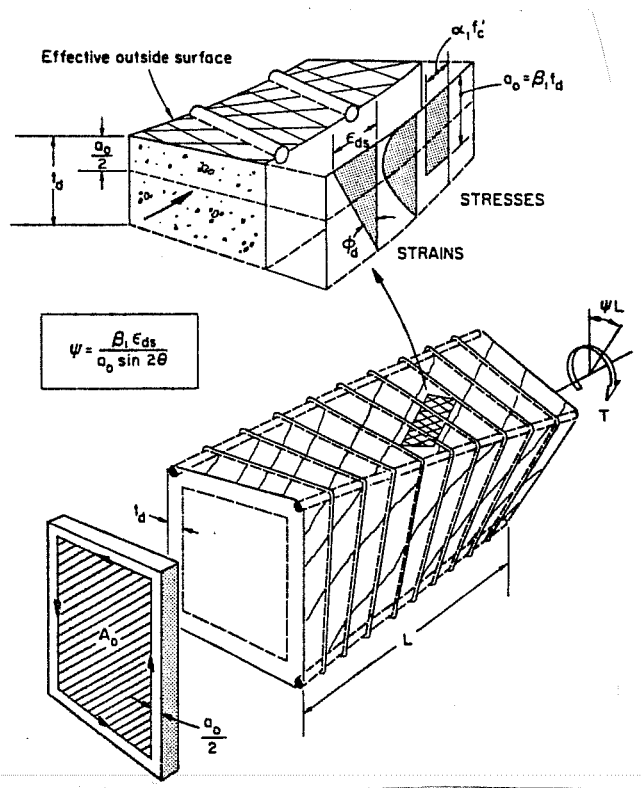

Figure 4.42 Deformed Shape of a Twisted Beam (from Ref. 14)

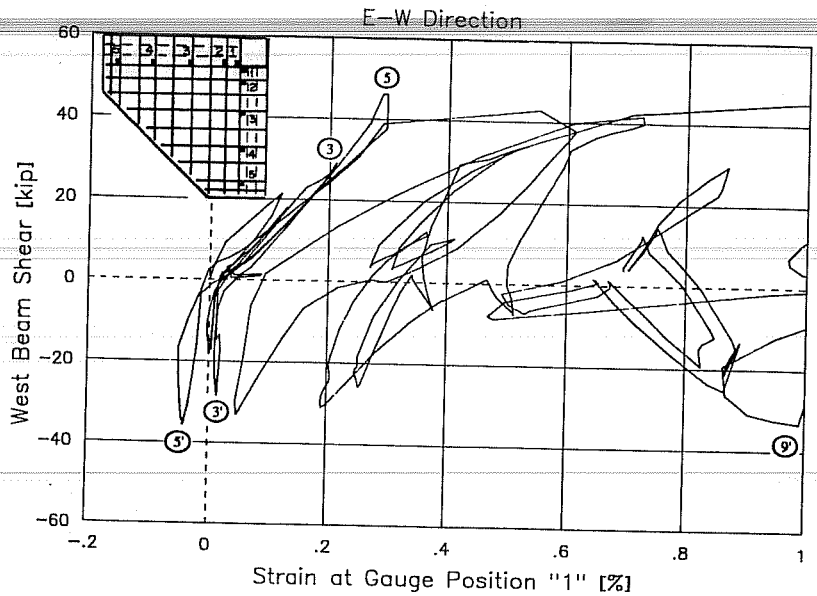

Figure 4.43 Specimen SB - West Beam Shear vs. Strain at Gauge Position "1"

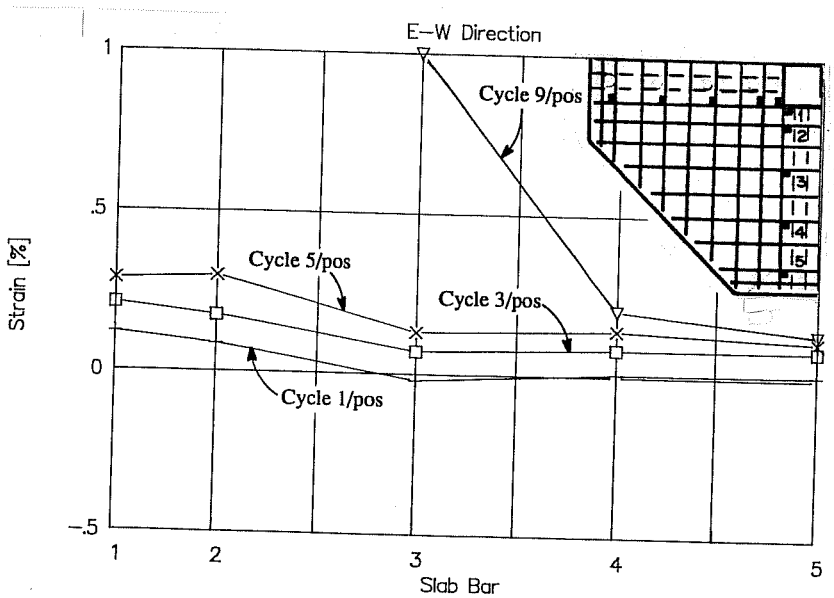

Figure 4.44 Specimen SB - Strains Across E-W Top Slab Bars

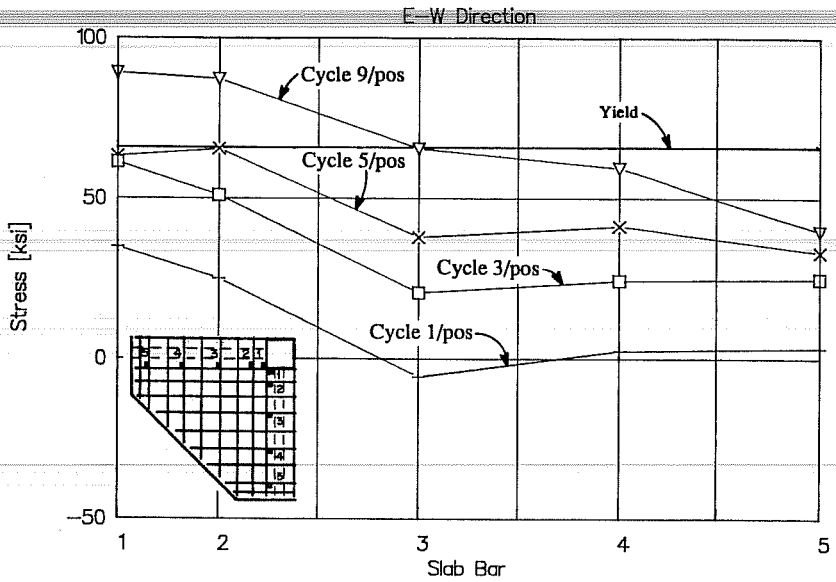

Figure 4.45 Specimen SB - Stresses Across E-W Top Slab Bars

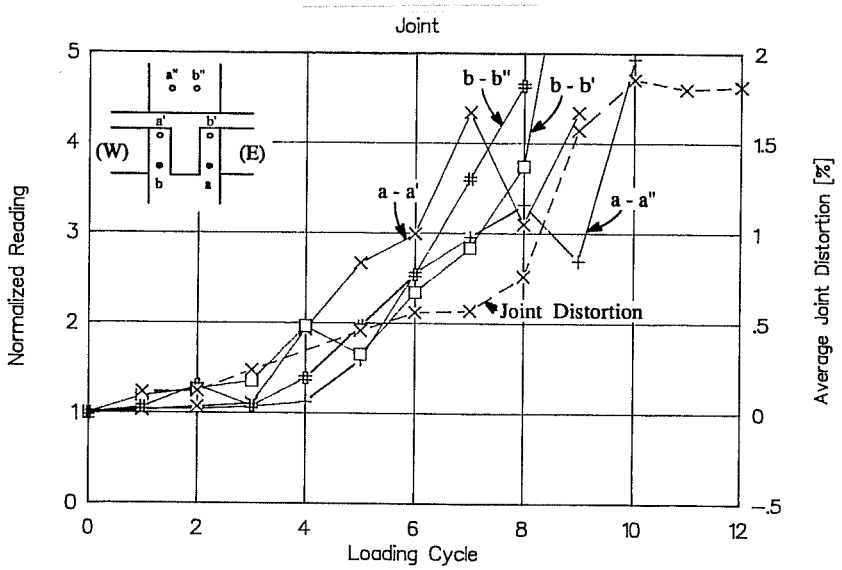

Figure 4.46 Specimen SB - Joint Pulse Velocity Measurement

curvatures to be reduced when the beam was displaced downwards. Inelastic strains in the slab bars also increased the energy dissipated (see Figure 3.28).

4.4.4 Joint. The steel angles behaved similarly to those in RB. First yielding in tension was detected during cycle 7 in the corner gauges and in compression during cycle 9/neg at the tip of the SW angle. Although specimen SB showed smaller joint distortions at cycles to 4% drift, strains in the steel angles were larger. Higher forces in the joint caused severe distress and bulging of the strut (see Figure 3.31). Permanent bending of bundled bars caused larger tensile strains than in RB. Joint collar strains were smaller at the same load levels than in RB (by a factor of 1/3 during cycle 5, for example). In test RB, joint forces were mainly resisted by parallel concrete struts in the column jacket. The horizontal component of the struts reacted against the lower portion of the steel angles stretching the lower joint collar and thus increasing the strains (see Figure 4.21). Conversely, the strut in specimen SB formed through the undamaged original core and the jacket, and was reacted by column and beam compressive stress blocks.

4.4.5 Ultrasonic Pulse Velocity. As in RB, pulse velocity measurements in the beams were almost constant during the test. Pulse velocity readings in the column increased slightly, thus suggesting that the column was monolithic. For example, upper column readings increased 3% on the average by the end of the test. Measurements across the joint (normalized with respect to the "zero" reading) are presented in Figure 4.46. Almost no joint damage occurred before cycle 4 so that readings remained constant. From cycle 5, readings increased with joint distortion. At large drift levels measurements were affected by joint cracking and spalling. A better correlation between pulse velocity readings and joint distortion was observed for SB than for RB, because the column core was undamaged.

4.4.6 Summary. Specimens RB and SB developed beam hinges which caused the joint to fail in shear. Bond along top beam bars was better in SB than in test RB because the concrete was stronger and beams were undamaged before the test. Bottom beam reinforcement lost bond strength across the joint. Joint forces in SB were mainly resisted by a concrete strut across the jacket and the original column core, whereas in RB, joint shear was resisted by a pair of struts formed in the jacket. With the different load transfer mechanism across the joint, column strains inside the joint were distinctly different in SB than in RB. Normal tension-compression loops and good bond were noted in SB. The slab was more stressed and the slab participation in negative bending larger in SB than in RB.

4.5 COMPARISON OF SPECIMENS SB AND SD

The difference in performance of jackets with bundled or distributed reinforcement is assessed by comparing specimens SB and SD.

4.5.1 Beams. In Figure 4.47, the yielding sequence in the E-W slab and beam bars is presented. Only working beam gauges are shown. E-W beam yielding occurred in cycle 5. The yielding sequence and strains were somewhat different from those in SB (see Figure 4.36).

In cycle 5/neg, bottom beam bar yielded at "e" (Figure 4.48) causing the neutral axis to rise. The strain gradient increased enough to yield the top beam bars at positions "a" (Figure 4.49), "b" and "c" and at position "6" in the bottom slab bar. Top slab bar at gauge location "1" was subjected to compressive stresses. Bond distress in the bottom beam bars progressed in subsequent cycles. As mentioned, top beam reinforcement yielded simultaneously along three positions and it is likely that bond loss occurred due to yield penetration. Yielding of beams marked the onset of nonlinear behavior of the joint (see Figure 3.41). In following cycles to 2% drift, some stiffness and strength degradation was noted (see Figure 3.35).

Forces on the joint were highest during cycle 9, and caused large joint distortion and severe joint damage which finally led to joint failure. At gauge position "h", the bar yielded during cycle 9/pos (Figure 4.47). In subsequent cycles, crushing in the bottom concrete caused large compression forces on the bottom bar which increased the bond distress. In cycle 9/neg (LS 286), during downward loading of the E beam, the W beam yielded at "a". After, the top bar was pulled through the joint losing bond. Splitting cracks were observed on top of the E beam and considerable crushing in the E beam was noted. Since the top bar lost anchorage in the tension side of the joint (E side) and through the joint, the bar was anchored in the compression face of the joint (W side), thus increasing the force to be resisted by the diagonal strut (see Figure 4.36b for SB, in which the same phenomenon is illustrated for bottom beam bars).

Bond loss along top and bottom beam bars contributed to pinching in the hysteretic response, especially after 4% drift as noted in the beam angle curves (Figure 3.37). With further cycling to 4%, there was a reduction in energy dissipated. Bond conditions deteriorated in cycle 11 when beam crushing penetrated into the joint. Average bond stresses along bottom bars reached a maximum of $u_m = 1190$ psi. in cycle 5/neg, whereas $DBI = 475$ psi. and $MBI = 1760$ psi..

N-S bottom reinforcement yielded in cycle 7 and top bars in cycle 11. N-S bars exhibited good bond behavior.

4.5.2 Column. The column showed elastic behavior as can be seen in the column angle curves. In general, original column strains were the same as in specimen SB.

The reinforcement of the jacket was distributed around the perimeter. In each quadrant, one bar was placed at the corner and two against the beams sides. Corner bars showed behavior nearly equal to that of the corner bars in specimen SB. Bars developed excellent bond behavior ($h/d_b = 18$), and exceeded the yield strain at some locations in cycle

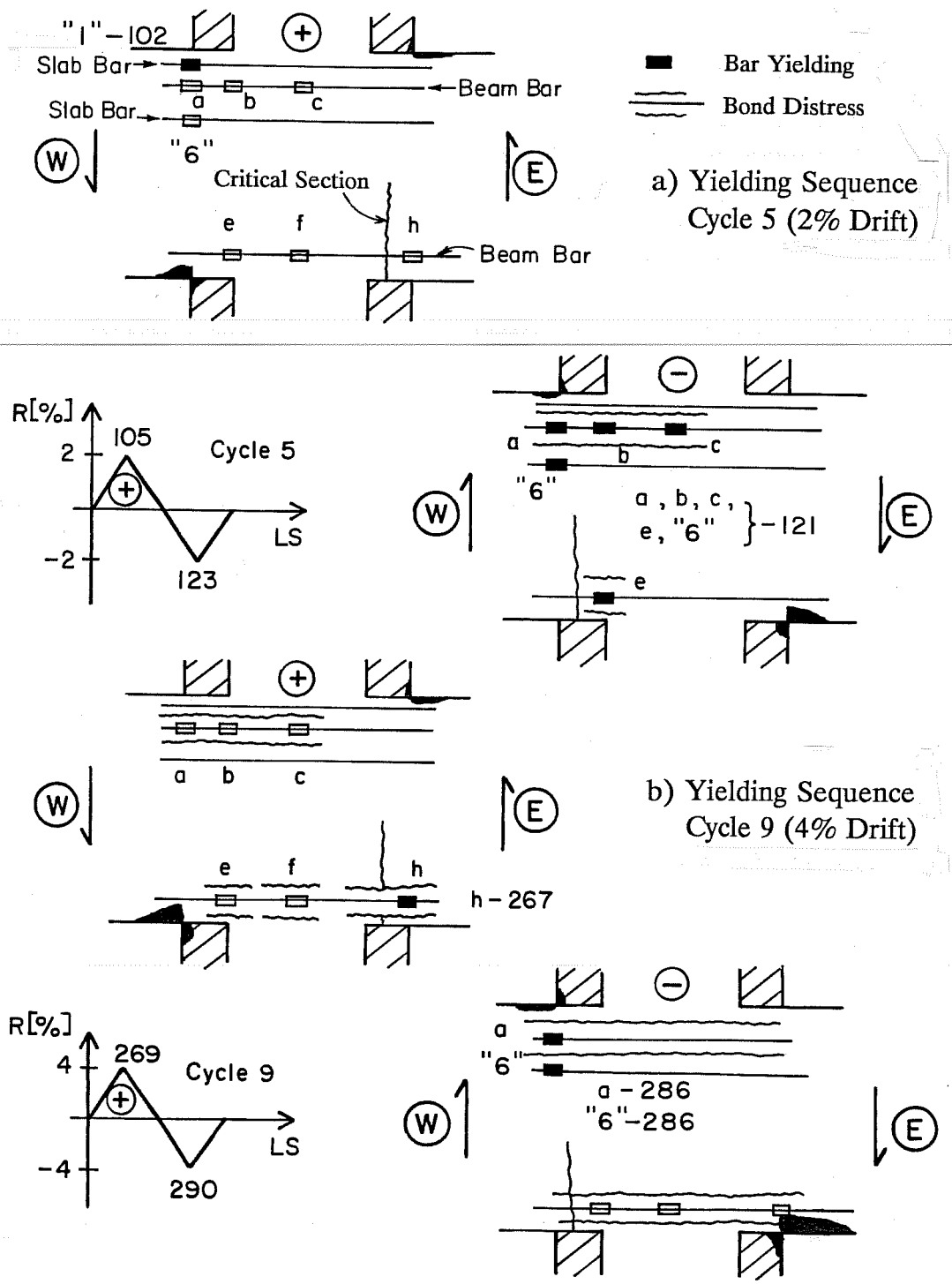

Figure 4.47 Specimen SD - Yielding Sequence (E-W Direction)

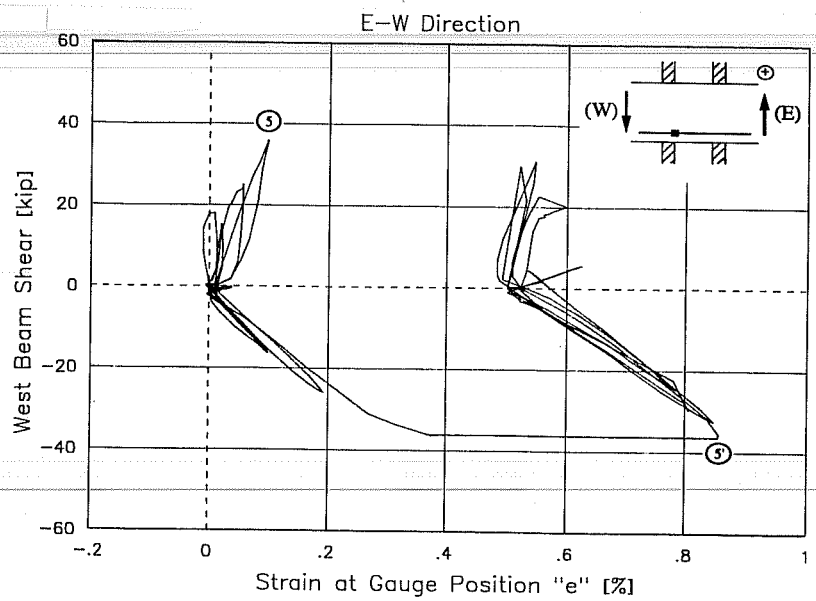

Figure 4.48 Specimen SD - West Beam Shear vs. Strain at Gauge Position "e"

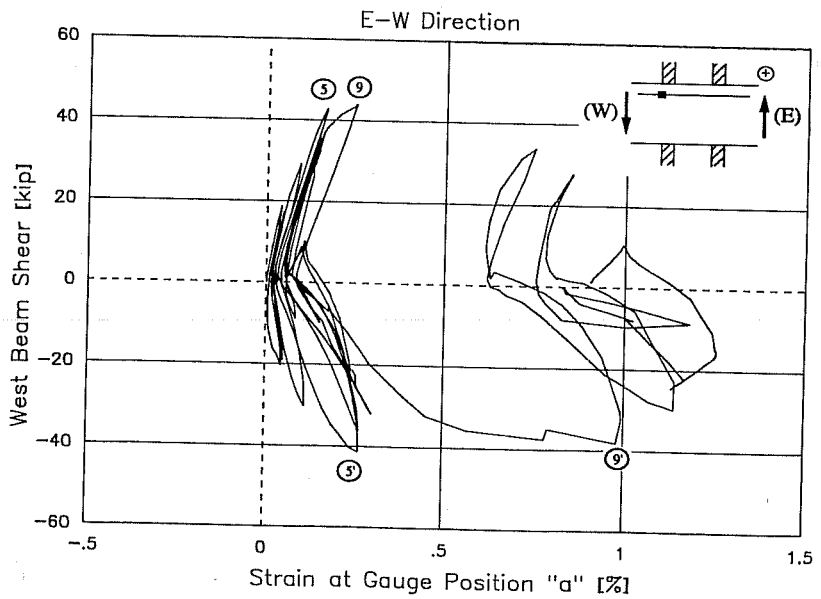

Figure 4.49 Specimen SD - West Beam Shear vs. Strain at Gauge Position "a"

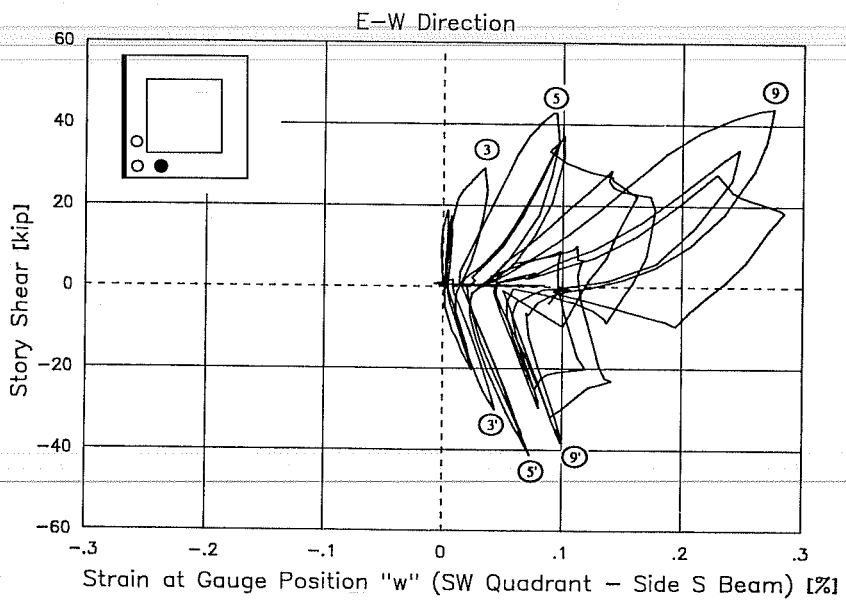

Figure 4.50 Specimen SD - Story Shear vs. Strain at Gauge Position "w" (Jacketed Column - Side Bar)

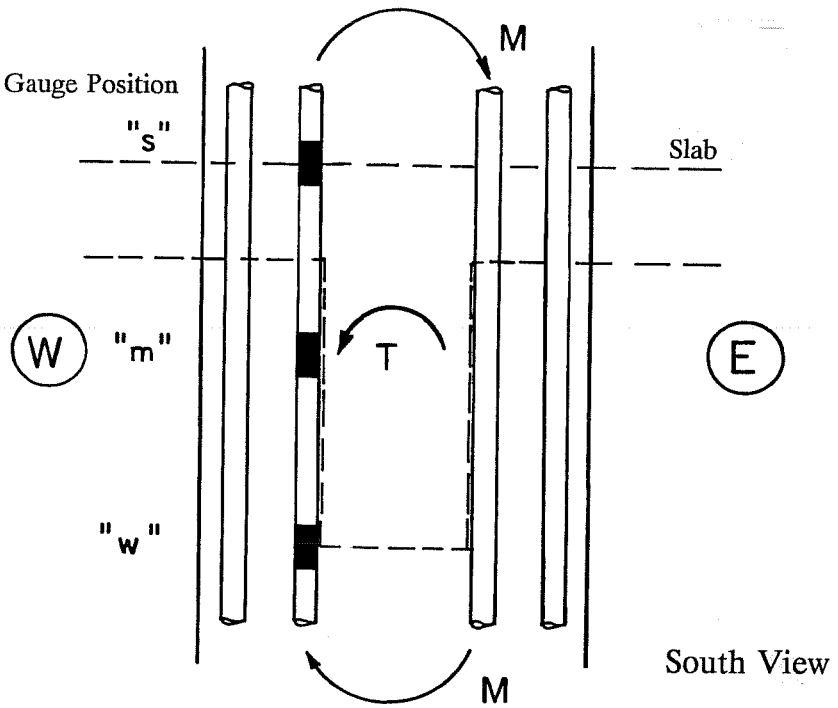

Figure 4.51 Specimen SD - Torsional Moment on Column Face

11. At the same load levels in a given cycle, larger strains were measured in test SD because the joint region was more flexible. Larger flexibility of the joint is confirmed by comparing the joint distortion curves for SB and SD. The distributed bars of the column reinforcement were the main reason for the difference (see Figures 3.31 and 3.41).

The bars placed against the beam sides performed differently from the lateral bar in the bundles of SB. In Figure 4.50, the story shear versus strain at position "w" in the bar contiguous to the S beam in the SW quadrant is shown. Positive loading applied compression on the lower column W face. Larger tensile strains were measured in positive half-cycles than in negative loading. Torsional moment transferred from the transverse beam caused the difference in bar strains (see Figure 4.51). The response is analogous to the column bars of specimen O (Figure 4.8). Strain at position "s" was alike (not shown). The bar showed good bond. Maximum bond stress was $u_m = 1135$ psi. in cycle 9, while the calculated bond indexes were $DBI = 525$ psi. and $MBI = 1750$ psi..

4.5.3 Slab. Only a few gauges worked in the E-W direction of SD. Most of the N-S gauges malfunctioned before testing started. Due to the lack of information, strain and stress distributions are not presented. Working gauges showed lower strains than in SB coinciding with the reduction in damage observed. Comparing strains in specimens RB, SB and SD, it is likely that the level of slab participation of SD was between the participation for RB and SB. Strains in the E-W top slab bar "1", for example, were 20% smaller than those in SB. Large stress reversals due to large tensile residual strains were recorded in the top bar at gauge position "1". Compressive stresses, as high as 80 ksi. (calculated from the cyclic strain history), were imposed and caused a small separation of the bar from the slab concrete. The E-W bottom bar "6" showed plastic strains 50% smaller than those in SB. The bar exhibited tensile stresses throughout the test.

4.5.4 Joint. Due to confinement requirements of Refs. 2 and 3, specimens SD and SD-B had four sets of five corner ties in the joint region. The corner ties had two 135-deg hooks and were spaced as were the column ties. Figure 4.52 shows the story shear versus strain of a corner tie located in the SW corner at midheight of the beam stem. The loops were C-shaped and showed increasing peak strains as test progressed thus coinciding with increasing joint distortion. Significant increment is observed at cycles to 4% drift during which large joint cracking and bulging of the core occurred. Corner ties remained elastic and confined effectively the joint core.

Consequent with the observation that the joint in SD was more flexible than in SB, larger strains in the steel angles at the same load levels in a given cycle were measured in SD than in SB. Yielding in the corner occurred in cycle 7 when the quadrant was subjected to highest biaxial tension. Steel angle tips yielded in compression in cycle 9/pos. In general, strains increased in cycles to 2% drift and especially at 4% drift due to bulging of the joint. The behavior of the joint collar was the same to that in specimen SB.

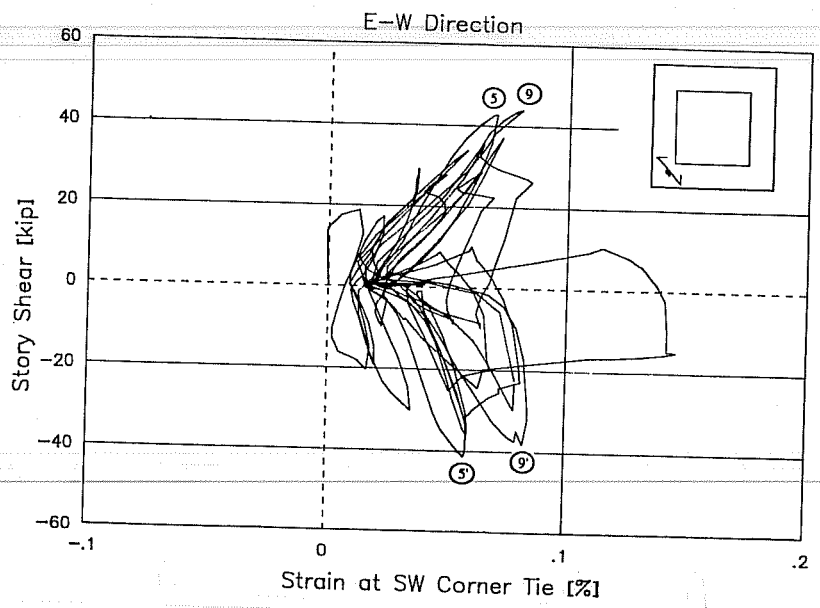

Figure 4.52 Specimen SD - Story Shear vs. Strain at Corner Tie

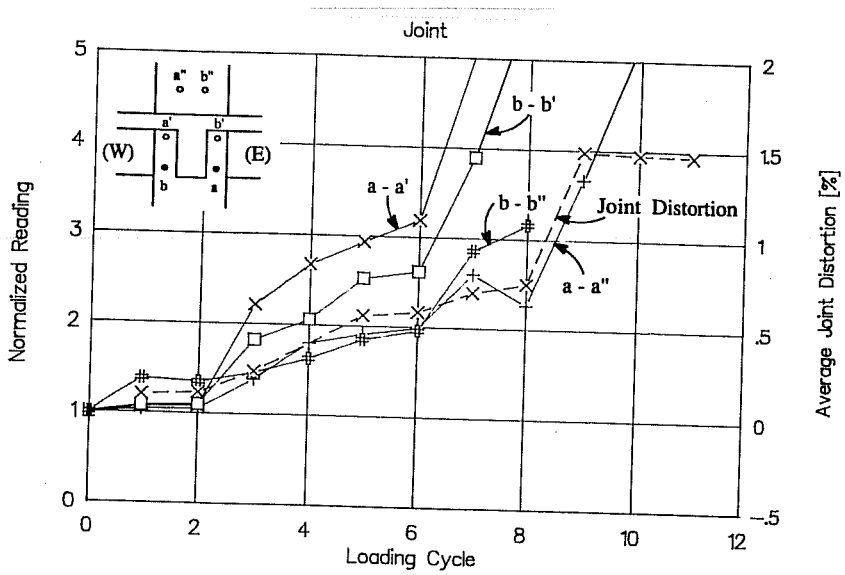

Figure 4.53 Specimen SD - Joint Pulse Velocity Measurement

4.5.5 Ultrasonic Pulse Velocity. Ultrasonic pulse velocity readings in the beam were similar to those in SB. Measurements in the column were indicative of monolithic behavior. Pulse velocity increased 3% on the average in the upper column, and 15% in the lower column, from the start to the end of the test. Joint readings were constant up to cycle 3 (Figure 4.53), in which first joint cracking was observed. Measurements increased with joint distortion up to cycle 7 during which considerable joint distress and yielding of the steel angles was recorded. Better correlation of pulse velocity measurements with joint distortion was observed.

4.5.6 Summary. Beam hinges formed and large shear forces from the beams were applied to the joint which failed at 4% drift. Unlike SB, top and bottom beam bars lost bond capacity contributing to the strength and stiffness decay, and pinching of the force versus deformation response shown in Chapter III (Figures 3.35 and 3.36). Jacketed column corner bars showed the same behavior as SB and exhibited good bond conditions. The bars against the beam faces resisted the torsional moment transferred from the transverse beams. The joint region was more flexible in SD than in SB, because column longitudinal bars in SD were distributed around the perimeter (versus bundles for SB). Weaker concrete might have contributed to the difference. The slab showed less damage than in SB which might be associated with smaller slab participation.

4.6 COMPARISON OF SPECIMENS SD AND SD-B

Comparison of specimens SD and SD-B helps to evaluate the effect of jacketing both beams and columns.

4.6.1 Beams. Beams were jacketed and the flexural strength was increased moderately. The beam jacket was reinforced with 2-#5 bars placed in each side of the beam under the slab, and 2-#4 bars placed at the bottom of the existing beam. Jacketed beam reinforcement was instrumented as shown in Figure 2.27. Strains in the longitudinal steel in the E-W beams are presented.

In Figure 4.54, the yielding sequence recorded in the E-W beam bars and slab bars next to the column is shown. The loading cycle and loading stage are also given. First beam yielding was measured at gauge "k" at the face of the jacketed column (Figure 4.55). Unlike specimens RB, SB and SD, the critical section was located at the face of the jacketed column. First cycles showed normal compression-tension strains. After yielding, large strain reversals took place when the load was alternated. Strain hardening was recorded in cycle 3. During downward loading, load versus strain curves showed stiffening associated with crack closing. The bar yielded in compression in cycle 9/pos. Large compressive stresses (up to 85 ksi., calculated from the measured cyclic strain history) caused buckling of the bar. Peak compressive and tensile stresses corresponded to the load peaks.

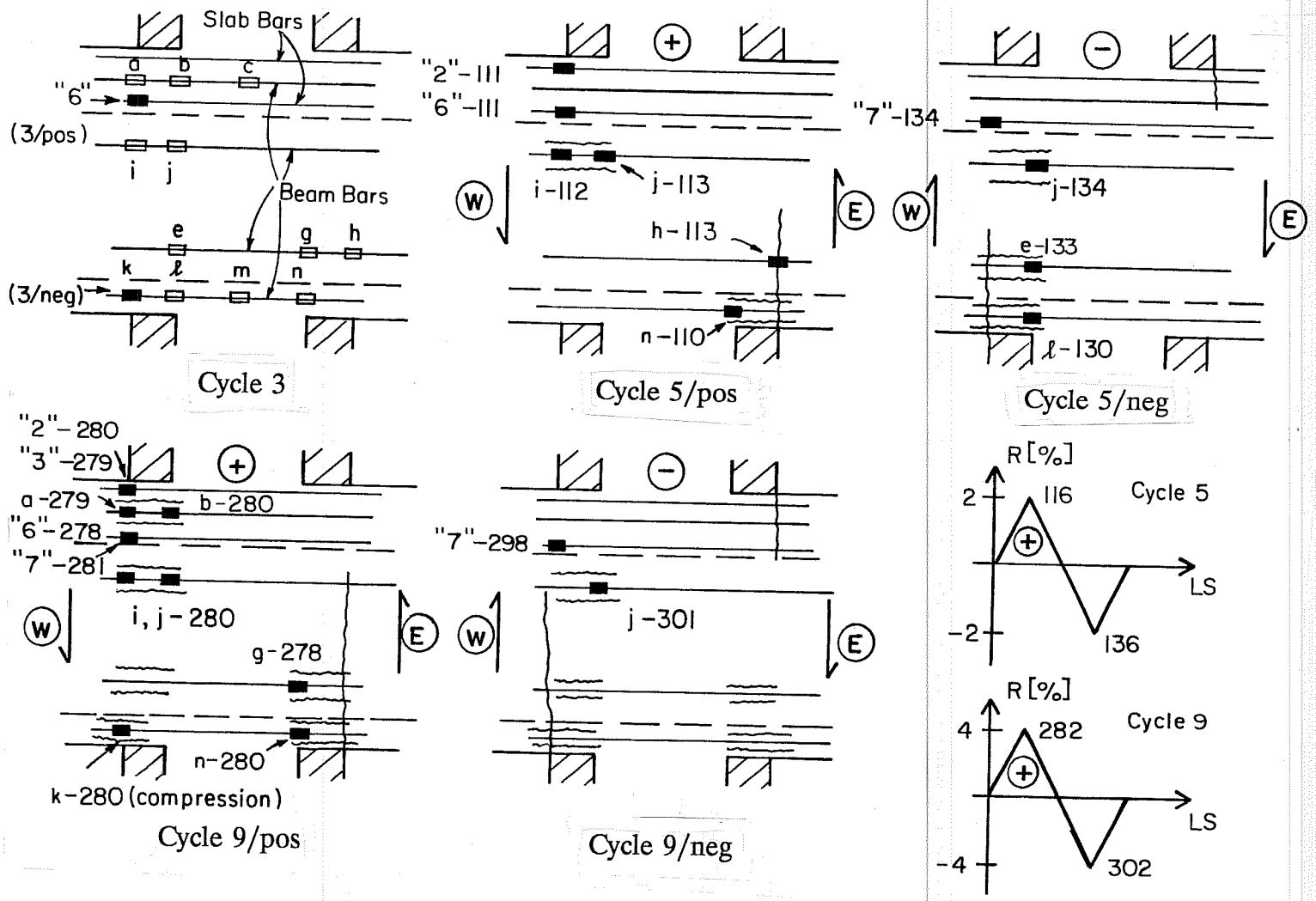

Figure 4.54 Specimen SD-B - Yielding Sequence (E-W Direction)

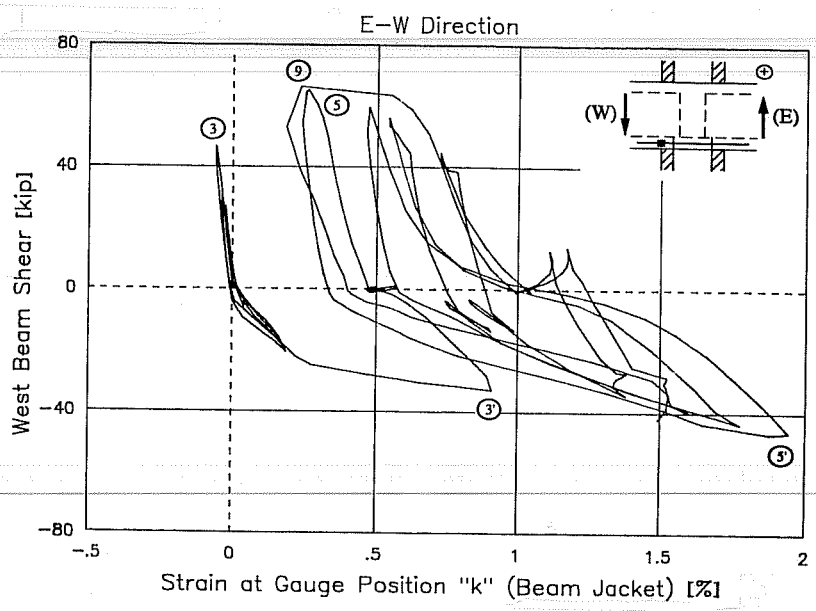

Figure 4.55 Specimen SD-B - West Beam Shear vs. Strain at Gauge Position "k" (Beam Jacket)

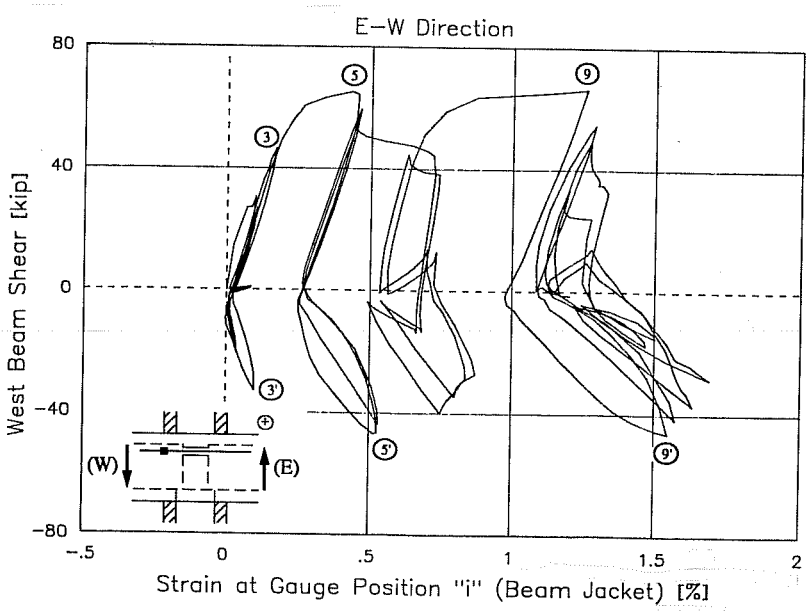

Figure 4.56 Specimen SD-B - West Beam Shear vs. Strain at Gauge Position "i" (Beam Jacket)

At gauge position "i" in the top jacket steel, C-shaped loops with tensile strains under upward loading as well as downward are shown in Figure 4.56. The bar was placed 2 in. below the slab. During positive moment, the neutral axis lay above the bars and the compression force from bending was resisted by concrete in the slab. During negative moment, the top jacket steel resisted the tensile bending force. Peak stresses, in tension only, coincided with the peak loads. Top bars in the beam jacket exhibited good bond (h/d_b =32, based on 20 in. column depth).

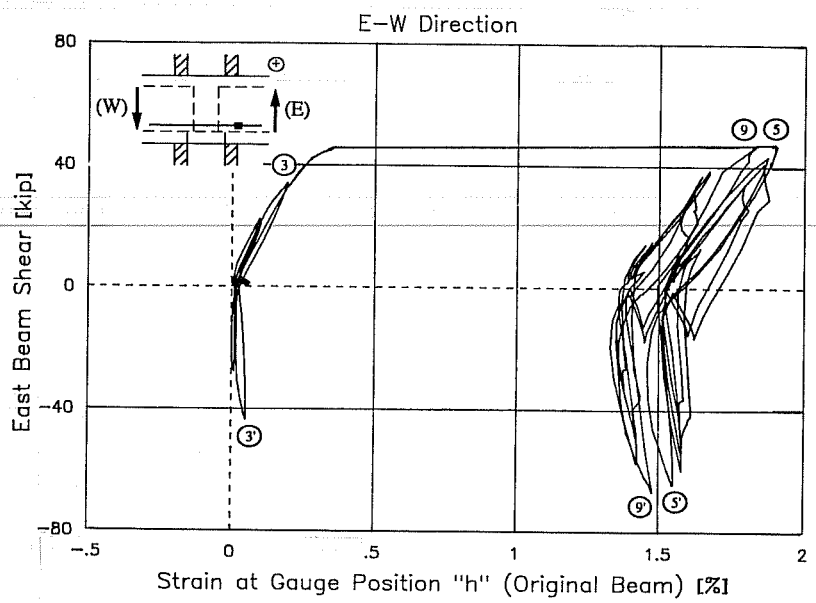

Figure 4.57 Specimen SD-B - East Beam Shear vs. Strain at Gauge Position "h" (Original Beam)

In Figure 4.57, the E beam shear versus strain at location "h" in the bottom steel of the existing beam is shown. The gauge was located at the face of the column and unlike specimens RB, SB and SD, C-shaped loops were recorded (see Figure 4.16, for RB). Before yielding, tensile strains were measured during positive and negative loading. The bottom bars in the existing beams were 5 in. above the soffit of the jacketed beam. During downward deflection, the neutral axis was near or under the bar resulting in tensile strains. After yielding, peak compressive stresses in the bottom bars of the existing beam occurred before the peak load was reached because compressive forces redistributed from the bar to the concrete while the crack was closing. In cycle 9/pos, yielding at position "g" indicates yield penetration. Bond behavior of bottom bars in the existing beams was better in SD-B than in tests RB, SB and SD, in which the bar was completely debonded. The addition of the beam jacket resulted in smaller tensile and compressive stresses on the bottom bars and bond failure was less likely.

In cycle 9/pos, more yielding was recorded (Figure 4.54). Top reinforcement in the existing beam yielded at positions "a" and "b" and at "i" and "j" in the jacketed beam.

Bottom bars yielded at "g" and "n". Yielding at "b", "g", "j" and "n" was evidence of propagation of plastic deformation from the column face into the joint.

In Figure 4.58, the stress distribution along the bottom bar in the beam jacket is shown. The bar exhibited excellent bond behavior. Stresses increased with the imposed drift angle and varied from compression in one side of the joint to tension in the other side. Maximum bond stress over 16 in. in cycle 9/pos, was $u_m = 1290$ psi., which was larger than the design bond index, $DBI = 1215$ psi. and the maximum bond index, $MBI = 955$ psi.. No bond distress was expected since $h/d_b = 40$ (calculated over the column depth, i.e. 20 in.).

In Figure 4.59, the stress distribution along the bottom bar in the existing beam during peak loads is shown. The bar was in tension throughout most of the test thus reducing the probability of bond loss. Maximum average bond stress was $u_m = 1430$ psi. in cycle 9/neg (calculated over a 16 in. length). The design bond index was 470 psi., and the maximum bond index was 1760 psi..

Strains in the N-S reinforcement (not shown) were similar to those in the E-W direction. First yielding in the N-S direction occurred in the bottom reinforcement of the jacketed beam in cycle 4 and in the bottom steel in the existing beam in cycle 7. Top beam reinforcement yielded in cycle 11.

4.6.2 Column. Column strains were smaller than beam strains. Strains in the original column showed the same behavior as that observed in SD. Column bars exhibited good bond behavior and there was no evidence of delamination between the existing column and the jacket.

Strains in bars in the jacketed column were the same as in SD, although in some cases smaller strains were measured at the same load levels in a given loading cycle. The longitudinal #10 bars in the jacket showed excellent bond characteristics ($h/d_b = 18$). Like in SD, bars placed against beam sides were effective in resisting column flexure as well as the torque transferred from the transverse beam. In Figure 4.60, the stress distribution along the NE corner bar is presented.

4.6.3 Slab. Slab behavior is compared with that of specimen SB because not enough information was available for specimen SD. Larger plastic strains were measured in SD-B than in SB. First yielding occurred in cycle 3 to 1% drift in the E-W top and bottom slab bars at positions "1" and "6", respectively. All the E-W bars that yielded exhibited strain hardening. N-S bottom slab bars yielded in cycle 7 and top bars in cycle 11.

In Figure 4.61, the stress distribution for E-W top slab bars during positive unidirectional cycles is presented. The distribution is similar to that of SB. The slab showed a nearly uniform stress distribution in cycle 9 to 4% drift. The distribution is used in Chapter V to evaluate the slab participation in resisting negative moments.

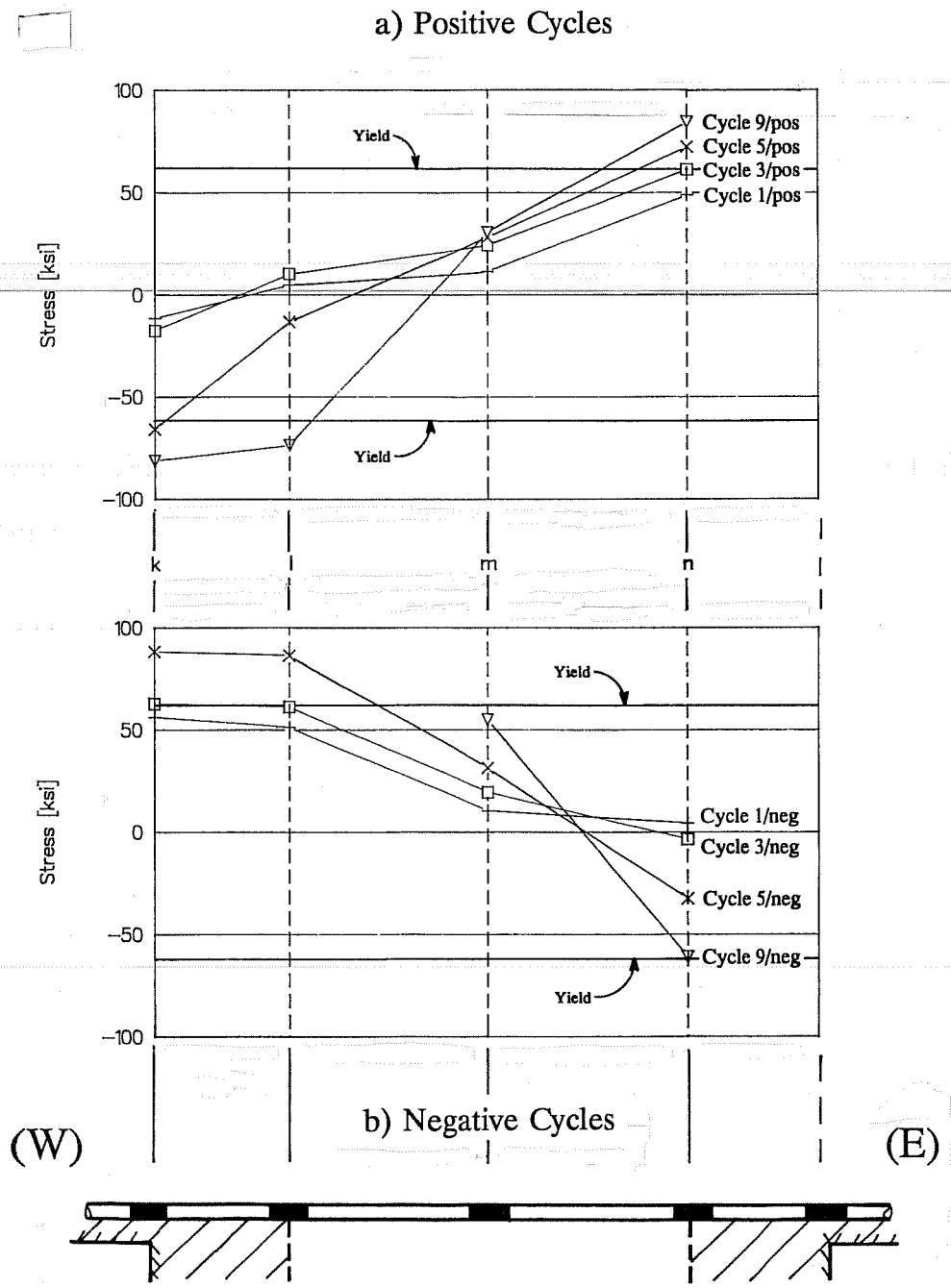

Figure 4.58 Specimen SD-B - Stress Distribution Bottom Bar (Beam Jacket)

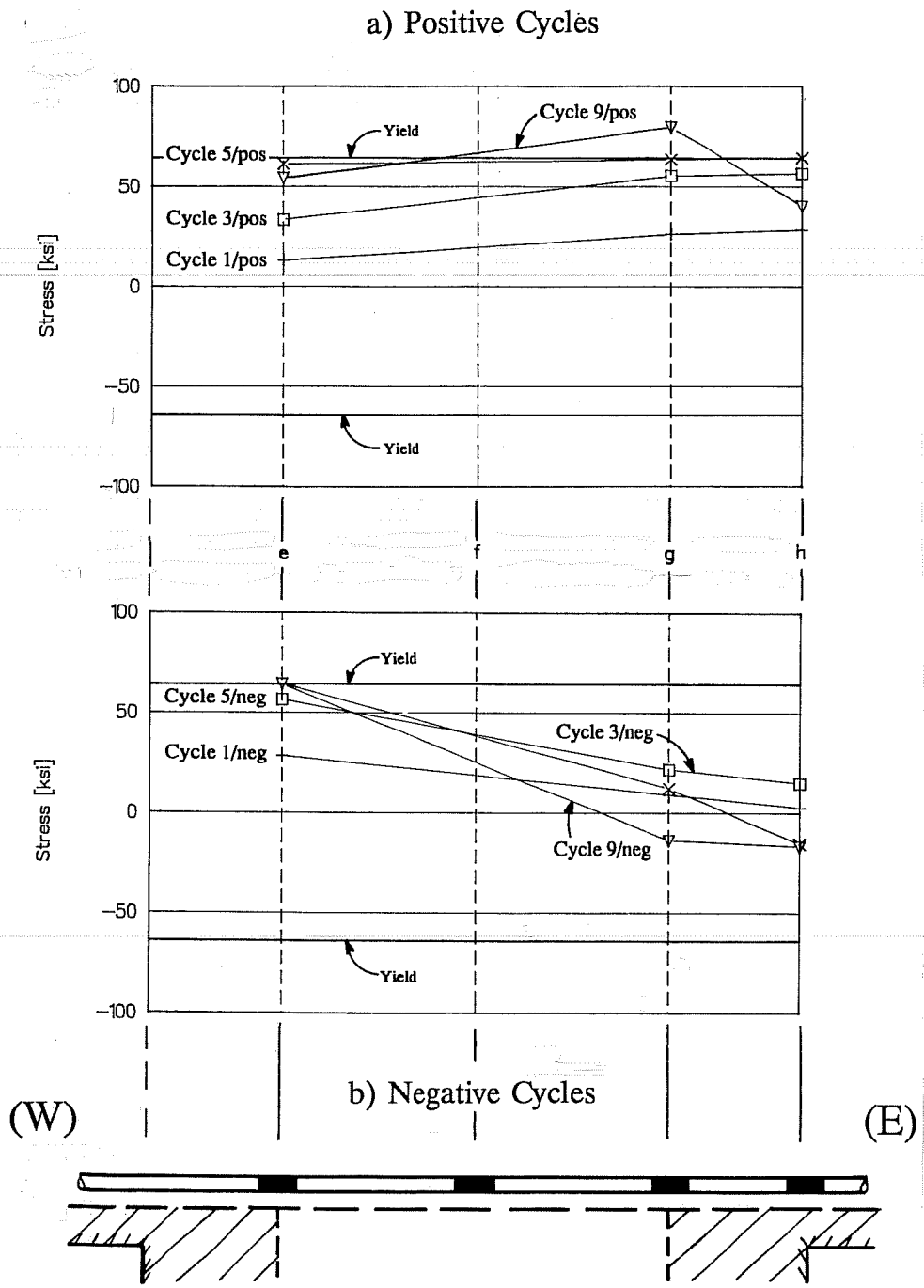

Figure 4.59 Specimen SD-B - Stress Distribution Bottom Bar (Original Beam)

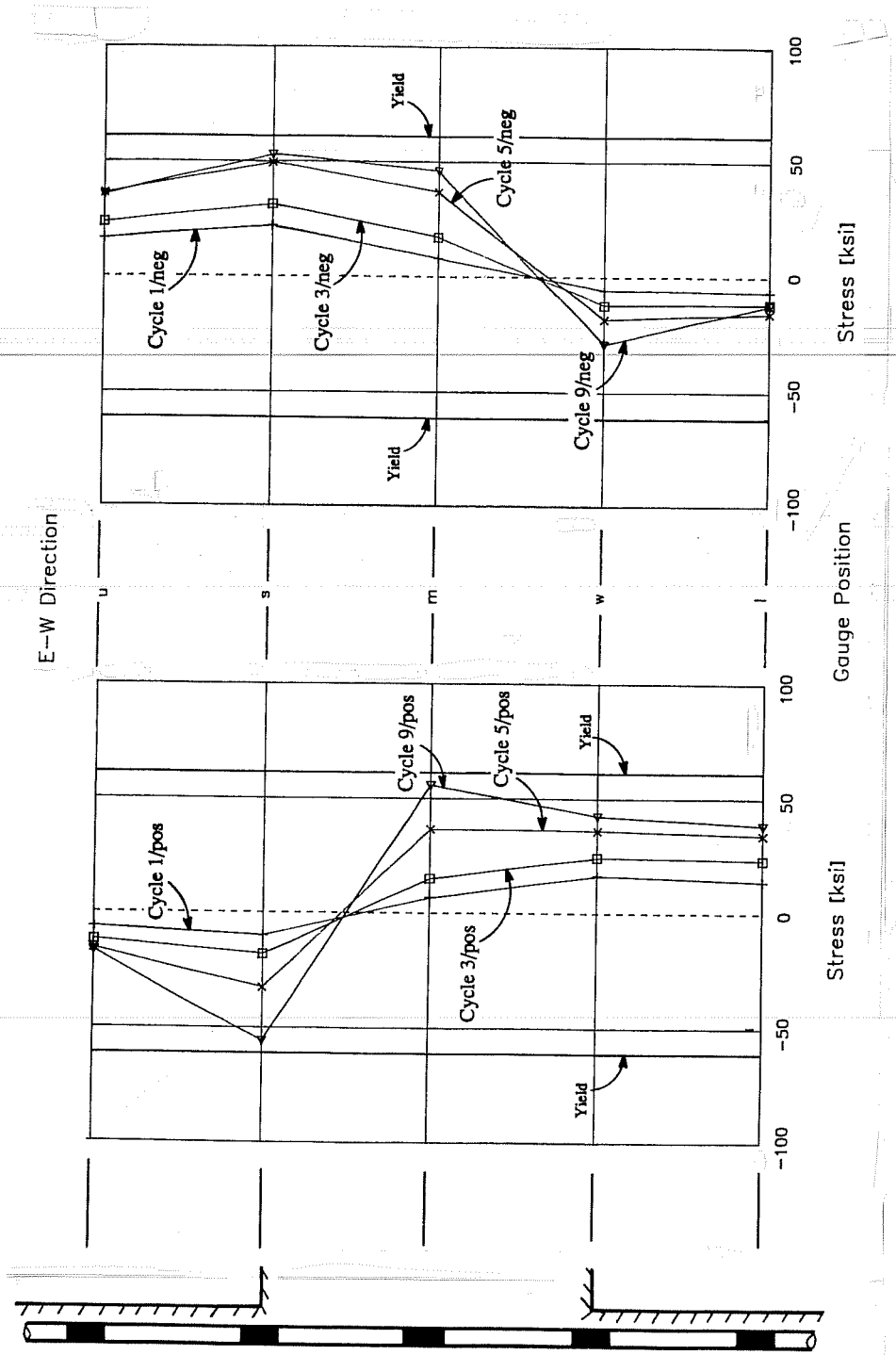

Figure 4.60 Specimen SD-B - Stress Distribution Column Bar (Jacketed Column - Corner Bar)

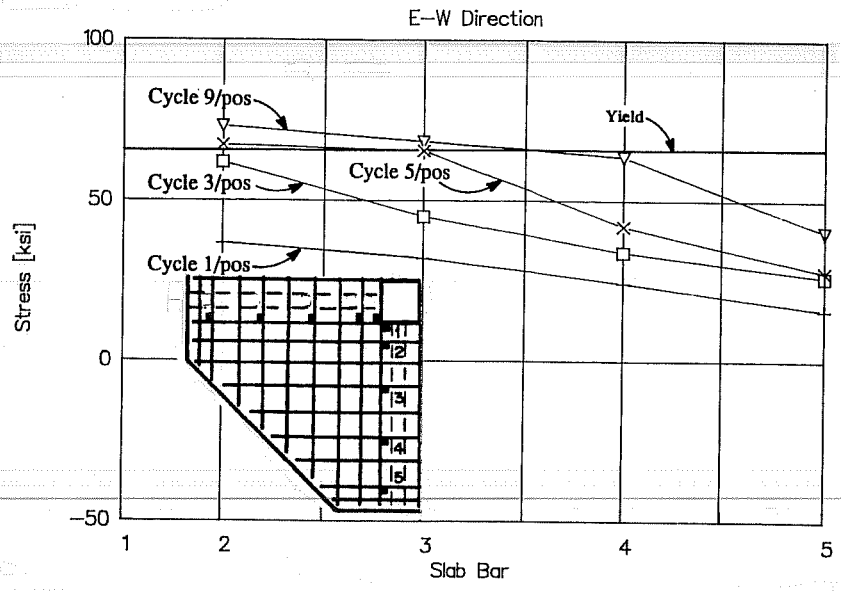

Figure 4.61 Specimen SD-B - Stresses Across E-W Top Slab Bars

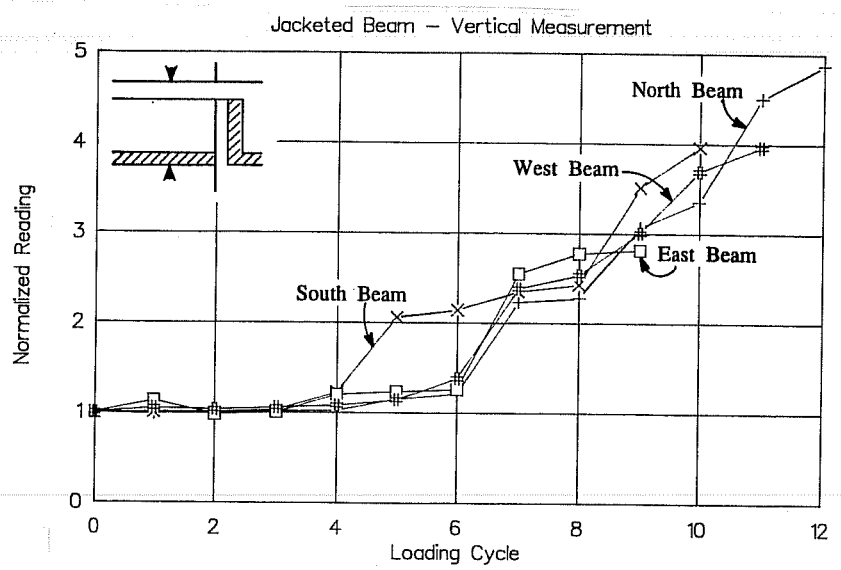

Figure 4.62 Specimen SD-B - Beam Pulse Velocity Vertical Measurement

4.6.4 Joint. Strains in the transverse steel in the existing column and the jacket were negligible. Corner tie strains at the same load levels in a given load cycle were higher than in SD. It is likely that the joint in specimen SD-B expanded more (see Figures 3.41 and 3.52), so that higher strains were measured. Larger joint shear stresses were applied, and the core was more cracked in SD-B than in SD. Corner ties yielded in cycle 11.

The joint confinement was enhanced because the beams were wider in specimen SD-B than in SD. First tensile yielding in the steel angles occurred in the corner in cycle 7 (bidirectional to 2% drift). Only one gauge, placed in the tip of the SW steel angle, measured yielding in compression during cycle 9/neg. The tips of the flanges of the steel angles were masked by the beams so that the behavior was somewhat different from SD, particularly for strains in the E-W joint faces. In the E-W joint faces, only tensile stresses were recorded except during bidirectional cycles. It is likely that the lateral confinement of the beams allowed bending of the steel angle with respect to an axis which passed through the steel angle tip. In the N-S sides, compressive strains at the tip were recorded as in specimens RB, SB and SD. The strain distribution across a transverse section of the steel angle (not shown) was Λ-shaped, with the corner in tension. Joint steel angles for SD-B had a lower strain gradient (smaller curvature) at loading peaks than for SD. The joint collars showed the same behavior as those in SD.

4.6.5 Ultrasonic Pulse Velocity. As described in Chapter II, direct readings were taken on beam and column faces, in the two loading directions, and from the beam soffit to the slab surface. The ratio of the vertical readings (at 9 in. from the column face) to the initial value for the four beams is shown in Figure 4.62. Readings were taken after each loading cycle. Curves for N, W, E beams were alike. No torsional damage was observed up to cycle 6 in the area where measurements were taken. The pulse velocity sharply increased after cycles 7, 9 and 11, during which torsional distress was evident. The curve for the south beam has a similar shape but the ratio increased in cycle 5. This is credited to the formation of torsional cracks across the line of measurement. The same behavior is observed in direct readings across the beams. From the observed response and the pulse velocity readings it is believed that monolithic behavior of the jacketed beam was assured throughout the test.

As in specimens RB, SB and SD, direct column readings indicated that the jacket remained well-bonded to the column. Readings at the end of the test increased from the start in 10% and 8% on the average for the upper and lower columns, respectively. Joint readings remained almost constant in the first two cycles. From cycle 3, pulse velocity increased up to cycle 5, after which measurements were inconsistent.

4.6.6 Summary. Like all rehabilitated specimens, SD-B behaved as a "strong column - weak beam" system developing beam hinges which led to joint failure. Although the existing beam bars were cast in the same conditions as in specimens RB, SB and SD (fresh concrete with slump higher than 5 in., and top bars cast above 17 in. of concrete), the bars in the existing beam showed better bond. The increase in beam depth due to beam jacketing resulted in smaller tensile and compressive stresses on top and bottom bars in the existing beam, and bond failure was less likely. Wider beams enhanced joint confinement. The slab participation was similar to that of SB though less damage was noted. Ultrasonic pulse velocity indicated composite behavior of beams and columns.

CHAPTER V - ANALYSIS OF TEST RESULTS

5.1 INTRODUCTION

An analysis of the general behavior of the specimens is presented in this chapter. Member contributions to drift angle and energy dissipation, useful for understanding the performance and mode of failure, are described. The stiffness of the specimens is evaluated using the equivalent stiffness and the peak-to-peak stiffness. Computed stiffness are compared with measured stiffness. The energy dissipation capacity of the subassemblages is assessed using the cumulative energy dissipated and the equivalent viscous damping ratio. Stiffness, strength and cyclic response characteristics used in the chapter are defined.

The analysis of results confirmed that jacketing of frame elements improved the response of the existing structure. Member contributions to drift angle and energy dissipation showed that rehabilitated specimens developed a "strong column - weak beam" response as opposed to the "strong beam - weak column" behavior of the existing structure. Rehabilitated specimens had slightly higher equivalent viscous damping ratio than the existing structure.

5.2 MEMBER CONTRIBUTION TO DRIFT ANGLE

In section 3.2.1, the components of drift angle (beam angle θ_b, column angle θ_c, and the drift component attributed to the joint distortion γ') were isolated and mathematical expressions for determining drift components were presented. The relative member contribution to drift angle was calculated as the ratio of the components of drift angle over the imposed drift angle R.

Member contribution to drift angle for specimens O and RB, during E-W positive cycles, are presented in Figures 5.1 and 5.2, respectively. Similar graphs were plotted for the other specimens (not shown here). Contributions in the N-S direction were similar (not shown). The variation of measured story shear is also shown in the figures (right edge vertical scale). The story shear helps to indicate the effect of the changes in a given portion of the structure on the strength of the specimen, and is particularly important to understand the mode of failure. In general, at large deformation levels, an increase in the participation of the most damaged element was accompanied with a severe loss of strength. For unidirectional cycles, the story shear shown is the same as the measured peak value. For bidirectional cycles, the story shear is the maximum value before the other direction was loaded. For specimen O (Figure 5.1), the beams contributed least to total deformation. The column contribution, which was largest at the first stages of the test, diminished by the end of the test when joint deformations contributed more to the total drift. After cycle 9, the joint contribution increased rapidly and accounted for 85% of the total drift by the end of the test. Specimen O can be considered to have failed in cycle 9 due to severe joint

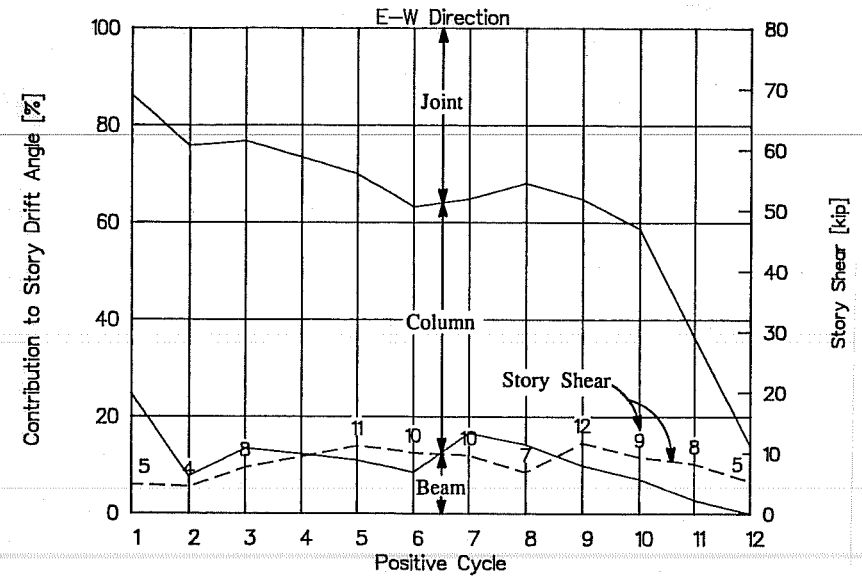

Figure 5.1 Specimen O - Member Contribution to Drift Angle (E-W Direction)

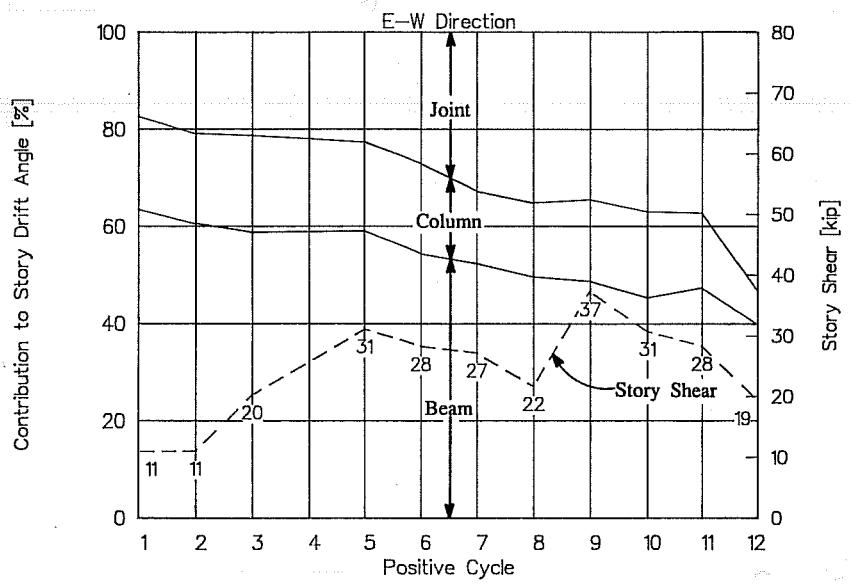

Figure 5.2 Specimen RB - Member Contribution to Drift Angle (E-W Direction)

distress which was aggravated by hinging in the columns and bond degradation of column bars in the joint. From cycles 9 to 12, the story shear decreased 55%, while the joint deformations increased dramatically. In Figure 5.2, the member contribution to E-W drift for specimen RB is shown. Comparison of contributions during tests O and RB shows that the behavior of the specimen was modified substantially. A "strong beam - weak column" system (test O) was changed to a "weak beam - strong column" system (test RB), in terms of strength and stiffness. In specimen RB, beams initially contributed 60% of the total deformation. Column contribution remained practically constant throughout the test, whereas the joint contribution increased steadily. During cycle 11, severe joint cover spalling occurred. From cycles 11 to 12, story shear dropped 48% with an increase of about

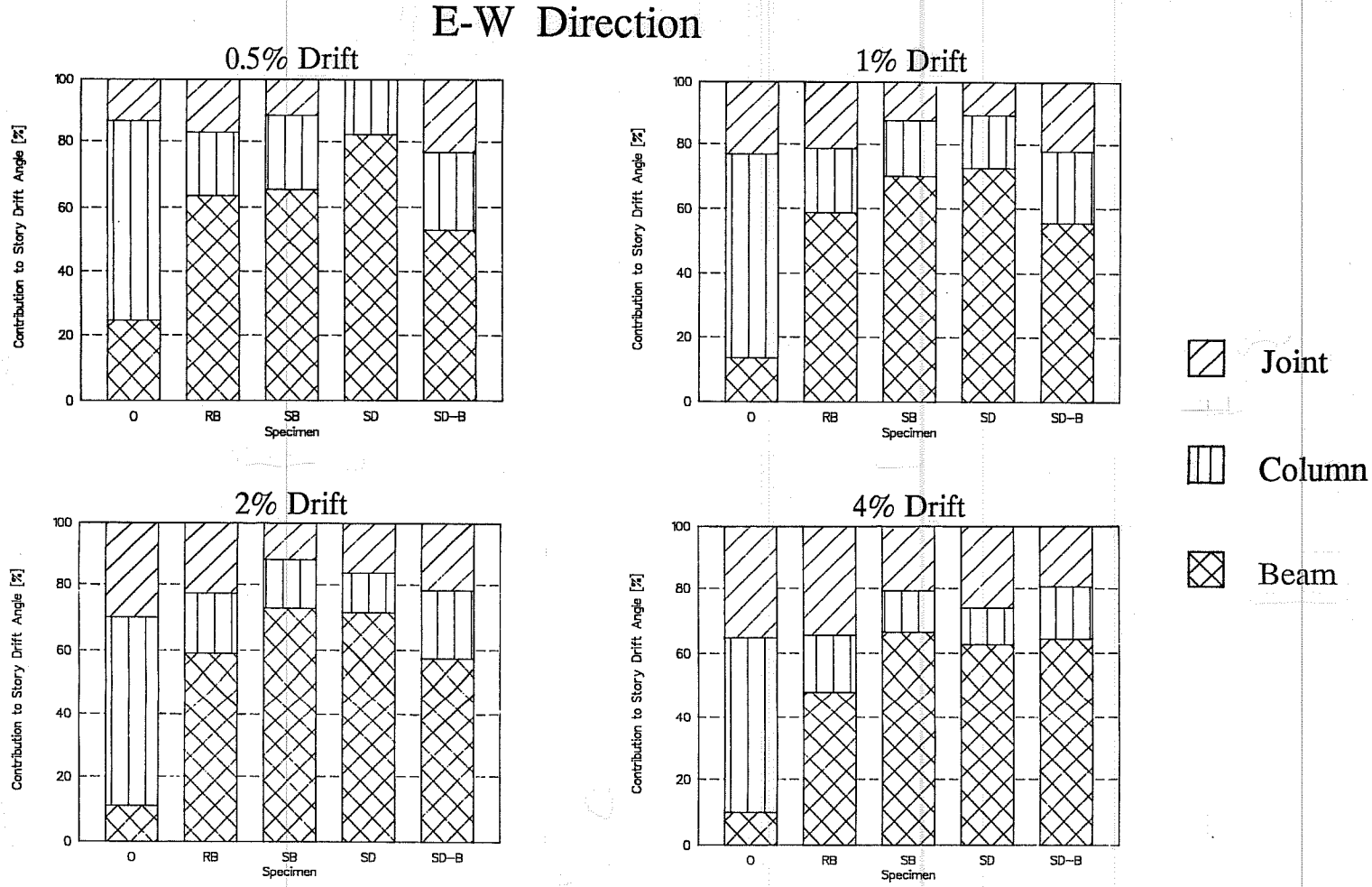

Figure 5.3 Member Contributions to Drift Angle (E-W Direction)

20% in the joint contribution. After failure, the increment contributed by the most damaged element, the joint, was smaller for the rehabilitated specimens than that observed in the existing structure. The joint steel cage proved to be effective confining the concrete core thus precluding an abrupt failure.

Member contributions to drift angle for all specimens in the E-W and N-S directions can be observed in Figures 5.3 and 5.4, respectively. Results in the E-W direction are presented for the first positive cycle to a given drift level, i.e. cycles 1, 3, 5, 9. In the N-S direction, negative cycles 4, 7 and 11 are shown. Cycles 7 and 11 were loaded bidirectionally. It is important to recognize that between cycles 4 and 7, and between 8 and 11, the specimen was deformed in the E-W direction only. Damage caused in the E-W direction generally affected the behavior (see Figure 3.57) and member contributions in the orthogonal direction. From Figures 5.3 and 5.4, it is clear that jacketing modified the behavior of the existing structure so that all rehabilitated specimens behaved as "strong column -weak beam" systems, in which beam contributions were the largest throughout the test. In general, the column contribution for all specimens decreased at drifts to 4%, while the joint contribution increased. The measurements coincide with the observed joint distress. It is interesting to note that at 0.5% drift, the joint component in the E-W direction for RB was a little larger than that of SB because the original joint core was severely damaged.

5.3 MEMBER CONTRIBUTION TO ENERGY DISSIPATION

The components of interstory drift were obtained multiplying the components of drift angle (θ_b, θ_c and γ') by the specimen height H. The energy dissipated by each component of interstory drift was then calculated as the area within the loops of the story shear versus interstory drift component relationship. Finally, the relative member contribution to energy dissipation was found by dividing the energy dissipated by each component of drift by the cumulative energy dissipated by the specimen. The latter was computed as the area within the loops of the story shear versus story drift relation. Both loading directions were analyzed.

Member contributions to energy dissipation in the E-W and N-S direction are presented in Figure 5.5 and 5.6, respectively. Comparing the member contribution to drift and energy, the similarity is obvious (see Figures 5.3 and 5.4). The joint contribution to drift and that for energy is nearly the same for positive cycles in the E-W direction and very similar for negative cycles in the N-S direction. Member contributions to energy dissipation confirmed that rehabilitated specimens developed a "strong column - weak beam" response as opposed with the "strong beam - weak column" behavior of the existing structure.

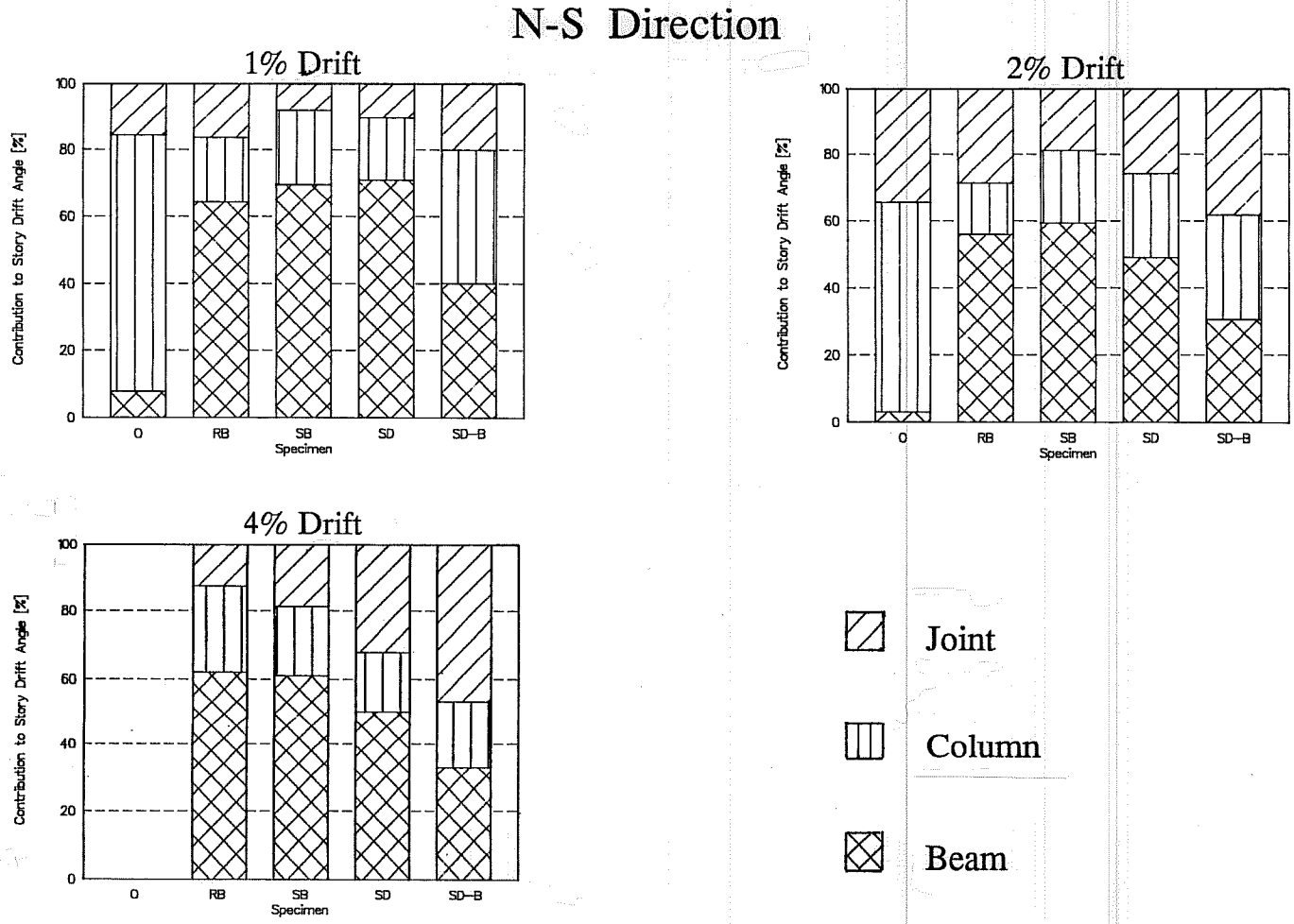

Figure 5.4 Member Contributions to Drift Angle (N-S Direction)

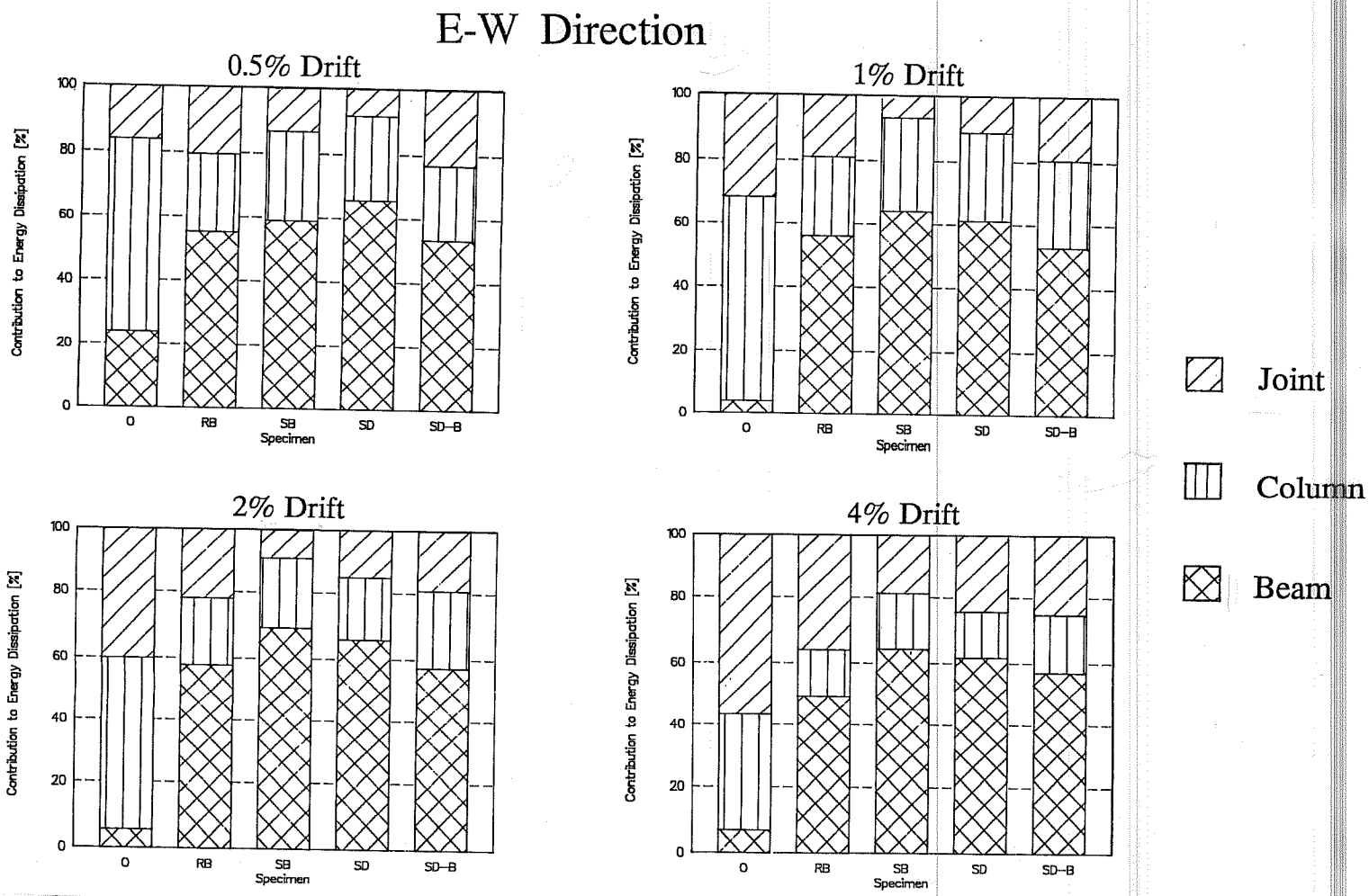

Figure 5.5 Member Contributions to Energy Dissipation (E-W Direction)

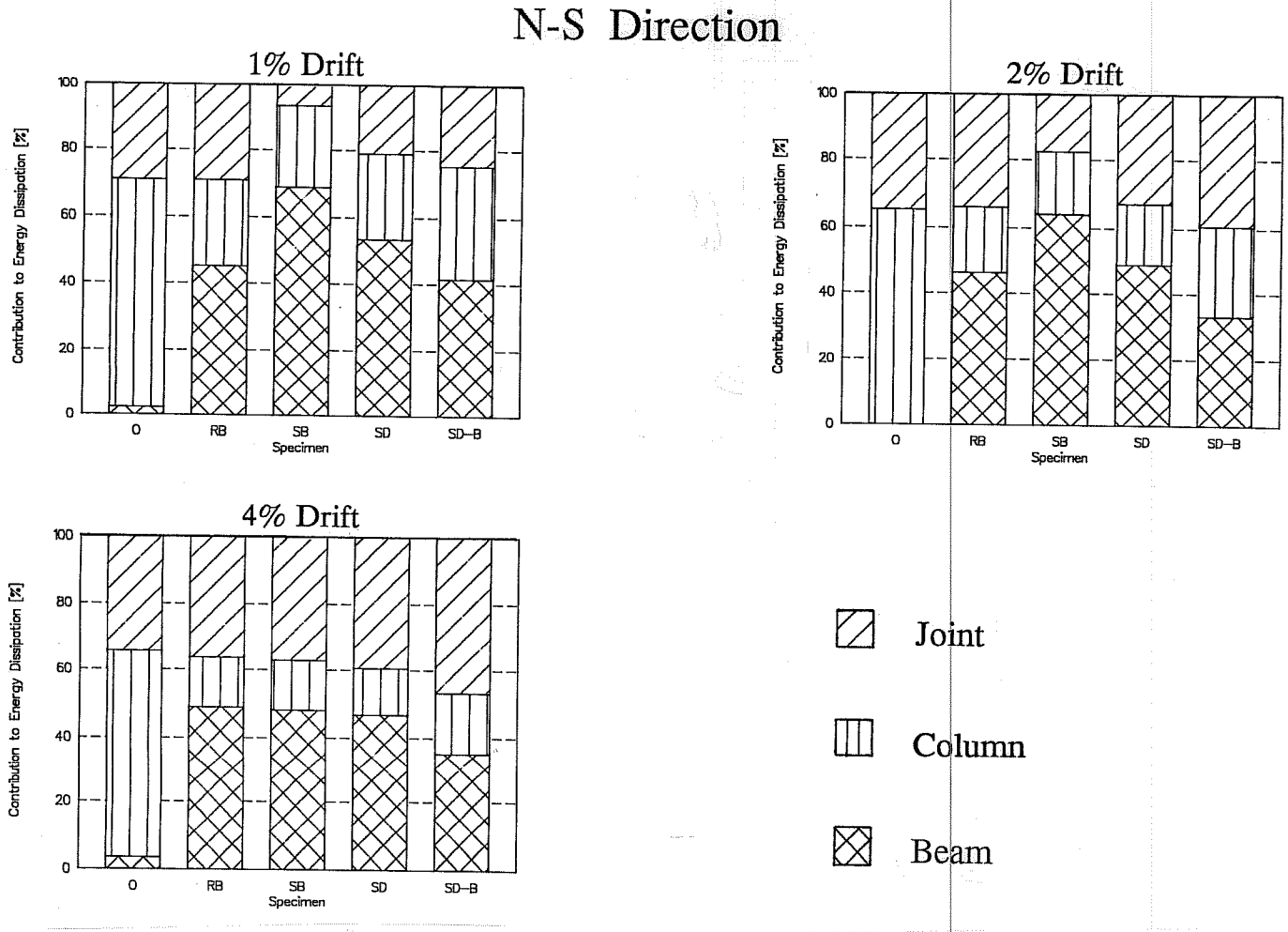

Figure 5.6 Member Contributions to Energy Dissipation (N-S Direction)

5.4 STIFFNESS

Satisfactory seismic design of structures requires that designers provide a balance of strength, stiffness, ductility and energy dissipation capacity. These characteristics must be based on a number of factors, including the type of ground motion, dynamic characteristics of the soil and the structure, structural system and material, and intended use of the building. Ideally, the stiffness should not degrade when loading cyclically, must be large enough to control drift and should be consistent with deformation limits of nonstructural components. Almost all reinforced concrete members experience stiffness degradation. Analytical studies on the effect of this phenomenon on the dynamic response of structures subjected to severe ground motions, have shown that stiffness degradation has the effect of reducing the amount of hysteretic damping. As a result, the system with degrading stiffness responds with larger accelerations than the nondegrading one (Refs. 7, 8). Stiffness degradation of reinforced concrete structures is attributable to concrete spalling, bond degradation, opening and closing of residual cracks, the Bauschinger effect in the reinforcing steel and decrease of the modulus of elasticity of the cracked concrete when subjected to alternating loads (Refs. 11, 22, 40, 44).

In this study, the stiffness of the specimens was evaluated using the equivalent stiffness (zero load or deflection to peak deformation in a half-cycle) and the peak-to-peak stiffness in both loading directions. Computed and measured stiffnesses will be compared.

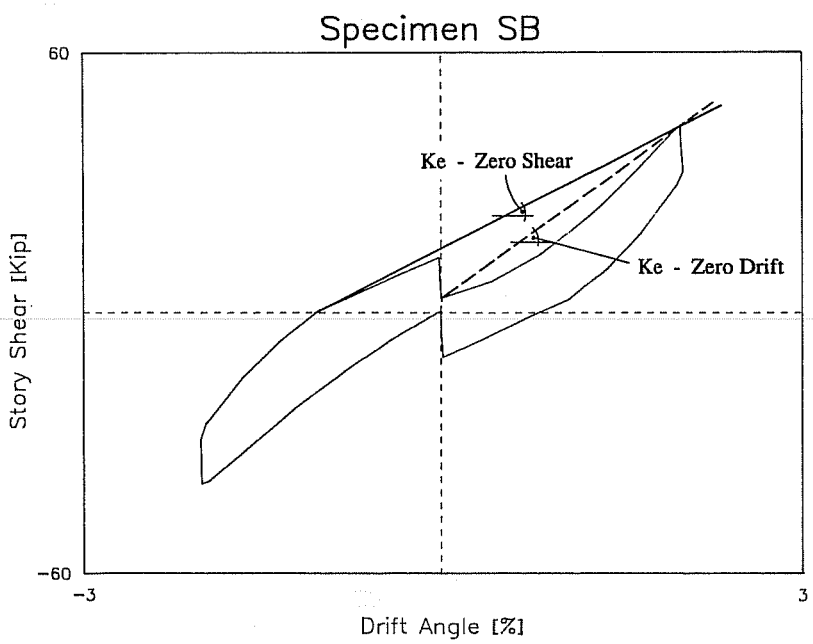

Figure 5.7 Definition of Equivalent Stiffness

5.4.1 Equivalent Stiffness. Stiffness deterioration in each half-cycle can be shown using equivalent stiffnesses. The definition of equivalent stiffness K_e in the story shear versus drift angle diagram is illustrated in Figure 5.7. A line is drawn from the point of zero story shear, at the beginning of the half-cycle in a loop, to the peak and is referred to as $K_{e,zero\ shear}$. The equivalent stiffness is defined as the slope relative to the abscissa. The point of zero story shear occurred, in general, in the previous loading half-cycle.

During bidirectional cycles, loading or unloading in one direction caused a decrease in the story shear in the other direction. The loading interaction was also evident when the beams in one direction were held at a zero drift angle. Under loading in the next half-cycle, a slightly different value of equivalent stiffness could also be defined, and is denoted as $K_{e,zero\ drift}$ (Figure 5.7). This stiffness is defined as the slope of the secant that joins the shear at zero drift to the peak load. Equivalent stiffness of a number of half-cycles were affected by the bidirectional interaction so that the use of $K_{e,zero\ drift}$ reflects the interaction. Values of $K_{e,zero\ drift}$ showed less scatter than those obtained using the definition of $K_{e,zero\ shear}$.

The equivalent stiffness concept does not reflect the shape of the hysteresis curves. A curve which follows an elasto-plastic response or a curve severely pinched near zero, will have the same equivalent stiffness as long as the initial and peak values are the same. The equivalent viscous damping, described in section 5.5.2 is used to indirectly measure pinching of the hysteretic response.

Figure 5.8 shows the notation used in Figures 5.9 and 5.10. Equivalent stiffnesses for specimen SB in the E-W direction are presented in Figures 5.9 and 5.10. The values are comparable to those observed in the N-S direction. Similar diagrams were plotted for other specimens (not shown). Equivalent stiffness $K_{e,zero\ shear}$ is shown in Figure 5.9. The stiffness deteriorated more rapidly in early stages of loading. First positive half-cycles showed larger stiffness in all specimens for two reasons. First, the story shear reached during positive half-cycles was a little larger than the one measured in negative half-cycles. Damage caused in a positive half-cycle affected the strength in the subsequent half-cycle. Second, the residual drift angle was smaller at the beginning of the first cycle to a new deformation level. Most of the stiffness degradation at a given deformation occurred in the first unidirectional cycle. Equivalent stiffness values decreased in subsequent cycles and were generally associated with loss of strength. This was especially the case in cycles to 4% drift angle. When bidirectional cycles were applied, deterioration progressed with cycling. Specimens showed severe stiffness deterioration when a new deformation level was applied. The equivalent stiffness $K_{e,zero\ shear}$ for the first unidirectional half-cycle at a given drift level (label 1U in Figure 5.8a), is presented in Table 5.1.

Equivalent stiffnesses $K_{e,zero\ drift}$ for specimen SB are presented in Figure 5.10. Stiffnesses of cycles 7/neg, 8/pos, 8/neg, 9/pos, 11/neg, 12/pos and 12/neg were larger and show less scatter than those calculated from zero shear.

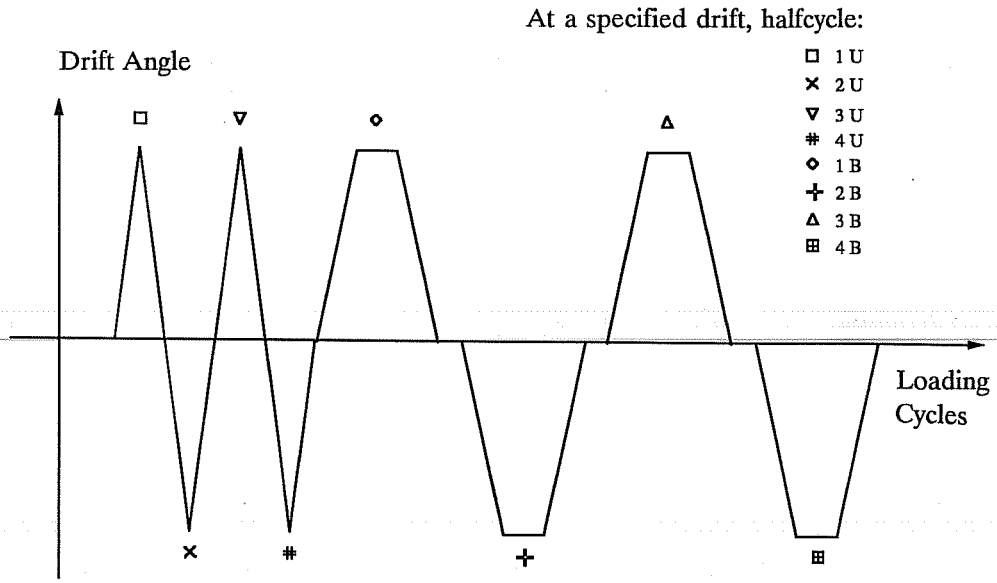

a) Notation for Equivalent Stiffness

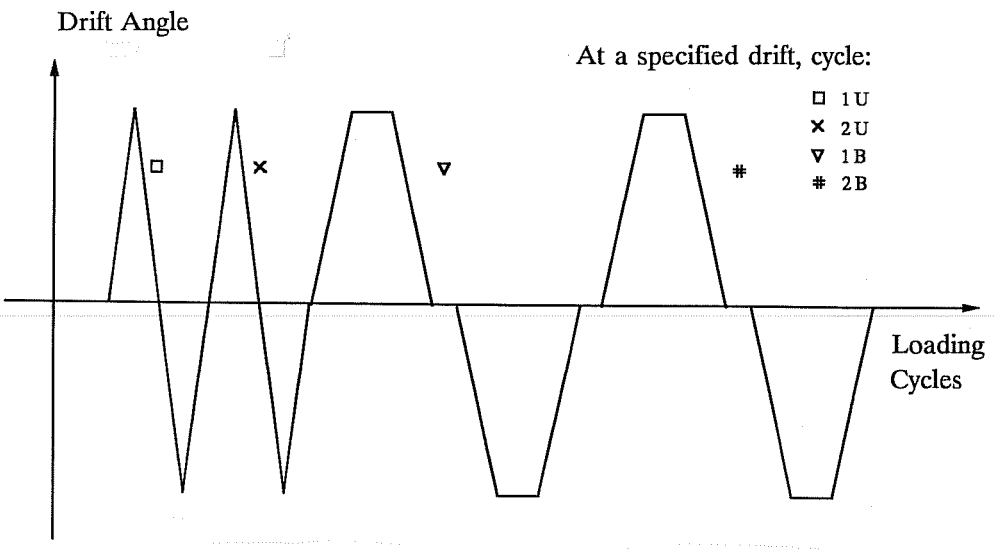

b) Notation for Peak-to-Peak Stiffness

Figure 5.8 Notation for Figures 5.9, 5.10 and 5.12

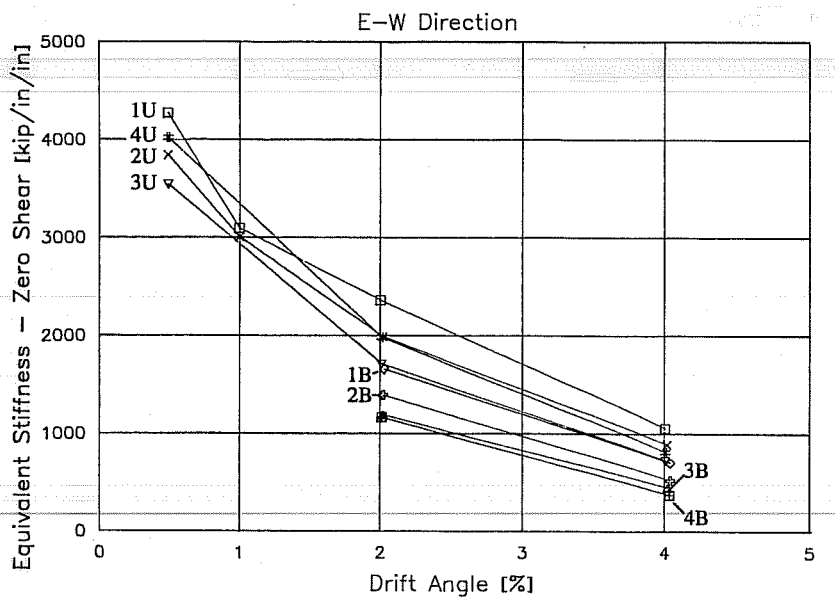

Figure 5.9 Equivalent Stiffness - Zero Shear (Specimen SB)

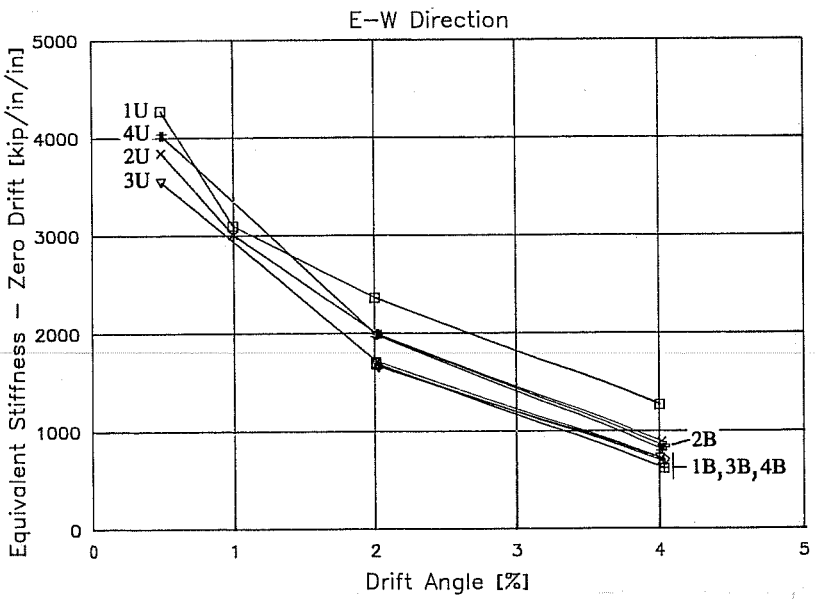

Figure 5.10 Equivalent Stiffness - Zero Drift (Specimen SB)

Table 5.1 Equivalent Stiffness $K_{e,zero\ shear}$

Story Drift Angle [%]	Specimen				
	O	RB	SB	SD	SD-B
0.5	965[a]	2201	4273	3747	6174
1	732	1877	3096	2852	4420
2	539	1394	2359	2000	3003
4	230	732	1055	865	1346

[a] Equivalent stiffness $K_{e,zero\ shear}$ of first unidirectional half-cycle at a given drift level, [kip/in/in].

5.4.2 Peak-to-Peak Stiffness.

Stiffness deterioration in full cycles can be assessed using peak-to-peak stiffness. The definition of peak-to-peak stiffness K_p is illustrated in Figure 5.11. Peak-to-peak stiffness is calculated as the slope relative to the abscissa of a line that joins story shear peaks in the same cycle. For bidirectional cycles (cycles 7, 8, 11 and 12), the stiffness was computed from the maximum values of story shear reached in the direction for which the stiffness is calculated. Due to the nature of the hysteresis loops and to the definition, peak-to-peak stiffness values were a little larger than equivalent stiffnesses for same cycles. Equivalent stiffnesses $K_{e,zero\ drift}$ had nearly the same values that peak-to-peak stiffnesses in cycles 7, 8, 11 and 12.

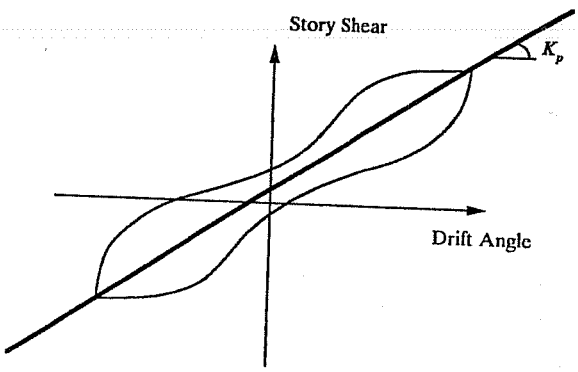

Figure 5.11 Definition of Peak-to-Peak Stiffness

Peak-to-peak stiffness versus E-W drift angle for specimen SB is found in Figure 5.12. Comparable values are observed in the other direction. Similar graphs were plotted for the other tests (not shown here). Data for peak-to-peak stiffness deterioration best follows a curve similar to that for equivalent stiffness. Guimaraes (Ref. 21), reported that the stiffness degradation of normal strength concrete specimens, i.e. less than 6000 psi., show a parabolic decay. The first cycles at a given deformation level showed slightly higher stiffnesses than subsequent cycles because the maximum values of story shear decayed progressively. Stiffness degradation was larger during cycles to 2% and 4% in which most of the joint softening, and crushing and spalling occurred. Peak-to-peak stiffness for the first unidirectional cycle at a given drift level (label 1U in Figure 5.8b), is given in Table 5.2.

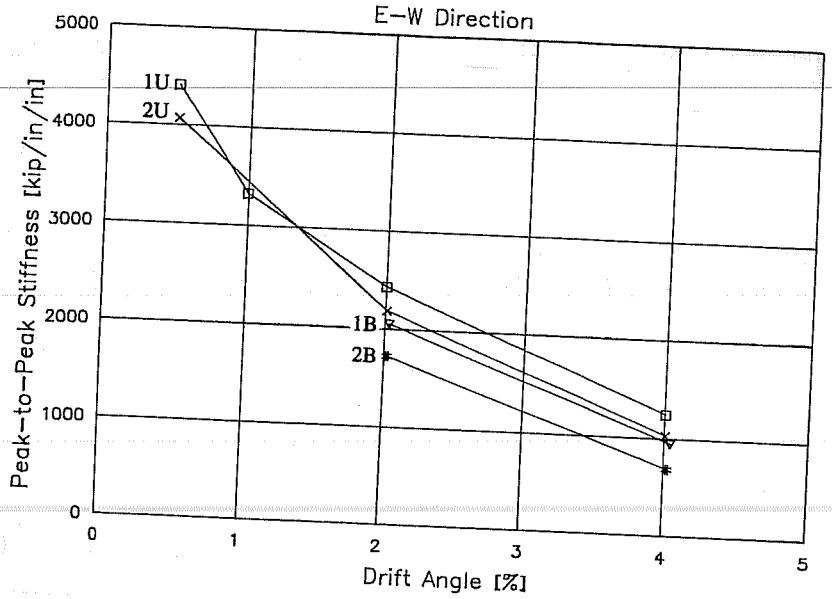

Figure 5.12 Peak-to-Peak Stiffness (Specimen SB)

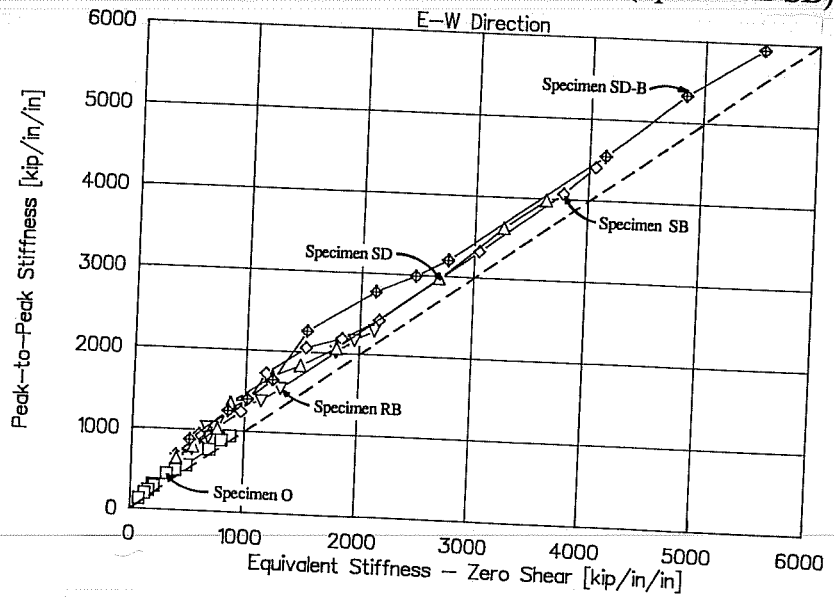

Figure 5.13 K_p vs. K_e (E-W Direction)

The relation of K_p and $K_{e,zero\ shear}$ in the E-W direction for all tests is shown in Figure 5.13. Equivalent stiffnesses at each cycle were the average of the measured stiffnesses in positive and negative half-cycles. Similar curves were plotted for $K_{e,zero\ drift}$ (not shown here). As mentioned previously, due to the nature of the hysteresis loops, peak-to-peak stiffnesses had higher values than equivalent stiffnesses (see Tables 5.1 and 5.2). It is interesting to note that data points best fit a straight line inclined at 45°. For mathematical modelling of the hysteresis rules, the stiffness relation obtained may be useful.

Table 5.2 Peak-to-Peak Stiffness K_p

Story Drift Angle [%]	Specimen				
	O	RB	SB	SD	SD-B
0.5	937[a]	2296	4407	3981	5923
1	761	2016	3324	2971	4547
2	559	1545	2427	2064	3201
4	291	911	1243	1023	1647

[a] Peak-to-peak stiffness K_p of first unidirectional cycle at a given drift level, [kip/in/in].

5.4.3 Theoretical Stiffness. The theoretical elastic stiffness of each specimen was calculated based on the contribution of beam, column and joint deformations. The theoretical stiffnesses were calculated only for the E-W direction. The procedure used was presented in Refs. 13 and 40. The beam and column elastic flexural deformations were calculated using the bending stiffness EI of the cracked section, which corresponds relatively well to the curvatures at loads approaching yield (Ref. 32). An estimate was made of the elastic shear deformation by taking twice the shear deflection of an uncracked member (Ref. 40).

The theoretical stiffness was obtained as $K_{th} = V_u / R_y$, where V_u was the predicted ultimate story shear for the specimens. In all tests, it corresponded to the ultimate joint strength, except in SD-B in which it corresponded to beam hinging. R_y was the drift angle at yield. V_u for ultimate joint strength was calculated as the story shear corresponding to the ultimate joint shear stress according to ACI 352. R_y was estimated as follows

$$R_y = R_{beam} + R_{column} + R_{joint} \tag{5.1}$$

The elastic flexural and shear deformations of the beams were calculated as

$$\delta_b = (P_i + P_j)\left(\frac{L_b^3}{3E_c I_e} + \frac{fL_b}{0.2E_c A_b}\right) \tag{5.2}$$

where $P_i + P_j$ = summation of beam tip loads at V_u. It was calculated from $P_i + P_j = 2V_u H/L$ (see Equation 2.1 in Chapter II)

L_b = beam span; distance from column face to hydraulic actuator

$E_c I_e$ = beam bending stiffness. For tests O, RB, SB and SD it was taken as $0.5 E_c I_g$ to account for cracking, in which E_c is the modulus of elasticity of beam concrete and I_g is the moment of inertia based on the gross concrete area of a beam 8 by 20 in. section. For specimen SD-B, $E_c I_e$ was taken as the bending stiffness of the cracked transformed section of the jacketed beam

f = form factor for shear, taken as 1.0

A_b = beam web area, $b_w d$.

Beam component of drift was computed as

$$R_{beam} = \frac{\delta_b}{192} \tag{5.3}$$

The elastic flexural and shear deformations of each column to mid-story height were estimated and doubled (assuming both half-columns are the same, see Figure 3.1)

$$\delta_c = 2 \left(\frac{V_u H_c^3}{3E_c I_e} + \frac{V_u f H_c}{0.2 E_c A_c}\right) \tag{5.4}$$

where V_u = ultimate story shear

H_c = column span

$E_c I_e$ = column flexural stiffness, taken in all tests as the stiffness of the cracked transformed section. E_c was the concrete modulus of elasticity of the transformed section

f = form factor for shear, taken as 1.2

A_c = gross concrete area.

The column component of drift angle was estimated as

$$R_{column} = \frac{\delta_c}{165} \tag{5.5}$$

No attempt was made to calculate the joint contribution to drift angle. Based of results of previous tests at the University of Texas at Austin (Refs. 21, 29, 31) it was assumed that the joint contribution was 50% of the column contribution, i.e. $R_{joint} = 0.5 R_{column}$.

Table 5.3 Theoretical and Experimental Stiffnesses

Test	Theoretical Stiffness K_{th} [kip/in/in]	Experimental Stiffness [kip/in/in]			
		Response Envelope @ 0.5%	At Yielding		
			K_y	Cycle	K_y/K_{th}
O	755	965	335	9/pos	0.44
RB	2890[a] 2870[b]	2175	1700	5/pos	0.59 0.59
SB	3580	4275	2225	6/pos	0.62
SD	3070	3745	2400	5/pos	0.78
SD-B	4820	6185	5145	3/pos	1.07

[a] Assumed fully monolithic section.
[b] Concrete jacket considered only.

Estimated values of K_{th} and measured stiffnesses are given in Table 5.3. Experimental values include the secant stiffness from the response envelope at 0.5% drift (section 3.9), and the measured stiffness at first yielding. First yielding of the flexural reinforcement wherever it occurred (in the slab, beams or columns) was determined from strain gauge readings (Chapter IV), and the stiffness was obtained as the ratio of the story shear to drift angle at the time of yielding.

Specimens were cracked in the first cycle to 0.5% drift. However, most tests exhibited higher stiffnesses than the predicted values, except RB (Table 5.3). As yield was approached, the stiffness was lower. This was particularly the case of specimen O which suffered significant damage before yielding. Measured stiffnesses at yield were lower than K_{th}, except for SD-B in which the prediction of stiffness agrees reasonably well with K_y. No single component (beam, column or joint) was found responsible for the flexibility of the subassemblages. This can be confirmed in the member contribution to drift angle discussed in section 5.2. Stiffnesses were also calculated based on gross sections for beams and columns. For jacketed members, the modulus of elasticity used was that of the concrete in the jacket. For specimens O, RB , SB and SD, the calculated stiffness based on gross sections was about twice the calculated stiffness in Table 5.3. For SD-B, the stiffness from gross sections was 2.6 times the stiffness based on cracked transformed sections (Table 5.3). Such a large factor can be attributed to the jacketed beams in SD-B. For specimen RB, K_{th} given in Table 5.3 was estimated (1) using the full column concrete section, and (2)

considering a hollow section with only the column jacket contributing to the stiffness. No difference was found between these values because, due to the position of the neutral axis, most of the existing column core was in tension. The contribution of the part located in the compression side next to the neutral axis was negligible. The estimation of K_{th} for all specimens was based on the assumption of monolithic behavior between the existing element and the concrete jacket. The measurements with the ultrasonic pulse velocity equipment, discussed in Chapter IV, indicated monolithic behavior.

5.5 ENERGY DISSIPATION AND EQUIVALENT VISCOUS DAMPING RATIO

5.5.1 Energy Dissipation. Major earthquakes release tremendous amounts of energy. If the building is to withstand the quake without endangering life safety, it must be capable of absorbing and dissipating energy through kinematic energy, viscous damping energy, recoverable elastic strain energy and irrecoverable inelastic (hysteretic) energy. Depending on the foundation flexibility, soil internal damping and radiation damping might also be sources of dissipation. It is clear that in a satisfactory design, the energy supply should be larger than the energy demand.

The energy dissipated during the tests was computed as the area within the hysteresis loops from the story shear - interstory drift relation. The interstory drift was obtained by multiplying the measured drift angle R by the column height H. During bidirectional cycles, the loading interaction represented by the decay in story shear, affected the area inside the loops.

The cumulative energy dissipated at peaks of positive cycles in the E-W and N-S directions is presented in Figures 5.14 and 5.15. Drift angles are also shown in the graphs. All the rehabilitated specimens dissipated much more energy than the existing structure. As expected, specimen SD-B dissipated the largest amount of energy. All specimens show similar trends for both loading directions.

The total cumulative energy dissipated at peaks of positive cycles (Figure 5.16) was calculated as the sum of the cumulative energies in the two loading directions, i.e. adding values in Figures 5.14 and 5.15. Energy dissipation increased in cycles to 4% drift angle as plastic deformations increased. For example, for specimens O, SB and SD-B the total cumulative energy dissipated by the end of the test was more than three times the energy dissipated before cycles to 4% drift were applied (cycles 9 through 12). For specimens RB and SB, the factor was about two.

5.5.2 Equivalent Viscous Damping Ratio. Internal damping can be the product of several mechanisms, which include plastic deformation of metals and the friction between intergranular faces in most structural materials, such as aggregate interlock in structural concrete (Ref. 37). Internal damping is classified as a function of the dependency on frequency. Coulomb damping, independent of frequency, is associated with the friction

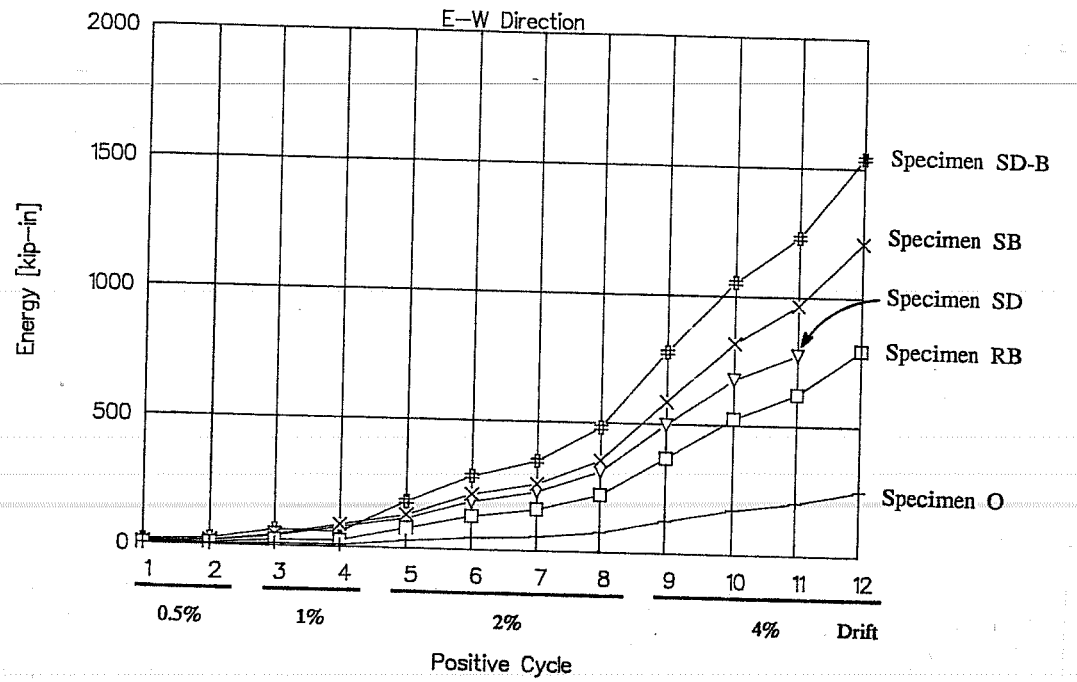

Figure 5.14 Cumulative Energy Dissipated (E-W Direction)

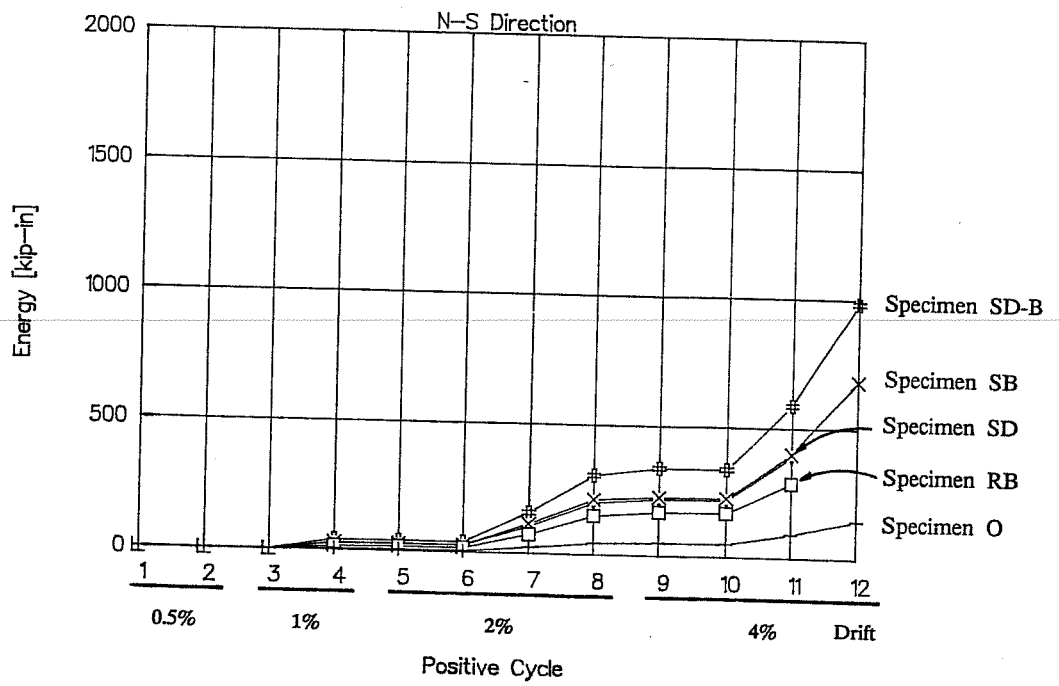

Figure 5.15 Cumulative Energy Dissipated (N-S Direction)

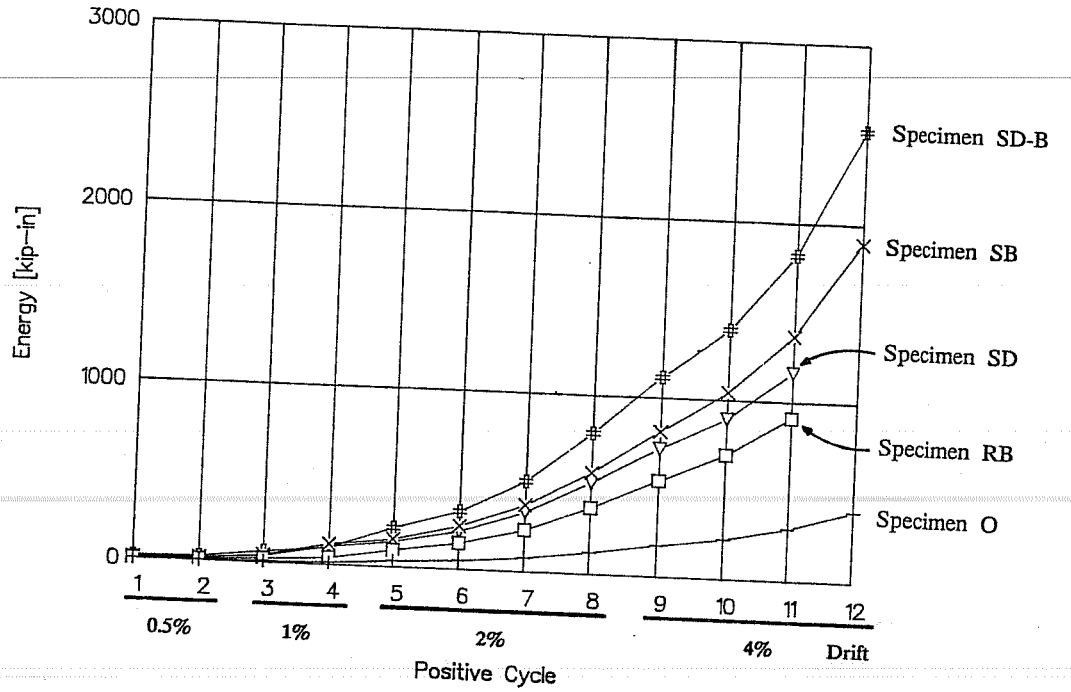

Figure 5.16 Total Cumulative Energy Dissipated

between intergranular surfaces, and is sometimes called hysteretic damping. Therefore, it necessarily involves nonlinear load versus displacement curves under static loads. The other energy dissipation mechanisms vary with the frequency and are generally referred to as viscous damping. Under low stress levels some materials, such as polymers for example, exhibit a damping which can be considered as linearly proportional to the rate of deformation.

It is possible to determine the amount of damping that would make a linear system respond with the same amplitude as a nonlinear structure subjected to a given periodic excitation. Equating the energy dissipated per cycle in the nonlinear structure to its linear equivalent, the equivalent damping can be computed. Although the equivalent damping is associated to the energy dissipated per cycle, i.e. related to the hysteretic damping, the equivalent damping is often referred to as equivalent viscous damping ratio (Ref. 37).

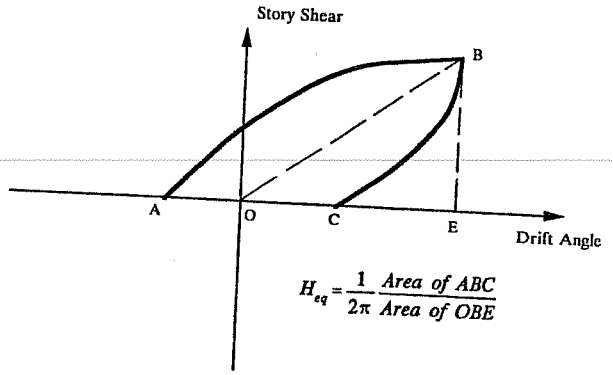

Figure 5.17 Definition of Equivalent Viscous Damping Ratio

The definition of equivalent viscous damping ratio H_{eq} is depicted in Figure 5.17. It was taken as the ratio of the dissipated energy within half a cycle to 2π times the strain energy measured at peak of an equivalent linearly elastic system. Values of the equivalent

viscous damping ratio were used to compare the energy dissipation capacity of the specimens and to indirectly measure pinching of hysteresis loops.

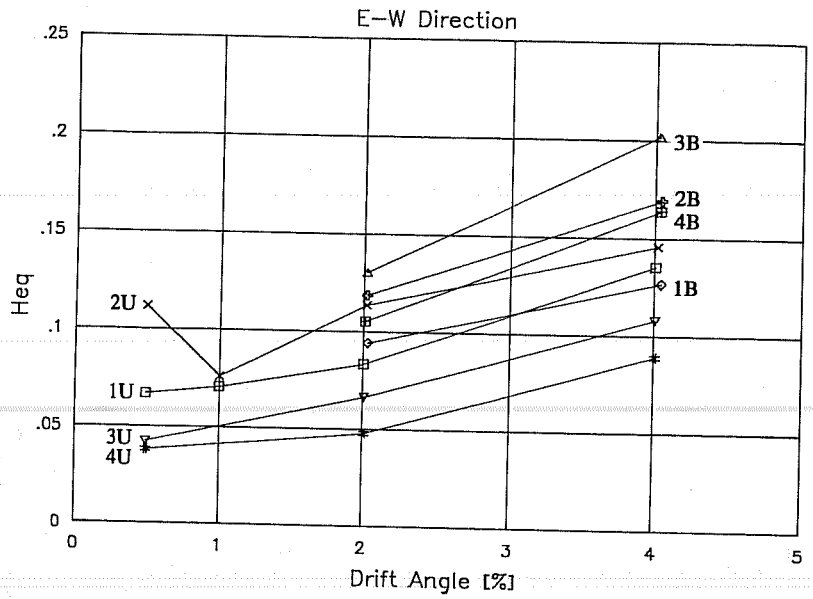

Figure 5.18 Equivalent Viscous Damping Ratio (Specimen SB)

The equivalent viscous damping ratio H_{eq} plotted against the story drift angle during E-W loading for specimen SB is shown in Figure 5.18. The energy dissipation capacity of specimen SB is used for illustration. Similar graphs were plotted for other tests in the two loading directions (not shown). The notation introduced in Figure 5.8 is applicable. In general, damping ratios increased with drift angle.

Typically, during unidirectional cycles to a given drift, the highest H_{eq} was calculated for the negative portion of the first loading cycle. At the beginning of such half-cycles, permanent deformation was larger than that for positive half-cycles, so that H_{eq} became larger. The lowest value occurred in the second negative half-cycle. Before this half-cycle was applied, the specimen had been subjected to 1.5 cycles to the same deformation level. Concrete damage, bond degradation, shear distress contributed to narrow the hysteresis loops.

As can be noted, damping ratios for bidirectional cycles were considerably higher. Larger values occurred due to the bidirectional interaction caused by the loading sequence devised for the experimental program. The energy dissipated from the point of zero shear was used to compute the equivalent viscous damping ratios in bidirectional cycles. Due to the rather low probability that the sequence used would occur during an earthquake, damping ratios for bidirectional cycles are not discussed in greater detail. In the N-S direction, only cycle 4 was unaffected by the bidirectional interaction.

Average values of equivalent viscous damping ratios in a given drift angle, $\bar{H}_{eq}$, for the E-W unidirectional loading are presented in Table 5.4. In all specimens, the variation of H_{eq} in a given deformation level was comparable thus allowing comparisons to be made. The variation was largest in cycles to 0.5% drift and lowest at drifts to 4%. In general, damping ratios were low and were quite similar in all tests.

Table 5.4 Average H_{eq} for Unidirectional Cycles

Story Drift Angle [%]	Specimen				
	O	RB	SB	SD	SD-B
0.5[a]	0.052	0.062	0.065	0.069	0.065
1[b]	0.074	0.081	0.074	0.081	0.077
2[a]	0.076	0.081	0.079	0.085	0.079
4[a]	0.109	0.108	0.120	0.117	0.111

[a] Average of four data points.
[b] Average of two data points.

Table 5.5 Sum of Normalized $\bar{H}_{eq}$

Specimen	O	RB	SB	SD	SD-B
Sum	4.00 (1.00)[a]	4.34 (1.09)	4.39 (1.10)	4.61 (1.15)	4.35 (1.09)

[a] Sum normalized with respect to specimen O.

To compare the energy dissipation capacities, equivalent damping ratios given in Table 5.4 were divided by the damping ratios for test O at a given drift angle. Then, the results presented in Table 5.5 were computed for each specimen by adding the ratios obtained. Taking specimen SD, for example, H_{eq} at 2% drift was normalized by dividing 0.085/0.076 = 1.12, where 0.076 is H_{eq} for specimen O. Repeating the process for all deformation levels, the following normalized H_{eq} are obtained: 1.33 (at 0.5% drift), 1.09 (at 1%), 1.12 (at 2%) and 1.07 (at 4%). The value reported in Table 5.5, i.e. 4.61, is the sum of such ratios. The energy dissipation capacity of the rehabilitated specimens was a little

higher than that for the existing structure. Thus total cumulative energy should not be used to compare specimen capability to dissipate hysteretic energy. Specimen SD shows a slightly higher values in Table 5.5 than specimens RB and SB. Beam inelastic deformations, which were more significant than in RB and SB, and column reinforcement layout (distributed vs. bundled bars) probably contributed to improve the energy dissipation capacity.

The quality of the hysteretic response of reinforced concrete members has been a matter of discussion. In this regard, two schools of thought are identified in seismic design. Full hysteresis loops may be considered by some as the only possible response of a structure to withstand a major earthquake. Others recognize that well proportioned and detailed reinforced concrete members can, and will, suffer some degree of pinching and stiffness degradation. The two performance criteria lead to different design standards and codes.

Recent studies (Ref. 28), have focused on the influence of the energy dissipation capability at the beam ends on earthquake response. Nonlinear time history analysis of buildings subjected to El Centro NS and Taft S69E records were performed. The hysteresis models were selected to simulate the pinching characteristics caused by bond deterioration. Equivalent damping ratios of 0.25, 0.15 and 0.10 at a ductility factor of 4.0 were used. The distribution of beam end ductilities in the structures analyzed, for equivalent damping ratios of 0.15 and 0.10, were comparable. The maximum response displacements were also similar. This means that the influence of pinching, assumed to be caused by bond distress, on the response was not very large for the range of H_{eq} considered. Kitayama et al. concluded that some pinching of the hysteresis diagram is acceptable, i.e. some bond deterioration of beam bars within a joint may be tolerable.

In other studies, it has been concluded that the effect of pinching on the response is a function of the amount of stiffness degradation and the frequency range, the greatest effect in the acceleration range (stiff structures) and lowest in the displacement range (Ref. 7). It was found that the effect of pinching on the response acceleration was 5% at most.

Structures designed so that large shear stresses are applied to the joint show pinching and stiffness decay in the hysteresis diagram, such as those observed in the rehabilitated specimens. However, in light of the results of the investigations mentioned above, the response of structures with pinched hysteretic behavior may be satisfactory when subjected to strong ground motions. Further analyses of such structures considering the influence of joint detailing, particularly in regard to possible bond deterioration, are necessary.

5.6 JOINT SHEAR STRENGTH

Joint shear strength is examined in terms of interstory shears. The ultimate story shear to cause joint failure was calculated as the story shear required to produce the maximum joint shear stress recommended by ACI 352 Committee Report (Ref. 4). Ultimate story shears were calculated as follows

$$V_{u,j} = \frac{v_j b_j h_j j_b}{H(1 - \frac{h_j}{L} - \frac{j_b}{H})} \tag{5.6}$$

where $V_{u,j}$ = ultimate story shear to produce joint failure
v_j = maximum joint shear stress
b_j = joint width
h_j = joint depth
H = column height
L = beam length
j_b = beam moment arm.

The joint geometry was determined according to Ref. 4 (Figure 5.19). The joint width was taken as the average of the beam and column widths. For all rehabilitated specimens, the column width was that of the jacketed column. For specimen SD-B, the beam width was that of the jacketed beam. The joint depth was taken as the jacketed column depth. The beam moment arm was taken as $7/8 \cdot d$, where d was the average effective depth of the beams in the direction of interest. Due to placement of the beam longitudinal steel, the effective depth for the E-W and N-S directions was slightly different. Member sizes in both directions varied a little. The largest effect of the effective depth on the ultimate story shear was 2% (specimen SD).

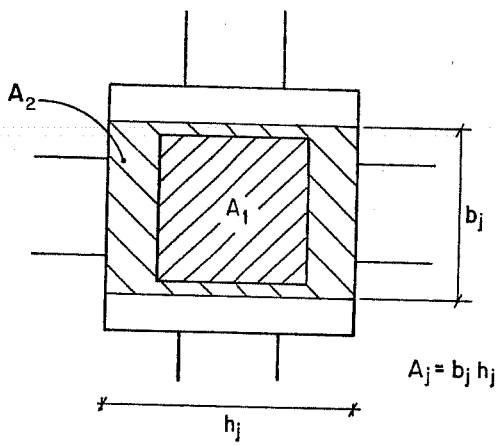

Figure 5.19 Joint Shear Area

In the derivation of Equation 5.6, it is assumed that the critical sections are immediately adjacent to the joint. As reported in Chapters III and IV, the beam critical section for specimens RB, SB, and SD was within the column jacket. The ultimate story shear, calculated using the assumption that critical sections are located at the original column face, were 5% smaller than those calculated with Equation 5.6 which represents an upper bound on the calculated story shears.

The maximum joint shear stress v_j was calculated as $v_j = \gamma\sqrt{f_c'}$, in which the constant γ depends on the joint classification. According to ACI 352, specimens O, RB, SB and SD are classified as "exterior joints" because the beams did not cover three-quarters of the width of the column so that a value of $\gamma = 15$ was used. Specimen SD-B is classified as an "interior joint" and $\gamma = 20$ was used. The joint region of the rehabilitated specimens consisted of two different concretes thus having distinct strengths. A weighted average of

the strength was computed to calculate the joint shear stress. The average strength was given by

$$A_j \sqrt{f'_{c,j}} = A_1 \sqrt{f'_{c,1}} + A_2 \sqrt{f'_{c,2}} \qquad (5.7)$$

where $A_j = b_j h_j$ = joint area
$f'_{c,j}$ = weighted average concrete strength
A_1 = gross area of existing column
$f'_{c,1}$ = strength of the existing column joint
$A_2 = A_j - A_1$ = area of column jacket included in joint area (see Figure 5.19)
$f'_{c,2}$ = strength of the jacketed column joint.

Dividing Equation 5.7 by A_j, and substituting $A_2 = A_j - A_1$, we have

$$\sqrt{f'_{c,j}} = \omega \sqrt{f'_{c,1}} + (1-\omega) \sqrt{f'_{c,2}} \qquad (5.8)$$

where $\omega = A_1/A_j$.

The calculated ultimate story shear and the measured maximum story shear for unidirectional and bidirectional cycles are given in Table 5.6 for cycles to 2% drift, and in Table 5.7 for the story shears in cycles to 4% drift. The ratios of measured to calculated story shears are shown in parenthesis.

Maximum measured bidirectional story shears were calculated as the maximum values given by square root of the sum of the squares of the E-W and N-S story shear components during peak biaxial displacements. Although there are no design guidelines for estimating the bidirectional joint shear strength, previous research programs at the University of Texas at Austin (Refs. 21, 29) have suggested that a circular (or elliptical) interaction diagram, using the unidirectional strength as the radius, could be used for design since it gives a safe estimate of the joint strength. A circular representation is implied in the ACI 352 Committee Report. To assess the joint strength under bidirectional loading, a circular or elliptical interaction curve was assumed. Rigorously, the interaction diagram is elliptical for all specimens but SB, due to the different ultimate story shears in orthogonal directions. The ratio of measured to calculated bidirectional story shears in Tables 5.6 and 5.7 were obtained from

$$Ratio = \sqrt{\frac{(V_{m,EW})^2}{(V_{u,EW})^2} + \frac{(V_{m,NS})^2}{(V_{u,NS})^2}}$$

where V_m = measured unidirectional story shear
V_u = calculated ultimate story shear.

Table 5.6 Calculated and Measured Maximum Story Shears at 2% Drift Angle

Test	Calculated Story Shear [kip]		Measured Story Shear [kip]	
	Uniaxial (E-W)	Biaxial	Uniaxial (E-W)	Biaxial
O	9.6 (1.17)	9.5 (1.16)	11.2	11.0 [6.1 - EW] [9.2 - NS]
RB	29.1 (1.07)	28.9 (1.19)	31.1	34.3 [20.0 - EW] [27.8 - NS]
SB	33.7 (1.47)	33.7 (1.65)	49.5	55.5 [33.8 - EW] [44.1 - NS]
SD	30.3 (1.41)	30.6 (1.51)	42.6	46.4 [26.1 - EW] [38.4 - NS]
SD-B	62.9 (1.02)	63.3 (1.16)	64.0	73.5 [42.8 - EW] [59.7 - NS]

Table 5.7 Calculated and Measured Maximum Story Shears at 4% Drift Angle

Test	Calculated Story Shear [kip]		Measured Story Shear [kip]	
	Uniaxial (E-W)	Biaxial	Uniaxial (E-W)	Biaxial
O	9.6 (1.22)	9.5 (1.08)	11.7	10.3 [5.3 - EW] [8.8 - NS]
RB	29.1 (1.28)	28.9 (1.17)	37.2	33.6 [17.8 - EW] [28.6 - NS]
SB	33.7 (1.58)	33.7 (1.43)	53.4	48.4 [26.7 - EW] [40.4 - NS]
SD	30.3 (1.45)	30.7 (1.41)	44.0	43.2 [18.3 - EW] [39.2 - NS]
SD-B	62.9 (1.05)	63.3 (1.03)	66.1	65.0 [33.7 - EW] [55.6 - NS]

Maximum story shears at 2% and 4% drift exceeded the calculated ultimate capacities. Calculated ultimate story shears were surpassed in both uniaxial and biaxial loading. The design recommendations in the ACI 352 Committee Report and the approach to estimate the weighted average strength (Equation 5.7) provide a safe estimate of the joint strength of the existing structure and of all the rehabilitated specimens. As was discussed in previous chapters, no transverse reinforcement was placed within the joint region of the existing column, following the design and construction practices of the 1950's. For constructibility and performance considerations, no transverse steel was placed in the joint of the rehabilitated subassemblages. To confine the concrete and the column jacket reinforcement not confined by the beams, a structural steel joint cage was assembled around the joint (see Figure 2.6). Thus, joint shear forces had to be resisted mainly by a diagonal concrete strut across the joint, which was fully effective at cycles to large drift levels (see Figure 1.1c). The joint cage effectively confined the core even after the joint failed in cycle 9. It is evident that the joint shear strength depends on the concrete compressive strength provided that the joint is adequately confined.

Ratios of measured to calculated unidirectional story shear were greater than one. The ratios were larger at 4% drift angle. Beam hinging and maximum story shears were reached in cycles to 4% drift. At 2% drift, the ratios ranged from 1.02 for SD-B to 1.47 to SB. The story shears, and therefore the ratios, increased an average of 7% at 4% drift.

Measured biaxial resultants of story shears were larger than the calculated strength assuming a quadratic interaction diagram. The largest ratios under biaxial load were obtained at 2% drift. At 4% drift, the biaxial resultants were about 8% less than at 2% because after joint failure, the E-W story shear component decreased very fast. For the same reason, at drifts to 4%, the ratios for biaxial loading were smaller an average of 7% than the unidirectional ratios.

The design guidelines of Ref. 4 are intended for structures in which beam hinging is expected in the primary seismic resisting system. Specimen O formed column hinges before the failure. Measured maximum unidirectional and bidirectional story shears were larger than the calculated ultimate strength both, at 2% and 4% drift. However, the design of "strong beam - weak column" systems, such as specimen O, subjected to earthquake loads should be avoided. It is clear that after jacketing the most damaged elements, namely the joint and columns, the strength of RB was smaller than that of SB and SD, which were jacketed with no previous damage. If 2% drift is anticipated as the deformation that a structure would undergo during a major seismic event, ACI 352 guidelines can be used to design rehabilitated joints (damaged or undamaged) which are adequately confined by transverse beams or joint reinforcement.

5.7 MEMBER STRENGTH AND SLAB PARTICIPATION

5.7.1 Member Strength. The beam and column strengths were calculated from measured material properties and dimensions, considering an equivalent rectangular stress block for concrete and assuming that plane sections remain plane. A perfect elasto-plastic model was assumed for the steel stress-strain behavior. Column capacities were computed for zero axial force since no external axial force was applied to the column. For the effective beam width for positive bending, flange widths suggested by Refs. 2 and 3 were used. For negative moment, the slab steel that contributed to the capacity was assumed to be bars within the same equivalent width. Capacities of jacketed members were calculated on the basis of monolithic behavior. Member strengths are independent of deformation level.

Table 5.8 Column and Beam Flexural Capacities [E-W Direction] (kip-in)

Test	Measured Column Moment[a] M_{test} [kip-in]	Column Flexural Capacity $M_{u,col}$ [kip-in]	Ratio $\frac{M_{test}}{M_{u,col}}$	Beam Capacity[b] $M_{u,beam}$ [kip-in]		Ratio $\frac{\Sigma M_{u,col}}{\Sigma M_{u,beam}}$
				Positive	Negative	
O	848.3	868.2	0.98	2668.3	2773.8	0.32
RB	2967.0	6882.4	0.39	2668.3	2773.8	2.53
SB	3871.5	7325.5	0.53	2703.0	2767.8	2.68
SD	3190.0	7125.0	0.45	2646.6	2725.5	2.65
SD-B	4792.3	8336.9	0.55	3320.1	3962.2	2.29

[a] Maximum column moment measured at the slab and at the beam soffit section.
[b] ACI effective width used for positive and negative beam moments.

The maximum measured column moments, at the slab section and at the beam soffits, and the column capacities in the E-W direction are given in Table 5.8. Beam flexural strength for positive and negative moments, and the ratio of column to beam bending strengths are also presented. Similar results were found for the N-S direction but are not presented here. The column flexural strength of specimen O was reached and column hinges were formed before the failure of the subassemblage. The behavior was typical of a "strong beam - weak column" design in which the ratio of column to beam

bending capacities is less than one. All rehabilitated specimens had stronger columns than beams. The response of the columns was essentially elastic with minor damage.

5.7.2 Slab Participation. The amount of slab that contributes to T-beam action is an important design consideration. Floor system strength, under positive and negative bending, is of particular interest because it must be considered for shear strength of the beams, the flexural strength of the columns and the strength of joints. Design guidelines for T-beam action under positive moment are based on an effective width (Refs. 2, 3). The effective width concept assumes that if the actual width of the flanges is replaced by a certain reduced width, simple bending theory can be applied to the effective beam cross section to correctly predict the flexural behavior of the entire slab-beam system. ACI provisions, based on the shear lag concept, imply that slab effectiveness far from the web is reduced because the stress distribution across the slab is not uniform with the stress in the slab decreasing with increasing distance from the web of the T-beam. Analytical results have shown that stress across the slab is actually fairly uniform, but that the slab farther away from the web does not behave as would be expected by simple flexural theory because the neutral axis changes with its distance from the web (Ref. 26). For negative flexure (slab in tension), there are no design guidelines to estimate the slab participation. Previous test programs at the University of Texas at Austin (Refs. 21, 26, 29, 31), have shown that counting only the tensile capacity of the reinforcement located in the effective flange width as specified by the ACI 318 Building Code in assessing the strength of the beam, leads to an underestimation of the negative moment capacity. The action of the slab is a function of the flexural deformations of the longitudinal beam (Ref. 36). As this beam is subjected to negative bending moment, the top surface of the beam elongates along the beam length. Because the slab is monolithically connected to the beam, the elongation is transferred through in-plane shear to the slab. The accumulation of shear along the length of the longitudinal beam results in slab tension that must be transferred through in-plane action to a section of the slab located at the interface of the transverse beam and the slab.

The total width of the specimens was 204 in. (see Figure 2.1). The slab width at each side of the beam was 98 in. for specimens O, RB, SB and SD, and 94.5 in. for specimen SD-B. The slab was reinforced with two layers of continuous #3 bars. Top bars were placed at every 12 in. and bottom bars were spaced at every 24 in.. Figure 5.20 shows the effective slab width which is the effective flange overhang on each side of the beam.

The effective slab width can be assessed through slab bar stresses. The effective slab width ratio was calculated as the ratio of the tensile force in the slab reinforcement over the maximum tensile force when all bars reach yielding.

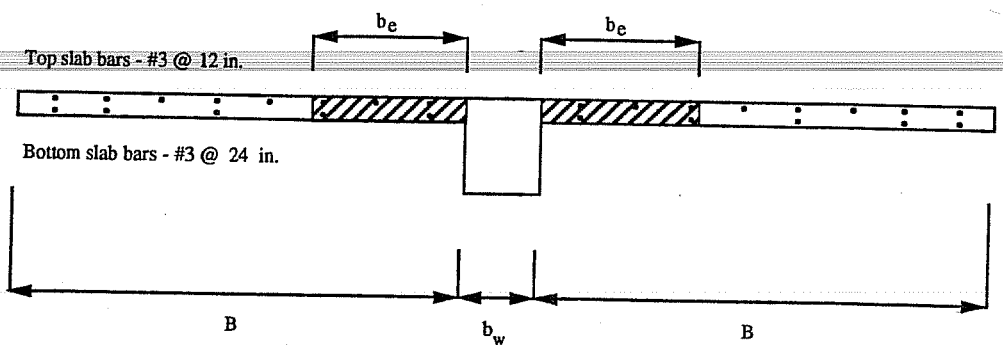

For specimens O, RB, SB and SD
b = 8 in.
B = 98 in.

Total slab width = 204 in.

For specimen SD-B
b = 15 in.
B = 94.5 in.

Figure 5.20 Effective Slab Width

Such ratio is expressed as

$$\frac{b_e}{B} = \frac{\Sigma A_s f_s}{\Sigma A_s f_y} \tag{5.9}$$

where b_e = effective slab width
B = total slab width
A_s = area of slab bar
f_s = stress of slab bar
f_y = yield strength of slab bar.

The effective slab width ratio was calculated from the stress distribution of the bars across the slab for positive peak cycles 1, 3, 5, and 9, as shown in Figure 4.29. Positive loading imposed tension on the slab of the W beam. The effective width was computed from the gauge locations in the top slab bars only, and in the top and bottom bars. In many cases, only top bars should be considered to participate in beam moment capacity because bottom bars are designed for gravity loads in the center of the slab and are not provided with sufficient anchorage to resist the bending moment at the face of the transverse beam under lateral loads. In these specimens, bottom slab bars were continuous across the transverse beams. Stresses were calculated from the strain history of top and bottom bars. Tensile stresses only were obtained at positive loading peaks. The slab participation was estimated for all specimens, except for SD in which most of the slab gauges malfunctioned

before the test. Although not enough data is available to estimate quantitatively the slab participation for SD, observation of the slab damage and analysis of some working gauges suggest that the slab participation for SD was lower than that for SB but higher than for RB.

Figure 5.21a shows the slab participation, in percent, considering top bars only, versus the imposed drift angle. The contribution of the top and bottom layers of reinforcement is presented in Figure 5.21b. The slab participation increased with drift angle. Effective slab width calculated from top bars only was a little higher than for top and bottom bars. It is clear that all the rehabilitated specimens showed greater slab participation than that of the existing structure at the same levels of deformation.

At 2% drift, the slab participation of specimen O was half that of the repaired specimen RB (Figure 5.21). Specimen SB and SD-B showed the largest participation at about 80% for top bars only and about 75% for top and bottom bars. Comparison of RB and SB shows that the slab participation of the repaired specimen was smaller than that of the undamaged specimen.

At 4% drift, the effective slab width ratios for specimens O and RB increased (Figure 5.21). The entire slab width was effective for top bars only in specimens SB and SD-B. For top and bottom bars, slab participation was 90%. Strain hardening of some top and bottom slab bars near the beam web is responsible for the large participation in specimens SB and SD-B. Comparable slab participation factors have been reported in other experimental programs (Refs. 21, 27, 29).

The slab participation estimated using slab bar stresses may not be a totally accurate measure of the moment resulting from the slab steel acting with the beam in negative bending, but it does indicate the increasing participation of the slab reinforcement in resisting lateral forces at large drift levels and indicates the influence of the transverse beams. The effect of the size of the transverse beam, and thus of the torsional stiffness, can be observed from comparison of the slab participation at low drift levels for SB and SD-B. Specimen SD-B had a torsionally stiffer transverse beam than SB and exhibited larger effective slab widths up to 2% drift. As torsional distress progressed in SD-B, the slab participation factors for the two specimens were nearly the same.

Slab participation can also be assessed through comparison of maximum measured moments and calculated beam capacities. Measured and calculated beam bending moments at 2% and 4% drift are given in Tables 5.9 and 5.10, respectively. Maximum beam moments were measured at the face of the existing column for specimen O, and at the face of the jacketed column for the rehabilitated specimens. Although the beam critical section for RB, SB and SD formed within the column jacket, measured moments were calculated at the face of the jacketed column. Moments at the existing column were only 5% larger.

In general, E-W moments increased slightly from 2% to 4% drift. At 2% drift, beams of the rehabilitated specimens had almost reached their maximum capacity so that

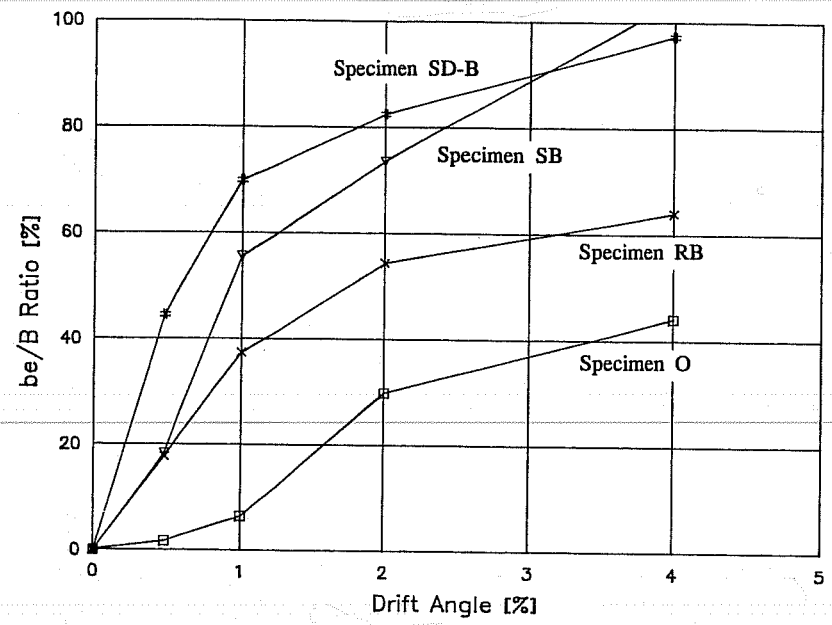

a) Top Bars

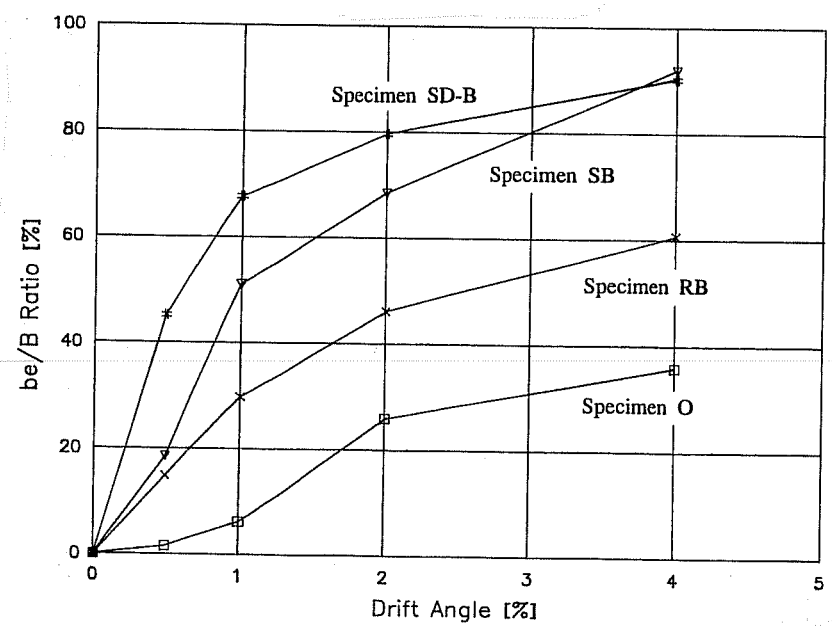

b) Top and Bottom Bars

Figure 5.21 Slab Participation

only small additional capacity was available at 4% drift. Additionally, bond deterioration and slip of the reinforcement reduced the effectiveness of the compression steel. In some cases, the "compression" reinforcement was actually in tension. This resulted in the neutral axis located above the top bars thus causing decrease in strength. Only the beam reinforcement in the jacket in SD-B strain hardened. Moments at 2% drift in the N-S beams typically decayed when reaching 4% drift (cycle 11). At this stage the specimen was in severe distress and the joint had failed (in cycle 9). As mentioned in Chapter III, the strength in the N-S direction was affected by the damage caused when loading in the E-W direction.

Beam flexural capacities were calculated with and without slab participation. Flexural capacities are independent of deformation level. Capacities were computed for beam rectangular section R_{calc}, and for several effective widths of the flange in T-section T_{calc}. Top and bottom slab bars were considered effective in the flange portion. Slab reinforcement outside the effective width was ignored.

For positive bending (slab in compression), the effective width suggested by Refs. 2 and 3 was used and corresponded to $b_e = 0.18\,B$ for specimens O, RB, SB and SD, and $b_e = 0.15\,B$ for specimen SD-B. The positive bending strength is not very sensitive to the assumed effective width because the capacity is governed by the bottom longitudinal beam reinforcement. Beam capacities R_{calc} and T_{calc}, and the ratio of measured to calculated beam moments are given in Tables 5.9 and 5.10.

Under negative bending at 2% drift, the beam capacity for O and RB was best estimated by the rectangular beam section strength. For the other specimens, $b_e = 0.30\,B$ was used. Same effective slab width was suggested in Ref. 21 for new structures built with normal and high strength materials. At 4% drift, the slab participation b_e/B was taken as 0.1 for RB, and 0.5 for the other rehabilitated specimens. Beam capacities based on rectangular and T-sections are also shown in Tables 5.9 and 5.10.

Pantazopoulou et al. (Ref. 39), have suggested effective slab widths of 1.5 beam depths up to yielding, increasing to approximately three beam depths for deformations that can be reasonably expected during severe earthquake loading. Such effective slab widths correspond to =0.3 and 0.6 which coincide with the values obtained for specimens SB, SD and SD-B at 2% and 4% drift, respectively. Other study has recommended the use of ACI effective slab width for negative bending (Ref. 19). For specimens SB, SD and SD-B, this approach would underestimate the moments at 2% drift by 33% on the average, and at 4% drift by 44% on the average.

The slab influence in beam moment capacity for rehabilitated specimens is clear in Tables 5.9 and 5.10. Calculation of beam capacities based on the rectangular section significantly underestimated the measured moments. Negative flexural moments were considerably affected by the participation of the slab reinforcement to beam strength. Beam capacities were obtained assuming that the strain distribution across the effective slab width was uniform. This implies that the beam strength under negative bending would depend

Table 5.9 Measured Beam Moments at 2% Story Drift and Calculated Moment Capacity

Test		Positive Moment [kip - in]					Negative Moment [kip - in]				
		M_{test} [a]	R_{calc} [b]	$\frac{M_{test}}{R_{calc}}$	T_{calc}	$\frac{M_{test}}{T_{calc}}$	M_{test} [a]	R_{calc} [b]	$\frac{M_{test}}{R_{calc}}$	T_{calc} [c]	$\frac{M_{test}}{T_{calc}}$
O	E-W	930	2398	0.39	2668	0.35	897	2326	0.39	2326	0.39
	N-S	919	2282	0.40	2472	0.37	835	2299	0.36	2299	0.36
RB	E-W	2291	2398	0.96	2668	0.86	2313	2326	0.99	2326	0.99
	N-S	2045	2282	0.90	2472	0.83	2135	2299	0.93	2299	0.93
SB	E-W	3359	2398	1.40	2703	1.24	3967	2346	1.69	3406	1.16
	N-S	2972	2327	1.28	2511	1.18	3540	2427	1.46	3452	1.03
SD	E-W	3243	2367	1.37	2647	1.23	3085	2301	1.34	3359	0.92
	N-S	2887	2303	1.25	2482	1.16	2876	2342	1.23	3358	0.86
SD-B	E-W	4074	2981	1.37	3320	1.23	5613	3493	1.61	4686	1.20
	N-S	3495	2864	1.22	3108	1.12	5328	3758	1.42	4921	1.08

[a] Maximum beam moment measured at the face of the joint.
[b] Calculated moment capacity as rectangular section.
[c] Calculated moment capacity as T-beam: b_e/B =0 for specimens O and RB, and 0.30 for SB, SD and SD-B.

Table 5.10 Measured Beam Moments at 4% Story Drift and Calculated Moment Capacity

Test		Positive Moment [kip - in]					Negative Moment [kip - in]				
		M_{test}[a]	R_{calc}[b]	$\frac{M_{test}}{R_{calc}}$	T_{calc}	$\frac{M_{test}}{T_{calc}}$	M_{test}[a]	R_{calc}[b]	$\frac{M_{test}}{R_{calc}}$	T_{calc}[c]	$\frac{M_{test}}{T_{calc}}$
O	E-W	942	2398	0.39	2668	0.35	950	2326	0.41	2326	0.41
	N-S	1010	2282	0.44	2472	0.41	690	2299	0.30	2299	0.30
RB	E-W	2743	2398	1.14	2668	1.03	2760	2326	1.19	2774	1.00
	N-S	2196	2282	0.96	2472	0.89	2047	2299	0.89	2299	0.89
SB	E-W	3347	2398	1.40	2703	1.24	4546	2346	1.94	3628	1.25
	N-S	2645	2327	1.14	2511	1.05	3358	2427	1.38	3668	0.92
SD	E-W	3213	2367	1.36	2647	1.21	3293	2301	1.43	3577	0.92
	N-S	2708	2303	1.18	2482	1.09	3085	2342	1.32	3568	0.86
SD-B	E-W	4058	2981	1.36	3320	1.22	5766	3493	1.65	4942	1.17
	N-S	3239	2864	1.13	3108	1.04	5045	3758	1.34	5171	0.98

[a] Maximum beam moment measured at the face of the joint.
[b] Calculated moment capacity as rectangular section.
[c] Calculated moment capacity as T-beam: b_e/B =0 for specimen O, 0.10 for RB, and 0.50 for SB, SD and SD-B.

only on the amount of slab reinforcement included in such flange. However, experimental data has shown that strain distribution is not totally uniform and varies with the distance from the column. Moreover, some slab bars close to the beam web went into strain hardening, while the farthest bars remained elastic. Also, the beam capacities were computed assuming strain compatibility in the cross section. At large deformation levels, particularly at 4% drift, the bond along some of top and bottom beam longitudinal reinforcement deteriorated and the bars slipped thus affecting the strain compatibility.

CHAPTER VI - CONSTRUCTION, DESIGN AND EVALUATION CONSIDERATIONS

6.1 INTRODUCTION AND SCOPE

Construction, design and evaluation considerations are presented in this chapter. The recommendations are based on the construction and observed performance of the specimens, and the analysis of test results presented in Chapters II through V of four large-scale reinforced concrete frame connections rehabilitated by jacketing. The construction and design considerations apply for cast-in-place reinforced concrete jacketing of moment resisting frame elements designed to resist earthquake motions. It is anticipated that 2% drift represents a reasonable estimate of the deformation that a structure will undergo during a major seismic event.

6.2 CONSTRUCTION CONSIDERATIONS

6.2.1 Surface Preparation. To have monolithic behavior of jacketed elements, the concrete surface must be roughened and cleaned appropriately. Previous research on shear transfer across new and existing concrete interfaces (Ref. 10) indicated that nearly any surface roughening preparation is adequate to transfer shear forces, as long as the exterior concrete paste (laitance, dust) is removed and some aggregate is exposed. The results of Ref. 10 did not appear to justify the use of a bonding agent. In this program, the surface was roughened using a hand chipping hammer (see Figure 2.13) and no bonding agent was applied to the surface. Small particles and dust were removed with a thick brush and a vacuum cleaner. Water may be used in lieu of vacuum cleaning. Compressed air should be used with caution because it might carry oil which will impair bond. Some design recommendations for rehabilitation of structures, such as Ref. 15, suggest the saturation of the concrete surface prior to casting the new concrete. To avoid excessive free water during casting, the concrete surface of the rehabilitated specimens was not wetted, except in specimen RB which was saturated. However, no difference was noted in the bond behavior along the concrete interface.

6.2.2 Perforations. Slab perforations are generally used to place the column jacket reinforcement, and to place and consolidate the concrete. The holes must be made as large as possible to reduce congestion of the reinforcement, and to facilitate placement and consolidation of the concrete. For placing the concrete for the beam jacket, slab perforations along the beam sides can be done in an alternating pattern to avoid forming weak planes in the slab (see Figure 2.14). To place the top reinforcement of the beam jacket, holes in the orthogonal beams can be drilled below the slab. The hole diameter must be large enough to accommodate any variation in the size of the beam jacket transverse reinforcement, and to allow concrete, especially grout, to penetrate the hole and improve bond around the bar. In this program, the hole was two times the bar diameter. It is important to note that in this series of tests, the time involved in the surface

preparation, and slab and beam perforations for specimen SD-B (columns and beams both jacketed) was nine times that for specimens with only columns jacketed. Threading of beam bars through the joint was very laborious. Jacketing of beams may not be cost effective for U.S. practice because very intensive labor is required.

6.2.3 Constructibility and Reinforcement Detailing.

6.2.3.1 Columns and Beams. Proper reinforcement detailing is of paramount importance to obtain satisfactory performance as well as for constructibility of the scheme. The thickness of the jackets must be large enough to permit construction operations to be carried out. A minimum thickness of 4 in. for columns, and 3 in. for beam sides must be considered. Transverse steel for columns and beams must have 135-deg hooks bent in the shop. In-situ hook bending is difficult and of variable consistency. Hooks intended to be bent to 135-deg may be closer to 90-deg hooks which have demonstrated very poor performance in past earthquakes. Column transverse steel can be provided by two L-shaped ties that overlap in diagonally opposite corners, as was done for the rehabilitated specimens (see Figures 2.3, 2.4, and 2.10 through 2.12). In a real structure, after the slabs have been perforated and the joint cage assembled, the ties can be stacked on the slab floor alternating overlapping corners at each layer. After the column longitudinal steel is placed, the ties can be lifted and secured. For columns with bundled reinforcement, tie hooks must accommodate the bundles and a special bend detail is necessary (Figure 2.3). For columns with distributed reinforcement, the L-shaped ties require standard bends and are more easily secured than in columns with bundled bars. The use of welded wire fabric for part or all the transverse steel along a member can be considered. Welded wire fabric cages have been used to improve the labor productivity and the construction quality (Ref. 21). However, careful construction scheduling, especially regarding the location of lap splices and casting procedures, is required. If corner ties are necessary, ⊏-shaped ties can be used outside the joint in lieu of the corner ties with 135-deg and 90-deg hooks used in this program (see Figures 2.4 and 2.5). The ⊏-shaped ties can be installed more easily, and are expected to perform as well as those used in these tests since the extension is anchored in the column core. For the beam transverse steel, U-shaped ties and inverted U-shaped ties can be considered (see Figures 2.5, 2.15 and 2.16).

6.2.3.2 Joint. To maintain joint shear strength through large deformations, joint confinement steel is needed to preserve concrete integrity. Joint confinement steel can be provided with ties placed in holes drilled through the beams. For the ties, in-situ bending of the hooks may be needed. Drilling of the beams is difficult and labor intensive, since the exact location of the beam reinforcement is unknown. Furthermore, as mentioned before, in-situ hook bending is arduous and unreliable. To eliminate ties and the need to drill holes through the beams, a structural steel cage can be used in the joint, similar to that used in this program (see Figures 2.6, 2.10 and 2.). The joint confinement cage has been used in some buildings; but, prior to this program, there was no experimental evidence regarding its effectiveness. The confinement cage performed satisfactorily and prevented concrete spalling other than the joint cover. The cage can be proportioned to provide an equivalent

confinement to that recommended in the ACI 352 Committee Report. The steel angles of the cage must be strong and stiff enough to provide confinement through the joint region. In this study, the steel angles were designed to resist the joint bulging through bending. Steel angles were dimensioned to provide confinement to the core equivalent to spiral reinforcement. An efficiency factor of 1/3 relative to the confinement of spirals was assumed in design. If the use of large steel angles reduces considerably the available space for concrete placement or if the jacketed column section is too large, diagonal flat bars forming a truss can be used (Figure 6.1). The diagonal flat bars are intended to help confining the joint concrete and column bars not confined by the transverse beams and steel angles, and to reduce the unsupported length of the steel angle. The cage collars are essential for adequate behavior of the cage and must be strong enough to resist bending of the steel angle. If corner ties with 135-deg hooks are used to confine additionally the joint region when distributed column bars are used, a welded wire fabric cage made with corner ties can be considered.

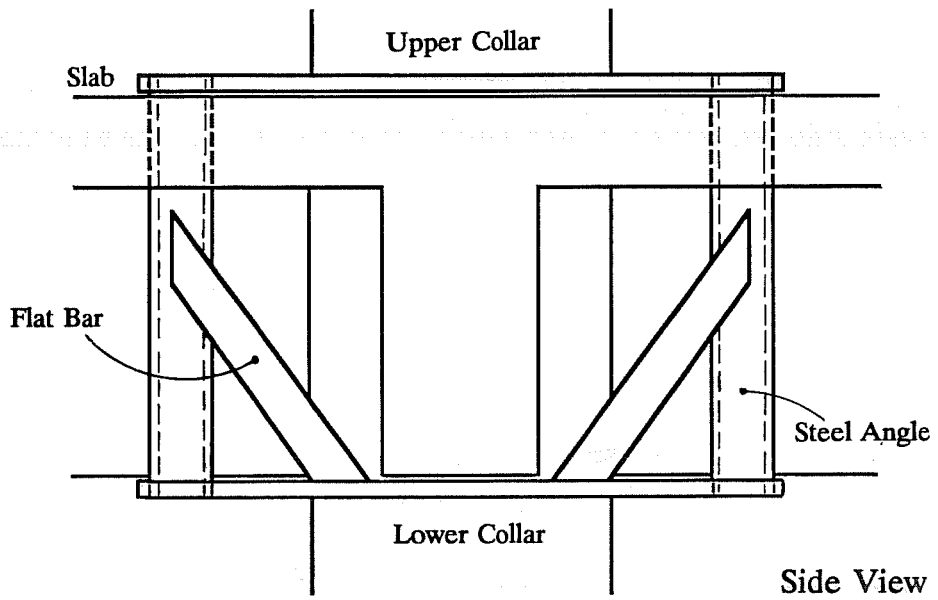

Figure 6.1 Joint Confinement Cage with Diagonal Flat Bars

6.2.4 Formwork. Formwork must be designed and constructed with large tolerances so that the contour of the existing structure is matched easily, and precision fitting is not needed. Formwork design should consider air release during casting. Vents are needed to allow air to escape as concrete fills the forms. Gaps at the top of the forms (under the slab) may serve this purpose. Large gaps may need to be partially sealed, and closed once the concrete has filled the forms. To facilitate placement of the concrete, the use of high-range water-reducing admixtures (superplasticizers) must be considered. The use of superplasticizers reduces the labor required for concrete placement and consolidation, and generally permits the concrete to flow more easily into congested spaces within the jackets. Beam jacketing requires the construction of large forms and the erection of supporting

frames to shore up the forms. The high cost of formwork in American construction practice must be considered if beam jacketing is used.

6.3 DESIGN CONSIDERATIONS

Based on the observed performance and the analysis of deformation and energy dissipation components, jacketing of frame elements proved to be an effective technique for rehabilitating the existing structure while maintaining the frame action of the structural system. The rehabilitated specimens behaved as a desirable "strong column - weak beam". Moreover, the rehabilitated subassemblages dissipated energy better. Beam hinging contributed significantly to deformation and energy dissipation throughout the tests. The rehabilitated specimens showed better stiffness, strength and total energy dissipation characteristics than those of the existing structure. In general, ACI Building Code Requirements can be used for designing a jacketing scheme. However, constructibility of the scheme must always be borne in mind.

6.3.1 Beam Critical Section. For jacketing of columns only, the location of the beam critical section should be taken into account. For specimens with jacketed columns only, the critical section was within the jacket. To design the beam for shear, it is safe to assume the beam critical section at the jacketed column face, whereas for beam flexure it is conservative to assume the critical section at the existing column face. The thicker the column jacket, the closer the critical section will be to the jacketed column face. For the specimen with jacketed beams and columns, the critical section formed at the jacketed column face.

6.3.2 Composite Behavior. Based on test results, it is clear that monolithic behavior of the specimens can be assumed. The contribution of the existing reinforcement should be taken into account when dimensioning and proportioning the jackets. For example, neglecting the participation of the existing beam flexural reinforcement is unconservative when checking the column to beam flexural capacity ratio intended to produce a "strong column - weak beam" system.

To estimate the stiffness at 0.5% drift of rehabilitated structures undamaged prior to jacketing, the cracked transformed moment of inertia of beams and columns can be used. The use of these values gave a reasonably good estimate of the measured stiffness. To simplify calculations, a fraction of the bending stiffness based on gross sections can be used as an alternative. For beams, a bending stiffness of $0.5E_cI_g$ can be considered. If the beams are jacketed, E_c corresponds to the modulus of elasticity of the jacket concrete. Similarly, a bending stiffness of $0.6E_cI_g$ can be used for jacketed columns. For the repaired specimen RB, the measured stiffness at 0.5% drift was about three quarters the estimated value using the procedure suggested above and considering the full column concrete section. From the test results, it was observed that the stiffness decreased 40% to 50% with increasing drifts from 0.5% to 2%.

6.3.3 Effect of a Damaged Column. Test results indicate that by jacketing the most damaged elements, the columns and joint, the strength at 2% drift and stiffness at 0.5% drift were about 65% and 50%, respectively, of the values obtained in the undamaged rehabilitated specimen.

6.3.4 Influence of Layout of Longitudinal Reinforcement in Column Jacket. The layout of the column jacket reinforcement influences both design and construction. Column bars may be distributed around the perimeter of the column or bundled in the corners. In this program, the specimen with bundles was stiffer than that with distributed bars. Both column bar layouts (distributed and bundled) showed good bond behavior. However, if the ratio of column to beam flexural capacities is lower than those for these tests, bundles are more prone to bond distress than distributed bars. Distributed column longitudinal reinforcement must be considered over bundles if the construction operations can be executed.

6.3.5 Effect of Beam Jacketing. Based on test results, beam jacketing can be considered for increasing the beam bending strength and for improving the bond behavior of the existing beam reinforcement. Due to a deeper beam, lower tensile and compressive stresses were applied to the existing top and bottom beam bars so that bond deterioration within the joint was less likely. Jacketing of beams also increased the confinement of the joint since the beams were wider. As mentioned before, beam jacketing may not be cost effective for U.S practice due to intensive labor and high costs of beam formwork.

6.3.6 Joint Shear Strength. No design recommendations exist for rehabilitated frame connections. From test results, it is clear that ACI 352 recommendations provided a safe estimate of the strength of jacketed joints with good joint confinement. Checking the joint shear strength in each direction will provide adequate bidirectional joint shear strength. For unidirectional loading, joint stresses of $15\sqrt{f'_{c,j}}$ and $20\sqrt{f'_{c,j}}$ should not be exceeded for "exterior" and "interior" type joints, respectively. The joints are classified according to ACI 352 based on the ratio of beam to column widths. The value $\sqrt{f'_{c,j}}$ is a weighted average of the square root of the concrete strength of the existing column and the jacketed column, based on their areas relative to the joint area (Figure 6.2). The uniaxial joint shear should be calculated from a beam hinge mechanism where the beam moment capacity accounts for increased stresses (due to higher yield strength than the nominal value and due to strain hardening) in longitudinal bars and for the participation of slab reinforcement. For all rehabilitated specimens, the beam critical section can be assumed at the jacketed column face. Measured story shears were larger than the calculated joint strength at 2% and 4% drifts. Figure 6.3 shows the maximum measured joint shear stresses for both loading directions during unidirectional and bidirectional cycles to 2% drift. Based on the joint geometry and joint classification suggested in ACI 352 Committee Report (Ref. 4), the envelope of maximum strength is also drawn. A circular interaction curve was assumed for bidirectional loading, in which the unidirectional strength is the radius. Specimens O, RB, SB and SD are classified as "exterior" joints because the beam width was less than three quarters of the column width.

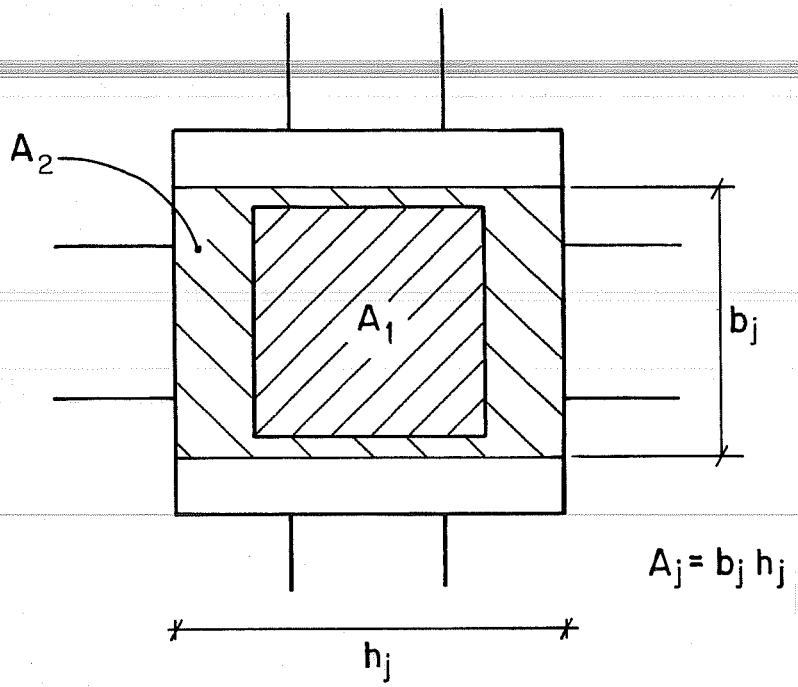

Figure 6.2 Joint Shear Area

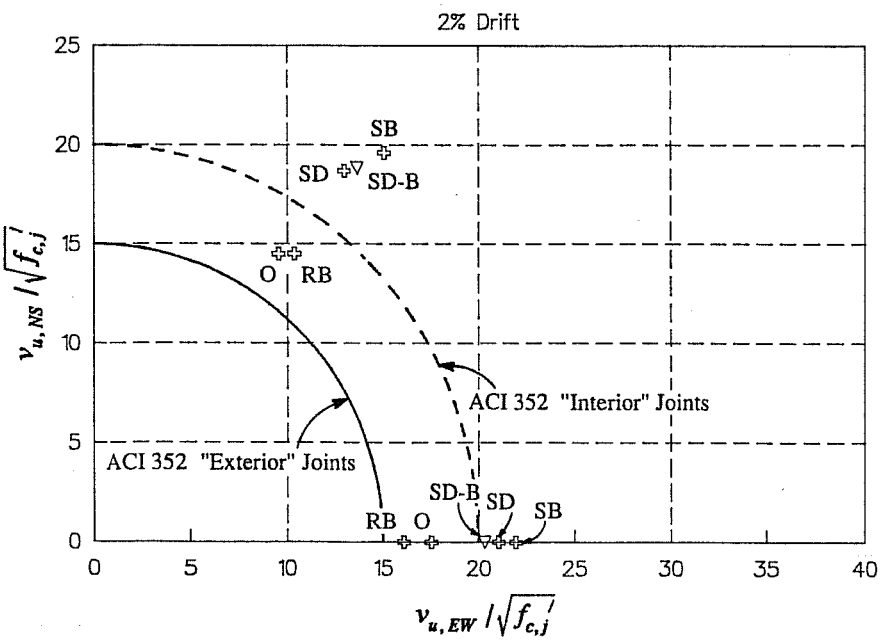

Figure 6.3 Joint Shear Stresses at 2% Drift

The use of $\phi = 0.85$ for rehabilitated joints might be justified if the construction quality is expected to be good. ACI 352 and ACI 318 specify a strength reduction factor of $\phi = 0.85$ intended for joints in new buildings. This factor considers the probability of understrength members due to variations in material strengths and dimensions, the inaccuracy of design equations, the degree of ductility and required reliability of the joint under seismic loads, and the importance of the joint in the structure. For rehabilitated structures, the ϕ factor should also include the level of damage and the quality of the workmanship. In the subassemblages tested, special care was given to detailing and construction of the jackets, particularly in the welds of the joint confinement cage. It is evident that if workmanship is substandard or if the joint is damaged, a lower reduction factor may be justified. The same consideration should be given to other strength reduction factors involved in the design of rehabilitation schemes.

6.3.7 Beam and Column Bar Development. For jacketed beams, the new beam bars should satisfy the ACI 352 criterion on bar development (ACI 352 suggests a minimum column depth to bar diameter ratio of $h/d_b = 20$ for new construction). The h/d_b ratio for the existing beam reinforcement should be checked and if it is below the minimum recommended, a larger column jacket or beam jacketing can be considered. To compute the h/d_b ratio, the location of the beam critical section should be taken into account. A similar review of column bars, especially bundled bars, should be made. Although not enough data is available on the response of bundles through joints subjected to large inelastic deformations, the effective h/d_b ratio for the bundle will be smaller than that based on a single bar. If the h/d_b ratio for beam and column bars is too small, it is likely that severe bond distress might occur within the joint. ACI 352 Committee Report requires checking the development of beam and column bars passing through the joint. In new construction, this criterion often controls the size of elements, especially columns. In rehabilitated buildings with jackets, column dimensions might be fixed due to economic considerations (to avoid foundation strengthening), occupancy, architectural and/or construction reasons.

6.3.8 Slab Participation. Beam strength enhancement from the slab reinforcement and flange areas, under positive and negative bending, must be considered because it will influence the required shear strength of beams, flexural strength of columns and strength of joints. To calculate the beam negative moment capacity, a total slab overhang equal to 20% of the transverse span can be considered for a damaged structure. For undamaged structures to be rehabilitated, a total overhang equal to half the transverse span can be used. For a building with geometry (beam span) different from that used in the specimens, the effective overhanging slab width on each side of the web can be taken as four times the slab thickness for a damaged structure, and ten times the slab thickness for an undamaged building. The effective slab width will then include the slab overhang and the beam width. Both top and bottom bars can be used in the calculations as long as bottom bars have enough anchorage in the transverse beams. Slab bars outside the effective slab are neglected in the calculations.

6.4 EVALUATION CONSIDERATIONS

Ultrasonic pulse velocity has been used in some buildings to evaluate the level of damage in the frame elements. However, based on this series of tests, the application of ultrasonic pulse velocity in a real structure appears to be limited, since previous measurements in the member, that serve as reference values, generally are not available. The use of absolute readings (without a reference value) to assess the damage of a member can be meaningless. The acquisition of the reference value from another location in the structure is not justified since pulse velocities depend on the density, cracking and moisture content of the concrete, and on the presence of steel reinforcement. In this program, the results of the pulse velocity were interpreted from readings normalized with respect to the measurement prior to testing. Based on these results, direct readings (across beams and columns) performed better than semidirect readings (diagonally through the joint). The need for diagnostic techniques is evident. Other non-destructive testing methods such as radar, delamination devices and tomography are still under development (Ref. 16).

CHAPTER VII - SUMMARY AND CONCLUSIONS

7.1 SUMMARY OF EXPERIMENTAL PROGRAM

An experimental program was implemented to assess the effectiveness of jacketing of frame elements. The investigation was aimed at studying the behavior of beam-column-slab joints rehabilitated by jacketing. Four large-scale reinforced concrete frame connections were tested after being repaired and/or strengthened by jacketing only columns, or both columns and beams. The specimen condition prior to the rehabilitation, i.e. damaged or undamaged, and the layout of the longitudinal reinforcement in the column jacket were also varied. The subassemblages were subjected to a bidirectional cyclic loading history to large deformation levels equivalent to 4% drift.

An interior joint representing a prototype structure, i.e. existing structure, was designed according to Mexican and American design practices of the 1950's. The structure was not detailed for ductile behavior. The floor system was designed for large gravity loads and the columns were not designed to carry significant lateral forces. As a result, the system consisted of a joint with weak columns and strong beams. Identical existing structures were rehabilitated by jacketing the columns only, and both the columns and beams. The column jackets were designed to have larger flexural capacities than those of the beams. The joints were subjected to large shear forces. The beam jackets were reinforced to increase moderately the bending capacity.

One specimen was tested to failure, repaired by jacketing the column with longitudinal reinforcement bundled in the corners of the jacket, and retested. The second model was undamaged prior to rehabilitation to permit a comparison of the effect of column damage on the response. To compare the influence of column bar bundles, the columns of the third subassemblage were jacketed with longitudinal reinforcement distributed around the perimeter. In the fourth structure, the column was jacketed using distributed column bars, and the beams were also jacketed. Beam and column jacket transverse steel was spaced to meet the requirements of ACI 318-83. Slab reinforcement was the same for all models, and consisted of #3 top bars spaced at 12 in. and #3 bottom bars spaced at 24 in.. Grade 60 deformed bars were used throughout. A structural steel cage was assembled around the joint to confine the joint concrete not confined by transverse beams, and to confine the column bars. The cage consisted of A36 structural steel angles and flat bars welded in situ.

7.2 CONCLUSIONS

A summary of test results is given. A summary of the construction, design and evaluation considerations, developed from the construction and observed performance of the specimens, and from the analysis of test results, is presented.

7.2.1 Summary of Test Results

7.2.1.1 Member Contributions to Drift Angle and Energy Dissipation. Member contributions to drift angle and energy dissipation showed that rehabilitated specimens developed a "strong column - weak beam" response as opposed to the "strong beam - weak column" behavior of the existing structure. All the rehabilitated specimens showed more favorable energy dissipation mechanisms than exhibited by the existing structure. Jacketing of frame elements proved to be effective for repairing and strengthening the existing structure.

7.2.1.2 Stiffness. The stiffness of all the specimens deteriorated more rapidly in early stages of loading. The stiffness decayed gradually with cycling. The application of a new deformation level further reduced the stiffness. The stiffness deterioration is attributed to concrete crushing and spalling, joint distress and bond damage. A reasonably good estimate of the stiffness at 0.5% drift was obtained using cracked transformed sections for jacketed members and half the moment of inertia based on gross sections for the existing beams not jacketed.

7.2.1.3 Energy Dissipation. All the rehabilitated specimens dissipated more energy than the existing structure. Equivalent viscous damping ratios were computed to measure indirectly the pinching of the load versus deformation curves and to compare energy dissipation capacities. In general, damping ratios were lower than 0.15 in unidirectional cycles and less than 0.20 during bidirectional loading. Rehabilitated specimens showed slightly higher damping ratios than the existing structure. Pinching of the hysteresis diagram is credited to joint distress, concrete damage, and bond deterioration or slip of the reinforcement. Differences in the amount of top and bottom beam reinforcement also contributed to pinching of the response. The amount of top reinforcement (including slab steel) was larger than the amount of bottom steel. After downward loading was completed, tensile residual strains in the top reinforcement were measured. During upward loading, the residual strains delayed crack closure and led to pinching of the load versus displacement curves.

7.2.1.4 Joint Shear Strength. The joints of the rehabilitated specimens failed at 4% drift after beam hinges formed next to the columns. Measured joint shear stresses for all specimens were higher than those recommended by ACI 352. For the rehabilitated specimens classified as "exterior" joints according to ACI 352, i.e. RB, SB and SD, joint shear stresses varied from $16.1\sqrt{f'_{c,j}}$ to $22.1\sqrt{f'_{c,j}}$ during uniaxial cycles to 2% drift, and from $17.9\sqrt{f'_{c,j}}$ to $24.8\sqrt{f'_{c,j}}$ during bidirectional loading. For specimen SD-B, classified as "interior" joint, joint stresses were $20.4\sqrt{f'_{c,j}}$ and $23.2\sqrt{f'_{c,j}}$ for uniaxial and biaxial loading to 2% drift, respectively. The value $\sqrt{f'_{c,j}}$ is a weighted average based on the effective areas resisting joint shear in the existing column and column jacket relative to the joint area. The results from the tests suggest that ACI 352 Recommendations can be applied to design rehabilitated joints using jacketing.

7.2.1.5 Slab Participation. The slab participation was evaluated using two methods. First, the effective slab width was estimated through slab bar stresses. At 2% drift, the effective slab width was 45% of the transverse span for the repaired structure and about 70% for the specimens which were undamaged prior to jacketing. In the second method, the effective slab width was calculated by comparing the maximum measured moments with calculated capacities. For this method, a good estimation of the beam capacity at 2% drift was obtained by considering the rectangular section for the repaired structure, and by taking 30% of the transverse span for the specimens which were undamaged prior to rehabilitation.

7.2.1.6 Effect of a Damaged Column. The results indicate that by jacketing the most damaged elements, the columns and joint, the strength at 2% drift and the stiffness at 0.5% drift of the repaired specimen were about 65% and 50% of the values obtained in the undamaged rehabilitated specimen.

7.2.1.7 Influence of Layout of Longitudinal Reinforcement in Column Jacket. In this series of tests, bundled bars and distributed reinforcement in the column showed good bond behavior. The specimen with distributed reinforcement was more flexible than that with bundled bars.

7.2.1.8 Effect of Beam Jacketing. Test results showed that lower stresses were applied on the existing reinforcement of jacketed beams. Joint confinement was also enhanced after jacketing the beams.

7.2.1.9 Joint Confinement. The structural steel cage assembled around the joint adequately confined the concrete and the column bars not confined by the transverse beams. No concrete spalling other than the joint cover was observed.

7.2.1.10 Ultrasonic Pulse Velocity. Ultrasonic pulse velocity measurements across jacketed columns and beams indicated composite behavior. Joint damage could not be readily correlated with pulse velocity measurements. Pulse velocity direct readings (across columns and beams) were more consistent than semidirect readings (diagonally through the joint).

7.2.2 Summary of Construction Considerations. Based on the construction and performance of the specimens the following construction considerations were developed. Concrete surface must be roughened and cleaned to obtain composite behavior. Slab perforations and holes through the beams must be as large as possible to facilitate placement of the steel, and placement and consolidation of the concrete. The time involved in the surface preparation, and slab and beam perforations of the structure with both beams and columns jacketed was nine times that for the specimens with jacketed columns only. Reinforcement detailing (hooks, bends) is of paramount importance for good performance and proper construction. It is preferable to fabricate transverse steel in the shop rather than on the site. Welded structural steel assemblies should be considered for confining the joint. Formwork must be designed to fit the shape of the existing structure without special or

expensive procedures. To release air pockets in congested regions in the jacket, vents or gaps should be provided in the top of the forms. The use of high-range water-reducing admixtures (superplasticizers) must be considered to improve concrete workability. Due to the intensive labor required for the surface preparation and perforations, and assemblage of the beam cages (especially threading the bars in the joint), and the high costs of formwork, beam jacketing may be uneconomical for American practice.

7.2.3 Summary of Design Considerations. Based on the performance of the specimens and the analysis of test results, the following design considerations were developed.

7.2.3.1 Beam Critical Section and Existing Reinforcement. In the design of structures rehabilitated using jacketing, the change in the mode of failure and redistribution of forces must be considered. Beam shear capacity must be sufficient to develop beam hinging. The location of the beam critical section, and the participation of the existing reinforcement and the slab reinforcement should be taken into account.

7.2.3.2 Layout of Longitudinal Reinforcement in Column Jacket. The layout of the column jacket longitudinal bars is an important design consideration. The use of column distributed reinforcement (versus column bundles) is appropriate to reduce the possibility of bond damage.

7.2.3.3 Stiffness. The stiffness at 0.5% drift can be estimated using a bending stiffness of $0.5E_cI_g$ for beams. If the beams are jacketed, E_c corresponds to the modulus of elasticity of the jacket concrete. Similarly, a bending stiffness of $0.6E_cI_g$ can be used for jacketed columns.

7.2.3.4 Joint Shear Strength. No design recommendations exist for rehabilitated frame connections. Based on the results, ACI 352 recommendations can be used to design rehabilitated joints using jacketing. Checking the joint shear strength in each direction will assure bidirectional joint shear strength. To compute the joint shear stress, a weighted average based on the effective areas resisting shear in the existing column and column jacket relative to the joint area should be used. Ideally, column and beam bars in the existing elements and jackets should satisfy the ACI 352 criterion for bar development. As minimum, longitudinal reinforcement in the jackets should fulfill this criterion.

7.2.3.5 Slab Participation. A total slab overhang equal to 20% of the transverse span can be used when calculating the negative beam flexural capacity for a damaged structure rehabilitated by jacketing. For undamaged structures, half of the transverse span can be used. For a building with beam spans different from those used in the specimens, the effective overhanging slab width on each side of the beam web can be taken as four times the slab thickness for a damaged structure, and ten times the slab thickness for an undamaged building.

7.2.4 Summary of Evaluation Considerations. The application of ultrasonic pulse velocity in real structures appears to be limited. Absolute readings are meaningless for evaluating the level of damage, if previous measurements in the member are not available.

7.3 SUGGESTED RESEARCH

An assessment of the effectiveness of frame jacketing as a rehabilitation technique was obtained from the analysis of test results. In light of the evaluation reached, additional research topics are suggested:

a) The use of structural steel for external joint confinement should be explored. Additionally, research on jacketing of frame elements using structural steel is necessary, particularly for beams. Technical and economical advantages and disadvantages in comparison with reinforced concrete jacketing should be included. Mathematical modelling of the behavior of such schemes should be carried out to examine the response of rehabilitated buildings subjected to different ground motions.

b) The use of welded wire fabric should be explored for rehabilitation of buildings to improve labor productivity and construction quality.

c) Development of reliable non-destructive testing methods must continue, especially for application to complex states of stresses. Screening methods are necessary to assess the in-situ bond capacity of bars within the joint of real structures.

d) Research on the slab participation must continue and may include, among other variables, slab thickness, transverse beam size, and the reinforcement ratio and layout. Slab participation of previously cracked floor systems after rehabilitation should be assessed. Correlation of isolated specimens with real structures is desirable.

e) Investigation of strength reduction factors and load factors for rehabilitated structures is needed.

f) To avoid drilling wide columns, the beam jacket reinforcement sometimes has been bent so that it surrounds the column and forms a horizontal haunch. An investigation of this scheme seems pertinent. Jacketing of columns in flat slab structures should also be examined.

g) Other topics may include the examination of the effect of pinching due to bond distress within the joints on the response of reinforced concrete structures subjected to seismic motions. Pinching of the response should be correlated with joint detailing. In this series of tests, bundled bars exhibited good bond behavior. It is

necessary to study the bond behavior of bundles in structures subjected to large inelastic deformations, in which the columns are less strong than those of this program. An equivalent beam depth to column bar diameter ratio for bundles is desirable.

BIBLIOGRAPHY AND REFERENCES

1. ACI Committee 318, "Building Code Requirements for Reinforced Concrete (ACI 318-63)," American Concrete Institute, Detroit, 1963, 144 pp.

2. ACI Committee 318, "Building Code Requirements for Reinforced Concrete (ACI 318-83)," American Concrete Institute, Detroit, 1983, 111 pp.

3. ACI Committee 318, "Building Code Requirements for Reinforced Concrete (ACI 318-89)," American Concrete Institute, Detroit, 1989, 353 pp.

4. ACI-ASCE Committee 352, "Recommendations for Design of Beam-Column Joints in Monolithic Reinforced Concrete Structures," (ACI352R-76)(Reaffirmed 1981), American Concrete Institute, Detroit, 1976, 19 pp.

5. Aguilar, J. et al., "The Mexico Earthquake of September 19, 1985 - Statistics of Damage and of Retrofitting Techniques in Reinforced Concrete Buildings Affected by the 1985 Earthquake," Earthquake Spectra, EERI, Vol. 5, No. 1, Feb. 1989, pp. 145-151.

6. Aktan, A.E., Karlsson, B.I., and Sozen, M.A., "Stress-Strain Relationships of Reinforcing Bars Subjected to Large Strain Reversals," Civil Engineering Studies No. 397, University of Illinois, Urbana, June 1973, 47 pp.

7. Al-Sulaimani, G.J., "Inelastic Response of Degrading and Nondegrading Systems Under Seismic Actions," Ph.D. Dissertation, The University of Texas at Austin, Aug. 1982, 317 pp.

8. Al-Sulaimani, G.J., and Roesset, J.M., "Design Spectra for Degrading Systems," Journal of Structural Engineering, ASCE, V.111, No. 12, Dec. 1985, pp. 2611-2623.

9. Applied Technology Council, "Evaluating the Seismic Resistance of Existing Buildings," Publication ATC-14, 1987, 370 pp.

10. Bass, R.A., Carrasquillo, R.L., and Jirsa, J.O., "Shear Transfer Across New and Existing Concrete Interfaces," ACI Structural Journal, Vol. 86, No. 4, July-Aug. 1989, pp. 383-393.

11. Bertero, V.V., and Bresler, B., "Seismic Behavior of Reinforced Concrete Framed Structures," Proceedings, Fourth World Conference on Earthquake Engineering, Santiago, Chile, 1969, 1, B-2, pp. 109-124.

12. Bett, B.J., Klingner, R.E., and Jirsa, J.O., "Behavior of Strengthened and Repaired Reinforced Concrete Columns Under Cyclic Deformations," PMFSEL Report No. 85-3, Phil M. Ferguson Structural Engineering Laboratory, The University of Texas at Austin, Dec. 1985, 75 pp.

13. Cheung, P.C., Paulay, T., and Park, R., "Interior and Exterior Reinforced Concrete Beam-Column Joints of a Prototype Two-Way Frame With Floor Slab Designed for Earthquake Resistance," Report No. 89-2, Department of Civil Engineering, University of Canterbury, Christchurch, New Zealand, Mar. 1989.

14. Collins, M.P., and Mitchell, D., "Shear and Torsion Design of Prestressed and Non-Prestressed Concrete Beams," PCI Journal, Sep.-Oct. 1980, pp. 32-100.

15. Comite Euro-International du Beton, "Assessment of Concrete Structures and Design Procedures for Upgrading (Redesign)," Bulletin D'Information No. 162, Lausanne, Aug. 1983, 288 pp.

16. Comite Euro-International du Beton, "Diagnosis and Assessment of Concrete Structures, State of the Art Report," Bulletin D'Information No. 192, Lausanne, Jan. 1989, 120 pp.

17. Corazao, M., and Durrani, A.J., "Repair and Strengthening of Beam-to-Column Connections Subjected to Earthquake Loading," NCEER Technical Report No. 89-0013, National Center for Earthquake Engineering Research, State University of New York at Buffalo, Feb. 1989, 99 pp.

18. Departamento del Distrito Federal, "Normas Técnicas Complementarias para Diseño y Construcción de Estructuras de Concreto," (In Spanish) Gaceta Oficial del Departamento del D.F., Nov. 26th., 1987, 73 pp.

19. French, C.W., and Boroojerdi, A., "Contribution of R/C Floor Slabs in Resisting Lateral Loads," Journal of Structural Engineering, ASCE, Vol. 115, No.1, Jan. 1989, pp. 1-18.

20. French, C.W., Thorp, G.A., and Tsai, W.J., "Epoxy Repair Techniques for Moderate Earthquake Damage," ACI Structural Journal, Vol. 87, No. 4, July-Aug. 1990, pp. 416-424.

21. Guimaraes, G.N., "Reinforced Concrete Frame Connections Constructed Using High Strength Materials," Ph.D. Dissertation, The University of Texas at Austin, Dec. 1988, 202 pp.

22. Jirsa, J.O., "Factors Influencing the Hinging Behavior of Reinforced Concrete Members Under Cyclic Overloads," Proceedings, Fifth World Conference on Earthquake Engineering, Rome, 1973, Paper 147, Vol. 2, 7 pp.

23. Jirsa, J.O., and Breen, J.E., "Influence of Casting Position and Shear on Development and Splice Length - Design Recommendations," Research Report No. 242-3F, Center for Transportation Research, Bureau of Engineering Research, The University of Texas at Austin, Nov. 1981, 45 pp.

24. Jirsa, J.O., "Repair of Damaged Buildings - Mexico City," Proceedings, Pacific Conference on Earthquake Engineering, New Zealand, Aug. 1987, Vol. 1, pp. 25-34.

25. Jirsa, J.O., "Programas de Rehabilitación de Edificios Peligrosos Ubicados en Zonas Sísmicas," (In Spanish) Proceedings, VI Latinamerican Seminar on Seismic Resistant Engineering, Mexico, Sep. 1990, 11 pp.

26. Joglekar, M.R., "Behavior of Reinforced Concrete Floor Systems Under Lateral Loads," Ph.D. Dissertation, The University of Texas at Austin, Dec. 1984, 228 pp.

27. Kitayama, K., Otani, S., and Aoyama, H., "Behavior of Reinforced Concrete Beam-Column Connections with Slabs," presented at the U.S.- New Zealand - Japan - China Seminar on the Design of Reinforced Concrete Beam-Column Joints for Earthquake Resistance, University of Canterbury, New Zealand, Aug. 1987.

28. Kitayama, K., Otani, S., and Aoyama, H., "Earthquake Resistant Design Criteria for Reinforced Concrete Interior Beam-Column Joints," Proceedings, Pacific Conference on Earthquake Engineering, New Zealand, Aug. 1987, Vol.1, pp. 315-326.

29. Kurose, Y. et al., "Study of Reinforced Concrete Beam-Column Joints Under Uniaxial and Biaxial Loading," PMFSEL Report No. 88-2, Phil M. Ferguson Structural Engineering Laboratory, The University of Texas at Austin, Dec. 1988, 146 pp.

30. Lee, D.L.N., "Original and Reparied R/C Beam-Column Subassemblages Subjected to Earthquake Type Loading," Report No. UMEE 76R4, Department of Civil Engineering, The University of Michigan, Apr. 1976, 206 pp.

31. Leon, R.T., "The Influence of Floor Members on the Behavior of Reinforced Concrete Beam-Column Joints Subjected to Severe Cyclic Loading," Ph.D. Dissertation, The University of Texas at Austin, Dec. 1983, 323 pp.

32. MacGregor J.G., "Reinforced Concrete Mechanics and Design," Prentice-Hall, Inc., New Jersey, 1988, 799 pp.

33. Martinez, J.E., "Repair of a Reinforced Concrete Beam-Column Subassemblage Subjected to Bidirectional Cyclic Loading," M.Sc. Thesis, The University of Texas at Austin, Dec. 1988, 60 pp.

34. Migliacci, A., et al., "Repair Techniques of Reinforced Concrete Beam-Column Joints," Final Report, IABSE Symposium on Strengthening of Building Structures - Diagnosis and Therapy, Venice, 1983, pp. 355-362.

35. Mindess, S., and Young, J.F., "Concrete," Prentice-Hall, Inc., New Jersey, 1981, 671 pp.

36. Moehle, J.P., "Observations on the Effect of Floor Slab on Behavior of Beam-Column-Slab Connections," presented at the Seminar on Earthquake Resistant Design of Reinforced Concrete Beam-Column Joints, Hawaii, May 1989.

37. Newmark, N.M., and Rosenblueth, E., "Fundamentos de Ingeniería Sísmica," Ed. Diana, Mexico, D.F., 1976, 680 pp.

38. Owen, G.N., Scholl, R.E., and Egbuonye, I.O., "Vibration Testing of an Epoxy-Repaired Full-Scale Reinforced Concrete Structure," Proceedings, Eight World Conference on Earthquake Engineering, San Francisco, 1984, Vol. 1, pp. 517-523.

39. Pantazopoulou, S.J., Moehle, J.P., and Shahrooz, B.M., "Simple Analytical Model for T-Beams in Flexure," Journal of Structural Engineering, ASCE, Vol. 114, No. 7, July 1988, pp. 1507-1523.

40. Park, R., and Paulay, T., "Reinforced Concrete Structures," John Wiley and Sons, New York, 1975, 769 pp.

41. Popov, E.P., and Bertero, V.V., "Repaired R/C Members Under Cyclic Loading," Earthquake Engineering and Structural Dynamics, Vol. 4, 1975, pp. 129-144.

42. Popov, E.P., and Ortiz, M., "Macroscopic and Microscopic Cyclic Metal Plasticity," Proceedings, Third Engineering Mechanics Division Specialty Conference ASCE, Austin, Sep. 1979, pp. 303-330.

43. Rosenblueth, E., and Meli, R., "The 1985 Earthquake: Causes and Effects in Mexico City," Concrete International Vol. 8, No. 5, May 1986, pp. 23-34.

44. Sozen, M., "Hysteresis in Structural Elements," published in the Applied Mechanics in Earthquake Engineering, Annual Meeting of the American Society of Mechanical Engineers, AMD Vol. 8, New York, Nov. 1974, pp. 63-98.

45. Teran, A., "Review of Repair Techniques for Earthquake Damaged Reinforced Concrete Buildings," M.Sc. Thesis, The University of Texas at Austin, Dec. 1988, 112 pp.

46. United Nations Industrial Development Programme, "Building Construction Under Seismic Conditions in the Balkan Region: Repair and Strengthening of Reinforced Concrete, Stone and Brick-Masonry Buildings," Vol. 5, First Edition, Vienna, 1983, 231 pp.

47. Zhu B., Wu M., and Zhang K., "A Study of Hysteretic Curves of Reinforced Concrete Members Under Cyclic Loading Taking Account of Local Contact," Journal of Tongji University, No. 1, 1980, pp. 63-75.